DETERMINING THE MOLECULAR STRUCTURE AND FUNCTION OF SODIUM CHANNEL

by

Ronald Adolphus Li

A thesis submitted in conformity with
the requirements for the degree of

Doctor of Philosophy

Graduate Department of Physiology
Faculty of Medicine
University of Toronto

The author has granted a non-exclusive licence allowing the National Library of Canada to reproduce, loan, distribute or sell copies of this thesis in microform, paper or electronic formats.

L'auteur a accordé une licence non exclusive permettant à la Bibliothèque nationale du Canada de reproduire, prêter, distribuer ou vendre des copies de cette thèse sous la forme de microfiche/film, de reproduction sur papier ou sur format électronique.

The author retains ownership of the copyright in this thesis. Neither the thesis nor substantial extracts from it may be printed or otherwise reproduced without the author's permission.

L'auteur conserve la propriété du droit d'auteur qui protège cette thèse. Ni la thèse ni des extraits substantiels de celle-ci ne doivent être imprimés ou autrement reproduits sans son autorisation.

0-612-41212-1

Canada

<center>

Determining structure and functions of Na$^+$ channel

Ronald A. Li

Ph.D. 1998

Department of Physiology

University of Toronto

ABSTRACT

</center>

The structure and functions of Na$^+$ channel were studied using mutagenesis in combination with biophysical probes such as Cd^{2+}, sulfhydryl-specific modifiers, various toxins and local anesthetics (LA). Since high-affinity blockade of cardiac Na$^-$ channels by Cd^{2+} is mediated by a cysteine residue in the pore, we first developed a strategy of studying the Na$^-$ channel pore structure by systematically replacing single residues in the putative pore region of Cd^{2+} insensitive rat skeletal muscle (rSkM1) Na$^+$ channels with cysteine. This allows identification of pore-lining residues, whose replacement with cysteine should confer enhanced Cd^{2+} sensitivity. Further 3-dimensional structural information was obtained by simultaneously substituting pairs of residues in distinct P-loops. Dual-replacements created channels with either enhanced or reduced Cd^{2+} sensitivity relative to the corresponding single mutants, suggesting coordinated Cd^{2+} binding and cross-linking by the inserted paired sulfhydryls. Since both processes require stringent geometric constraints (<3.5Å) and multiple consecutive adjacent residues in one P-loop could very often approach a single residue in another P-loop, our results indicate that the Na$^-$ channel pore is highly flexible and most of that flexibility resides in Domain IV (DIV).

We next looked for correlations between pore flexibility and channel functions by examining the role of pore-lining residues in Na$^+$ channel ion-selectivity. Specifically, we measured permeability and ionic current ratios of single mutant channels in the presence of different monovalent and divalent cations. Mutations of members of the proposed selectivity filter (i.e. aspartate, glutamate, lysine and alanine in domains I-IV respectively or DEKA for short) of Na$^+$ channels had little effects except K1237 in DIII.

However, we identified three other residues (W1531, D1532, G1533), all in DIV, which are critical determinants of ionic selectivity. Coincidentally, DIV is the most flexible domain. These data not only redefine the Na^+ channel selectivity filter but further suggest a possible role of pore flexibility in selectivity.

Pharmacologically, we examined the effects of pore mutations on μ-conotoxin (μ-CTX) and LA binding. We identified several pore residues which are critical for interacting with the peptide toxin via either electrostatic (E758, D1241) or hydrophobic (W402, W1239, W1531) interactions. Pore mutations (D400C, W402C, E403C, E755C, E758C, K1237C, W1239C, D1241C, A1529C and W1531C) also affected LA binding. In particular, mutations of W1531 in domain IV completely abolish lidocaine binding to Na^+ channels without affecting drug access. We conclude that this trytophan forms part of the local anesthetic binding site (LABS). Taken together with its role in ionic selectivity and toxin binding, our results suggest that W1531 is critical for normal channel functioning.

To map the spatial relationship between the pore and the LABS, we employed the novel strategy Anchor-Linker-Drug (ALD) wherein the agent was made up of a drug moiety linked to an anchor via a linker. Specifically, the LA benzocaine was tethered to the sulfhydryl specific chemical group methanethiosulfonate (MTS) via a hydrocarbon chain. Benzocaine-based methanethiosulfonate derivatives produced typical but irreversible local anesthetic actions in cardiac channels and the mutant rSkM1 channels (Y401C) containing a cysteine at the equivalent location as the cardiac channels. Such effects were readily reversible in rSkM1 upon drug washout indicating the specificity of these drugs to the pore cysteine. By varying the linker length, ALD also allows determinations of the spatial relationship between the pore cysteine and the LABS. We find that the two functional domains are structurally adjacent to each other. Our strategy also provides a potential method for developing a heart-specific antiarrhythmic using the novel strategy.

EXAMINATION COMMITTEE

SUPERVISOR

Dr. Peter Backx
Department of Physiology
University of Toronto

INTERNAL EXAMINERS

Dr. Peter Pennefather
Department of Pharmacology
University of Toronto

Dr. John Roder
Department of Immunology
University of Toronto

Dr. Michael Salter
Department of Physiology
University of Toronto

EXTERNAL EXAMINER

Dr. Harry Fozzard
Department of Pharmacological & Physiological Sciences
University of Chicago

ACKNOWLEDGEMENTS

"Life is like riding a bike, you have to keep moving in order to maintain balance."

"The bitter and the sweet come from the outside, the hard from within, from one's own efforts."

Dr. Albert Einstein

CONTENTS

LIST OF FIGURES

LIST OF TABLES

LIST OF ABBREVIATIONS

Anchor-linker drug	ALD
Batradotoxin	BTX
μ-conotoxin	μ-CTX
Putative Na$^+$ channel selectivity filter	DEKA
Dithiothreitol	DTT
Human heart sodium channel	hH1
Local anesthetic	LA
Local anesthetic binding site	LABS
Long QT	LQT
Methanethiosulfonate	MTS
Benzyl methanethiosulfonate	MTSBN
Methanethiosulfonate benzocaine	MTSBZ
Methanethiosulfonate ethylammonium	MTSEA
Sodium 2-sulfonatoethyl Methanethiosulfonate	MTSES
2-Triethylammonium ethyl Methanethiosulfonate	MTSET
2-Hydroxyethyl methanethiosulfonate	MTSHE
Rat skeletal muscle sodium channel	rSkM1 (μ1-2)
Saxitoxin	STX
Scanning Cysteine Accessibility Method	SCAM
Tetradotoxin	TTX
Wild-type	WT

CHAPTER 1
INTRODUCTION

1.1   *Overview*

Action potentials in excitable cells such as neuronal and cardiac cells are the result of complex interactions of dozens of different classes of ion channels and pumps (Figure 1.1). The voltage-gated Na^+ channel class is responsible for the increase in Na^+ permeability during the initial rapid rising phase of the action potential. Upon membrane depolarization, Na^+ permeability increases rapidly leading to an influx of Na^+ ions into the cell along its concentration gradient. Within a few milliseconds Na^+ channels inactivate and Na^+ permeability decreases back to the baseline level. The channels remain inactivated until the membrane repolarizes. Once repolarized, channels return to the closed states and are be ready again for reopenings upon subsequent depolarization.

The rapid and transient increase in Na^+ permeability results in rapid depolarization of cells. Depolarization by the Na^+ current subsequently activates voltage-gated Ca^{2+} channels (L- and T-type) allowing Ca^{2+} ions to enter cells. Once inside, Ca^{2+} ions can either directly modulate or indirectly act as an intracellular second messenger causing for example the release of neurotransmitters or trigger other intracellular biochemical events (e.g. phosphorylation and gene expression) thereby leading to biological functions such as secretion, metabolism, contraction and excitability.

Eventually, membrane repolarization is achieved by the outward flow of K^+ ions through many different K^+ channels (i.e. I_{to} which is responsible for the early rapid repolarization, $I_{K\ ATP}$ which is normally closed except during ischemia or hypoxia when ATP concentration falls, I_{Ks} which activates very slowly and is stimulated by β-adrenergic agonists, I_{Kur} which activates ultra-rapidly and is sensitive to 4-AP block; I_{K1} whose rectification properties result in elimination of this current during the plateau phase of the action potential and is important for setting the resting membrane potential; $I_{K(Ach)}$ which are activated by acetylcholine and also contribute to repolarization during

Figure 1.1

Top Panel: A typical action potential in a cardiac cell.

Middle Panel: Na^+, Ca^{2+} and K^+ conductances during an action potential. Upward and downward deflections indicate conductances of inward depolarizing and outward repolarizing currents flowing through the corresponding channels.

Bottom Panel: Entry of Na^+ ions through Na^+ channels generates the initial upstroke (Phase 0). Efflux of K^+ ions through i_{to} channels leads to early partial repolarization (Phase 1). The balance between the net efflux of K^+ ions through i_K, i_{K1} and i_{to}, etc and the net influx of Ca^{2+} ions through Ca^{2+} channels leads to a plateau phase (Phase 2). Net efflux of K^+ ions through i_K, i_{K1} and i_{to} channels (Phase 3) and i_K and i_{K1} channels (Phase 4).

2

g_{Na}

g_{Ca}

g_K
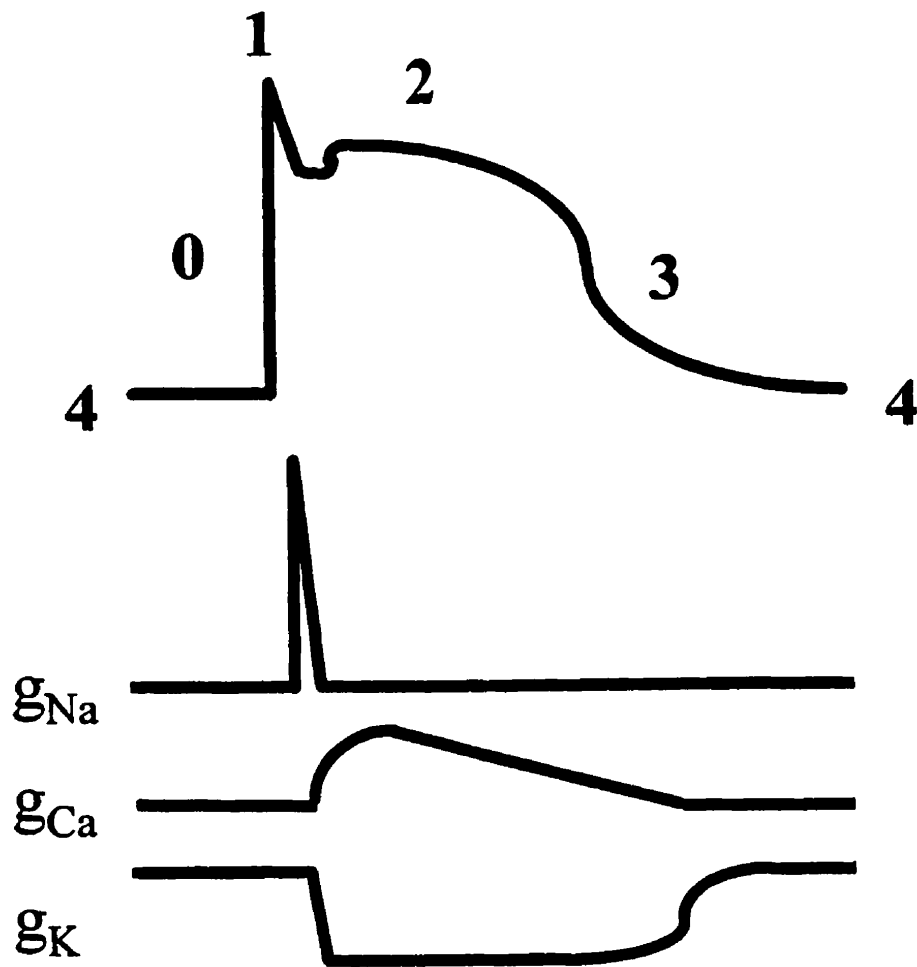
Phase 0	Phase 1	Phase 2	Phase 3	Phase 4

Na^+ $\leftarrow$

K^+ $\rightarrow$

Ca^{2+} $\leftarrow$

K^+ $\rightarrow$

K^+ $\rightarrow$

K^+ $\rightarrow$

Fast Na^+ channel

K^+ channel (i_{to})

Ca^{2+} channels K^+ channels (i_K, i_{K1}, i_{to})

K^+ channel (i_K, i_{K1} i_{to})

K^+ channel (i_K, i_{K1})
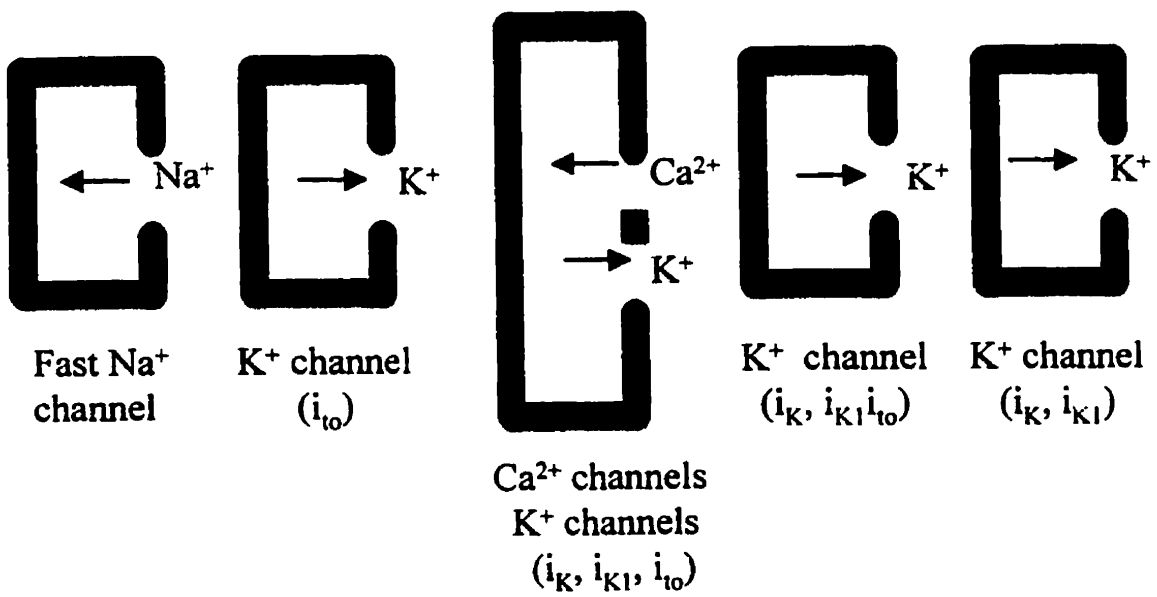
phase 3 especially in the SA-node).

Not only do voltage-gated ion channels mediate action potentials in electrically excitable cells, other channels and ion transporters are also of physiologic importance. To name a few, Cl^- channels are involved in cell volume regulation, stabilization of membrane potential, signal transduction as well as transepithelial transport (Steinmeyer et al., 1991; Berger et al., 1993); $Na^+ K^+$ ATPase pump which hyperpolarizes cells by pumping 3 K^+ ions out for 2 Na^+ ions in; Na^+/Ca^{2+} exchanger which provides a depolarizing current during systole in heart; ligand-gated ion channels such as nicotinic acetylcholine and GABA receptors which mediate ion conductance at chemical synapses (Grenningloh et al., 1987a, b; Schofield et al., 1987; Role and Berg, 1996; Colquhoun and Patrick, 1997; Kimura, 1998), etc. There are also nonselective channels which play critical roles in regulating a variety of different physiological processes. The channels listed so far are however only small samples of the many known to exist in mammalian excitable tissues. Nevertheless, this thesis focuses on the studies of structure and functions of voltage-gated Na^+ selective channels. In this chapter, I will provide a general background on what have been known about Na^+ channels. Specific goals and experimental approaches will be described in subsequent chapters.

1.2   Why study ion channels?

As mentioned, voltage-gated ion channels play a significant physiologic role in excitable tissues by monitoring initiation and propagation of action potentials which is critical for signaling. Ion channels are also important for many forms of inter- and intracellular communication. Defects in ion channels and their operation can alter normal physiology and lead to many forms of pathologies. Recombinant DNA techniques have identified many inherited ion channel diseases caused by mutations in genes encoding for various ion channels (see Table 1.1). Furthermore, ion channels are the primary receptors for a variety of clinically important drugs such as antiarrhythmic agents (Grant, 1991; Hille, 1992; Hondeghem and Katzung, 1977), local anesthetics, neuroprotective agents and calcium channel antagonists (Hille, 1992) etc (see also Table 1.1). Detailed

4

Table 1.1

Summary of ion channel diseases.

Channel Type	Disease (ion-channel gene)	Drug

Na^+ channel:
 	
● Cardiac
 	
● Skeletal muscle
 	
● Epithelial
	● Long QT Syndrome: LQT3 (SCN5A)
	
	● Cardiac Arrythmias
	
	● Torsade de Pointe
	
	● Paramyotonia Congenita (SCN4A)
	
	● Hyperkalemic Periodic Paralysis (SCN4A)
	
	● Masseter-muscle rigidity (SCN4A)
	
	● Liddle's Syndrome (ENaC): hereditary
	
	hypertension and pseudoalsostronism
		● Anticonvulsants (carbamazepine, phenytoin, valproic acid,
		
		etc)
		
		● Class I antiarrhythmics
		
		  IA: disopyramide, procainimide, quinidine, etc.
		
		  IB: lidocaine, mexiletine, phenytoin, tocainide,
		
		  IC:encainide, flecanide, propafenone, etc.
		
		● Local anesthetics (bupivacaine, cocaine, lidocaine,
		
		mepivacaine, tetracaine, etc)

K^+ channel	● Long QT Syndrome: LQT1 (KVLQT1), LQT2 (HERG)	● Class III antiarrhythmics (clofilium, dofetilide, sotalo, amiodorant, N-acetylprocainimide, etc) ● Antidiabetics (glipizide, glyburide, tolazamide, etc) ● Antihypertensive drugs (diazoxide, minoxidil, etc) ● Potassium channel agonist (adenosine, aprikalim, levcromakalim. nicorandil, pinacidil, etc)
Ca^{2+} channel	● Muscular Dysgenesis	● Class IV antiarrhythmics (diltiazem, verapamil)

	• Malignant Hyperthermia (RyR1) • Central core storage disease (RyR1)	• Antihypertensive drugs (amlodipine, diltiazem, felodipine, isradipine, nifedipine, verapamil, etc) • Antianginal drugs (amlodipine, diltiazem, felodipine, nifedipine, verapamil, etc)
Cl⁻ channel	• Thomsens's Myotonia Congenita (CLCN1) • Becker's Generalized Myotonia (CLCN1) • Hyperkalemic Periodic Paralysis (CACNL1A3) • Myotonia Levior (CLCN1) • Cystic Fibrosis (CFTR) • Hypercalciuric nephrolithiasis (CLCN5)	• Anticonvulsants (clonazepam, phenobarbital, etc) • Hypnotic or anxiolytic drugs (clonazepam, diazepam, lorazepam) • Muscle relaxants (diazepam)

understanding of the structure, pharmacology and physiology of these ion channels and their underlying molecular mechanisms can allow better understanding of the molecular basis of abnormal electrophysiology in diseases such as LQT and others related to ion channel defects. The new knowledge gained in turn will enable improvements in diagnosis of these diseases and better strategies for therapeutic drug design and disease treatment.

1.3   Analogies between enzymes and ion channels

Ion channels are intrinsic membrane proteins that catalyze the transfer of ions across the cell membrane. Passage of ions requires ion channels because the lipid bilayers creates an energy barrier (about 30kT) thereby preventing ions from freely crossing the cell membrane (Hille, 1992). Ion channels are analogous to enzymes in many aspects (Eisenberg, 1990; Miller, 1992). Channel pores are able to discriminate between different ions in solution and yet allow the passage of selective ions at rates as high as millions of ions per second. For instance, K^+ channels can discriminate against Na^+, Mg^{2+} and Ca^{2+} ions very effectively and yet conduct more than 2×10^6 K^+ ions per second through the pore. Channel pores are in fact the equivalence of active sites in enzymes, which selectively transfer substrates to products. Like enzymes, pores also do not influence the direction of reaction (i.e. the direction of ion flow) but only the rate at which the reaction occurs. This rate in turn is dependent on the electrochemical gradient across the cell membrane (see 1.4 for details regarding this electrochemical driving force) which is analogous to the chemical free energy in enzymatic reactions. In other words, the transfer process (catalytic reaction) does not require coupling of energy from an exogenous source; ions simply flow passively down the electrochemical gradient. Like enzymes, ion channels reduce the free energy required to overcome the rate-limiting barrier imposed by the lipid bilayer. Moreover, ion channels also exhibit saturation kinetics which can be described by the Michaelis-Menton kinetics because unitary current saturates at high ion concentrations. Like enzymes, channels are also subject to allosteric regulations (which is equivalent to voltage-dependent gating) by inhibitors (e.g. blockers) and modifiers (e.g. local anesthetics) as well as biochemical processes such as phosphorylation via the G-

7

protein pathway. Finally, the dynamic behaviour of channel pores (Chapter 3) which is critical for ionic selectivity (Chapter 4) is also similar to the essential active site motion of numerous enzymes.

The major difference between ion channels and enzymes lies on the fact that enzymes generally catalyze reactions between distinct distinguishable biochemical molecules (i.e. transition from one chemical structure to another) whereas ion channels distinguishes chemical species on the basis of location. Accordingly, if an enzyme catalyzes the following reaction

$$A \leftrightarrow B \hspace{5cm} \text{Equation 1.1}$$

then the direction of this reaction is determined by the difference in the chemical free energy between B (the product) and A (the reactant) which is given by

$$\delta G = G_B - G_A \hspace{5cm} \text{Equation 1.2}$$

where G_B and G_A are the Gibbs free energy per mole of B and A respectively. When the intrinsic energy of A is greater than B (i.e. $G_A > G_B$), the reaction will proceed *on average* from A to B (i.e. a spontaneous reaction). To a good approximation, the free energy of any chemical species at low concentrations is determined by

$$G_X = RT\ln[X] + G^o_X \hspace{4cm} \text{Equation 1.3}$$

where [X] is the concentration of chemical X and G^o_X is the standard free energy of X (which is directly related to the chemical stability of X). δG for the reaction between A and B is therefore given by

$$\delta G = RT\ln([B]/[A]) - (G^o_A - G^o_B). \hspace{3cm} \text{Equation 1.4}$$

The term $RT\ln([B]/[A])$ is the ideal gas term while $\delta G^o = G^o_A - G^o_B$ is the intrinsic

potential energy difference between molecules A and B.

In the case of ion channels, [A] and [B] represent the concentrations (actually activities when solutions are non-ideal) of the permeant ions on the inside and outside of the membrane respectively. δG^0 is actually V_m which is equivalent to the standard free energy term and represents the difference in electrical potential energy between ions on the inside and outside. Equation 1.4 can be readily appreciated by considering the special case of equilibrium when $\delta G = 0$. Rearranging 1.4 gives

$$E_X = V_m = RT \ln [X]_{outside}/[X]_{inside} \qquad \text{Equation 1.5}$$

which is the Nernst equation where E_X is the ionic equilibrium or Nernst or reversal potential for the ion species X. E_X is indeed an electrical measure of the ion distribution across the cell membrane. When a particular type of ion channel opens, the electrochemical force drives the membrane potential of the entire cell toward the Nernst potential of that particular channel until equilibrium is reached. The direction of ion flow is determined by the net electrochemical driving force for ion movement across the membrane which comprises of two terms: the entropic energy associated with concentration gradients across the membrane (i.e. $RT \ln [X]_{outside}/[X]_{inside}$), plus all other energy changes which in this case arise from the electrical term (i.e. V_m). This net driving force is given by

$$\delta G_X = V_m - E_X \qquad \text{Equation 1.6}$$

When more than one type of channel opens, a balance between the Nernst potentials of both channels will be reached depending on the relative conductance and numbers of channels. The new equilibrium will be closer to the Nernst potential of the dominant channel. The approximate Nernst potentials for Na^+, K^+, Ca^{2+} and Cl^- channels are respectively +70, -98, +150 and -30 to -65 mV. At rest, K^+ channels dominate and therefore the resting membrane potential (-70 to -80 mV) is closer to its Nernst potential.

1.4   *Biophysics of ion channels*

Movements of ions across lipid membranes via ion channels down the electrochemical gradient result in electrical currents. Ion channels therefore are characterized by the electrical conductances which is defined by the Ohm's law.

$$I_X = g_X E \qquad\qquad\qquad \text{Equation 1.7}$$

where I_X is the ionic current carried by the ion species X through its channel. g_X is the corresponding conductance and $E = \delta G_X$ is the driving force as defined in Equation 1.6. The reciprocal of g is the resistance symbolized as R (i.e. $R = 1/g = E/I$). The total electrical conductance of a membrane is the total sum of all ionic conductances (i.e. ion channels) connected in parallel. i.e. $G_{total} = g_{Na} + g_K + g_{Cl} + ... +$. Note that the conductances/resistances of voltage-gated ion channels are highly voltage- and time-dependent depending on the intrinsic properties of a particular type of channel. Indeed, this serves as the fundamental basis of mediation of electrical signals in excitable cells.

Biological membranes are hydrophobic lipid bilayers that separate intracellular and extracellular charges by an extremely thin insulating layer (about 30A) without allowing them to move across. This charge separation across the bilayer in turn generates an electric field (E) and a voltage difference (i.e. membrane potential. V_m). In physical terms. membranes act like capacitors. This capacitance (C) is defined as,

$$C = Q/E \qquad\qquad\qquad \text{Equation 1.8}$$

where Q is the charge across the cell membrane for a given membrane potential difference E. C has units of farad (F) which is Coul/V. Typically, all cell membranes have a specific capacitance (i.e. capacitance per area) of about 1 $\mu F/cm^2$ (Cole, 1968; Almers, 1978). This value is quite constant even among membranes from different cell types. Since the total capacitance of a particular cell is the product of its total surface area and the specific capacitance, bigger cells for a given membrane potential have higher

total capacitance and are therefore capable of storing more charges. For the same reason, cells that possess extensive membrane invaginations (e.g. cardiac myocytes and their T-tubules), which significantly increase their total cell surface area, have higher capacitances than would be calculated from simple dimensional measurements of the cell.

When ion channels open, ions flow according to the electrochemical gradient and the membrane either charges or discharges itself depending on the direction of current flow. By differentiating Equation 1.8, the rate of change of the potential when a current I_C flows across the membrane is

$$dE/dt = I_C/C = -E/RC \qquad \text{Equation 1.9}$$

The negative sign indicates the capacitor is discharging in this case. The solution of the above first order differential equation is

$$E = E_O \exp(-t/\tau) \qquad \text{Equation 1.10}$$

where $\tau = RC$ is the so called membrane time constant. Physically, it represents the time needed to discharge the total charge to $1/e$ of their previous value. Since specific capacitance is relatively constant, measurements of τ allows estimation of specific membrane resistance. τ ranges from 10 μs to 1s in different resting membranes (Hille, 1992) reflecting the number of active (open) ion channels, and hence the specific resistance, differ vastly between different cell types at rest.

The properties of lipid bilayers and ion channels can be readily represented as capacitors and resistors respectively (Figure 1.2). Consider a single ion channel when ions flow according to the electrochemical gradient, two components of the electrochemical force, namely the electrical flux (J_{et}) and the chemical (diffusional) flux (J_{dit}), are present. The electrical flux is defined as

$$J_{et} = \delta_{et}E \qquad \text{Equation 1.11}$$

11

Figure 1.2

Equivalent electrical circuit representation of the biological membrane. The branches represent ionic currents with their corresponding electromotive forces. The variable resistors denote ion channel conductances are variable and dependent on time and voltage. The total membrane conductance at any given time is the sum of all ionic conductances at that time. See text for details.

Out

$$V_m$$

C_M

g_{Na} g_K

E_{Na} E_K

$$G = g_{total}$$
$$= g_{Na} + g_K + g_{Cl} + ...$$

In
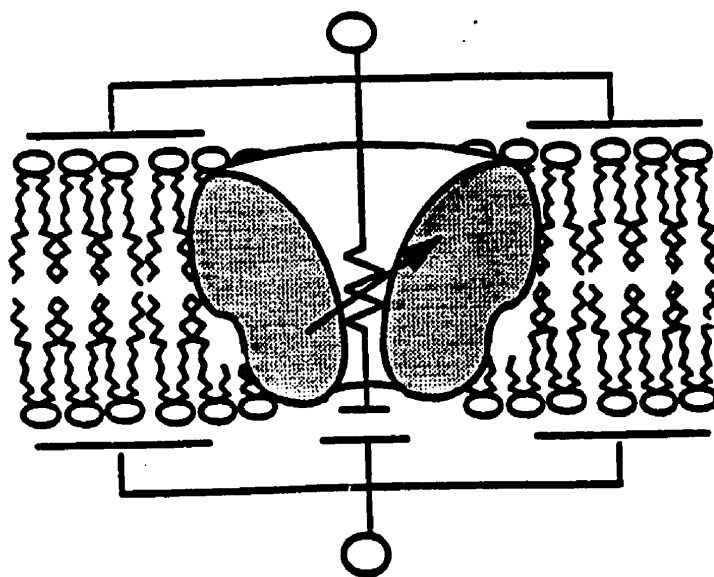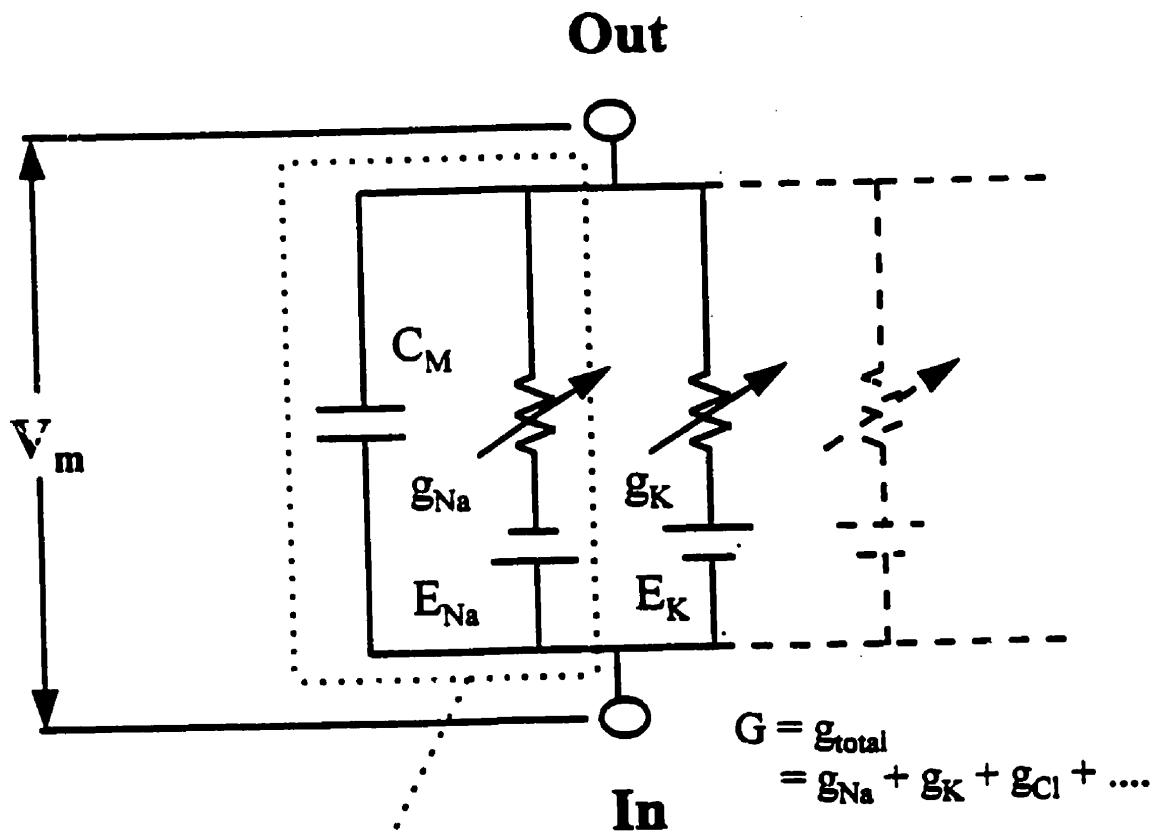
where $\delta_{el} = \mu z[C]$ is the electrical conductivity and $E = -\delta V/\delta X$ is the electrical field. μ is the mobility, z is the ionic valence. $[C]$ is the ion concentration. V is the electric potential and X is the membrane thickness.

According to the Fick's law for diffusion in one dimension, the diffusional flux across the membrane is defined as

$$J_{diff} = -D \, \delta[C]/\delta X \qquad \text{Equation 1.12}$$

where D is the diffusion coefficient. The negative sign indicates that the flux flows from high to low concentrations.

Assuming independence of the electrical and diffusional forces. we can write the total flux as

$$J_{Total} = J_{el} + J_{diff}$$
$$= -\mu z[C] \, \delta V/\delta X - D \, \delta[C]/\delta X \qquad \text{Equation 1.13}$$

Using the Einstein's relation between diffusion and mobility $D = kT\mu/q$ and rearranging Equation 1.13. we get

$$J_{Total} = -(\mu z[C] \, \delta V/\delta X + \mu RT/F \, \delta[C]/\delta X) \qquad \text{Equation 1.14}$$

Equation 1.14 is the Nernst-Planck equation (NPE). At equilibrium. the net flux across the membrane is zero. therefore

$$0 = -(\mu z[C] \, \delta V/\delta X + \mu RT/F \, \delta[C]/\delta X)$$
$$\delta V/\delta X = -RT/zF * 1/[C] * \delta[C]/\delta X$$
$$\int_{X1}^{X2} (dV/dX)*dX = -RT/zF \int_{X1}^{X2} (d[C]/[C]dX)*dX$$

Change variables:
$$\int_{X1}^{X2} dV = -RT/zF \int_{[C]1}^{[C]2} (d[C]/[C])$$

14

$$V_2 - V_1 = -RT/zF \ln [C]_2/[C]_1$$

i.e. $\quad V_m (J=0) = V_{in} - V_{out} = RT/zF \ln [C]_{out}/[C]_{in}$ $\qquad$ Equation 1.15

Equation 1.15 is the Nernst equation.

The above mathematical equations and physics laws form some of the fundamental basis of Hodgkin and Huxley's independent/electrodiffusion theory for understanding properties of ion channels. These equations are valid only when the channels are open and conducting ions. However, channels pores are not always open. These proteins shuffle between open (O), closed (C) and inactivated closed (I) conformations depending on time and cellular conditions. The processes governing transitions between these different states or conformations are collectively known as gating (see also 1.8). Since there are usually around 100-2000 channels of a particular type present in the membrane of a cell, the total ionic current (I_{tot}) resulting from all the ion channels of that type can be expressed as:

$$I_{tot} = N_X * P_X * i_X \qquad \text{Equation 1.16}$$

where $i_X = g_X * \delta G_X$ (equation 1.7) is the unitary current flowing through one single ion channel, P is the probability of the channel being open which is usually a function of time and voltage, N is the total number of channels of a particular type present in the cell. Note that the direction of ion flow however is determined by δG_X (equation 1.6; i.e. the net electrochemical driving force) but not the number of channels or their efficiency (i.e the rate of ion transfer). Each channel undergoes instantaneous transitions between open conducting (O) and closed non-conducting (C & I) states in a time and voltage dependent manner. For example, a Na^+ channel is closed at hyperpolarized potentials (e.g. -80 mV or more negative), opens stochastically following depolarization of the cell membrane and subsequently goes into closed inactivated states. When recording a macroscopic current, it looks "smooth" however since the average behaviour of hundreds or even thousands of channels is being observed (Figure 1.3).

Figure 1.3

Illustrative diagram demonstrating idealized currents recorded from single Na^+ channels (A) and whole-cell/macroscopic currents (B). Individual single channel openings are stochastic events. Summation of thousands of these events gives macroscopic current which displays the average behavior of these channels.

A
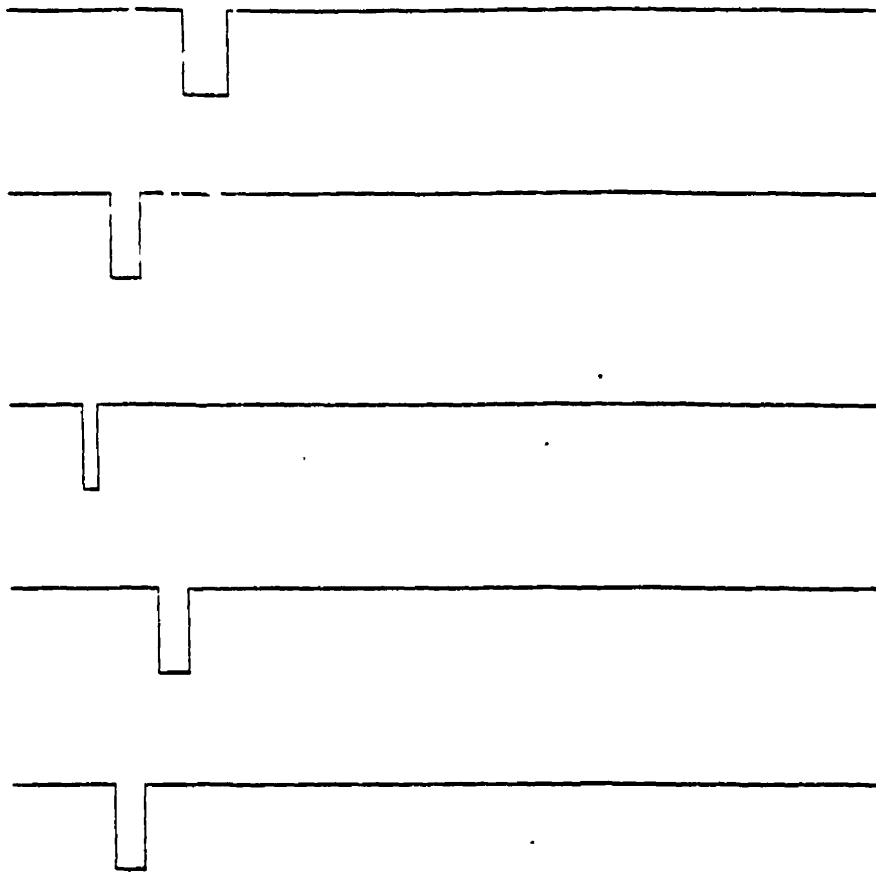
B
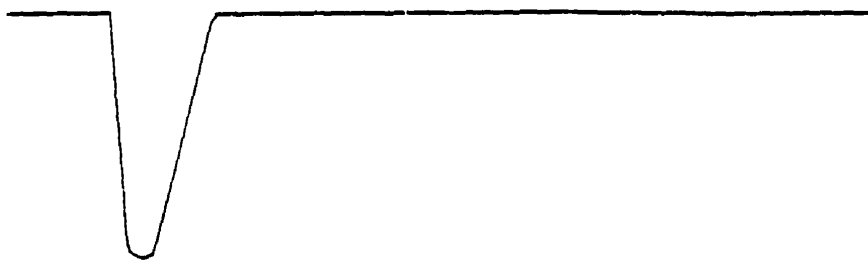
1.5   *Molecular structure of ion channels*

Most voltage-gated ion channels belong to a single super-family of membrane associated proteins which consist of pseudo-symmetrically arranged homologous subunits or repeats surrounding a central pore (Anderson et al., 1993). Although most channels are associated with auxillary regulatory protein subunits (e.g. $\beta 1$ and $\beta 2$ in brain Na^+ channel, $\beta 1$ in skeletal muscle Na^+ channel, $\alpha 2$, β, γ and δ in L-type Ca^{2+} channel, etc) that are required for normal functioning. The α subunits are the subunits which by themselves can form a functional channel (for review, see Catterall, 1992 and Isom et al., 1994). In fact, these α subunits possess all the structural components required for basic ion channel functions. The general structure of the principal α subunits of Na^+, Ca^{2+} and a subset of K^+ channels such as the "Shaker-like" voltage gated K^+ channels is based on the same motif. In the case of the Na^+ channel α subunit, it is a single polypeptide made up of about 2.000 amino acids. Four homologous repeats (DI-IV) are predicted from the primary amino acid sequence and hydropathy analysis. Each of these repeats/domains in turn comprises of six transmembrane spanning segments (S1-6) (Anderson et al., 1993). The region between S5 and S6 inserts back into the membrane to form part of the channel pore and is known as the P-loop or P-segment (P for pore or permeation) (Stevens, 1991; Backx et al., 1992; Catterall, 1991; Ellinor et al., 1995; Heinemann et al., 1992; Noda et al., 1989; Satin et al., 1992; Terlau et al., 1991) (Figure 1.4). The $\alpha 1$ subunit of Ca^{2+} channel also has a similar topology. In contrast to Na^+ and Ca^{2+} channels which are both single polypeptides consisting of four homologous domains, K^+ channels are homo- or hetero-tetramers (Jan and Jan, 1989). Each of the four monomeric subunits is a separate gene product resembling a single domain of Na^+ and Ca^{2+} channels (Figure 1.4). In all cases, the four monomers or domains are pseudo-symmetrically arranged to form a barrel-like structure with the P-loops as extensions from each of the four subunits dipping into the central axis of the channel to form part of the ion-conducting pore (Figure 1.5). These short stretches of P-loops comprise the selectivity filter where selective ion coordination occurs. S4 contains a cluster of positively charged arginines and lysines and is the major component of the voltage sensor in voltage-gated ion channels (see also 1.8.i). Inactivation is mediated by a tethered inactivation particle (i.e. the ball and chain)

18

Figure 1.4

(A) The putative topological arrangements of the principal α-subunits of Na^+ and Ca^{2+} channels showing four homologous internal repeats each with six transmembrane segments (S1-S6). The S4 segment carries a ribbon of positively charged residues and is reponsible for voltage-sensing. The four P-loops which are located between S5 and S6 in each repeat domain form a major part of the channel pore.

(B) In contrast to Na^+ and Ca^{2+} channels which consist of one single polypeptide comprised of four (I-IV) similar repeats. K^+ channels are constructed from non-covalent tetrameric assembly of four single subunits (monomers). Each of these monomers resembles a single domain of Na^+ or Ca^{2+} channel.

Na+ & Ca2+ channel

out

in

N

I

II

III

IV

C

K+ channel

N

C
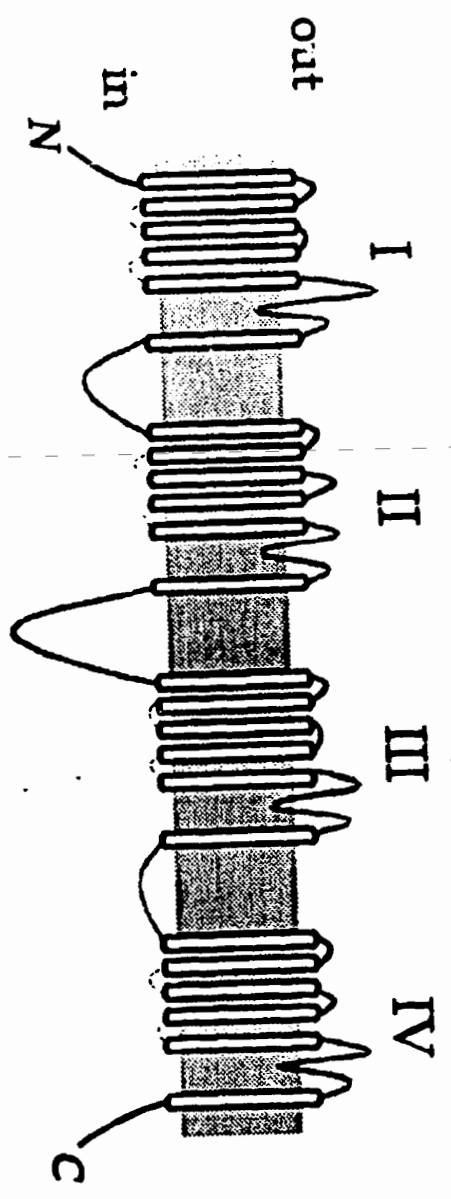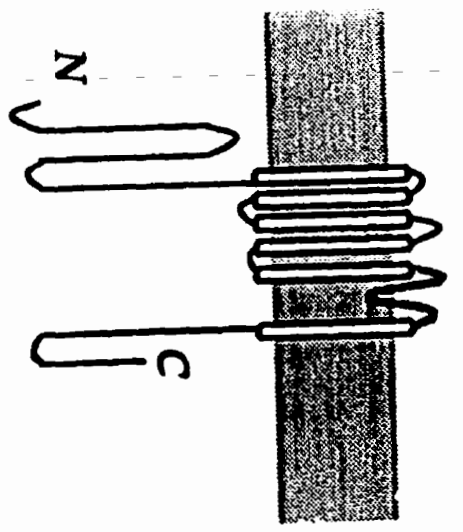
which is located within the III-IV linker in Na⁺ channel and at the N-terminal end of K⁺ channel monomers. This inactivation particle swings into the cytoplasmic mouth of the pore to physically occlude the permeation pathway (see also 1.8.2). These processes of gating will be discussed in more details in subsequent sections.

1.6   *Ion channel pore*

The 3-dimensional molecular structures of ion channel pores have always intrigued biophysicists. Understanding their structures will shed light on the chemical basis of permeation, ionic selectivity and the high throughput rates (typically $>10^6$ ions per sec) of these channel proteins. Previous permeation studies using organic cations suggest that the selectivity region (filter) in Na⁺ channels is rectangular in shape and that the channel has an hourglass appearance with the selectivity filter joining two large vestibules (Hille. 1971) (Figure 1.5). A rigid static pore model has often been assumed to account for many biophysical observations (Hille, 1992). This model received further support from recent crystallization and X-ray analysis of a K⁺ channel from *Streptomyces lividans* (KcsA K⁺ channel) (Doyle et al., 1998). These authors propose that the pore of the KcsA K⁺ channel is constructed of an inverted teepee with the selectivity filter opened into a wider cavity and tunnel lined with hydrophobic residues to the inside (Doyle et al., 1998). While these investigators suggested that the teepee structure is likely to be a general feature other K⁺ channels (Doyle et al., 1998), Na⁺ and Ca²⁺ channels however may employ different methods for ion permeation than their K⁺ channel counterparts implying potential structural and functional differences underlying the fundamental architectures of their pores. For example. in Ca²⁺ channels the side chains of specific glutamate residues from the four P-loops are essential for ionic selectivity (Kim et al., 1993; Mikala et al ., 1993; Yang et al., 1993) whereas main chain carbonyl oxygen are required for selectivity in K⁺ channels. Therefore. whether the same rigid model is applicable in Na⁺ and Ca²⁺ channels remains unclear at this stage. In Chapter 3 of this thesis, I will describe a novel strategy that we developed to study the 3-dimensional structure of the Na⁺ channel pore using multiple cysteine mutagenesis. The conclusion of this study is that the P-loops. like the active sites of many enzymes, are indeed highly

Figure 1.5

(A) Top view of an ion channel demonstrating the P-loops dip towards the central axis of the channel to form part of the pore. The four homologous domains of Na^+ and Ca^{2+} channels are linked together via inter-domain linkers whereas K^+ channels are made up of individual monomers.

(B) Cross-sectional view of an ion channel. A funnel-shaped structure with 2 wide vestibules open to both sides of the channel connected by a restricted portion which acts as the selectivity filter. A static rigid pore model is traditionally assumed which contrasts to the flexible pore model described in Chapter 3. The inactivation particle is also indicated. It is tethered on the cytoplasmic side and binds to a receptor during inactivation thereby physically occluding the channel pore.

(C) Cartoon of a voltage-gated Na^+ channel. K^+ and Ca^{2+} channels are similar in arrangements except the K^+ channel is tetrameric. The four domains of Na^+ and Ca^{2+} channels may be arranged in an asymmetrical fashion. One domain has been removed for easier presentation. The membrane spanning domains are arranged as a barrel-like structure with an ion-conducting pore in the centre. The P-loops form the outer part of the channel pore and is the active site for ionic selectivity.

TOP VIEW

A Na$^+$/Ca^{2+} channel   K$^+$ channel

Inter-domain linker

II

I   Na$^+$ III

IV

B **RIGID & STATIC MODEL**

OUT   Na$^+$

IN

Inactivation ball

C P-loop

I   II   III
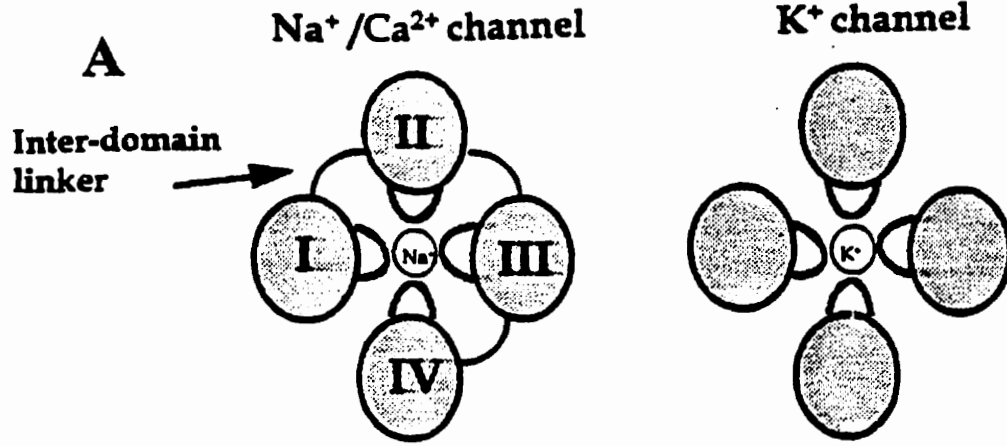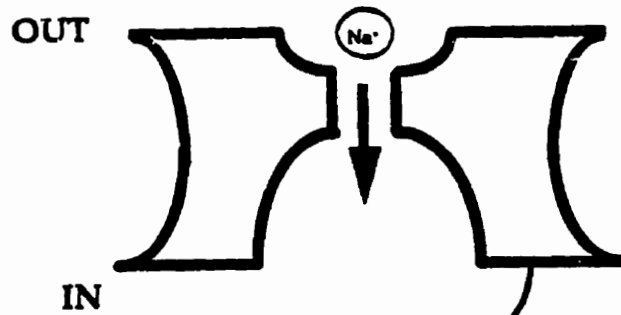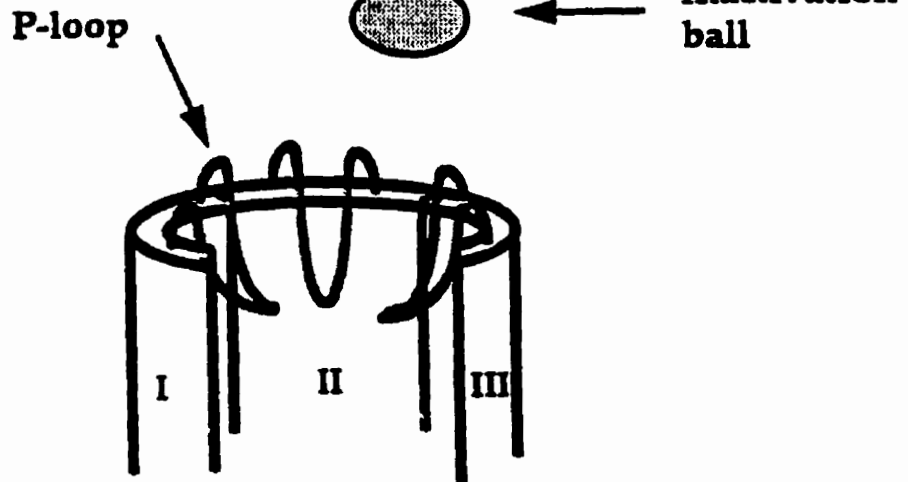
flexible structures on the millisecond time scale, making static structural models pointless due to thermal motions. Previous structural models have proposed that the pore is made up of α-helices and β-strands (Yellen et al., 1991; Lipkind and Fozzard, 1994; Soman et al., 1995; Guy and Durell; 1995). While these secondary structures are well suited for forming the structural framework of proteins because of their highly ordered structures, they also greatly restrict regional flexibility. Flexible regions in other proteins are often random coil/loop structures, as are the flexible active sites of many diffusion limited enzymes (Branden and Tooze, 1991; Cottrell et al., 1995; Creighton, 1993; Fersht, 1985; Lan et al., 1995; Larson et al., 1995; Pompliano et al., 1990; Tanaka et al., 1993). Loop structures permit high degree of flexibility thereby allowing chemical groups from different amino acids to be placed at optimal positions in space to catalyze a particular reaction (MacKinnon, 1995). P-loop flexibility is also consistent with recent studies in other ion channels (Ellinor et al., 1995; Liu et al., 1996; Sun et al., 1996; Yellen et al; 1994) and the notion that ion channels are enzymes (Eisenberg, 1990). The role of channel flexibility in normal channel functioning will be further investigated and discussed in Chapter 3, 4 and 7.

1.6.1   The P-loops form the permeation pathway

Potassium channels are the most extensively characterized group of voltage-gated ion channels. The diversity of this group of channels arises from the tetrameric assembly of these channels which permit heterologous association of different subunit types (MacKinnon, 1991; Miller, 1991). Studies of the *Shaker* K^+ channel and its mammalian homologues provided the first insights into the molecular basis of permeation in voltage-gated channels. This major advance was made with the cloning of the Shaker locus in *Drosophila melanogaster* (Tempel et al., 1987). This locus encodes a family of alternatively spliced transcripts that codes for transient K^+ channels (Papazian et al., 1987). Three other subfamilies have also been cloned from Drosophila namely *Shal, Shab* and *Shaw*. Homologous mammalian genes have been described for each subfamily (Salkoff et al., 1992). The core or membrane spanning regions (i.e. S1-S6) of the K^+ channels within each subfamily share approximately 40% amino acid identity whereas

the amino and carboxy termini tend to be quite variable (Salkoff et al., 1992).

Even with the clones available, the location of the pore through which ions permeate was not known until MacKinnon and Yellen identified the P (pore or permeation) region (Yellen et al., 1991; Hartman et al. 1991). This P-region with striking sequence conservation even among a large array of K^+ channels occurs between the fifth and sixth membrane spanning regions (S5-S6), alternatively known as SS1-SS2 or the P-loops. All K^+ channels known possess the signature sequence (GYG) within the P-region and this sequence is critical for K^+ selectivity (Heginbotham et al., 1992; Heginbotham et al., 1994). Blocking studies of the *Shaker* K^+ channels with the scorpion venom, charybdotoxin (CTX) and the organic cation tetraethylammonium (TEA) provide some of the first evidence that this short stretch of residues in the P-loop is extracellular and in fact turns back into the membrane to form the channel pore (MacKinnon and Miller, 1989; Miller, 1990).

1.6.2   *P-loops form part of the Na^+ channel pore*

The P-loops in all four homologous repeats are highly conserved among Na^+ channels from different tissue subtypes (Table 1.2) (Noda et al., 1984; Noda et al., 1986; Auld et al., 1988; Salkoff et al., 1987; Trimmer et al., 1989; Rogart et al. 1989, Anderson et al., 1993). However, there are many differences between the P-loop sequences of Na^+, K^+ and Ca^{2+} channels (Hille, 1992). While a 4-fold symmetry is generally assumed in homomeric K^+ channels due to their identical monomeric subunits, accessibility scanning studies have suggested asymmetric contributions of each of the four homologous domains of Na^+ channel (Chiamvimonvat et al., 1996a, Perez-Garcia et al., 1997; Tsushima et al., 1997a, b). Furthermore, mutagenesis of "analogous" residues in the P-segments of homologous domains often result in different functional changes. For instance, mutation of a P-loop tryptophan residue in DIV (i.e. W1531) of rat skeletal muscle (rSkM1) Na^+ channel renders the channel non-selective for monovalent cations while mutations of analogous residues in the other three domains (DI: W402C, DII: W756C and DIII: W1239C) did not display the same effects on ionic selectivity

25

Table 1.2 Aligned sequence of the P-loops (S5-S6 linkers) of all four domains of brain. heart and skeletal muscle Na$^+$ channels. The sequences are strikingly conserved.

Domain I

Brain	R L M T Q D F W E N L Y Q
Heart	R L M T Q D C W E R L Y Q
Skeletal muscle	R L M T Q D Y W E N L F Q

Domain II

Brain	R V L C G E W I E T M W D
Heart	R I L C G E W I E T M W D
Skeletal muscle	R I L C G E W I E T M W D

Domain III

Brain	Q V A T F K G W M D I M Y
Heart	Q V A T F K G W M D I M Y
Skeletal muscle	Q V A T F K G W M D I M Y

Domain IV

Brain	Q I T T S A G W D G L L A
Heart	Q I T T S A G W D G L L S
Skeletal muscle	E I T T S A G W D G L L N

26

(Tsushima et al., 1997a). Indeed not only are the four P-loops asymmetrical but the four domains also contribute differently to channel functions.

Similar to the K^+ channel studies, pore blockers have been used to identify the role of the P-loop in pore formation in Na^+ channels. Tetrodotoxin (TTX) and saxitoxin (STX) are among some of the most commonly used Na^+ channel pore blockers. Neutralization of charged residues in the P-loop in all four homologous repeats, which are conserved between TTX-sensitive and TTX-insensitive isoforms, influence TTX block and single channel conductance (Noda et al. 1989; Terlau et al., 1991). Like TTX, divalent cations of the group IIB series (Cd^{2+}/Zn^{2+}) block Na^+ channels in a subtype-specific fashion (Frelin et al., 1986). Interestingly, the TTX-sensitive channels are Cd^{2+}/Zn^{2+}-insensitive and vice-versa (Backx et al., 1992). Recognizing that Cd^{2+}/Zn^{2+} binds to cysteines in solution with high affinity highlighted a naturally occurring variant in the P-loop of these isoforms involving a cysteine residue (C373). Conversion of C373 in DI to tyrosine (i.e. DI-C373Y) in rat heart Na^+ channel abolished sensitivity to Cd^{2+} block but dramatically increased TTX sensitivity by 100-fold (Satin et al., 1992). Interestingly, the complementary mutation in the skeletal muscle Na^+ channel (DI-Y401C) rendered the channel TTX-resistant and Cd^{2+}- and Zn^{2+}-sensitive (Backx et al., 1992). Analysis of the voltage-dependence of divalent block established that the intra-pore location of this residue and the fractional electrical distance of the binding site was about 20% from the outside in both native and expressed channels, despite marked differences in Cd^{2+} affinity (Backx et al., 1992).

Additional evidence for the crucial role of the P-loops in determining the permeation properties of the Na^+ channel came from mutagenesis experiments of the P-loop residue lysine in domain III which conferred Ca^{2+} channel permeation properties onto the Na^+ channel (Heinemann et al., 1992), and the tryptophan in domain IV (Tsushima et al., 1997b) which abolished the ability of the pore to discriminate Na^+ against other monovalent cations such as K^+, Cs^+ and NH_4^+. The roles of pore-lining or P-loop residues in rat skeletal muscle (rSkM1) Na^+ channel in ion permeation and selectivity will be further discussed in Chapter 4.

27

1.7   *Ionic selectivity*

The Na^+ channel pore is highly selective for Na^+ ions over other physiological ions: the selectivity sequence is $Na^+ \approx Li^+ > K^+ > Rb^+ > Cs^+$ (Begenisich, 1987; Hille, 1992; Tsushima et al., 1997). Similarly, other ion channels are selectively permeable to some ions but preclude permeation of others. How ion channels display such extreme selectivity while maintaining high throughput rates ($>10^6$ ions sec^{-1}) remains elusive. Several theories have been proposed to account for this ionic selectivity. The molecular sieve model states that it is the pore size which determines the permeability of different ions through the pore (Bezanilla and Armstrong, 1972; Hille, 1973). In other words, permeability cuts off at a definite ionic size. Ions in solution are hydrated and therefore their hydrated radii need to be considered. A cation in solution attracts the negative end of the water molecule electric dipole (i.e. the oxygen atom) and tries to maintain this hydrogen bond as much as possible. However, permeant ions need to be dehydrated before they can cross the selectivity filter. Water dehydration is a highly unfavorable energetic process. Therefore, ions must fit snugly in the pore and an appropriate surrogate hydrogen shell within the channel so that the energy lost by dehydration and gained by coordination is balanced (Bezanilla and Armstrong, 1972; Hille, 1973). Ions whose ionic radii that are too large cannot be fit while ions that are too small cannot be dehydrated effectively. Thus the selectivity filter selects ions based on both ionic radius (larger ions) and thermodynamic factors (smaller ions). Since the pore size is critical in ion selection, this model also predicts that the ability of the selectivity filter of a highly selective channel to stretch is very limited. This theory is supported by the crystallography recently obtained from the KcsA K^+ channel by Doyle et al. (1998). Consistent with the theory, it shows that the K^+ selectivity filter is comprised of carbonyl oxygens (which are responsible for dehydrating permeating K^+ ions) and is constrained in an optimal geometry to allow proper coordination of a dehydrated K^+ ion but not the smaller dehydrated Na^+ ion (Doyle et al., 1998).

The above molecular sieve model leads immediately to the ion-binding model (Lauger, 1973; Hille, 1975). It was developed from the Eyring rate theory (Eyring et al.,

28

1949) and proposes that ions do not diffuse freely along the pore but bind at certain saturable site(s) within the channel while passing through (Hille, 1975). These binding sites may correspond to the "sieve" mentioned above and are mathematically represented as energy barriers or wells. Different ions bind with different affinities as a result of different barrier heights and well depths. Pore selectivity is the result of these differences in ion binding properties. The permeating ions simply "jump" from one energy well to another while permeating the pore following the rules that each well can only be singly occupied at a time and that an ion cannot pass over a well without first dwelling in it (Hille, 1992). Indeed, the observation that unitary currents saturate at very high permeant ion concentrations, which is analogous to saturation of enzymatic rate at high substrate concentrations lends support to this saturable binding site model. This theory can also account for observed deviations that arise from the independent/electrodiffusion theory (Hille, 1975). While this ion-binding theory is useful in explaining many permeation properties, its literal interpretation of "one energy well corresponds to one discrete physical binding site" from the original model is sometimes ambiguous (Dang & McClesky, 1998). Energy wells are indeed mathematical representation of changes of potential energy during permeation and do not necessarily translate into discrete physical entities (i.e. binding sites) especially for the low-affinity ones. They might simply represent steps of potential energy that the permeant ion experiences during the process of permeation. For instance, a low energy well may qualitatively represent weak ion binding within a wide vestibule (Dang & McClesky, 1998), stepwise dehydration of ions (Eigen & Winkler, 1971), a discrete low-affinity binding site (Hille, 1971, 1972, 1975) or even channel-ion interactions that do not lead to binding. Indeed, crystallography recorded in the presence of permeating ions reveals that hydrated ions spend a fraction of their times in "cavities" without creating deep energy wells (Doyle el al., 1998) is consistent with the last possibility.

When considering the above models, it is necessary to consider the electrostatic field generated from an ion as well. For example, a cation can polarize its immediate environment thereby bringing the negative ends of dipoles closer to itself to achieve stabilization. Given that the polarizability of the surrounding medium is minimal at the

29

centre of the bilayer, it is easy to understand the presence of vestibules or cavities flanking the selectivity filter since their presence is capable of overcoming the electrostatic destabilization resulting from the low dielectric bilayer by simply allowing an ion to remain hydrated. This structural design enables ions to reach the selectivity filter from the cytoplasm or outside via a low resistance pathway thereby facilitating a high throughput.

There are one-ion pores (e.g. SR K^+ channels, AChR channel) and multi-ion pores (K^+ channel, Ca^{2+} channels, Na^+ channels, gramacidin channels) in the ion binding model. One-ion pores can accommodate only one ion in the pore at a time but may possess several different ion-binding sites thereby allowing permeation of several different kinds of ions (Hille, 1992). They are relatively short compared to multi-ion pores such that the electrostatic field of an ion occupying the pore is sufficient to prevent a second ion from entering even if multiple binding sites exist. One-ion pores are characterized by a simple rectangular hyperbola Michaelis-Menton saturation kinetics, concentration-independent and constant permeability ratios, conductance and reversal potential as monotonic functions of mole fraction when measured in the presence of two permeant ions, etc. In contrast, multi-ion pores (i.e. single-file pores) are longer than one-ion pores and are capable of accommodating more than one ion simultaneously in single file (Yellen, 1987).

Electrostatic repulsion generated within multiply occupied pores reduces ion binding affinity thereby making high ion flux rates possible (Hille and Schwartz, 1978; Almers et al., 1984; Hess and Tsien, 1984; Yellen, 1984; Neyton and Miller, 1988; Shumaker and MacKinnon, 1990). Multi-ion pores are more complex and display characteristics like analomous mole-fraction, concentration dependent permeability ratios, unusual conductance-activity relationship other than a simple saturation curve, etc. Ironically, while this multiple ion-binding site model comprehensively explains many of the biophysical properties observed, mutagenesis studies have suggested that the permeation pathway is comprised of a very short region flanked by two wide vestibules (Heginbotham et al., 1994; Hidalgo & MacKinnon, 1995; Miller, 1996; Ranganathan et

al., 1996; Holmgren et al., 1992) which is inconsistent with a long narrow pore consisting of multiple binding sites (Yellen, 1984; French & Shoukimas, 1985; Neyton & Miller, 1988). More recently, a revised model proposes that permeation through a pore containing a single high-affinity binding site flanked by low-affinity non-selective sites/regions (i.e. bulk within vestibules) is equally sufficient to explain ionic selectivity, high flux rates and multi-ion behaviours observed in many channels (Kiss et al., 1998; Dang & McClesky, 1998) in a way that is more consistent with the above molecular studies mentioned.

Another way to account for permeation selectivity is to suggest that ion channels behave like ion carriers or exchangers. Ion permeation involves ion binding and subsequent changes of the pore structure in order for the ion to permeate. In other words, ion permeation is a dynamic process. This is also analogous to the well-known active-site motion, which is essential for many enzymatic reactions. Protein motions may lead to very interesting effects on ion transport (Lauger, 1973, 1987; Ciani, 1984). Depending on the time-scale, motions coupled to ion transfer may influence the observed electrical behaviour such that a single-ion pore may be perceived as a multi-ion pore (Ciani, 1984). Since all hypotheses have their limitations, a combination of these approaches is usually required to explain ionic selectivity and the process of permeation.

1.8 Na^+ channel gating

Ion channel pores are not always open. Pore opening is indeed highly regulated by a process called gating. Availability of the pore is tightly controlled by conformational change of the channel proteins which is a highly voltage-dependent process. Membrane voltages (i.e. the transmembrane electrical fields) trigger these changes in molecular structure thereby affecting ion permeability. Gating is classically separated into two distinguishable processes namely activation and inactivation. According to the Hodgkin and Huxley model of channel function, these gating processes are imagined as gates that reside on the channel protein. Depolarization causes Na^+ channels to open (activate) and then spontaneously close (inactivate) within several milliseconds. Once they close

31

inactivate, the channels need to be repolarized before they are ready for reopening upon subsequent depolarizations. In other words, they need to recover from inactivation. Having said that, ion channels display a number of distinct molecular structures with very distinct functional properties as a function of time and voltage. Shown below is a typical 3-state scheme for Na^+ channel.

$$C \longleftrightarrow O$$
$$\searrow \quad \swarrow$$
$$I$$
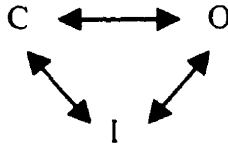
where C, O and I represent closed, open and inactivated states respectively. Note that it is an over-simplification to assume one closed, one open an one inactivated state. Realistically, ion channels very often show more than three states. In fact we can assume as many states as required to fit our experimental data. Most ion channels can usually be best described by assuming 5 or 6 C states, one O state and 1 or 2 I states. It is intriguing that the 5 closed states of the channel have molecular correlates (Kuo & Bean, 1994). The rate constants for transitions between these different states are highly voltage-dependent. Activation and inactivation are the processes that control these rate constants. In other words, these gating processes collectively govern the probability of channel opening (P from equation 17) which in turn control access of ions for the pore. Since P is characterized by both processes of activation and inactivation, it can be written as

$$P = P^a_x * P^i_x \qquad\qquad \text{Equation 1.18}$$

where P^a_x and P^i_x respectively represent the probabilities of the activation and inactivation gates of channel X being open. Many drugs and toxins bind preferentially to one state or a subset of these states or molecular conformations thereby changing the rate constants between certain states (or the probability being in certain states) and/or creating new drug-bound state(s) thence modifying channel behaviors. Activation, inactivation and the coupling between these two gating processes are discussed in greater details below.

32

1.8.1 *Activation*

Hodgkin and Huxley (1952) recognized that the permeability of voltage-gated ion channels is dependent on the membrane potential. They further proposed that charged "gating particles" must exist within the membrane to respond to the transmembrane electric field thereby ultimately controlling the activation (m) gates and drives the permeability changes. These gating particles appear to be charged amino acid residues within the membrane spanning segments (S4) and their movement has been detected as gating current (Armstrong and Bezanilla. 1973) and indirectly measured using fluorescent probes (Mannuzzu et al., 1996; Cha and Bezanilla. 1997). Gating currents can be measured in the absence of ionic fluxes by replacing permeant ions with impermeant ions or application of channel blockers (Armstrong and Bezanilla. 1973. 1974; Keynes and Rojas, 1973; Armstrong, 1981) provided the gating steps are not affected in the presence of these agents. Upon depolarization. activation of Na^+ channels exhibits rapid and highly voltage-dependent outward gating currents which precedes the final opening of the channel (Armstrong & Bezanilla, 1973; Keynes and Rojas, 1973). Such outward gating current could result from outward movements of positive gating particles or alternatively from inward movements of negative charges. If repolarization is given after a short depolarizing pulse (0.5 to 1 ms) before channel inactivation takes place (inactivation is a slower gating process, see section 1.8.2), a rapidly diminishing "tail gating current" will be observed. This indicates that channels close (deactivate) without inactivating. A decaying transient inward gating current is accompanied with this tail current as the gating charges return (an inward movement) to their original positions before activation (Armstrong & Bezanilla, 1973). This observation indicates that the process of activation is readily reversible. Such reversibility is further demonstrated by the observation that the total outward movement of gating charge (Q_{on}) during activation is equal to the total inward movement (Q_{off}) after activation or during deactivation (Armstrong & Bezanilla. 1974; Armstrong, 1981).

Gating current is the result of movements of gating charges or particles. But what are these particles and where are they located? Inspection of the amino acid sequence of

33

the Na^+ channel α-subunit reveals that while most of the transmembrane segments are quite hydrophobic. S4 carries a ribbon of positively charged amino acid residues and is therefore well suited to act as the gating apparatus for voltage-sensing. A positive charged residue. either lysine or arginine. is found at every third amino acid within this segment (Noda et al.. 1984. 1986: Salkoff et al.. 1987; Tanabe et al.. 1987; Papazian et al.. 1987; Tempel et al.. 1988; Baumann et al.. 1988; Ellis et al.. 1988; Kayano et al.. 1988). Moreover. this motif of positive charges followed by two hydrophobic residues is absolutely conserved in all cloned Na^+ channels as well as highly conserved in voltage-gated Ca^{2+} and K^+ channels (Table 1.3). This leads to the prediction that the S4 segments might serve as a critical component of the voltage sensor (Noda et al.. 1986; Catterall. 1988; Numa. 1989; Guy and Conti. 1990).

In addition to deductions from the primary sequence. the S4 hypothesis is further supported by numerous mutagenesis studies of both Na^+ and K^+ channels. If S4 is indeed part of the voltage sensor. its charges (basic amino acids) are expected to move through the electric field upon depolarization. Recent studies have demonstrated that the second and third basic residues of the S4 segment of domain IV (i.e. D4:R2 and D4:S3) of the human skeletal muscle (hSkM1) Na^+ channel translocate completely from an internally accessible to an externally accessible position in response to depolarization (Yang and Horn. 1995; Yang et al.. 1996. 1997). Similar physical displacement of S4 residues has also been demonstrated in the *Shaker* K^+ channel (Mannuzzu et al.. 1996: Larsson et al.. 1996).

Another piece of evidence supporting the role of S4 in voltage sensing comes from mutations of positively charged S4 residues (lysine or arginine) to neutral (glutamine) or negatively charged residues in rat brain Na^+ channels affected the voltage dependence of gating (Stuhmer et al.. 1989). Not only were the mid-points for half-maximal activation shifted. the steepness of activation was also affected suggesting a change in the apparent gating charge. Neutralization of S4 positive charges in *Shaker* K^+ channels also led to similar results (Papazian et al.. 1991; Liman et al. 1991; Logothetis et al.. 1992).

Table 1.3 Homologous sequences of S4 segments

Aligned single-letter amino acid sequences of the S4 segments of rat brain Na⁺ channel, rat skeletal muscle Na⁺ channel, human heart Na⁺ channel, rat skeletal muscle Ca²⁺ channel and Drosophila Shaker K⁺ channel. All four homologous repeats are shown for Na⁺ and Ca²⁺ channels. Roman numerals in bracket indicate the corresponding domain. Conservative arginine (R) and lysine (K) residues are in bold letters.

Segment	Channel	Amino acid sequence
IS4	Na⁺	S A L **R** T F **R** V L **R** A L **K** T I S V I P G L **K**
IS4	Ca²⁺	**K** A L **R** T F **R** V L **R** P L **R** V L S G V P S L Q
IIS4	Na⁺	G L S V L **R** S F **R** L L **R** V F **K** L A **K** S W P
IIS4	Ca²⁺	L G I S V L **R** C I **R** L L **R** L F **K** I T **K** Y W T
IIIS4	Na⁺	G A I **K** S L **R** T L **R** A L **R** P L **R** A L S **R** F E
IIIS4	Ca²⁺	S V V **K** I L **R** V L **R** A L **R** P L **R** A I N **R** A **K**
IVS4	Na⁺	**R** V I **R** L A **R** I G **R** I L **R** L I **K** G A **K** G I **R**
IVS4	Ca²⁺	I S S A F F **R** L F **R** V M **R** L I **K** L L S **R** A E
S4	K⁺	**R** V I **R** L V **R** V F **R** I F **K** L S **R** H S **K** G L Q

35

Interestingly, certain S4 residues seem to play a more significant role in governing activation than others in homologous positions of other domains suggesting assymetrical contributions of each S4 segments to activation in Na^+ channels (Stuhmer et al., 1989; Chen et al., 1996; Kontis and Goldin, 1997). Even mutations of S4 residues within the same domain showed different effects on gating suggesting that even individual charges from the same segment contribute differently to this gating process. Furthermore, the effects of neutralization are not additive suggesting some degree of cooperativity and a non-linear relationship between these individual charges and gating valence (Papazian et al., 1991; Liman and Hess, 1991; Logothetis et al., 1992, 1993; Tytgat et al., 1993).

Not only the positively charged residues in S4 influence channel gating but substitutions of S4 hydrophobic residues in both Na^+ and K^+ channels also have profound effects on channel activation (Auld et al., 1990; Lopez et al., 1991; McCormack et al., 1991, 1993; Fleig et al., 1994; Aggarwal and MacKinnon, 1996). Hydrophobic leucine residues in S4, which occur as highly conserved leucine heptad repeat (McCormack et al., 1991, 1993; Garcia et al., 1997), also play a significant role in gating. In K^+ channels, these leucine residues are found every seven amino acids and occur five times in a row starting from the S4 and ending in the beginning of S5. In other proteins, these leucine heptad repeats signify regions of interchain interactions. Replacements of the first and second S4 leucines with valines dramatically shift the activation gating curve negatively by 70 to 100 mV while changing the one close to S5 shifts the curve positively by 20 mV indicating the significance of these residues (McCormack et al., 1991). Mutations of other hydrophobic residues in S4, without changing the charged residues, alter the voltage range within which gating charges move but not the total number of gating charge (Aggarwal & MacKinnon, 1996). Therefore, S4 hydrophobic residues may act as "lubricants" for S4 movements. In contrast, mutations of hydrophobic residues in other membrane spanning segments do not have major effects on channel activation (Lopez et al., 1991; Li et al., 1998). These findings further confirm that S4 plays a unique role in voltage sensing and channel activation.

Stabilization of the geometry of the positively charged S4 segments which sit within the highly hydrophobic lipid bilayer requires the presence of nearby negative residues in S2 and S3 which form electrostatic salt-bridges with S4 positive charges (Durrel and Guy; 1996). Neutralization of these negative charges located in vicinity of S4 are therefore expected to influence channel activation. In fact, neutralization of negatively charged S2 and S3 residues in Shaker K^+ channel either shifts activation in the depolarizing direction or renders channels non-functional due to disruption of protein maturation suggesting both functional and structural importance of these residues as countercharges (Papazian et al. 1995; Seoh et al., 1996; Tiwari-Woodruff et al., 1997). In Chapter 5, I will describe the effects of neutralizing several absolutely conserved S3 negatively charged aspartate residues in rat skeletal Na^+ channels on gating. In brief, neutralization of negative S3 Asp results in changes in gating that resemble the effects of neutralization of positive S4 charges.

The exact mechanism by which the S4 segments serve as the voltage-sensor is unknown. Guy and Conti (1990) proposed that S4 segments are helices that undergo α-helix-β-sheet transition and propagate outward to a region of the channel which is not normally in a helical orientation in order to move charged residues outward. There is however no direct experimental evidence to support this model. Furthermore, in order to account for the steepness and voltage-dependence of activation observed in most K^+ and Na^+ channels, a translocation of an equivalent of at least 10-14 elementary charges across the transmembrane electric field is required (Schoppa et al., 1992; Sigworth, 1993; Zagotta et al., 1994a,b; Aggarwal & MacKinnon, 1996; Seoh et al., 1996; Sigg & Bezanilla, 1997). This implies that each of the four S4 segments needs to move an equivalent of at least 2.5 elementary charge across the membrane upon each depolarization.

Several questions arise from this scenario. How can the S4 segment possibly move that many charges (2.5 basic residues plus the intervening residues) across the transmembrane field so reversibly and so quickly in relation to the kinetics of activation and deactivation? Horn and colleagues (1997) hypothesize that upon depolarization S4

37

charges traverse the membrane through a short "S4 channel" which spans the hydrophobic core of the protein with a physical length of no longer than 11 Å (Yang & Horn. 1995; Yang et al.. 1996, 1997). This S4 channel is nevertheless distinct from the ion-conducting pore (Figure 1.6). In particular. the S4 segment in DIV translocates a minimum distance of 5 A through this S4 channel in response to depolarization leading to channel activation (Yang & Horn, 1995; Yang et al., 1996, 1997). These investigators further suggest that the short S4 channel contains at most only one positive residue in response to each depolarization thereby explaining the rapid reversibility of activation while obviating the need for a large number of countercharges. Nonetheless, the exact mechanisms still remain speculative.

1.8.2 *Inactivation*

While activation controls voltage-dependent opening of ion channels. inactivation is responsible for their rapid closure and ensures the transient nature of Na^+ current. Inactivation of Na^+ channel can be removed by treatment of the cytoplasmic face of the channel with proteolytic agents (Rojas & Armstrong, 1971; Eaton et al.. 1978; Oxford et al., 1978; Hoshi et al.. 1990). These results have led to the proposal of the "ball and chain" mechanism for Na^+ channel inactivation (Figure 1.4B). According to this model, an inactivation particle (ball) is tethered on the cytoplasmic surface of the channel which diffuses to a receptor site in the cytoplasmic mouth of the pore thereby physically plugging the pore (Armstrong, 1981). With cloning of ion channels, this hypothesis has received considerable support not only in Na^+ channels but also the *Shaker* and related K^+ channels by identification of cytoplasmic domains on the channel which physically occlude the pore (Zagotta et al.. 1990; West et al., 1992).

The use of site-directed anti-peptide antibodies directed against various regions of the Na^+ channel has located a segment of the channel which is required for fast-inactivation (Vassilev et al., 1988, 1989). Antibodies directed against the short intracellular segment connecting homologous domains III and IV (i.e. the III-IV linker) selectively inhibited Na^+ channel inactivation (Vassilev et al.. 1988; Vassilev et al., 1989).

Figure 1.6

Schematic depictions of S4 and its channel during hyperpolarization and depolarization. The S4 channel is distinct from the ion-conducting pore but yet unidentified. The domain in the foreground is not shown for clarity. Upon depolarization. the positively charged S4 segments move outward through the corresponding S4 tunnels leading to channel activation (opening).

Ion conducting pore

S4

S4 tunnel

depolarization

+ + +

+ + +

- - -

- - -
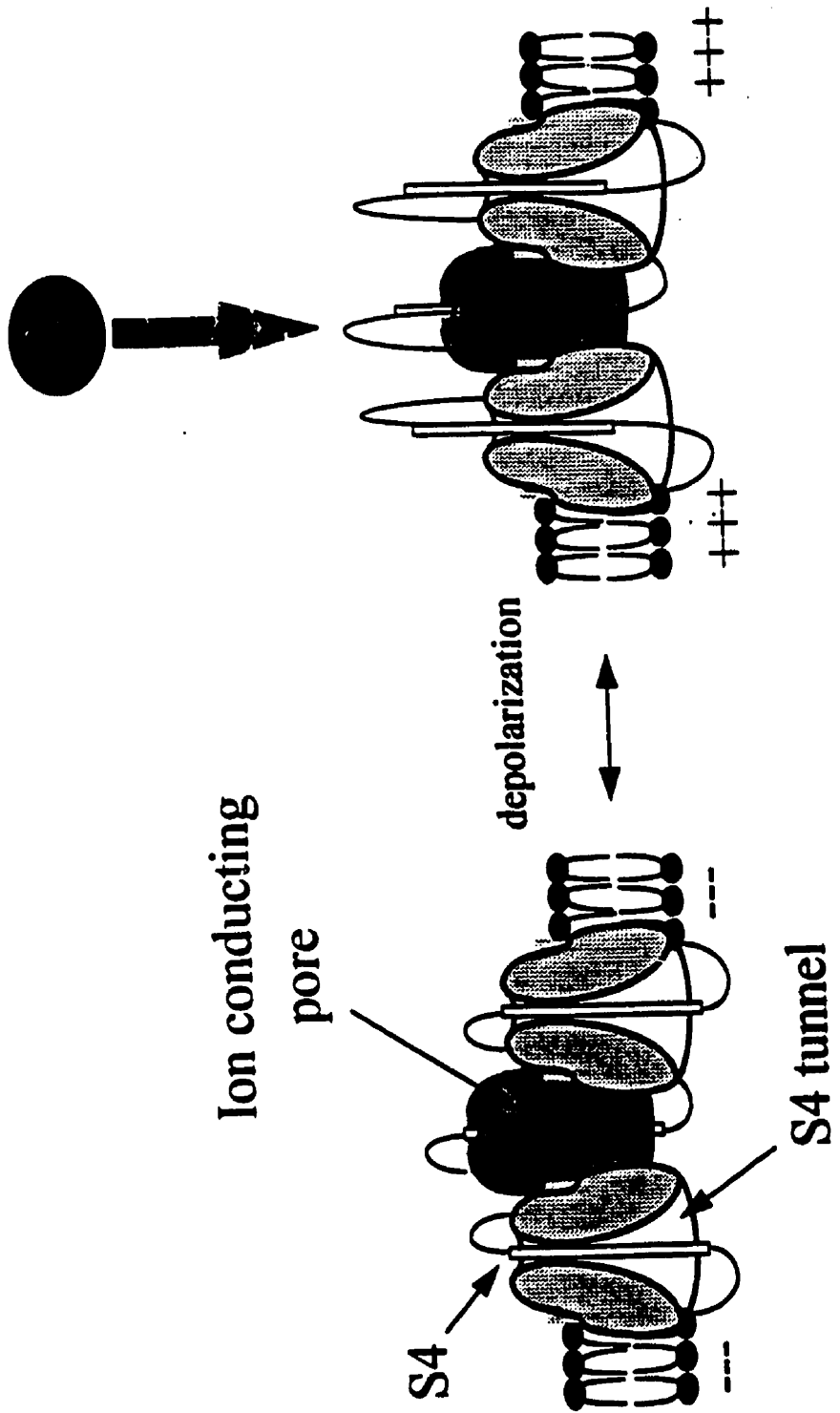
The sequence of this III-IV linker also shows striking conservation even among different Na⁺ channels further support its potential role in inactivation. Indeed. deletions of III-IV linker greatly slows inactivation (Stumer et al.. 1989). Mutations of the hydrophobic triplet isoleucine-phenylalanine-methionine (IFM) located within the linker to glutamines (i.e. IFM-QQQ) completely abolish fast-inactivation with most of the effects reside in the F-Q substitution (West et al.. 1992). Furthermore. application of the synthetic peptide acetyl-KIFMK-amide to inactivation deficient Na⁺ channels restores a fast current decay resembling inactivation (Eaholtz et al.. 1994). Based on these results. it is widely accepted that the IFM motif serves as the inactivation particle of Na⁺ channel and occludes the pore by blocking the cytoplasmic mouth of the channel during inactivation. This hypothesis is further supported by recent studies involving introduction of a cysteine in the IFM motif that shows the substituted cysteine is accessible to sulfhydryl-modifying agents only during closed and open states of the channel but is buried and inaccessible during inactivation when the inactivation particle is bound to its receptor (Kellenberger et al., 1996; Vedantham and Cannon. 1998).

Unlike the inactivation particle itself. the receptor for this particle is not well defined. It has been suggested that several hydrophobic residues located in IVS6 may form part of the receptor for the inactivation ball because of the locations of several natural mutations associated with muscle myotonia within this segment (Rojas et al.. 1991; Cannon and Strittmatter. 1993) and mutations of other S6 residues all disrupt Na⁻ channel inactivation (McPhee et al.. 1994). The local anesthetic receptor. which has been long thought to be located on the cytoplasmic side of the channel pore. is also believed to comprise certain S6 residues (Ragsdale et al., 1994). Indeed. the S6 segments have been suggested to line the cytoplasmic mouth of the pore in all families of voltage-gated ion channels thereby contributing to the receptor sites for numerous different classes of intracellular blockers and drugs, and in the case of Na⁺ channel. also forms part of the inactivation receptor.

However, the story is not straightforward and is complicated by the observation that application of the KIFMK peptide to certain S6 mutant channels (F1764A and V1774A of rat brain Na^+ channel) rescue inactivation implying that the inactivation receptor may remain intact in these S6 mutants (McPhee et al., 1995). In other words, these S6 mutations may destabilize the inactivated state without disrupting the actual drug binding receptor. Recently, the S4-S5 intracellular loops in each of the four domains have been suggested to be another potential candidate for forming part of the docking site for the inactivation particle (Isacoff et al., 1991; Yang et al., 1994; Holmgren et al., 1996; Mitrovic et al., 1996; Tang et al., 1996; Filatov et al., 1997; Smith and Goldin, 1997; McPhee et al., 1998). Obviously, further experiments are required to fully identify this molecular receptor for fast-inactivation.

In addition to fast-inactivation which results in rapid closure of the channel by occlusion of the pore as mentioned above, Na^+ channels also undergo slow-inactivation which occurs only after prolonged depolarization (Adelman & Palti, 1969; Chandler & Meves, 1970). The two inactivation processes are distinguished by their recovery kinetics. While channels recover from fast-inactivation within several milliseconds, recovery from slow-inactivation requires tens of seconds or longer (Adelman and Palti, 1969; Ruff et al., 1987; Simoncini and Stumer, 1987; Ruben et al., 1992). Slow inactivation plays a significant physiological role in determining membrane excitability by modulating the availability of Na^+ channels (Ruff et al., 1988; Cummins and Sigworth, 1996). Defects in slow inactivation underlie the pathophysiology of many muscle diseases (Cannon, 1996; Cummins and Sigworth, 1996; Hayward et al., 1997). The mechanism is however only poorly understood. The structural determinants of slow-inactivation are also not as well defined as fast-inactivation. Pore residues have been suggested to play a role in mediating this gating process implicating its homology to C-type inactivation observed in K^+ channels (Tomaselli et al., 1995; Balser et al., 1996). Interestingly, slow-inactivation is unaffected when fast-inactivation is removed by either protease treatment or mutagenesis (Rudy, 1978; Cummins and Sigworth, 1996; Featherstone et al., 1996) or when the movement of the inactivation particle (i.e. the fast-inactivation gate) is blocked by specific antibodies or chemical agents (Vassilev et al.,

1989; Vedantham and Cannon, 1998). Similarly, only slow inactivation is inhibited by external alkali metal cations while fast inactivation remains unaffected (Townend and Horn, 1997). Therefore, fast- and slow-inactivation are likely to be independent processes (Vedantham and Cannon, 1998) but however not mutually exclusive (Vedantham and Cannon, 1998). In addition to fast- and slow-inactivation, a form of ultra-slow inactivation, whose recovery kinetics are within the range of hundreds or even thousands of seconds, has also been reported in Na^+ channels (Fox, 1976; Todt et al., 1997).

The mechanisms of inactivation of Na^+ and K^+ channels share many similarities. For example, both N-type inactivation in Shaker K^+ channel and fast Na^+ channel inactivation lead to rapid inactivation or closure of the channel by occlusion of the cytoplasmic mouth of the pore by an inactivation particle (Hoshi et al., 1990; Zagotta et al., 1990). Hydrophobic amino acid residues are essential in both cases. Furthermore, the inactivation gate receptors of both Na^+ and K^+ channels may have similar three-dimensional molecular structures since non-inactivating K^+ channel whose native inactivation particle has been removed, recognizes the Na^+ channel inactivation particle and restores rapid inactivation despite there being no amino acid sequence identity between the two different channel inactivation particles (Patton et al., 1993). It has been suggested that C-type inactivation is the result of closure of the external portion of the pore (Armstrong, 1971; Choi et al., 1991; Hoshi et al., 1991; Yellen et al., 1994). Interestingly, mutation of a pore residue (DI W402C) in Na^+ channel also affects slow-inactivation (Tomaselli et al., 1995; Balser et al., 1996). Despite these similarities, N-type and C-type inactivation of K^+ channels are distinct but tightly coupled processes (Hoshi et al., 1991) whereas the concurrent concept of fast- and slow-inactivation of Na^+ channels are separate and independent (uncoupled) processes (Rudy et al., 1978; Patlak, 1991).

1.8.3 Activation-inactivation coupling

According to the original Hodgkin and Huxley model, both channel activation and inactivation are voltage-dependent processes (as *m* and *h* gates respectively) and are

43

independent of each other. Since both activation and inactivation gates are charged and can move through the membrane field, both processes of activation and inactivation are therefore predicted to produce gating currents with time course comparable to the kinetics of both gating processes. However, it is known that inactivation leads to gating charge immobilization and does not result in gating currents (Armstrong & Bezanilla, 1977; Bezanilla & Armstrong, 1974, 1975; Armstrong, 1981). In fact when inactivation is removed by proteolytic digestion, immobilization decreases (Armstrong & Bezanilla, 1977; Nonner, 1980). These observations are inconsistent with independent gating and a coupled inactivation model was proposed (Hodgkin and Horowicz, 1960; Hoyt, 1965; Goldman and Schauf, 1972).

The coupled model can be readily appreciated by examining the 3-state scheme shown in beginning of this section. Though channels can inactivate from the closed conformation, they do so at a very slow rate (Horn et al., 1981). Therefore, access of the inactivation particle to its receptor is basically available only when the activation gate is open (i.e. when channels are in the open conformation). Armstrong (1981) proposed that the inactivation particle or its vicinity may be charged but since it only moves through a small distance within the membrane field, the current generated, if any, is negligible. In fact much of the inactivation particle (i.e. the IFM motif) is uncharged (West et al., 1992) and the flanking positively charged residues have little effects on inactivation (Patton et al., 1992). Moreover, while the inactivation particle is bound to its receptor, it acts like a foot-in-the-door and hinder closing of the activation gate and subsequent return of gating charges to their original positions. This coupling model therefore accommodates both the absence of gating current and gating charge immobilization during inactivation. Nonetheless, inactivation shows voltage-dependence because it cannot occur until activation takes place. In other words, inactivation of Na^+ channel derives its apparent voltage dependence from coupling to the highly voltage dependent process of activation (Bezanilla and Armstrong, 1977; Nonner, 1980; Aldrich et al, 1983; Zagotta and Aldrich, 1990). This hypothesis is further supported by gating current and mutagenesis studies of Na^+ channels (O'Leary et al., 1995; Chen et al., 1996; Kontis and Goldin, 1997a, b). In fact, neutralization of positive charges in the putative S4 voltage-sensor very often have

profound effects on inactivation as well as activation indicating disruption of the coupling between these processes (Stumer et al., 1989; Chen et al., 1996; Yang et al., 1997; Kontis and Goldin, 1997a, b).

The molecular mechanism of activation-inactivation coupling is still poorly understood. It is believed to involve regions all over the channel including those remote from the voltage-sensor and inactivation gate. Previous reports have demonstrated that naturally occurring mutations of human skeletal muscle Na^+ channels found in paramyotonia congenita decouple inactivation from activation (Chahine et al., 1994; Ji et al., 1996). In all of these cases, rate and voltage dependence of inactivation were slowed and lost (either partially or totally) while recovery from inactivation was hastened. These are the results of disruption of the functional linkage between the voltage-sensor and the inactivation gate. In Chapter 5, I will describe two Asp residues located in S3 which also seem to be responsible for this activation-inactivation coupling.

1.9   *Modulation of Na^+ channel functions*

Na^+ channel functions can be modulated in a number of different mechanisms. As mentioned (section 1.5), many forms of Na^+ channels are associated with auxiliary subunits. They are also important modulators of channel functions. Co-expression of the α-subunits of neuronal and skeletal muscle Na^+ channels in *Xenopus* oocytes with the β_1-subunit increases current amplitude, accelerates fast inactivation, shifts steady-state inactivation curve in the hyperpolarizing direction, slows the rate of entry into slow inactivation and accelerates activation kinetics (Zhou et al., 1991; Isom et al., 1992; Bennett et al., 1993; Cannon et al., 1993; Patton et al., 1994; Nuss et al., 1995; Chang et al., 1996;). The effects of β_1-subunit on the cardiac subtype is however not certain (Cohen & Levitt, 1993; Makita et al, 1996b; Nuss et al., 1995; Qu et al., 1995; Makielski et al., 1996). The mechanisms by which β_1-subunit modulates Na^+ channel functions have been studied using both biochemical and mutagenesis methods (Chen and Cannon, 1995; Makita et al., 1996b; McCormick et al., 1998).

Channel functions are further modulated by cAMP dependent phosphorylation (Catterall, 1994). While all forms of Na^+ channels known to date are modulated by protein kinase C (West et al., 1991, 1992; Numann et al., 1991; Li et al., 1993; Numann et al., 1994; Bendahhou et al., 1995; Qu et al., 1996; Murray et al., 1997), protein kinase A (PKA) affects only the neuronal and cardiac but not the skeletal muscle subtype (Smith & Goldin, 1992, 1995). The sites of phosphorylation have been identified (Murphy et al., 1993, 1996). Phosphorylation at some of these sites selectively affects channel conductance while at others affect gating and other channel properties. In fact, specific pattern of phosphorylation result in specific functional consequences reflecting the complex nature of channel regulation via this pathway (Gershon et al., 1992; Li et al., 1993; Murphy et al., 1993; Schreibmayer et al., 1994; Frohnwieser et al., 1995; Smith and Goldin, 1995, 1997; Murphy et al., 1996; Cantrell et al., 1997; Frohnwieser et al., 1997).

Other forms of Na^+ channel modulation come from co- and post-translational glycosylation which are critical for channel conductance, subunit interactions, protein transport (Schmidt et al., 1985; Schmidt & Catterall, 1987; Wollner et al., 1987; James & Anew, 1989; Cohen & Levitt, 1993; Bennett et al., 1997), as well as regulation of gene expression and tissue specificity at the transcriptional level (Kallen et al. 1990; Yang et al., 1991), etc.

1.10 Na^+ channel pharmacology

A number of toxins (e.g. TTX, STX, μ-CTX, etc) and blockers (Cd^{2+}, Zn^{2+}, local anesthetics, etc) act specifically on voltage-gated Na^+ channels by various mechanisms. These agents have been valuable tools in channel localization, identification and purification as well as characterization of their structure and functions. Historically, they were used to separate currents flowing through different ion-selective channels. For example, tetraethylammonium (TEA) ions selectively block many types of K^+ channels and tetrodotoxin (TTX) blocks Na^+ channels. Advances in molecular biology and chemistry techniques allow manipulations of both toxins and channels thereby providing

46

even further insights into the structure/function of Na⁻ channel.

1.10.1 Na^+ channel toxins

Na⁻ channel toxins were classified by Catterall (1994) into 6 major classes based on their mechanisms and sites of action.

Class I toxins are positively charged water-soluble heterocyclic guanidines. Examples of this class of toxins are tetrodotoxin (TTX) from puffer fish (*Fugu*), salamanders (*Taricha*), frogs (*Atelopus*) and mollusks (*Hapalochlaena*), and saxitoxin (STX) from dinoflagellates (*Gonyaulax*). μ-conotoxins (μ-CTX), a polypeptide toxin isolated from the sea snail *Conus geographus*, also belongs to this category (see also Chapter 6). Class I toxins are among the most toxic substances known to the mankind. They typically have dissociation constants (K_D) within the nanomolar range. Class I toxins inhibit Na^+ current by binding to a site which is thought to be located on the extracellular side of the pore thereby physically plugging the outer entrance of the ion-conducting channel pore. Toxin binding is also thought to involve extensive electrostatic interactions between the toxin guanidinium groups and some carboxylic side chains (from glutamates and aspartates) in the pore (Li et al., 1997).

Class II toxins consist of batrachotoxin (BTX) from frogs (*Phyllobates*), veratridine from plants (*Lilaceae*), aconitine from plants (*Aconitum*), pumiliotoxins from frogs (*Dendrobates pumilio*), and grayanotoxin from rhododendrons. These toxins are lipid-soluble alkanoids (except grayanotoxin, included because of its functional similarity) and can freely diffuse across the lipid bilayer. They inhibit (block or slow) inactivation and shift channel activation to more hyperpolarizing potentials. The result is activation followed by sustained opening of Na^+ channels at resting membrane potential. For this reason, Class II toxins are also referred to as alkaloid channel activators. They also alter channel selectivity (Albuquerque, 1971; Albuquerque et al., 1973; Catterall & Beneski, 1980; Narahashi, 1986; Brown, 1988). Since Class II toxins have effects on both channel activation and inactivation, their binding site is thought to involve regions

of the channel that coordinate both gating processes.

North African α scorpion (*Leiurus quinquestriatus*) toxins and sea anemone (*Condylactis, Anthopleura* and *Anemonia* species) toxins belong to Class III toxins. These toxins are polypeptides that either slow or block channel inactivation. They also enhance binding of Class II toxins to their receptor by as much as 20-fold (Catterall, 1981). Class III toxins are believed to bind to the voltage-sensing apparatus of sodium channels since the voltage-dependence of Class III toxin binding closely parallels the voltage-dependence of channel activation.

North American β scorpion (*Centruroides, Tityus* and *Androctonus* species) toxins are Class IV toxins. They modify Na^+ channel activation and enhance binding of Class II toxins. However, channel inactivation is unaffected by these toxins.

Cyclic polyether compounds such as brevetoxins (from *Ptychodiscus brevis*), icthytoxin and ciguatoxin (from *Gambierdiscus toxicus*) are Class V toxins. They shift the voltage dependence of channel activation in the hyperpolarizing direction and cause repetitive firing. Class V toxins also enhance the effects of Class II toxins but do not compete with Class III toxins (Catterall & Gainer, 1985). Finally, Class VI toxins consist of toxins isolated from *Goniopora* slow channel inactivation but also do not compete with Class III toxins (Barchi, 1988).

In Chapter 6, I will describe identification of several pore residues that are critical determinants of the binding of a Class I toxin, μ-CTX, to the rSkM1 Na^+ channels.

1.10.2 *Anti-arrhythmics and local anesthetics:*
Interactions with Na^+ channels

Antiarrhythmic drugs are classically classified into four types (types I to IV) according to the methods originally proposed by Vaughan Williams (1981). In type I (e.g. lidocaine), the drugs primarily inhibit Na^+ current by interacting with the Na^+

48

channels (Figure 1.7). In type II (e.g. propranolol). the agents are sympatholytic drugs that block β-adrenergic receptors. In type III (e.g. amiodarone). they are drugs that prolong the repolarization phase of the action potential without appreciable blockade of the Na⁻ currents. In type IV (e.g. verapamil), the drugs are Ca^{2+} channel antagonists. It is type I drugs that are of primary interest of this thesis because of their effects on Na⁻ channels.

Type I class antiarrhythmics are also commonly used as local anesthetics to achieve anesthesia. Type I is further subclassified by Harrison and others (1981) into types IA (e.g. quinidine. procainimide. disopyramide. cibenzoline), IB (e.g. lidocaine. tocainide. mexilitene. morcizine) and IC (e.g. encainide. flecainide. lorcainide. propafenone. indecainide). Type IA are drugs that depress phase 0 of the action potential. slow its conduction and prolong repolarization. In contrast, type IB shortens repolarization and depress phase 0 only in abnormal tissues but not the normal ones. Type IC markedly depresses phase 0 and slow conduction while having little effects on repolarization (i.e. overall action potential duration). This Vaughan Williams classification method was solely physiologically based and was derived at a time when knowledge in electrophysiology was not as extensive.

Drugs classified according to this method often show multiple properties. Drugs from different classes show similar properties while the effects of drugs from the same class may not be identical. Dissatisfaction has led a group of basic science and clinical investigators meeting in 1991 in Sicily to consider new approaches of classification. The so called Sicilian Gambit classifies antiarrhythmics more systematically based on their actions and underlying arrhythmogenic mechanisms. The Vaughan Williams method is nevertheless useful as a form of general framework for understading the clinical electrophysiologic properties of antiarrhythmics.

How do Type I antiarrhythmics and local anesthetics modulate Na⁻ currents? There are two major classes of action: tonic block and use-dependent (or frequency-dependent or phasic) block. It should be pointed out that the term "drug block" refers to

49

Figure 1.7

Schematic diagram demonstrating the three states of Na^+ channels and their interactions with local anesthetics (LA). Hydrophilic LAs can bind to the local anesthetic binding site (LABS) only when both activation (m) and inactivation (h) gates are open i.e. when the hydrophilic pathway is available. In contrast, hydrophobic LAs can bind to the LABS (via the hydrophobic pathway) even while the gates are closed by diffusing across the bilayer membrane. Polar amphiphilic drugs are capable of taking both pathways. Drug-bound channels need to release the drug molecules before they can recover from inactivation. Therefore, LAs slow recovery from inactivation (see Chapter 7 for further details).

△ = Hydrophobic LAs

◁ = Hydrophilic LAs

◀ = Amphiphilic LAs

m: activation gate
h: inactivation gate

Open

Closed

Inactivated

activation

inactivation

recovery

OUT

IN

m

h
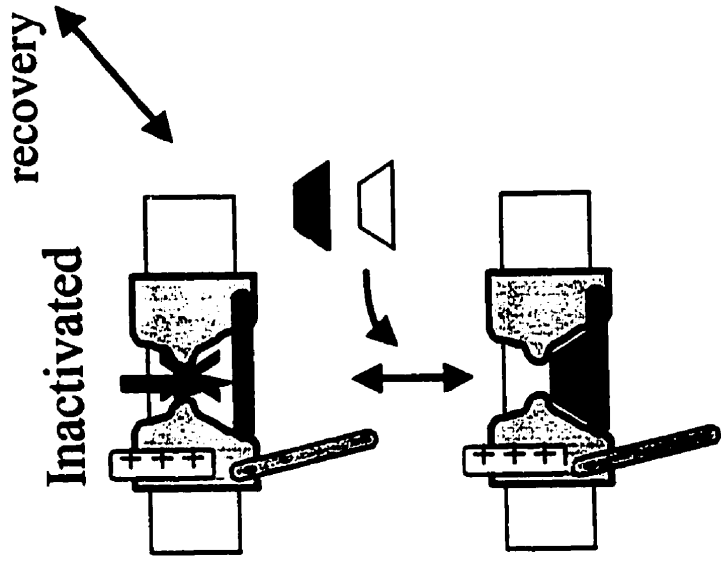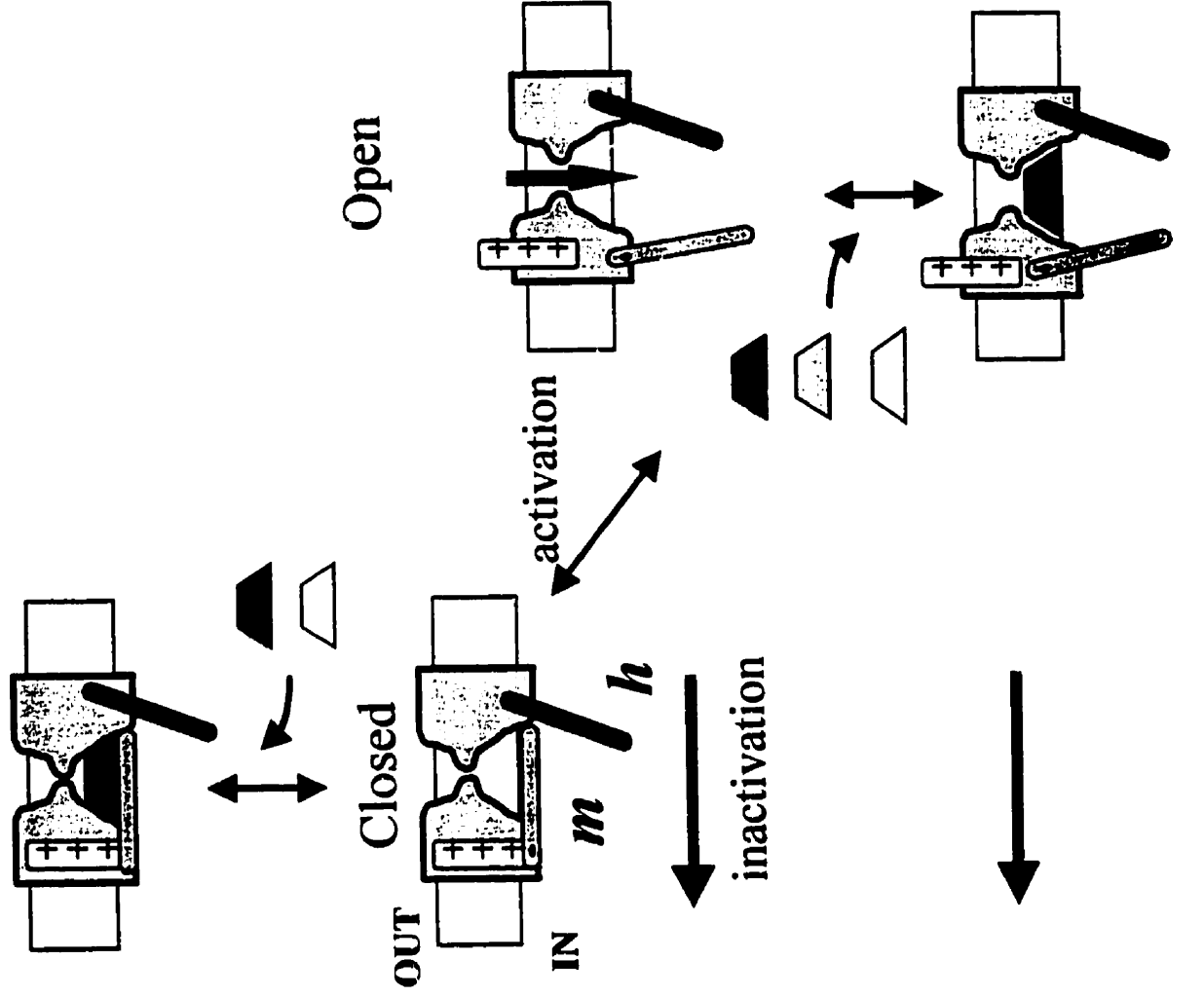
the reduction of ionic flux as a result of drug binding to the channel by whatever means and does not necessarily imply a physical "plugging" of the channel pore. For example. stabilization of the non-conducting inactivated states by preferential drug binding to these conformations will also lead to an apparent reduction in ionic current. Drug binding is a dynamic reversible process depending on the affinity of the drug receptor (i.e. the local anesthetic binding site), whose exact constituents are presently unknown, as well as access to this receptor site. In general. tonic block represents block of sodium current at very low stimulation frequency (<0.25 Hz) and primarily reflects drug binding to resting or open channels. In contrast, use dependent block is additional block caused by high frequency repetitive stimulations or depolarizations (>1 Hz) as a result of accumulation of drug-bound inactivated channels between pulses since these channels recover more slowly from inactivation. The degree of use-dependent block is dependent on drug polarity with the hydrophobic ones (e.g. benzocaine) showing least use-dependence because these drugs are able to bind and unbind to the LABS very rapidly thereby reaching equilibrium very quickly and hence no accumulation of block.

Two hypotheses have been proposed to account for the mechanisms of channel blockade by local anesthetics: 1) modulated receptor and 2) guarded receptor hypotheses. The former proposes that drug binding to Na^+ channels is highly state-dependent and different states of the channel possess different affinities for drugs whereas the latter hypothesizes that there is only one receptor site for drug with a constant drug binding affinity but only accessibility to this site is shielded differently in different states. These hypotheses will be discussed in greater details in Chapter 7. I will also describe in Chapter 7 the identification of a pore residue in mammalian Na^+ channels which is critical for local anesthetic binding. In Chapter 8. I will then describe the use of a novel strategy, the "Anchor-Linker-Drug" strategy, which we develop to study the spatial relationship between the outer pore and the local anesthetic binding site as well as to develop a tissue-specific local anesthetic which targets specifically and exclusively to the cardiac Na^+ channels. The development of a cardiac-specific anti-arrhythmic agent is highly desirable because many of the currently available therapies for treatment of electrical disturbances developed in cardiac arrhythmias are ineffective owing to their

side-effects on Na^+ channels in tissues other than the heart (Chapter 8).

1.11   Scanning Cysteine Accessibility Method (SCAM)

With advances in molecular biology, more and more protein clones are becoming available at a breathtaking pace. With the primary sequences in hands, mutagenesis is routinely exploited to study structure-function relationships of proteins. Combination of these molecular techniques and electrophysiology has provided important insights into structure-function of ior channels. Common mutagenic strategies involve generation of chimeric constructs from related genes, random mutagenesis, deletion mutagenesis, strategically placed point mutations and scanning mutagenesis, etc. In particular, the Scanning Cysteine Accessibility Method (SCAM) is employed throughout this thesis to investigate the structure-function relationships of Na^+ channels.

The scanning mutagenesis strategy involves substitution of a series of amino acids of a protein with another residue. Alanine and cysteine are commonly chosen as the target residues for reasons listed below. Alanine substitution merely replaces the original side chain with a conservative methyl group thereby allowing examination of the functional importance of the chemical identity of the native side chain. In addition, alanine does not normally alter the main chain conformation as do amino acids such as glycine and proline. Therefore, alanine substitution is generally well tolerated. Replacement with cysteine has similar advantages as alanine substitution but further allows post-translational protein modifications at specific sites because of the reactivity of the thiol side chain for sulfhydryl modifiers and its sensitivity to the redox state of the immediate cellular environment (see below). In both cases, the major idea of this scanning approach is that alanine or cysteine substitutions remove the unique structural and/or functional properties of the side chain of the native residue at a given position of the protein of interest thereby allowing screening of functionally or structurally critical amino acid residues.

The Scanning Cysteine Accessibility Method (SCAM) was first introduced by

Falke et al (1988) and Akabas et al (1992) to study a bacterial sensory receptor and acetylcholine receptor respectively. The strategy has also been used in structural and functional studies of a number of other channel proteins such as the aspartate receptor (Falk et al, 1988, Pakula et al.. 1992), colicin (Todd et al.. 1989. Jakes et al.. 1990). bacteriorhodopsin (Altenbach et al.. 1990), dopamine receptor (Javitch et al.. 1995). cyclic nucleotide-gated (CNG) channel (Sun et al.. 1996), cystic fibrosis transmembrane conductance regulator (CFTR) (Cheung & Akabas. 1996). K^+ channels (Yellen et al.. 1994; Lu and Miller. 1995; Kurz et al.. 1995; Pascval et al.. 1995) and Na^+ channels (Tsushima et al.. 1997a, b; Li et al.. 1997), etc. The method involves replacement of individual amino acids with cysteines using site-directed mutagenesis followed by assessment of the ability of aqueous-limited polar sulfhydryl-specific modifiers to modify the side chain of the substituted residues (Figure 1.8). Like all other mutagenesis studies, SCAM also makes certain basic assumptions that might critically influence data interpretation. SCAM assumes that amino acid replacements do not result in global and nonspecific alterations of the structure and function of the protein of interest and that the side chain of the substituted cysteine lies in an orientation similar to that of the native wild-type residue. Addition of aqueous-limited sulfhydryl-specific modifying agents should react more readily with cysteine sulfhydryls exposed to the aqueous phase than with sulfhydryls exposed to the lipid or internal face of the protein. In other words, residues whose side chains project into the lumen of the channel are accessible whereas those buried within the lipid membrane or protein are not. Change in current or other channel properties such as gating upon reaction between the substituted sulfhydryl and its modifier would indicate that the residue in question is accessible and modified thereby allowing identification of both location and functional importance of the residues being studied. It should be pointed out that. however, it is dangerous to overinterpret these results since it is possible that application of sulfhydryl modifiers as biophysical probes could result in trapping of a subset of channel states which may not be true representatives of the real dominant states.

Some of the most commonly used biophysical probes in SCAM studies are metal ions such as Zn^{2+}. Cd^{2+}, Ag^+ and methanethiosulfonate (MTS) derivatives. MTS agents

54

Figure 1.8

Schematic representation of Scanning Cysteine Accessibility Method (SCAM).

A) A cysteine substituted mutant channel is sensitive to aqueous-limited sulfhydryl-specific biophysical probes (e.g. Cd^{2+}. Zn^{2+} MTS-derivatives, etc) only if its side-chain is exposed to the aqueous phase. Side-chain orientation is assumed to be the same as that of the original native residue in WT channels.

B) Mutant channel is insensitive (i.e. same as wild-type) to sulfhydryl reagents if the substituted side-chain is buried within the protein.

A

I

IV II

S

III

B

I

IV II

III SH
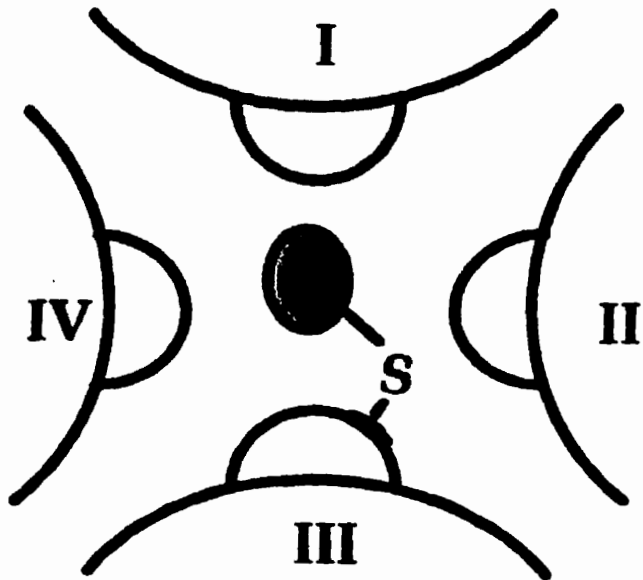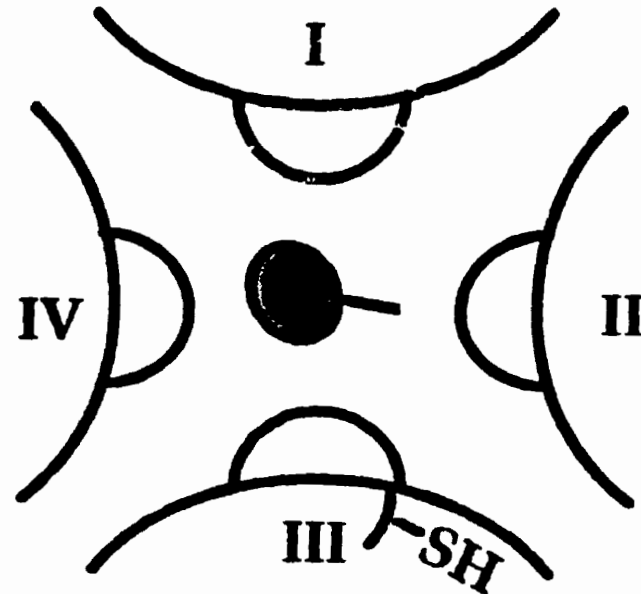
Biophysical Probe

Cd²⁺, Zn²⁺
Sulfhydryl Modifying Reagents

Cysteine Residue
Accessible to Probe

→ ↑ Sensitivity

Cysteine Residue
Buried within Protein

→ Sensitivity = Wild-Type

such as $CH_3SO_2SCH_2CH_2NH_3^+$ ($MTSEA^+$), $CH_3SO_2SCH_2CH_2NMe_3^-$ ($MTSET^+$), $CH_3SO_2SCH_2CH_2SO_3^-$ ($MTSES^-$) and $CH_3SO_2SCH_2CH_2$ C_6H_6 (MTSBN) are reactive mixed disulfides that covalently modify the inserted cysteines by attaching to the free sulfhydryls in the aqueous environment either positively charged, negatively charges or neutral moieties. Addition of these MTS derivatives therefore allows changes of the chemical identity of the inserted cysteinyls, at a post-translational level, with specific chemical groups possessing unique properties and charges of choice. Recent studies involving the use of these sulfhydryl modifiers (Yang and Horn, 1995; Larsson et al., 1996; Yang et al., 1996, 1997) and sulfhydryl-specific fluorescent tag (Mannuzzu et al., 1996) in combination with different electrophysiological protocols have provided direct physical evidence that S4 segments undergo physical translocation during channel activation. These dynamic structural information regarding channel proteins cannot be obtained even from crystallography. In addition, since strict geometric constraints are required in order for two cysteines to either crosslink or form a coordination site for binding of group II divalents, paired cysteine mutagenesis has been used to study structural dynamics and to estimate physical distances in proteins. Therefore, SCAM is a very powerful technique to investigate structures and functions of ion channels.

1.12 *Summary and perspectives*

Understanding the Na^+ channels at the molecular level is of such physiologic importance as this class of proteins underlies the fundamental basis of electrical signalling in all excitable cells in higher organisms. Advances in areas such as molecular biology, electrophysiology and pharmacology have further accelerated our pace of understanding of these proteins and their interactions with drugs. More effective and rational drug designs are anticipated within the next decade as more is known about these proteins.

The subsequent chapters describe research that I conducted over the past three years. They are meant to add more information to the existing body of knowledge concerning the Na^+ channel in terms of its pore structure (Chapter 3), molecular

functions: ionic selectivity (Chapter 4) and channel gating (Appendix), and pharmacology of toxin (Chapter 5) and local anesthetic (Chapter 6) binding as well as the development of a novel agent (i.e. Anchor-Linker-Drug or ALD) to study the spatial relationship between the channel pore and local anesthetic binding site (Chapter 7) of Na^+ channels. The ALD strategy that we employed further provides a foundation for development of a cardiac specific antiarrhythmic which is clinically desirable since many of the current therapies are ineffective owing to their side effects on channels other than the cardiac. This approach can be generalized and applied in designs of other tissue-specific agents.

CHAPTER 2

GENERAL METHODS

In this chapter, I will describe the general methods employed in all studies presented in this thesis including molecular biology, heterologous expression and voltage-clampling techniques etc. Specific experimental protocols are further presented in the individual pertinent chapters.

2.1   *Molecular Biology*

For mutagenesis, a 1.9 kb BamH I-Sph I (for domain I mutations) and 2.5 kb Sph I-Kpn I (for domain II, III and IV mutations) fragment of the rSkM1 Na⁺ channel (Trimmer et al., 1989) were subcloned into pGEM-11f⁺ and pGEM-7f⁺ (Promega, Madison, WI) respectively. Mutations were introduced by site-directed mutagenesis using uracil-enriched single-stranded DNA (Kunkel, 1985). The mutation was confirmed by dideoxy nucleotide sequencing (Sanger et al., 1977) prior to subcloning into the expression vector pGW1-CMV (British Biolabs, Oxford, UK) containing the full length Na⁺ channel clone. The final clone was re-sequenced to ensure the desired mutation was present.

2.1.1   *Site-specific Mutagenesis*

2.1.1.1 *Kinase Reaction*

Kinase reaction was performed to add phosphate to the 5' end of the mutagenic oligo for latter extension (i.e. polymerase reaction) after annealing with a single-stranded DNA template of the phagemid vector (i.e. pGEM) carrying a cassette of the Na⁺ channel clone. Oligo (3 μl, 20 μg/ml), 10X kinase buffer (2 μl), 10 mM ATP (2 μl), T4 kinase (1 μl, 6 unit) and dH₂O (12 μl) were mixed together and incubated at 37°C for 90 min for the kinase reaction to take place. The mixture was then incubated at 65°C for 10 min to heat inactivate the kinase.

2.1.1.2 *Preparation of single-stranded DNA template*

A pGEM vector carrying a cassette was first transfected into CJ 236 or BW 313 cells. These two strains of cells are *dut⁻ ung⁻* and lack the corresponding gene products dUTPase and uracil-N-glycocylase. Deficiency of these enzymes result in elevated level of dUTP and suppressed replacement of uracil by thymine in DNA. The process of transformation is described in section 2.2.1.1. A well separated colony was grown overnight in 2 X YT broth (2 mL). The overnight culture (1 ml) was inoculated into a 250 mL flask containing 2 X YT (40 mL) with ampicilin (50 μg/ml). The entire culture was incubated at 37°C and grown to an OD$_{600}$ reading of 0.3-0.5 before the helper phage M13K807 (100 μl) was added. The culture was incubated again at 37°C overnight with vigorous shaking. The overnight culture was poured into a 50 ml sterile polypropylene centrifuge tube and spun at 5,000 rpm for 15 min at 4°C. The supernatant was isolated and poured into another 50 ml centrifuge tube and spun at 5,000 rpm for 15 min at 4°C. RNAse (10 μg/μl, 20 μl) was added and incubated at room temperature for 30 min to degrade the presence of any RNA. 2.5M NaCl/20% PEG 800 (10 ml) was next added and incubated on ice for 1 hour. The phagemids were collected by centrifuging at 7,000 rpm for 20 min. The supernatant was discarded and the pellet was resuspended in TE buffer (400 μl) and transferred to a 1.5 ml microtube. The suspension was chilled on ice for 30 minutes followed by centrifugation at 5,000 rpm for 2 minutes to remove the insolubles. The supernatant was then transferred to another microtube. The entire mixture (400 μl) was extracted with TRIS-equilibrated phenol (400 μl). The extraction process was repeated 5 times with phenol: chloroform: isoamyl alcohol and 3 times with chloroform :isoamyl alcohol to purify the single-stranded template DNA. 3M NH$_4$OAc (1/10 volume) and 100 % ethanol (2.5 volume) was added and the final mixture was incubated at -70°C for at least 30 min for DNA precipitation. The DNA mixture was spun at 4°C for 15 min and the pellet collected was washed with 70% cold ethanol, air dried and resuspended in TE (20 μl).

2.1.1.3 *Annealing reaction*

Template DNA (2 µl, 300ng), the mutagenic oligo* (1 µl, 10 pmol) and 10X annealing buffer (1 µl) (see 2.6 for incredients) and water (6 µl) were mixed together. The entire mixture was heated to a temperature 20°C higher than the T_m of the oligo for 5 min and then allowed to cool slowly to RT. The mixture was then placed on ice for 5 min. While on ice, 10X synthesis buffer (1 µl) (see also 2.6), T4 DNA ligase (1 µl) and T4 DNA polymerase (1 µl) were added to the mixture, incubated in 25°C water bath for 5 min, followed by 37°C water bath for 2 hours to produce double-stranded circular phagemids. Unlike the template, the newly formed DNA strand containing the mutagenic oligo carried thymine instead of uracil. The mutagenesis reaction mixture (5 µl) containing the heteroduplex molecules was transformed into DH5α competent cells (50 µl) which produce normal *dut* and *ung* gene products. The original non-mutagenic uracil-containing DNA template will be degraded within DH5α cells thereby increasing the efficiency of recovery of mutant DNA.

2.1.1.4 *Screening for mutation*

At least 3 well isolated colonies from each transformation of mutagenesis product were cultured and screened for the desired mutation by dideoxy nucleotide sequencing.

2.1.2 *Sequencing*

Plasmid DNA to be sequenced was first denatured by treating with alkali. DNA (0.5-1.0 pmol, 20 µl) was added to 2M NaOH/2 mM EDTA (2 µl), mixed and incubated at 37°C for 5 min for denaturation. The mixture was placed on ice, to which 3M sodium acetate (pH 6.0, 7 µl) was added to neutralize the DNA solution. 95% ethanol (75 µl) was added and then placed on ice for 10 min for DNA precipitation. The mixture was spun at 13,000 rpm for 10 min. DNA pellet was collected and washed with 75% ethanol (400 µl). Denatured DNA (0.5-1.0 pmol including 1 µg M13) was combined with the sequencing

primer* (0.5 pmol) and the sequencing reaction buffer (2 μL) (see 2.6). The reaction mixture was brought up to 10 μL with dH$_2$O and the annealing reaction was allowed to proceed at 65°C for 2 minutes. The reaction mixture was then allowed to cool at room temperature for 30 minutes and chilled on ice. To the annealed template-primer. DTT (0.1M. 1 μl), labelling mix (diluted 1:5, 2 μl), [α-^{32}P]dATP (5 μCi, 0.5 μl) and T7 DNA polymerase (3.25 units) (Amersham, Cleveland. OH) were added. The mixture was mixed thoroughly and incubated at room temperature for 5 minutes. 4 tubes were labelled 'A'. 'T'. 'C' and 'G' and each filled with the appropriate dideoxy termination mix (2.5 μl). These tubes were pre-warmed to 45°C. Lacking the 3' hydroxyl group, dideoxy nucleotide is incapable for further extension. Polymerase reaction therefore stopped whenever a dideoxy nucleotide was incorporated resulting in fragments of different lengths terminated at every 'A', 'T', 'C' or 'G' in the appropriate reaction tubes. The completed labeling reaction from above was transferred to each of the 4 'A', 'T'. 'C', 'G' labeled tubes in 3.5 μl aliquots. The tubes were incubated at 37°C for 5 minutes followed by addition of the stop solution (4 μl to each tube), mixed and stored on ice. The samples were heated to 80 °C for 10 minutes for denaturation, then loaded (3 μl each) to a polyacrylamide gel.

The loaded gel was run at 100 V for 6 hours followed by exposure to a film (Kodak. Toronto, Canada). The sequence was read to confirm the presence of the desired mutation.

* Mutagenic oligos and sequencing primers were pre-designed. Concentration of oligo/primer was determined by reading the optical density at 260 nm (OD$_{260}$). The concentration was calculated using the equation: Concentration (pmol/μl) = OD$_{260}$ / (0.01 * N) where N is the number of bases the oligo/primer contains.

2.1.3 *Molecular Subcloning*

Once the desired mutation was confirmed by sequencing, the cassette carrying the mutation in the pGEM vector was subcloned first into the vector p64T* which carries the full length of rSkM1 Na$^+$ channel gene subcloned at BgII sites. p64T* was chosen because

it lacks the convenient restriction sites BamH1. Sph1 and Kpn1. The full-length gene carrying the mutation in p64T* was then spliced into pGW1H for protein expression at BglII sites (Figure 2.1) Plasmid DNA was transformed and amplified in the DH5α strain of E.Coli and extracted using the conventional miniprep method for all subcloning purposes. Extracted DNA was cut with proper restriction enzymes and ligated with the appropriate fragments. Ligated DNA was transformed, re-amplified and extracted as above. cDNA (in GW1H) for oocyte injection was prepared using Qiagen spin columns instead of miniprep for purity reasons. These procedures are described in details below.

2.1.3.1 Transformation

Competent DH5α cells were kept as aliquots (20 μl) frozen at -70°C. The cells were allowed to sit on ice for 15 min before transformation for thawing. DNA (3 μl, 0.01 μg/μl) was added to the DH5α cells. The mixture was incubated at 37°C for 15 minutes. LB (500 μl) was then added to the transformed cells, mixed and spread on a LB/Ampicilin agar plate. The plate was incubated at 37°C overnight.

2.1.3.2 Miniprep

The standard miniprep procedure was used for preparing DNA for all subcloning purposes. A well isolated colony was grown in LB (2 ml) overnight at 37°C. The overnight bacterial culture was spun at 3,000 rpm for 10 min. The supernatant was discarded and the bacterial pellet was collected. Solution I (150 μl) was added to the pellet and vortexed for 30 sec to mix. Solution II (300 μl) was added to the mixture to lyze the cells. The mixture was inverted very gently for 5-6 times to mix. Solution III (250 μl) wa. added 5 min after addition of Solution II for neutralization. The mixture was again inverted 5-6 times to mix and then centrifuged at 13,00 rpm for 15 min. The supernatant was transferred to a fresh microfuge tube to which 100 % ethanol (2X volume) or isopropanol (0.7X volume) was added. The microfuge tube containing the DNA was placed on ice for 1 hour for DNA precipitation. The DNA pellet was collected and vacuum dried. dH₂0 (50 μl) was added to

Figure 2.1   64

Flow diagram showing subcloning of mutagenic cassettes encoding for DII. III and IV (SphI-KpnI) into the expression vector pGW1H. Subcloning of DI cassettes was similar except BamHI-SphI sites were employed.

.

KpnI

SphI

pGEM

BglI *SphI* *KpnI*

BglI

64T*

KpnI/SphI Digestion

+

Ligation

rSkM1 in 64T*

BglI

+

BglI cut
Dephosphorylated GW1H

Ligation

KpnI *KpnI*

KpnI

rSkM1 in GW1H

KpnI

Correct

Incorrect

Empty

↓ *KpnI*

↓ *KpnI*

↓ *KpnI*

5 kb & 6 kb

10 kb & 1 kb

5 kb
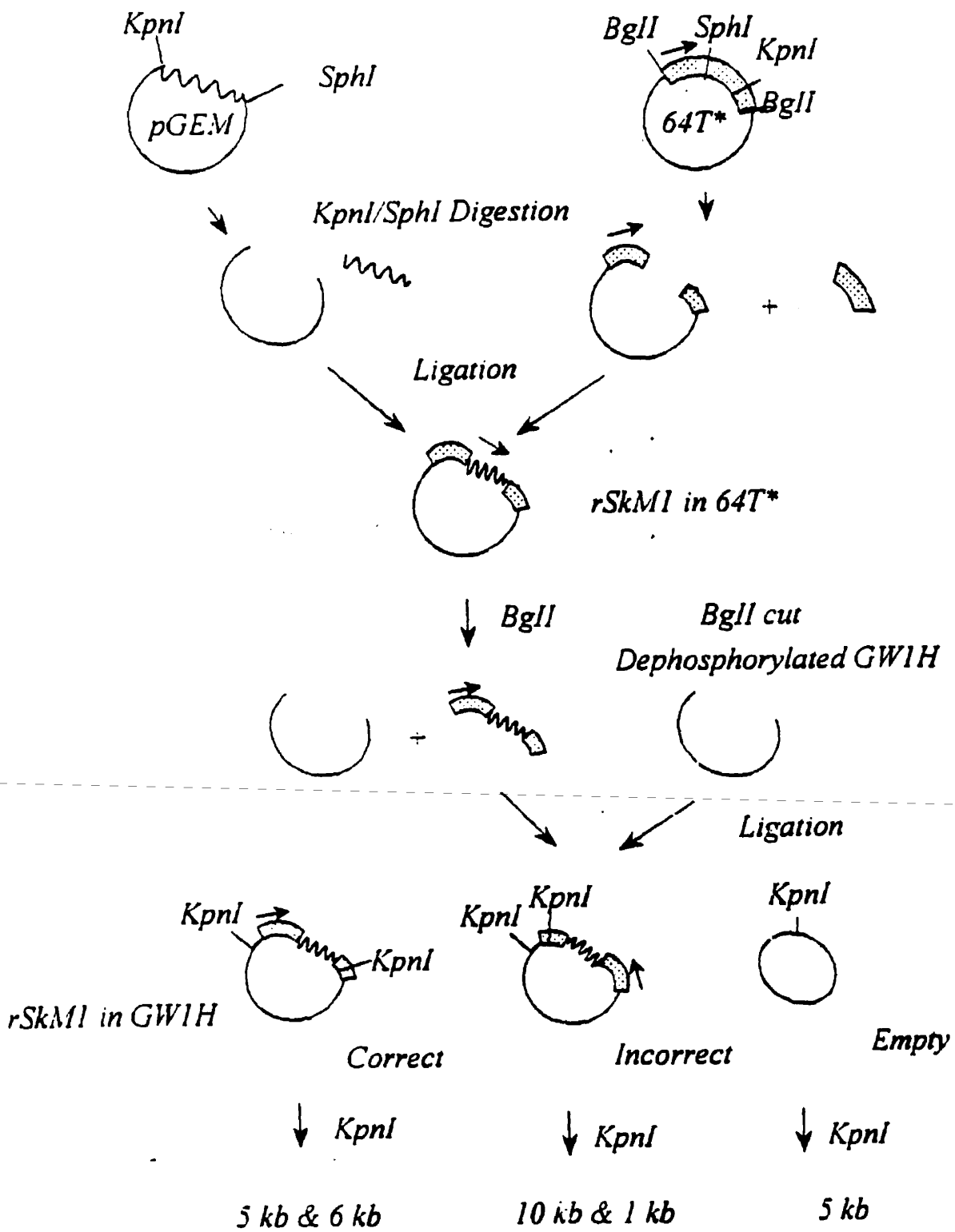
dissolve the pellet.

2.1.3.3 *Restriction digestion of DNA*

pGEM vectors (Promega, Madison, WI) carrying the mutagenic cassettes encoding for domain I were cut with BamH1-Sph1 while those for domains II. III and IV were cut with Sph1-Kpn1. The digested fragments were separated in a 10% agarose gel dissolved in 1X TAE solution with ethidium bromide (10 µg/100 ml) using electrophoresis. The gel was run for at least 1 hour at 100 V. The desired fragments containing the mutations (i.e. 1.9 kB for pGEM-I1f and 2.5 kB for pGEM-7f) were cut using a razor blade. Similarly, the vector 64T* (3 kb) containing the full-length rSkM1 Na⁻ channel gene (6 kb) at BglI sites was cut with BamH1-Sph1 and Sph1-Kpn1 to yield 7.1 kb and 6.5 kb fragments respectively. Appropriate fragments were ligated together (see 2.2.4). Similarly, full-length gene carrying the desired mutation in p64T* was cut and subcloned into pGW1H at BglI sites.

2.1.3.4 *Dephosphorylation*

pGW1H was dephosphorylated prior to subcloning to minimize self-circularization because of the presence of two identical cohesive ends after restriction digestion with BglI. BglI cut pGW1H was precipitated with 100 % ethanol (2X volume) on ice for 30 min then spun at 13,000 rpm for 10 min. The pellet was collected, washed with 70% cold ethanol. vacuum dried and dissolved in dH_2O (90 µl). 10X Calf Intestine Phosphatase (CIP) buffer (10 µl) and CIP (0.5 µl) were added. The mixture was incubated at 37°C for 30 min to dephosphorylate and subsequently at 85°C for 15 min to heat inactivate the enzyme. The mixture was cooled slowly at room temperature for 20 min before the DNA was precipitated with ethanol as before. The DNA pellet containing the dephosphorylated vector was dissolved in dH_2O (10 µl).

2.1.3.5 *Ligation*

For ligation, the vector was mixed with the fragment to be ligated in a 1:5 ratio by weight of DNA. Ligase (1 unit), 10X ligase buffer (1 µl), 10 mM ATP (1 µl) were added to the mixture. The volume of the final reaction mixture was brought up to 10 µl with dH$_2$O. The ligation mixture was incubated at 16°C for 1 hour before transformation into competent DH5α cells on an agar/ampicillin plate.

2.1.3.6 *Screening of ligation products*

At least 5 distinct colonies from each ligation product were grown for screening of the desired products. DNA was extracted using miniprep as described in section 2.2.1.2. For Na⁻ channel clones in p64T*, successful incorporation of the mutagenic fragment was tested by digesting the corresponding clone with BgII to yield the full-length 6.0 kb gene and the 3.0 kb vector. For clones in pGW1H, proper orientation of the Na⁻ channel gene was tested by digestion with KpnI. There were three possibilities: correct orientation, incorrect (backward) orientation and empty vector. Correct orientation should yield two bands each of 5.1 and 5.9 kb in length. In contrast, backward orientation would yield a 1 and a 10 kb fragments. Empty vector would yield a single 5 kb band indicating absence of the gene (Figure 2.1).

2.1.3.7 *DNA Purification*

The Qiaprep Spin Plasmid kit (QIAGEN Inc., Chatworth, CA) was used to purify cDNA for injection into *Xenopus* oocytes. DH5α cells were transformed with appropriate cDNA and grown in LB broth (5 ml) overnight at 37°C. The overnight culture was spun down and the pelleted bacterial cells were resuspended in Buffer P1 (250 µl) and transferred to a microfuge tube. Buffer P2 (250 µl) was then added and the mixture was gently inverted for 5 times to mix. Buffer N3 (350 µl) was added 5 min after addition of Buffer P2 and the mixture was inverted 5 times to mix as before. The final mixture was spun at 13,000 rpm

for 10 min. The supernatant obtained was added to a Qiaprep column placed in a 2 ml collection tube and spun at 13.000 rpm for 1 min. The flow-through was discarded. Buffer PE (0.75 ml) was added to the spin column and spun at 13.000 rpm for 1 min. The flow-through was again discarded and the spin column was spun again at 13.000 rpm for an extra 1 min to remove any residual wash buffer. Finally, the spin column was placed in a 1.5 ml microfuge tube and dH_2O (50 μl) was added and allowed to stand for 1 min. The eluant containing the cDNA was collected by centrifuging at 13.00 rpm for 1 min. Typical yield of cDNA this method was 10-20 μg.

2.3   Heterologous Expression

The *Xenopus* oocyte system is repeatedly used in this thesis for expression of all Na^+ channel clones and is described in detail below.

2.3.1   *Xenopus Oocyte Expression System*

The *Xenopus* oocyte expression system was first introduced by Gurdon in 1971 as a means to study various aspects of the control of gene expression (Gurdon et al., 1971). Injection of cDNA into the nucleus or mRNA into the cytoplasm led to the expression of functional proteins by the oocytes. It was in 1982 that Barnard and co-workers first demonstrated that various types of ion channels and receptors could be expressed in oocytes after injection of mRNA isolated from the appropriate tissues (Barnard et al., 1982). In this thesis, this expression system was used in combination with mutagenesis to study the structure and function of Na^+ channels.

2.3.1.1 *Oocyte Isolation*

Adult female *Xenopus laevis* (Nasco, Ft. Atkinson, WI) was anesthetized by immersion in 0.25% tricaine (Sigma Chemical Co., St. Louis, MO) solution for 10-15 min. A small incision (7-10 mm) was made on the anesthetized frog in the abdomen. Stage V or

VI oocytes (Figure 2.2) were removed from Ovarian lobes were pulled out from the incision and placed in sterile ND96+++ solution. A simple suture was used to close the incision. The surgerized frog was placed in water to allow for recovery. Ovarian lobes were teased open and broken into smaller clumps. The oocytes were placed into a 15 ml tube and rinsed with Ca^{2+} free OR-2 solution for 3-4 times until clear. The oocytes were transferred to another 15 ml tube filled with 2 mg/ml collagenase (Type 1A, Sigma) in OR-2 for digestion. The digestion was done at room temperature for about 45 minutes until many single isolated oocytes were released. Caution was made to ensure cells were not overdigested. After digestion was complete, oocytes were rinsed with OR-2 3-4 times and then transferred to a petri dish for screening under microscope. Only healthy stage V or VI oocytes (Figure 2.) were selected for injection. Oocytes with white spots developed on their animal pole were discarded. Selected oocytes were placed in ND 96+++ solution containing 2.5% fetal bovine serum (FBS) to promote the removal of the follicular layer. Defolliculated oocytes were ready for injection and stored in ND 96+++ at room temperature. Solution was changed daily to keep the oocytes healthy.

2.3.1.2 Injection of cDNA

50 nl of cDNA (final concentration: 0.1-1.0 μg/μl) encoding for the α subunit of wild-type (rSkM1) or mutant channels, and the rat brain β_1 subunit (Isom et al., 1992) (ratio of α: β_1 subunit by weight was 1:5) were injected into the nucleus of healthy, stage V-VI oocytes from the dark-colored animal pole using a 10 μl micropipettor. All cDNA dilutions were made by adding appropriate volume of DEPC (diethylpyrocarbonate) water to the QIAGEN cDNA prepared as described in 2.3. Injected oocytes were incubated at room temperature in ND96+++ solution for 24 to 72 hours for protein expression.

2.4 Electrophysiology

Voltage-clamp is a powerful technique. Except for a brief period required for charging the membrane after stepping to a new voltage, the capacitive current arising from

the membrane capacitance is eliminated as the membrane potential is held constant. Since the membrane potential is held constant, the currents that flow are proportional to the membrane conductance (i.e. number of open channels) and any changes in kinetics of a particular type of ionic current can be addressed as changes in functional properties of this channel.

2.4.1 Two-electrode Oocyte Clamp

Whole-cell current recordings of *Xenopus* oocytes expressing the desired channels were done at room temperature (20-22°C) using a two-electrode voltage-clamp amplifier (OC-725A, Warner Instruments, Hamden, CT) as outlined in Figure 2.2. The voltage-electrode is responsible for detecting the membrane potential relative to the ground. This measured potential is compared to the pre-set command voltage at the amplifier. The current electrode injects a current equal in magnitude but opposite in direction to the currents going through the open ion channels to counteract with their effects and bring the membrane potential back to the command voltage thereby voltage-clamping the membrane potential constant. Whole-cell currents flowing through the ion channels are measured by determining how much current is needed to maintain the membrane potential at a particular command voltage. Microelectrodes (TW120F-6, World Precision Instruments, Sarasota, FL) were agarose-plugged to maintain stability and filled with 3 M KCl and had a final resistance of 1-3 MW. Electrode penetration was achieved by advancing the electrode into the oocyte until it dimples the membrane and finally visibly pops into the cell. Whole-cell currents were typically evoked by step depolarizations from -60 to +50 mV with 10 mV increments from a holding potential of -120 mV. The currents were digitized at 10 kHz and low-passed filtered at 1-2 kHz (-3 dB). A P/4 protocol was utilized for leak and capacitance subtraction. Current records and data were collected using custom-written software.

2.4.2 Single Channel Recording

Oocytes expressing whole-cell currents between 5 and 10 μA were chosen for s

70

Figure 2.2

Two-electrode voltage-clamp set-up and a healthy stage V-VI *Xenopus* oocyte.

Feedback circuit representation of the two-electrode oocyte clamp set-up. The cell can be considered as a simple RC circuit where C_m is the membrane capacitance and R_m the membrane resistance. R_I and R_V represents the resistance of the current and voltage electrodes respectively. R_{others} represents resistances from other sources such as the bath solution and the bath ground. The amplifier (A) is designed such that $V_{Command}$ is always equal to V_m, the output to the current electrode is therefore $V_{out} - V_m - V_{command}$.

Two electrode voltage-clamp

$V_{command}$ — A

$V_{out\,put}$
$= V_m - V_{command}$

R_v R_I

Oocyte

V_m

R_m C_m

R_{others}
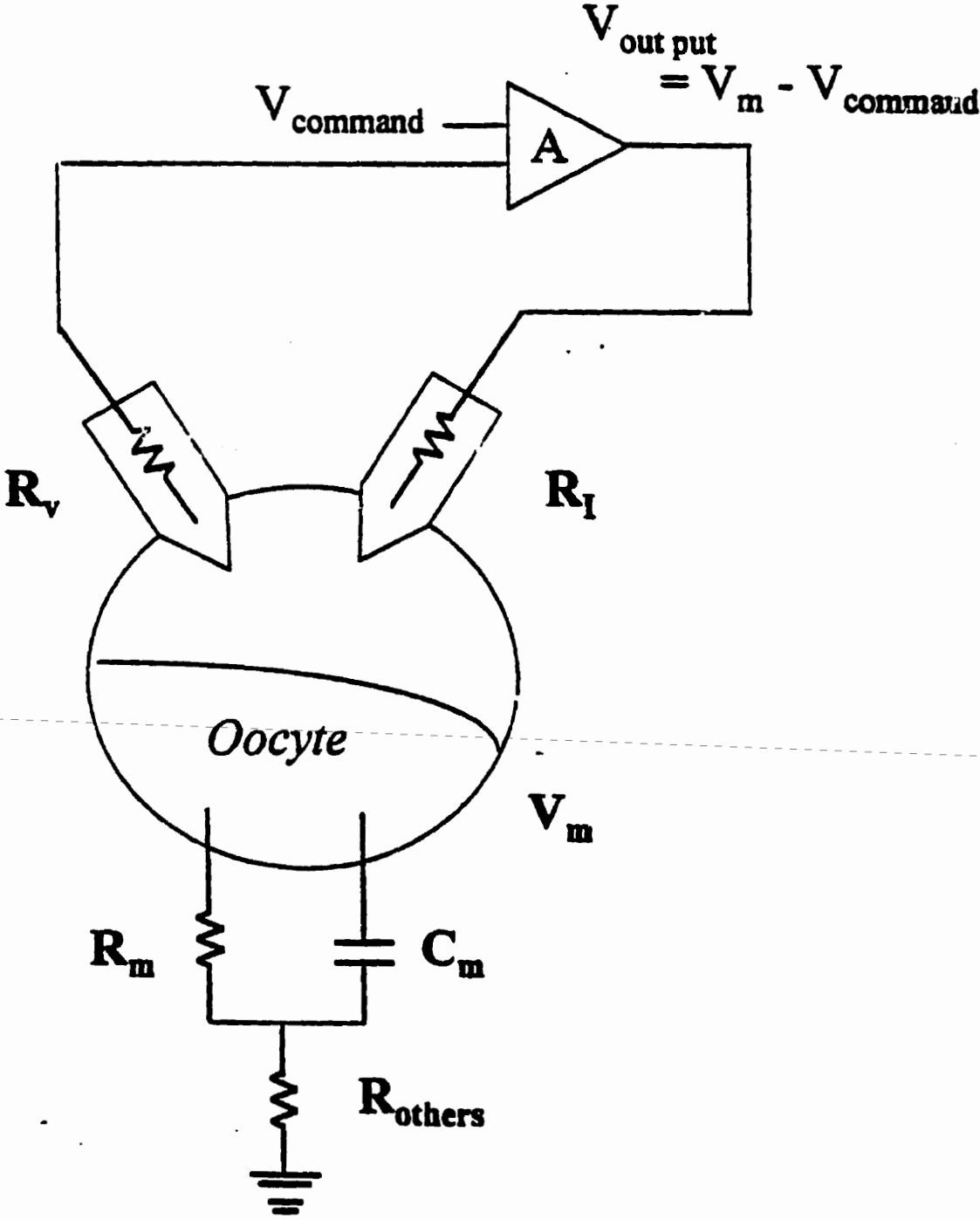
ingle-channel recording. The vitelline membrane was removed prior to any recording. Oocytes were placed in a hypertonic stripping solution to promote shrinkage. As the oocyte shrunk, the vitelline membrane detached from the cell membrane and appeared as a transparent spherical coating around the oocyte. It was mechanically removed with a pair of fine watchmaker forceps under a light microscope. Oocytes were extremely fragile when defolliculated and any contact with the air-water interface during transferring was avoided.

Single-channel currents were measured in the cell-attached (inside out) configuration (Hamill, Marty, Neher, Sakmann and Sigworth, 1981) (Figure 2.3A) at room temperature using an integrating headstage (Axopatch 200A, Axon Instruments, Foster City, CA, USA). Data were sampled at 10kHz and low-pass filtered (4-pole Bessel, -3 dB at 2 kHz). Electrodes were fabricated from 1.5 mM outer diameter thin-walled borosilicate glass (1BBL, World Precision Instruments Inc., Sarasota, FL) pulled on a Sutter puller, fire-polished and coated with Sylgard to reduce the glass capacitance. Final resistance was 5-10 MΩ. A high K$^-$ bathing solution was used to zero the cell membrane potential. The glass electrode is brought into contact with the membrane surface of the oocyte. Application of gentle suction, without breaking into the cell as in the case of whole-cell patch-clamp recording, leads to the formation of a giga-ohmn seal between the pipette and the lipid bilayer. Due to the small size of the electrode and the highly resistant seal, single or several ion channels can be isolated in the patch and the specific currents flowing through these channels are captured. Electrophysiological recordings can be performed either in the cell-attached inside-out configuration with the patch remains intact or in the excised inside-out mode (Figure 2.3B) where the membrane patch is mechanically ripped off from the membrane. In the cell-attached mode, the intracellular contents remain undisturbed whereas in the inside-out patch the millieu of the cytoplasmic side can be controlled.

Figure 2.3

Different cell-recording configurations.

Single-channel and macropatch recordings can be done in the on-cell or cell-attached patch mode (A). The patch can be pulled off the cell to form the inside-out or excised patch configuration (B). Alternatively, cell patch can be ruptured to form the whole-cell configuration (C). The excised-patch and whole-cell configurations have the advantage of total control over the cytoplasmic millieu.

A
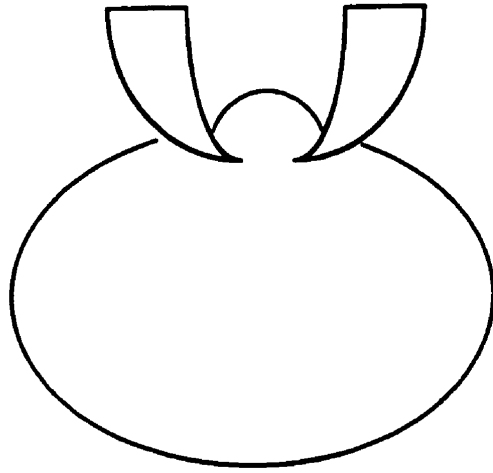
B
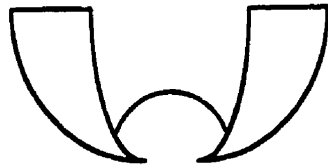
C
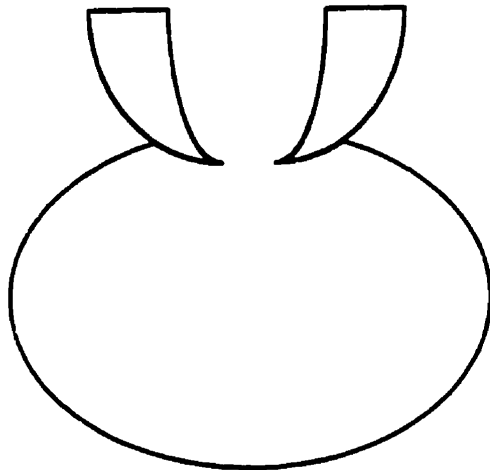
2.4.3 Whole-cell Patch-clamp

The standard whole-cell patch-clamp recording configuration (Figure 2.3C) was used to record sodium current from transfected HEK cells or cardiac myocytes. All recordings were performed at room temperature (20-22°C) using the whole-cell patch clamp method with an Axonpatch 200A amplifier (Axon Instruments, CA, USA). Microelectrodes were pulled from thin-walled borosilicate glass (1.5mm diameter, World Precision Instruments, Sarasotoa, FL) using a Flaming-Brown micropipette puller (Sutter Instruments). The pipette tip was heat polished with a heating filament (model MF-83, Narushige, Tokyo, Japan) and the final resistance was typically 2-5 MΩ when filled with pipette solution. Uncompensated series resistance was typically 2-5 MΩ and compensation was typically 60-80%.

In contrast to the two-electrode oocyte clamp, whole-cell patch-clamp consists of only one micropipette electrode for both voltage recording and current passing. The microelectrode is initially brought into contact with the membrane surface. Gentle suction allows formation of a tight seal between the pipette and a patch of the membrane. Once a patch is formed, subsequent suction will rupture the attached patch of the membrane resulting in a low-resistance access of the micropipette to the whole cell. After membrane rupture, the cell was allowed to dialyse for 1-3 minutes before experiments. Cell capacitance was estimated both automatically by custom-designed software and manually by integrating the area of the capacitance transients. Currents were digitized at 2 to 10 kHz and stored off-line for analysis.

2.5 Data Analysis

All data were analyzed using the commercially available softwares Ionview and Origin (Microcal). Specific mathematical equations used to obtain fits of experimental data are described in pertinent chapters.

For single-channel recordings, data were idealized using the 50% amplitude criterion to identify channel openings and closings. Idealized channel openings were used to generate data such as first latency, single channel conductance, unblocked- and blocked-times, closed- and open-times, probability of openings and the number of opennings per sweep, etc (Colquhoun and Sigworth, 1983). Equations used for data fitting are described in pertinent chapters. All patches studied were stable for at least 500 Colquhoun sweeps (depolarizing pulses).

2.6   *Solutions*

The recipe for all solutions mentioned in this chapter is given in Table 2.1. Specific solutions used in certain experiments are described in pertinent chapters.

Purpose	Solution	Ingredients
Mutagenesis	10X annealing buffer	20 mM Tris (pH7.4), 2 mM MgCl₂, 50 mM NaCl
	10X synthesis buffer	0.4 mM each dNTP, 0.75 mM ATP, 17.5 mM Tris (pH 7.4), 3.75mM MgCl₂ and 1.5 mM DTT.
Miniprep	Solution I	50 mM Glucose, 25 mM Tris (pH 8), 10 EDTA
	Solution II	200 mM NaOH, 1% SDS
	Solution III	3M KAc, 11.5% AcOH
Electrophoresis	50X TAE buffer	0.04M Tris base, 5.7 % Glacial acetic acid, 0.002M Na₂EDTA.2H₂0 (pH 8.5)
Oocyte Isolation	OR-2	88 mM NaCl, 2 mM KCl, 1 mM MgCl₂ and 5 mM HEPES (pH 7.6).
	ND96⁺⁺⁺	96 mM NaCl, 2 mM KCl, 1.8 mM CaCl₂, 1 mM MgCl₂ and 5 HEPES, 50 mg/ml gentamicin, 5 mM pyruvate and 0.5 mM theophylline (pH 7.6).
2-electrode voltage-clamp	ND96	96 mM NaCl, 1 mM BaCl₂, 1 mM MgCl₂ and 5 mM HEPES (pH 7.6).
Whole-cell Patch-clamp	Bath solution	140 mM NaCl, 1 mM MgCl₂, 10 mM HEPES (pH 7.4)
	Pipette solution	35 mM NaCl, 105 mM CsCl, 10 mM HEPES (pH 7.4)
Single Channel Recording	Hypertonic stripping solution	280 mM KAsp, 10 mM HEPES (pH 7.4)
	Bath solution	140 mM KCl, 10 mM HEPES (pH 7.4)
	Pipette solution	140 mM NaCl, 1 mM MgCl₂, 10 mM HEPES (pH 7.4)
Macropatch Recoding	Bath solution	140 mM KCl, 10 mM HEPES (pH 7.4)
	Pipette solution	140 mM NaCl, 1 mM MgCl₂, 5 mM BaCl₂, 10 mM HEPES (pH 7.4)

CHAPTER 3

THE STRUCTURE OF P-LOOPS AND THE Na⁺ CHANNEL PORE

3.1 *Abstract*

The 3-dimensional structure of the Na⁻ channel pore was studied using Scanning Cysteine Accessibility Method (SCAM). Single cysteine substitutions of individual P-loop residues in the rat skeletal muscle (rSkM1) Na⁻ channel produced channels sensitive to current blockade by extracellular Cd^{2+} and susceptible to modifications by sulfhydryl-reactive agent revealing residue side-chains lining the pore. The proximity of these pore-lining residues was assessed by simultaneously replacing two residues in distinct P-loops with cysteines. Dual cysteine replacements create channels which are ultra-sensitive or insensitive to Cd^{2+} block relative to the individual single mutants, suggesting coordinated Cd^{2+} binding and cross-linking by the inserted sulfhydryl pairs. Since both processes of Cd^{2+} coordination and disulfide bridge formation require strict geometric constraints, this strategy allows identification of residue pairs capable of approaching one another to within 3.5 Å. The interaction pattern demonstrates that multiple consecutive adjacent residues in one P-loop could very often interact with a single residue in another P-loop. One possible explanation for these observations is that the P-loops, like the active sites in many enzymes, are flexible on the time scale of Cd^{2+} binding and sulfhydryl modification. Furthermore, cross-linking of certain P-loop residues appears to affect ion permeation and selectivity. Our results suggest that P-loop dynamics might play a crucial role in Na⁻ channel function.

3.2 *Introduction*

Previous modeling (Hille. 1992; Noda et al., 1984; Guy and Durell, 1995; Lipkind and Fozzard, 1994; Soman et al.. 1995) and mutagenesis experiments (Terlau et al.. 1991; Satin et al., 1992; Heinemann et al., 1992; Backx et al., 1992) have established that P-loops are critical determinants of catalytic permeation properties of Na⁻ channels. These

P-loops are located between S5 and S6 in the four homologous repeat domains of Na⁻ (Noda et al., 1984) and Ca^{2+} channels (Ellinor et al., 1995) and are located at analogous positions in K⁻ (Mackinnon and Miller, 1989) and cyclic nucleotide-gated channels (Heginbotham et al., 1992; Sun et al., 1996). Four P-loops, pseudosymmetrically arranged, are necessary to form a functional pore (MacKinnon, 1991; Catterall, 1995). While other regions, such as the fifth (S5) and sixth transmembrane (S6) segments (Lopez et al., 1994) as well as the S4-S5 loops (Isacoff et al., 1991), of voltage-gated channels influence permeation, P-loops are the principal determinants of ion selectivity. Based on mutagenesis experiments, various structural models for P-loop backbones have been proposed: β-strands with β-hairpin loops (Yellen et al., 1991; Lipkind and Fozzard, 1994; Soman et al., 1995), random coils (Sun et al., 1995; Perez-Garcia et al., 1996) and a-helices with β-turns (Guy and Durell, 1995). Detailed 3-dimensional information on the relationship of P-loop residues to one-another has been obtained using mutant cycling analysis of toxin binding to channels (MacKinnon and Miller, 1989; Gross and MacKinnon, 1995; Hidalgo and MacKinnon, 1995; Ranganathan et al., 1996). More recently, crystallization and X-ray analysis of the pore of a primitive K⁻ channel, which comprises of 2 transmembrane segments, have been obtained (Doyle et al., 1998). However, NMR or crystallographic approaches to such large intrinsic proteins as Na⁻ and Ca^{2+} channels are not yet available. P-loops structures of these channels therefore still remain obscure. Indirect approaches have been employed to deduce the structures of these regions.

In this chapter, I will describe a novel approach that we use to assess the molecular architecture of the pore of Na⁻ channel by using Cd^{2+} as a biophysical probe of mutant channels in which one or two P-loop residues are replaced by cysteines. Cd^{2+} was chosen because: 1) its ionic radius (0.92 A) (Cotton and Wilkinson, 1992) is nearly identical to Na⁻ (0.95 A), 2) it binds free sulfhydryls with high affinity in a "near-covalent" manner (Cotton and Wilkinson, 1992) and, 3) it can coordinately bind to multiple free sulfhydryls with a tetrahedral geometry, as observed in Zn^{2+}-finger proteins (Vallee and Falchuk, 1993) and metallothionins (Shaw et al., 1992), while binding very

weakly to oxidized sulfhydryls (Torchinsky, 1981). Thus. Cd^{2+} is ideal for identifying P-loop residues lining the channel pore following cysteine replacements. Furthermore. Cd^{2+} is well suited to map the spatial relationship between residues in channel pores where pairs of P-loop residues from distinct domains are replaced by cysteine. In our double cysteine mutant channels. changes in sensitivity to Cd^{2+} block of ionic currents. compared to single-cysteine mutants. can identify residue pairs capable of interacting by Cd^{2+} coordination or formation of disulfide linkages. A similar strategy was used by Benitah et al (1996) in Na^+ channels and Krovetz et al (1997) in K^+ channels to determine residue proximity.

In this study. the pattern of P-loop residue pairs capable of coordinately binding Cd^{2+} or forming disulfide bonds suggests a possibility that P-loops are remarkably flexible on the time scale of Cd^{2+} binding and coordination. While this suggestion is incompatible with static molecular sieve models for channel pores (Hille. 1992), it is not totally unexpected especially given the analogy between ion channels and enzymes (Eisenberg, 1990: Miller. 1992). Indeed. ion channel proteins are enzymes catalyzing the selective passage of ions across the cell membrane in which the pore forms the active site (Eisenberg, 1990: Miller. 1992); many well-studied enzymes have active sites formed by highly flexible "random-coil" loop structures (Creighton. 1993: Branden and Tooze. 1991) and flexibility is crucial for both selective substrate binding and catalytic activity (Pompliano et al.. 1990: Larson et al., 1995: Lan et al., 195: Nicholson et al.. 1995). In general. our data are most consistent with "unstructured" loop models for Na^+ channel P-loops which form the active site and further suggest that P-loop flexibility may be critical for selective ion permeation. Thus. our results support dynamic pore models (Lauger. 1987) wherein ion passage requires motion of the pore in addition to movements of the traversing ion.

3.3   Methods and Materials

3.3.1   Electrophysiological recording

Oocytes were bathed in ND96 (section 2.5.1). Variable concentrations of $CdCl_2$ were added as required from a 1M stock solution. When needed, methanethiosulfonate-ethylammonium (MTSEA) was added at a concentration of 1 mM and dithiothreitol (DTT) at a concentration of 10 mM in ND96. The application of MTSEA and DTT was achieved by washing at least 30 ml of the solution while the oocytes were depolarized every 2 s to -10 mV from a holding potential of -120 mV. All recordings were done at 21-23°C.

3.3.2   Estimation of the dissociation constant (K_D) for Cd^{2+} binding of single cysteine mutants

The dissociation constant, K_D, for Cd^{2+} binding to the channel was estimated using least-squares fitting of the dose-response curves to the equation:

$$I / I_o = K_D / (K_D + [Cd^{2+}])$$ Equation 3.1

where I and I_o represent Na^+ currents measured in the presence and absence of Cd^{2+} respectively. Statistical significance for changes in Cd^{2+} binding was determined by comparing the experimentally estimated K_D (mean±S.E.M.) between single-cysteine mutant and wild-type rSkM1 (i.e. WT) channels using a paired Student's t test (p<0.05).

3.3.3   Analysis of double-cysteine mutants to assess coordinated Cd^{2+} binding

When Cd^{2+} binds independently to the two cysteines inserted into P-loops of distinct domains of the Na^+ channels we expect the dissociation constant for Cd^{2+} block of Na^+ current to be directly determined by the dissociation constants measured for the

individual single-cysteine mutants. Specifically, the predicted dissociation constants for the double-mutant, $K_{D,pre}$, for independent binding of Cd^{2+} to the two cysteines is given by the equation:

$$1/K_{D,pre} = 1/K_D^1 + 1/K_D^2 , \qquad \text{Equation 3.2}$$

where K_D^1 and K_D^2 represent the dissociation constants for the single-cysteine mutants 1 and 2. Therefore, $K_{D,pre}$ was compared to the observed dissociation constant (i.e. $K_{D,ob}$) in order to assess whether coordinated Cd^{2+} binding occurred in the double-cysteine mutants. A one-way analysis of variance for three groups was employed (Bogartz, 1994) in order to assess whether the measured mean of $1/K_{D,ob}$ differed statistically from the estimated mean $1/K_{D,pre}$ predicted from Equation 3.2. This test takes into account the measured variance of K_D^1, K_D^2 and $K_{D,ob}$ in determining statistical significance ($p<0.05$). Alternatively, when the two inserted cysteine residues are geometrically arranged to simultaneously bind a Cd^{2+} ion and provide only coordinated Cd^{2+} binding, we expect the dissociation constant for the double-cysteine mutant channel (i.e. $K_{D,co}$) is given by:

$$K_{D,co} = K_D^1 \exp[-(\delta G_2 + \delta G_d)/kT]$$
$$= K_D^2 \exp[-(\delta G_1 + \delta G_d)/kT] , \qquad \text{Equation 3.3}$$

where δG_1, and δG_2 are the free energies of Cd^{2+} binding to sites 1 and 2 respectively (expected to be negative), δG_d is the distortional and entropic free energies required for the protein to coordinately bind Cd^{2+} (expected to be positive), k is Boltzmann's constant and T is the absolute temperature. Thus for coordinated Cd^{2+} binding, $(\delta G_2 + \delta G_d)$ and $(\delta G_1 + \delta G_d)$ represent the stabilization energy contributed by Cd^{2+} binding to the second site. Therefore, the average stabilization energy for Cd^{2+} coordination could be directly obtained by measuring K_D^1, K_D^2 and $K_{D,ob}$.

3.3.4 Single-channel data analysis

Single-channel recordings were idealized by using the 50% amplitude criterion to identify channel openings and closings. Idealized channel openings were used to generate unblocked- and blocked-time density distribution histograms and the number of opennings per sweep (Colquhoun and Sigworth, 1983). Mean unblocked times were estimated by fitting unblocked-time density histograms to a mono-exponential function using a non-linear least squared algorithm. Mean blocked-times were estimated by fitting the mean blocked-time histogram with either a mono- or bi-exponential function (Colquhoun and Sigworth, 1983). The goodness of fit was estimated by calculating the F-statistics and using the F-distribution ($p < 0.05$). All patches studied were stable for at least 500 sweeps (depolarizing pulses).

3.4 Results

3.4.1 Single-cysteine substitutions of P-loops residues

Single-cysteine mutant channels were created (Akabas et al., 1992) and probed with both Cd^{2+} and sulfhydryl reactive compounds in order to identify side-chains of P-loop residues which line the pore (Backx et al., 1992). All single-cysteine replacements studied (Figure 3.1), except G1238C, produced functional channels with normal gating properties. Figure 3.2A shows sample Na^+ currents measured in oocytes before (solid line) and after (broken line) extracellular addition of 100 μM extracellular Cd^{2+} in wild-type (WT), Y401C W402C and E403C. Clearly, all three mutants have an elevated sensitivity to Cd^{2+} compared to the wild-type. This is more clearly illustrated in Figure 3.2B which displays the relative whole-cell conductance at varied extracellular Cd^{2+} for the wild-type and three mutants shown in Figure 3.2A. From such dose-response, estimates of the dissociation constant for Cd^{2+} binding to the channel pore can be obtained (see 3.3.2). In order to quantify the increase in sensitivity to Cd^{2+} of mutant channels, where P-loop residues are replaced by cysteine, Figure 3.2C outlines the ratio

Figure 3.1

(A) The putative topology of Na⁻ channels showing four homologous internal repeats each with six transmembrane segments (S1-S6). The four P-loops which are located between S5 and S6 in each repeat domain form a major part of the channel pore. The approximate location of residues mutated in our study are marked by a thickened portion of the COOH-terminal portion of the P-loop (i.e.. SS2 domain).

(B) Partial alignment sequences along with the corresponding residue numbers of the P-loops in the region which were mutated in our experiments. The mutated residues are marked as a capital letters.

(C) Three outcomes of introducing pairs of cysteine residues into distinct homologous repeat domains of Na⁻ channels are possible. Coordinated Cd^{2+} binding is expected if the two inserted sulfhydryls are sufficiently close to one another. Cross-linked channels are expected to be insensitive to current block by Cd^{2+} and will become more Cd^{2+}-sensitive by reduction with DTT. If the two inserted cysteines are distant from one another. we expect Cd^{2+} to bind independently.

A

I   II   III   IV

N
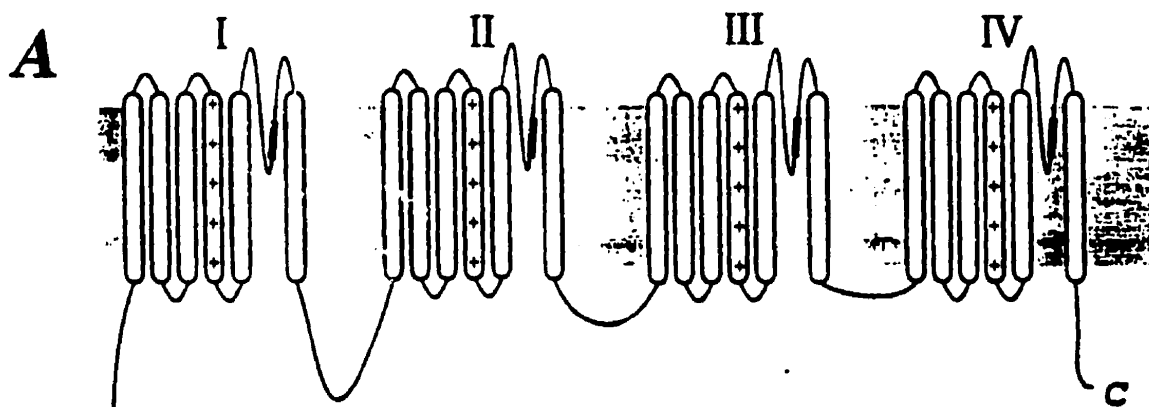
B

| Domain I | q d **Y W E** n |
| | 401 402 403 |

| Domain II | g e **W I E** t |
| | 756 757 758 |

| Domain III | f k **G W M D** |
| | 1238 1239 1240 1241 |

| Domain IV | s **A G W D** g |
| | 1529 1530 1531 1532 |

C

Coordinated Binding   *Cross-linked*   *Independent Binding*
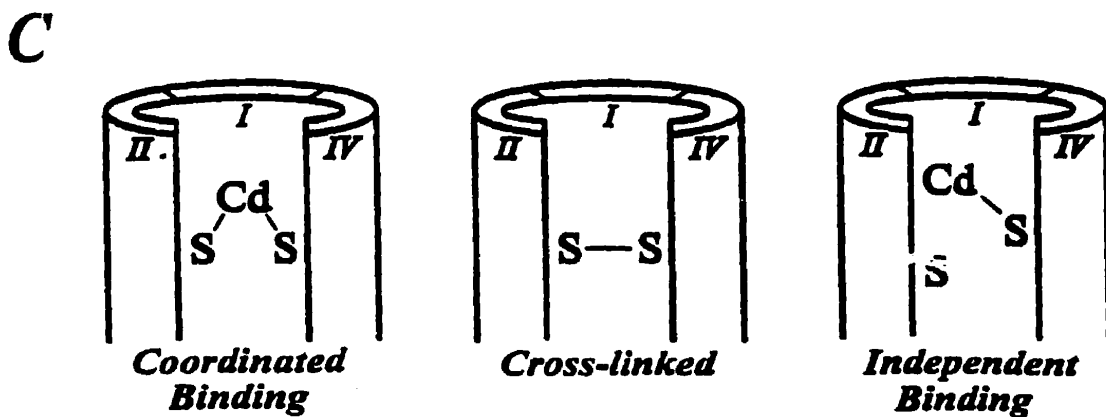
Figure 3.2

(A) Raw current traces of wild-type. Y401C. W402C and E403C channels recorded in oocytes following depolarization to -10 mV from a holding potential of -120 mV with (broken line) and without (solid line) 100 μM extracellular Cd^{2-}. The amount of current reduction is much greater for the mutant channels (Y401C. W402C and E403C) than for the wild-type channels. The currents amplitude have oeen scaled for ease of comparison. Peak currents in μA were: 3.8. 3.5, 3.5 and 2.0 for WT, Y401C. W402C and E403C respectively.

(B) Plots of the fraction of peak current remaining as a function of the extracellular $[Cd^{2-}]$ for the same channels shown in (A). Curve fits allow estimation of the dissociation constants (i.e. K_D) for Cd^{2-} binding to the channel pore.

(C) Summary of the Cd^{2-} block in single-cysteine mutants. The ratio of the estimated K_D for Cd^{2+} block of current in single cysteine mutants divided by the wild-type channels (i.e. $K_{D,Mut}/K_{D,WT}$) for control conditions and following the application of 0.5 mM methane-thiosulfate-ethylammonium (MTSEA) to oxidize the inserted free sulfhydryls. For each mutants. except W756C, $K_{D,mut}$ was significantly reduced (p < 0.001) more than 3-fold which was abolished by the application of MTSEA.

B

C

$K_{D, Mut} / K_{D, WT}$
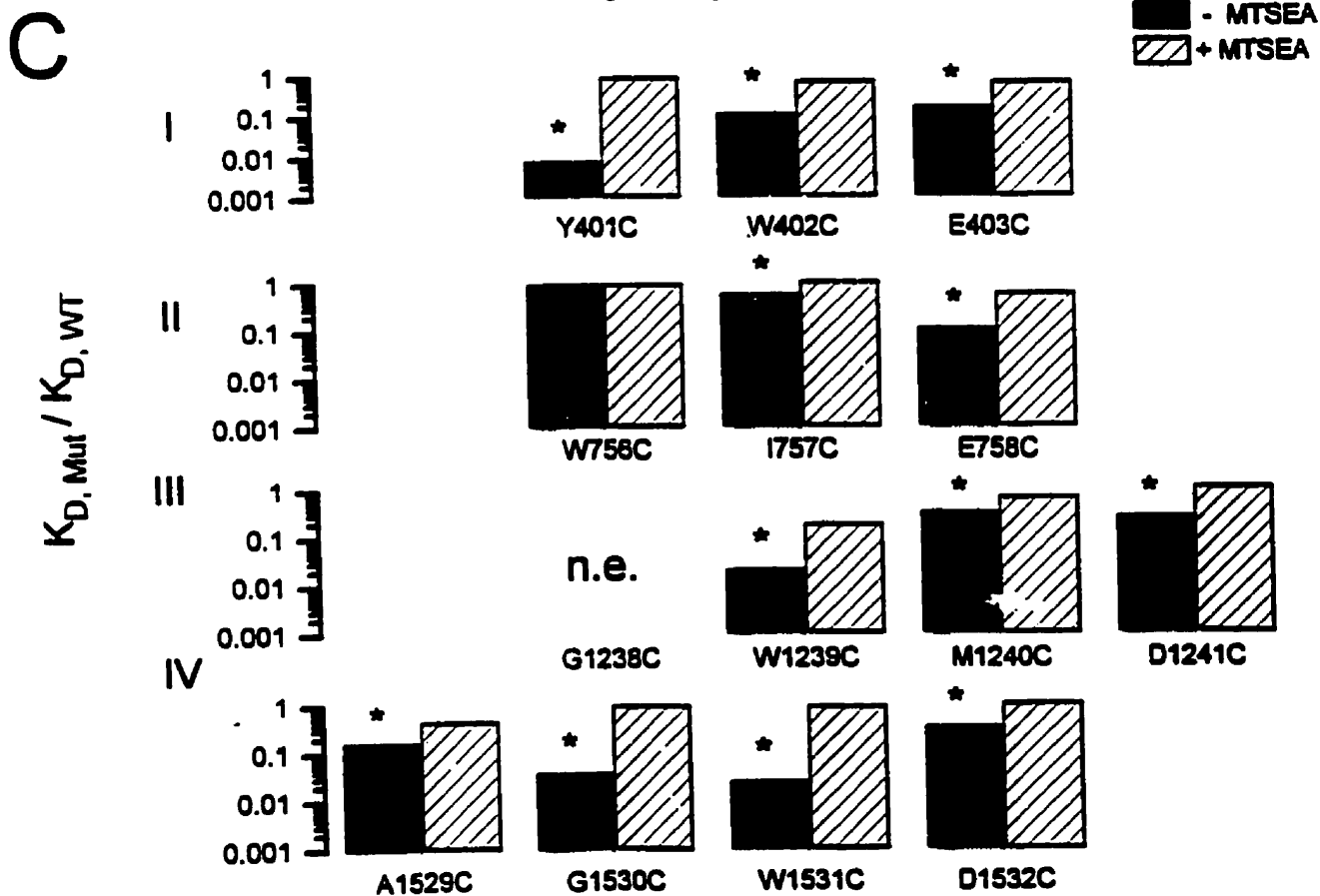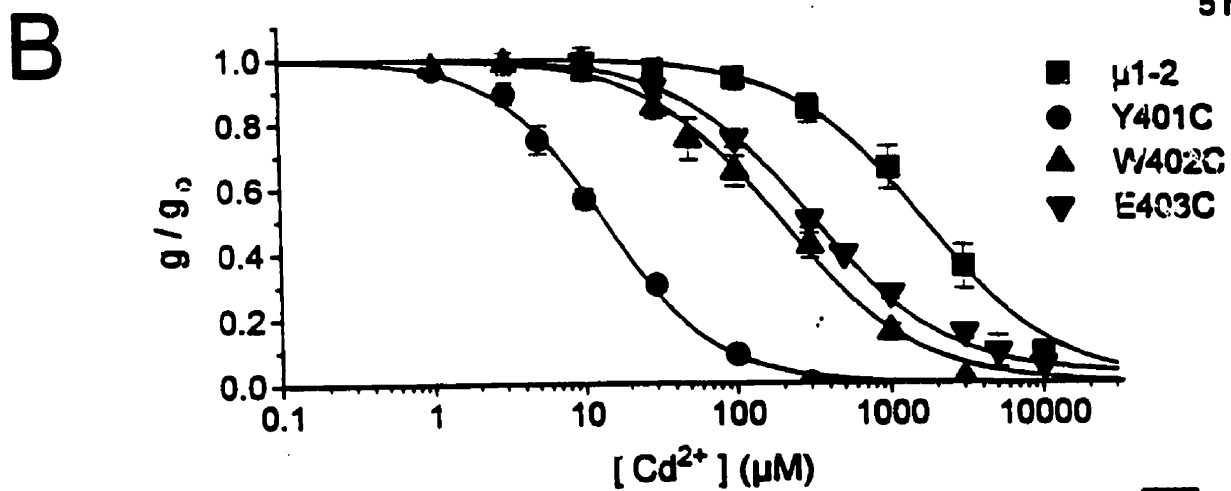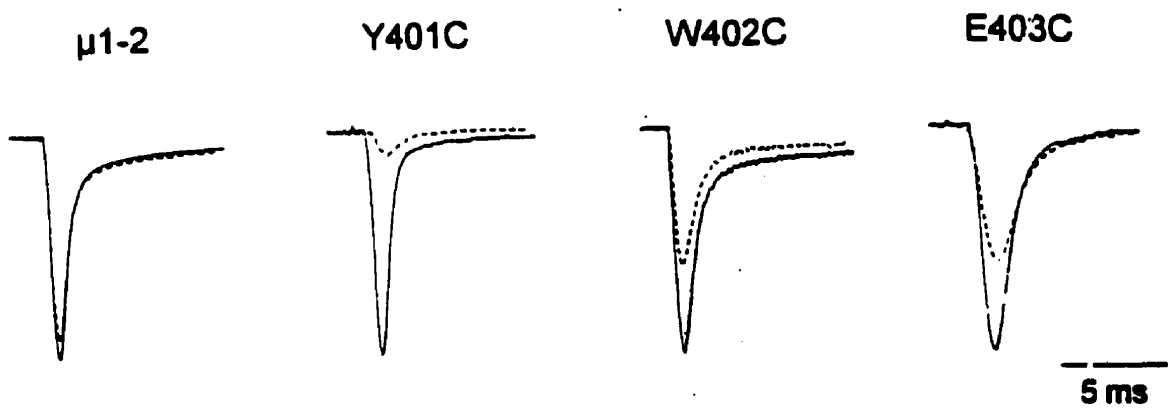
- MTSEA
+ MTSEA

Table 3.1

Dissociation constants (K_D) for Cd^{2+} of WT and mutant Na^+ channels before and after MTSEA modification. Numbers in parenthesis represent the number of determinations. N/A, not applicable. n.e., no expression.

Mutants	IC_{50} (μM)	IC_{50} (μM) after MESEA modification
WT (rSkM1)	$1.8 \pm 0.4 \times 10^3$ (3)	N/A
Y401C	$1.3 \pm 0.3 \times 10$ (5)	$1.6 \pm 0.1 \times 10^3$ (3)
W402C	$2.0 \bullet 0.1 \times 10^2$ (4)	$1.2 \pm 0.1 \times 10^3$ (3)
E403C	$2.8 \pm 0.2 \times 10^2$ (5)	$1.2 \pm 0.2 \times 10^3$ (5)
W756C	$1.6 \pm 0.1 \times 10^3$ (4)	$1.6 \pm 0.4 \times 10^3$ (2)
I757C	$2.0 \pm 0.2 \times 10^2$ (2)	$8.8 \pm 0.7 \times 10^2$ (3)
E758C	$4.9 \pm 0.3 \times 10^2$ (8)	$1.0 \pm 0.1 \times 10^3$ (3)
G1238C	n.e.	n.e.
W1239C	$3.7 \pm 1.0 \times 10$ (3)	$3.2 \pm 0.3 \times 10^2$ (2)
M1240C	$5.7 \pm 0.3 \times 10^2$ (3)	$1.2 \pm 0.1 \times 10^3$ (2)
D1241C	$4.5 \pm 0.5 \times 10^2$ (3)	$1.9 \pm 0.3 \times 10^3$ (3)
A1529C	$3.0 \pm 0.6 \times 10^2$ (3)	$8.0 \pm 0.6 \times 10^2$ (2)
G1530C	$6.8 \pm 0.9 \times 10$ (4)	$1.7 \pm 0.2 \times 10^3$ (3)
W1531C	$4.6 \pm 0.5 \times 10$ (5)	$1.6 \pm 0.3 \times 10^3$ (6)
D1532C	$6.0 \pm 0.7 \times 10^2$ (8)	$2.3 \pm 0.3 \times 10^3$ (2)

of the estimated dissociation constant for the single-cysteine mutants ($K_{D,mu}$) to the wild-type ($K_{D,WT}$) measured before (shaded bars) and after (hashed bars) oxidation with external application of MTSEA (methanethiosulfonate-ethylammonium). Table 3.1 lists the measured dissociation constants (i.e. mean±SE) for the same channels. All channels (except W756C) had significantly (p < 0.01) increased sensitivities to block by Cd^{2+} (i.e. smaller dissociation constants. K_D) compared to WT channels (Figure 3.2B). Extracellular application of MTSEA. which rapidly oxidizes free sulfhydryls forming Cd^{2+} insensitive disulfide complexes (Akabas et al.. 1992; Torchinsky, 1981), abolished high affinity block by Cd^{2+} (Figure 3.2C). This establishes that enhanced Cd^{2+} sensitivity depends on the free sulfhydryls inserted into the pore since Cd^{2+} binds weakly to oxidized sulfhydryls (Torchinsky. 1981). The elimination of Cd^{2+} sensitivity by MTSEA could be readily reversed by the sulfhydryl reducing agent dithiothreitol (DTT) (data not shown) while reduction with DTT did not affect channels not previously exposed to MTSEA. These data suggest a possibility that two, three or four adjacent consecutive P-loop residues might have their side-chains exposed to the external face of the permeation pathway thereby allowing interactions with Cd^{2+} ions. At first glance these results, which are similar to results in other ion channels, (Akabus et al.. 1992; Pascual et al.. 1995; Kurz et al.. 1995; Gross and MacKinnon. 1995; Perez-Garcia et al.. 1995) are difficult to reconcile with α-helical or β-strand 2° structures, assuming P-loops are relatively rigid and immobile. However, as shown below, the assumption of P-loop immobility is not valid on the time-scale of sulfhydryl modification and Cd^{2+} binding. Nevertheless, our findings are consistent with "random-coil" loop structures for P-loops like that observed for active sites in many enzymes (Creighton, 1993; Branden and Tooze. 1991).

A comparison of the $K_{D,mut}/K_{D,WT}$ ratio between different mutants uncovers unexpected differences between residues in homologously aligned locations from distinct P-loops (Figure 3.1). For example, Y401C is exquisitely sensitive to Cd^{2+} in comparison to W756C which has wildtype sensitivity while G1530C has intermediate sensitivity. Furthermore, mutant channels with cysteine replacements at homologous alignment positions in different repeat domains do not generally have similar affinities for Cd^{2+}

binding. These results argue against a symmetrical arrangement of the residues at equivalent alignment locations between P-loops of different domains. In spite of large variations in Cd^{2+}-sensitivity between different single-cysteine mutants. MTSEA was able to access all positions equally as measured by the elimination of high affinity Cd^{2+} block and that whole-cell currents were reduced in all channels. except W756C. following MTSEA treatment. providing additional support for the conclusion that these P-loop residues line the the extracellular face of the pore.

3.4.2 *Double-cysteine substitution of P-loops residues from distinct internal repeat domains*

To discriminate further between various models for the P-loop structure and to obtain detailed 3-dimensional relationships between various pore-lining residues. double-cysteine mutants were created by combining single-cysteine mutants from distinct P-loops. Since coordinated Cd^{2+} binding and disulfide cross-linking of the two nearby inserted cysteines require very restricted geometries (i.e. S- Cd^{2+} bonds are 2.1 Å and S-Cd^{2+}-S angles are 108° while S-S bonds are 2.05 Å and the angle between two Cd^{2+}-S bonds is 70-100°) (Torchinsky, 1981: Careaga and Falke, 1992: Balaji et al.. 1989), these double-mutant channels provide an opportunity to determine detailed structural information on spatial relationship between side-chains of pore residues.

Figure 3.1C illustrates the three potential outcomes expected following insertion of cysteine pairs into the channel pore. First, if the two inserted sulfhydryls are spatially oriented in the correct manner. coordinated Cd^{2+} binding could occur and thereby enhance sensitivity to Cd^{2+} block of current compared to single-cysteine mutants (Vallee and Falchuk, 1993; Cotton and Wilkinson. 1992). Enhanced Cd^{2+} binding results from the stabilization energy derived from the formation of two simultaneous bonds between the Cd^{2+} ion and the two free sulfhydryls as described by equation 3.1 (section 3.3.3). Alternatively, cross-linking of proximal inserted cysteines, which is strongly favored by the oxidizing extracellular environment (Figure 3.2), will create relatively Cd^{2+}-

insensitive channels that are predicted to become Cd^{2+}-sensitive following DTT application. Finally, if the substituted cysteines are far apart. Cd^{2+} will bind independently and, in that case, the dissociation constant for Cd^{2+} block of whole-cell current (i.e. $K_{D,Pre}$) can be predicted from the sensitivity of the single-cysteine mutants as described by equation 3.2 (section 3.3.3). Therefore, when the ratio of the experimentally observed K_D (i.e. $K_{D,OB}$) to $K_{D,Pre}$ is significantly different from 1, evidence for either cross-linking or coordinated Cd^{2+} binding is obtained.

Remarkably, all double-cysteine mutant channels created (except W402C/I757C and those constructed with G1238C) formed functional channels. Figures 3.3A & 3.3B show typical results for Y401C/E758C channels: the measured dissociation constant for Cd^{2+} block ($K_{D,ob}$) for Y401C/E758C channels was 1353 ± 382 μM (mean ± SD, n=7) compared to 12 μM predicted for independent binding (i.e. K_D(Y401C) = 13.7 ± 3.0 μM (n=6) and K_D(E758C) = 454 ± 47 μM (n=7)). Following reduction with DTT, the K_D for Cd^{2+} block decreased about 1200-fold to 1.1 ± 0.2 μM (n=4). In this mutant, reduction by DTT caused an increase in whole-cell currents by about 2.5-fold: DTT-reduction also caused comparatively large increases in whole-cell current and/or conductance in other cross-linked mutants studied. The increase in current invariably occurred in 'ess than 30 s after DTT application. indicating rapid separation of the cross-linked cysteines. Furthermore, reduction with DTT enhanced the sensitivity of cross-linked channels to Cd^{2+} blockade (see below). Subsequent to DTT reduction, Cd^{2+}-sensitive Y401C/E758C channels and other reduced cross-linked double-cysteine channels could be made Cd^{2+}-insensitive again by applying 1 mM MTSEA (data not shown).

Data for the double-cysteine mutants created with Y401C. W402C and E403C are summarized in Figure 3.4, which depicts the ratio of the experimentally measured $K_{D,ob}$ for Cd^{2+} binding to double-cysteine mutant channels divided by the predicted $K_{D,pre}$ before (shaded bar) and after (hatched bar) the application of DTT. Table 3.2 lists the measured $K_{D,ob}$ values (i.e. mean ± SE). Many double mutants showed evidence for disulfide crosslinking: $K_{D,ob}/K_{D,pre}$ was above 1 before DTT and/or decreased significantly after

Figure 3.3

(A) Na⁻ current tracings of Y401C. E75SC and Y401C/E758C mutant channels in response to depolarization to -10 mV from a holding potential of -120 mV before (solid traces) and after (broken traces) the addition of 100 μM Cd^{2+} extracellularly. Na currents for Y401C/E758C channels are shown before and after the addition of DTT.

(B) Dose-response curves of the normalized peak Na⁻ current as a function of the extracellular [Cd^{2+}]. The channels become about 1200-fold more sensitive to Cd^{2-} (K_D changes from 1353 + 382 μM to 1.1 ± 0.2 μM) following the addition of 2 mM DTT.

A

Y401C E758C Y401C / E758C (before reduction) Y401C / E758C (after reduction)

5 ms

B

- ● Y401C
- ▲ E758C
- ■ Y401C / E758C (before reduction)
- ▼ Y401C / E758C (after reduction)
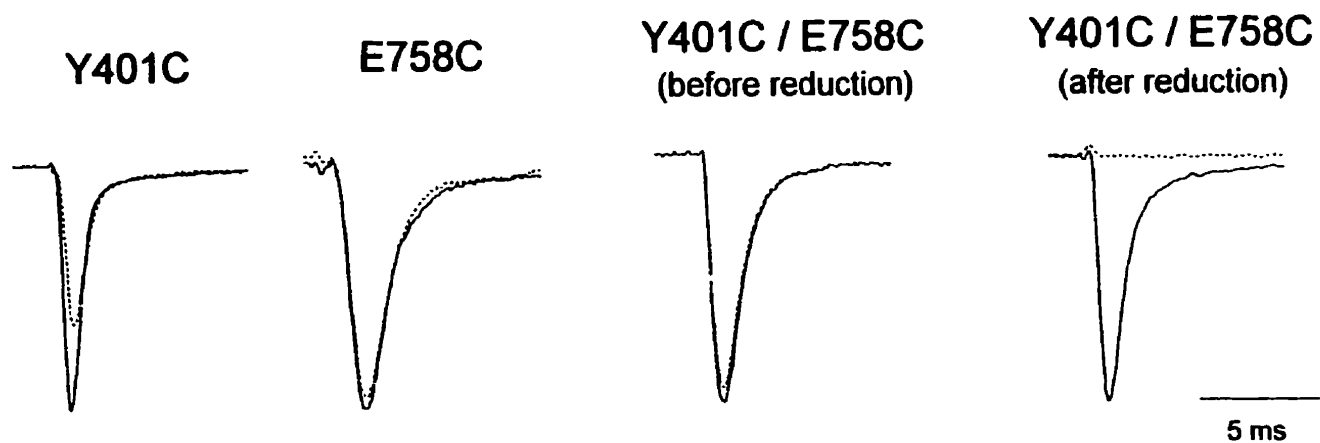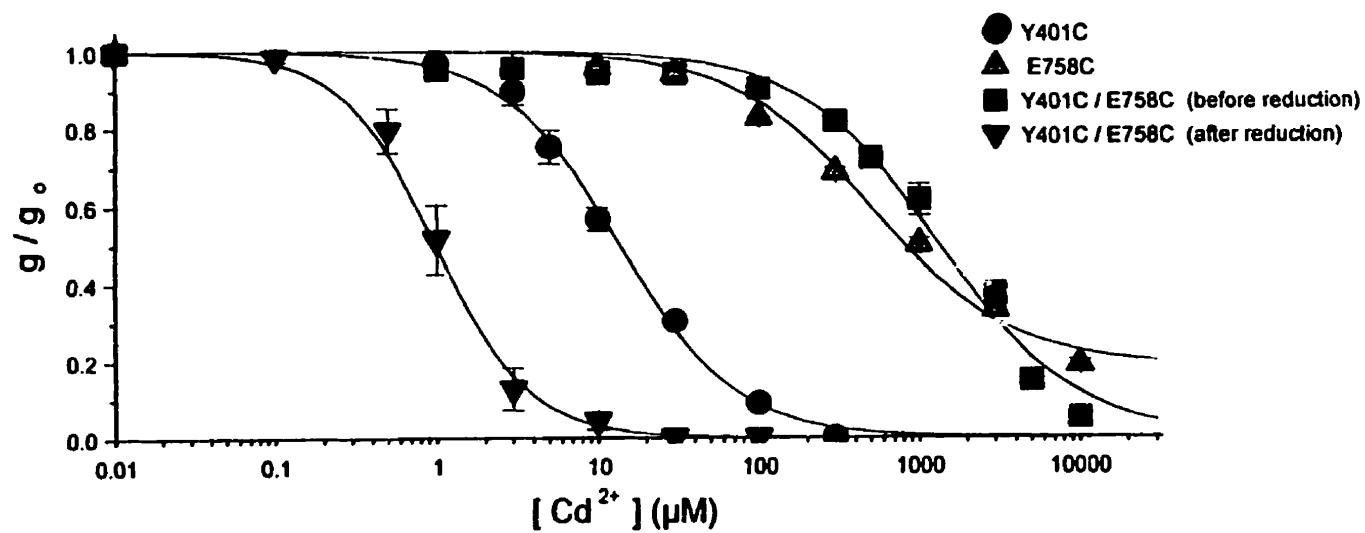
Figure 3.4

Ratios of the predicted dissociation constant. $K_{D,pre}$ to the experimentally observed dissociation constant. $K_{D,ob}$ for all the double mutants studied before (shaded bars) and after (hatched bars) reduction by DTT. $K_{D,pre}$ is estimated from the dissociation constants recorded for the single-cysteine mutant channels assuming independent binding of Cd^{2+} to the inserted cysteines in double-cysteine mutants. (see 3.3). For the mutants with ratios of $K_{D,ob}/K_{D,pre}$ around one, we assume that the two inserted cysteines are binding Cd^{2+} independently. Values of $K_{D,ob}/K_{D,pre}$ substantially below one (the broken lines), suggest coordinated binding of Cd^{2+}. When $K_{D,ob}/K_{D,pre}$, is significantly above one or is decreased below one following reduction. we conclude that the two cysteines are at least partially cross-linked under oxidizing conditions and can coordinately bind Cd^{2+} following reduction.

$$K_{D,pre} = (1/K_D^1 + 1/K_D^2)^{-1}$$
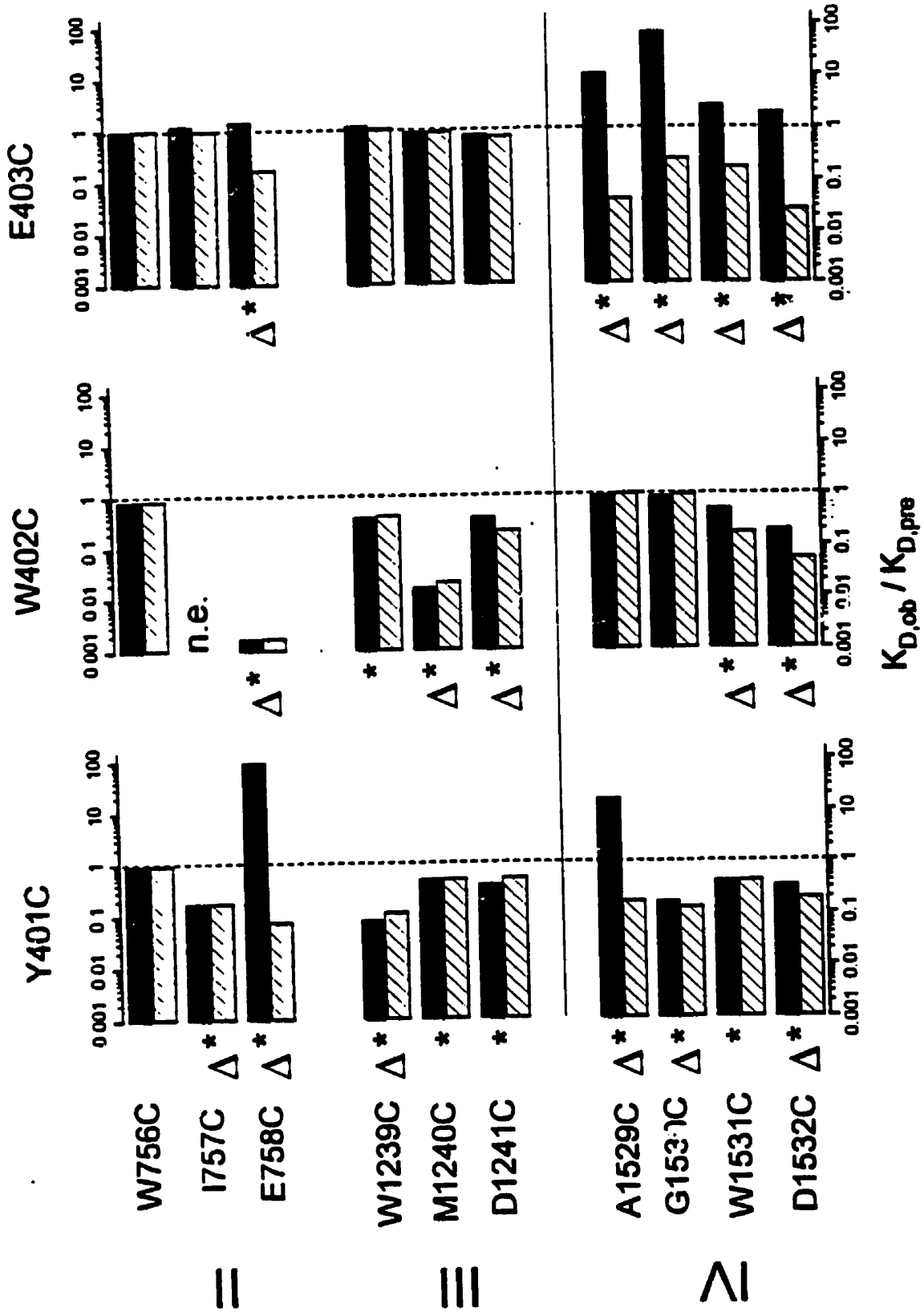
Table 3.2

Dissociation constants (K_D) for Cd^{2+} block of double mutants observed before and after DTT reduction (means ± S.E.M.). Mutants that are statistically different (p<0.05) from the predicted values are indicated by asterisks. Numbers in parenthesis represent the number of determinations. n.e., no expression.

	Y401C OBSERVED K_D (μM)		W402C OBSERVED K_D (μM)		E403C OBSERVED K_D (μM)	
	NON-REDUCED	REDUCED	NON-REDUCED	REDUCED	NON-REDUCED	REDUCED
W756C	$1.2 \pm 0.1 \times 10$ (3)	$1.2 \pm 0.1 \times 10$ (3)	$1.4 \pm 0.1 \times 10^{-7}$ (3)	$1.4 \pm 0.2 \times 10^{-7}$ (2)	$2.4 \pm 0.3 \times 10^{-7}$ (4)	$2.4 \pm 0.2 \times 10^{-7}$ (2)
I757C	2.1 ± 0.4 (5)*	2.1 ± 0.5 (2)*	n.e.	n.e.	$1.4 \pm 0.2 \times 10^{-7}$ (7)	$1.1 \pm 0.3 \times 10^{-7}$ (2)
E758C	$1.2 \pm 0.1 \times 10^{-1}$ (2)*	$9.3 \pm 1.8 \times 10^{-1}$ (5)*	$2.5 \pm 0.7 \times 10^{-1}$ (7)*	$2.5 \pm 1.0 \times 10^{-1}$ (3)*	$1.6 \pm 0.9 \times 10^{-7}$ (5)	$1.9 \pm 0.2 \times 10$ (5)*
W1239C	$7.8 \pm 5.5 \times 10^{-1}$ (5)*	1.1 ± 0.3 (3)*	$1.2 \pm 0.1 \times 10$ (7)*	$1.3 \pm 0.1 \times 10$ (3)*	$3.7 \pm 0.2 \times 10$ (6)	$3.2 \pm 0.2 \times 10$ (3)
M1240C	6.0 ± 0.3 (7)*	6.1 ± 0.1 (2)*	2.3 ± 0.7 (7)*	3.0 ± 0.1 (3)*	$1.6 \pm 0.4 \times 10^{-7}$ (8)	$1.6 \pm 0.3 \times 10^{-7}$ (3)
D1241C	4.7 ± 0.7 (5)*	6.3 ± 0.6 (4)*	$5.2 \pm 0.6 \times 10$ (9)*	$2.8 \pm 0.3 \times 10$ (4)*	$1.3 \pm 0.1 \times 10^{-7}$ (9)*	$1.2 \pm 0.2 \times 10^{-7}$ (3)*
A1529C	$2.1 \pm 0.5 \times 10^{-2}$ (4)*	2.1 ± 0.1 (3)*	$1.1 \pm 0.5 \times 10$ (3)	$1.2 \pm 0.2 \times 10$ (3)	$1.5 \pm 0.1 \times 10^{-7}$ (7)*	5.9 ± 1.8 (7)*
G1530C	1.8 ± 0.6 (7)*	1.4 ± 0.4 (2)*	$4.4 \pm 0.5 \times 10$ (7)	$4.8 \pm 0.8 \times 10$ (2)	$3.6 \pm 1.7 \times 10^{-1}$ (6)*	8.3 ± 1.2 (5)*
W1531C	4.2 ± 1.0 ( )*	4.2 ± 0.8 (3)*	$1.9 \pm 0.3 \times 10$ (8)*	6.4 ± 0.9 (3)*	$9.7 \pm 5.0 \times 10$ (7)*	6.4 ± 1.0 (6)*
D1532C	4.2 ± 1.4 (7)*	2.4 ± 0.3 (4)*	$3.0 \pm 1.0 \times 10$ (6)*	7.9 ± 3.6 (4)*	$5.1 \pm 1.6 \times 10^{-2}$ (5)	7.2 ± 2.6 (4)*

DTT application in E403C/E758C, A1529C, G1530C, W1531C, D1532C, and Y401C/E758C, A1529C channels. We conclude that the inserted sulfhydryls in these double mutants are able to approach one another to within 2.05 Å under oxidizing conditions. Following the application of 10 mM DTT for 8-10 min, cross-linked double mutants became ultra-sensitive to Cd^{2+} application compared to the corresponding single mutants indicating an ability to coordinately bind Cd^{2+}. Double mutants having $K_{D,ob}/K_{D,Pre}$ ratios significantly (p<0.05) below 1 in the presence of DTT are indicated by asterisks (*) in Figure 3.4. The double-mutants with $K_{D,ob}/K_{D,Pre}$, ratios less than 0.37, which corresponds to stabilization energies above 1 kT, are labeled with triangles (Ranganathan et al., 1996). Stabilization energies above 1 kT are deemed sufficient in magnitude to clearly identify pairs of side-chains capable of "cross-talking" or interacting by coordinately binding Cd^{2+} and therefore having their sulfur atoms approach one another to within 3.5 Å (Shaw et al., 1992; Torchinsky, 1981; Careaga and Falke, 1992; Balaji et al, 1989). Inspection of Figure 3.4 shows remarkable patterns for interacting pairs of residue side-chains, suggesting considerable pore flexibility. For example, E403C cross-talks with 4 adjacent consecutive P-loop residues in D-IV while Y401C talks with the same residues although the stabilization energy was slightly below 1 kT for the Y401C/W1531C mutant. On the other hand, E758C and D1532C can communicate with three consecutive residues in D-I. Both Y401C and W402 are rather promiscuous, cross-talking with residues in all other domains, often with multiple consecutive residues. Assuming no major disruption of the channel pore by double-cysteine replacement and after addition of sulfhydryl reactive agents, these results are inconceivable for pore models assuming fixed alignments between P-loops regardless of the underlying secondary structure and strongly suggest that Na^+ channel pores, like the active-site in many enzymes, are highly flexible (Creigton, 1993; Pompliano et al., 1990; Elofsson et al., 1991; Larson et al., 1995; Lan et al., 1995; Nicholson et al., 1995).

Even for relatively unstructured domains, like loop regions and random coils, geometric and steric constraints prevent side-chains of three consecutive residues from simultaneous interacting with a single site without backbone motion and flexibility

(Creighton. 1993). The amount of movement required to account for our observations depends on the local secondary structure assumed but. for extended loop structures. requires residues to translate a minimum of 7 Å over-and-above that allowed by side chain motion. Similar large amplitude excursions and long-ranged collective motions have also been observed in more ordered α-helical structures in proteins with known crystal structures (Careaga and Falke. 1992) using a similar double-cysteine strategy. Figure 3.4 further shows that. in reduced channels. the $K_{D.ob}/K_{D.Pre}$ ratio follows clear patterns which are well illustrated by mutants involving W402C with domain IV: $K_{D.ob}/K_{D.Pre}$ is lowest for W402C/D1532C and progressively increases towards W402C/A1529C. This pattern suggests that Cd^{2+} coordination occurs most optimally for W402C interacting with D1532C and becomes increasingly more difficult for adjacent residues. probably due to the increased channel distortion required to trap the Cd^{2+} ion. Therefore. in spite of the large degree of P-loop flexibility in domain IV, W402 appears to interact preferentially with D1532. suggesting that W402 is physically closer to D1532 than to other D-IV residues. This preferential interaction pattern of a P-loop residue with specific residues in other domains is generally observed. Therefore, we can tentatively identify pairs of P-loop residues from distinct domains which are most closely aligned with one another. Generally, pairs of residues deemed as nearby neighbors are rarely at equivalent positions in the putative alignment sequence (Figure 3.1). For example from the above arguments. W402 is judged to be most closely aligned with E758 in D-II. M1240 in D-III and D1532 in D-IV, none of which match the alignment sequence shown in Figure 3.1B. This lack of correspondence between P-loop residues located at homologous locations in the different repeat domains of the Na^+ channel are consistent with previous single-channel results in single cysteine mutant Na^+ channels (Chiamvimonvat et al., 1996).

99

3.4.3 Underlying mechanism for the enhanced Cd²⁺ sensitivity in double-mutant channels

Single-channel recordings (Figure 3.3C) were used to establish the mechanism underlying the enhanced Cd^{2-} sensitivity of reduced Y401C/E758C mutants. Figure 3.5 shows typical single-channel recordings at −80 mV for Y401C, E758C, and reduced Y401C/E758C channels recorded from inside-out cell attached patches in the absence (A) and presence (B) of Cd^{2-}. All recording were made in the presence of 10 mM fenvalerate, which maintains Na^+ channels in the open state for tens to hundreds of milliseconds (Backx et al., 1992). For Y401C channels, Figure 3.5B shows representative single-channel sweeps measured in the presence of 5 µM Cd^{2-} in the pipette. Notice the discrete flicker blockade of the unitary current in Y401 channels (i.e., represented by O) often lasting several milliseconds which was not observed in the absence of Cd^{2-}. Cd^{2-} totally occludes the passage of Na^- ions (i.e., represented by C) consistent with Cd^{2-} binding within the permeation pathway. The corresponding blocking-time histogram, illustrated in Figure 3.5C, could be adequately fit by a mono-exponential function, as expected if a single Cd^{2-} binding site exists within the pore. The estimated average block-time of Cd^{2-} ions within the pore (i.e., equal to the estimated time constant for the mono-exponential fit of the block-time histogram) was 1.43 ms for this Y401C (average 1.36 ± 0.12 ms, n = 3).

By contrast, E758C channels have a very different signature with respect to Cd^{2-} block. In the presence of 400 µM Cd^{2-}, E758C channels also show discrete reductions of unitary currents but these channels are blocked to a subconductance level establishing that Cd^{2-} binding to the channel does not fully prevent the passage of Na^- ions (Figure 3.5B). The corresponding blocked-time histogram in Figure 3.5C was well fit with a mono-exponential function demonstrating that only a single Cd^{2-}-binding site exists within the pore of these channels. The average residence time estimated for the E758C patch shown in Figure 3.5B was 2.4 ms (average 2.21 ± 0.19 ms, n = 3).

Figure 3.5

Single-channel recordings of Y401C, E758C and reduced Y401C/E758C mutant channels following fenvalerate application at -120 mV (Backx et al., 1992).

(A) Currents recorded in Y401C, E758C, and Y401C/E758C channels in the presence of 10 μM fenvalerate which is added to maintain the channels in the open state for tens to hundreds of milliseconds.

(B) Currents recorded in Y401C and reduced Y401C/E758C mutants channels with 5 μM extracellular Cd^{2+} and in E758C channels with 400 μM Cd^{2+}. Cd^{2+} caused full closures of the Y401C and Y401C/E758C channels while blocking E758C channels to a sub-conductance level (closed level indicated by the broken line). In the presence of 5 μM Cd^{2+} the double-mutant channel Y401C/E758C displayed bursts of short-lived blocking events separated by long-lived blocking events not seen in either single-mutant. These long-lived blockages likely represent the "trapping" of the Cd^{2+} ion as a result of simultaneous interactions with the two free sulfhydryl groups.

(C) The mean block-time histograms are shown for the channels illustrated in A for Y401C, E758C, and Y401C/E758C channels. The blocked-time histograms could be adequately fit using a mono-exponential equation for Y401C and E758C channels, while a bi-exponential function was required for Y401C/E758C channels. Note: the same axes are different in the different panels. See text for further details.

(D) The mean unblocked-time (i.e., open-time) histogram is shown for the same channels illustrated in B. For Y401C, E758C, and Y401C/E758C channels the unblocked time histogram could be adequately fit using a mono-exponential function.
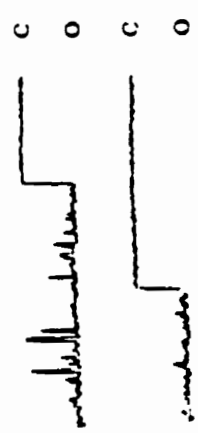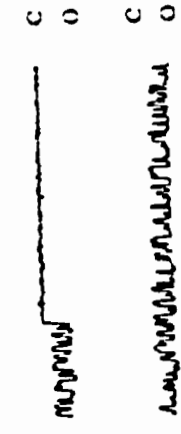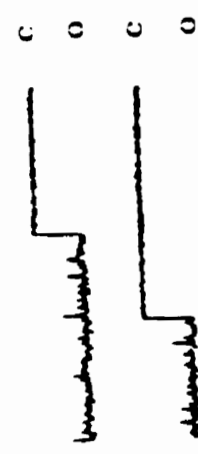
Y401C   E758C   Y401C/E758C
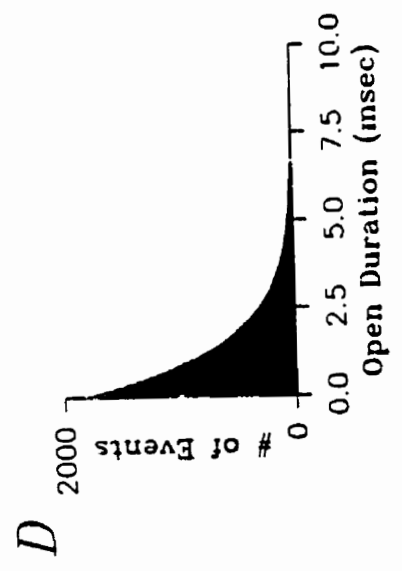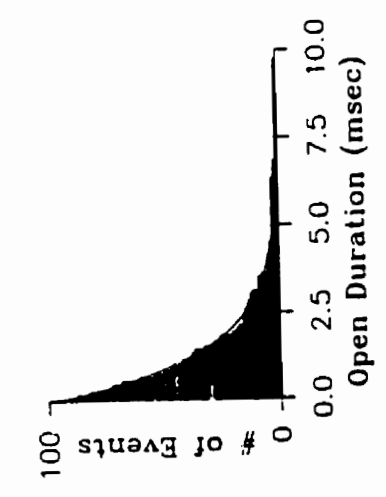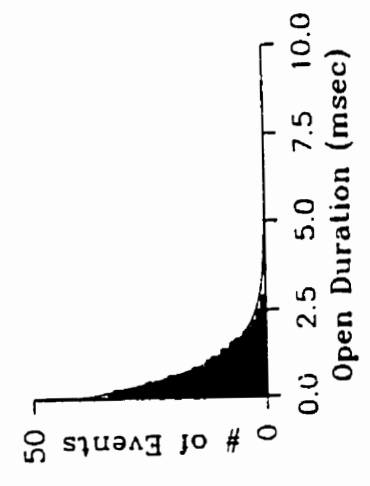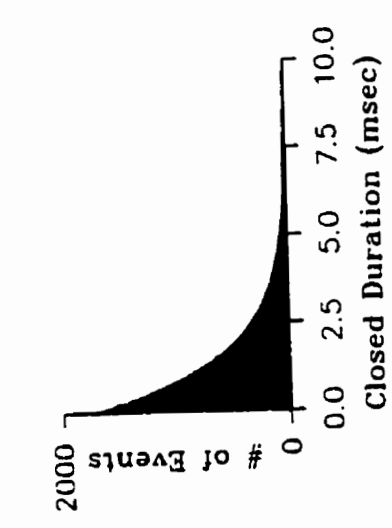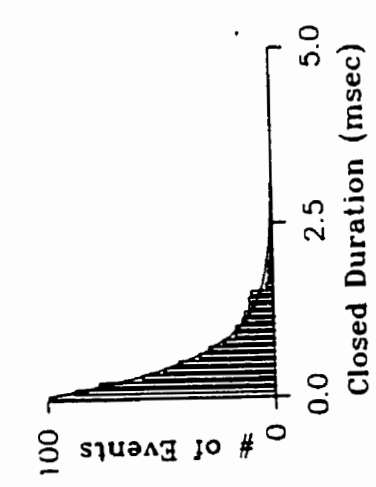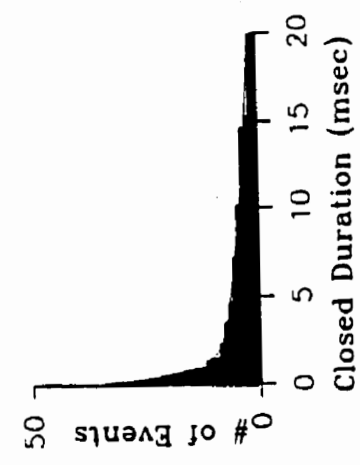
By comparison with the corresponding single-cysteine mutant channels, reduced Y401C/E758C channels showed a very different blocking pattern. As depicted in Figure 3.5B, 5 μM Cd^{2+} caused complete interruptions of the unitary currents through reduced Y401C/E785C channels, like Y401C channels. However, simple inspection reveals that in these channels there are two distinct blocking times: repeated rapid closures are separated by very long-lived closures. As a result of these long closures, very little current passes through the channel in the presence of 5 μM Cd^{2+}, accounting for the very low dissociation constant measured for these channels following reduction (Fig. 3B). The presence of two distinct blocking times is confirmed in Fig. 5 C which shows that adequate fitting to the blocked-time histogram required a bi-exponential function. The two estimated mean blocking times for this Y401C/E758C channel in the presence of 5 μM Cd^{2+} were 0.91 ms and 13.53 ms (average 1.10 ± 0.05 ms and 13.91 ± 0.09 ms, n = 3).

The presence of two distinct blocking times in reduced Y401C/E758C channels reveals the presence of two binding sites or two binding states of the channel. It is important to note that the smaller mean blocking time (i.e., 1.10 ms) in Y401C/E758C channels is similar to the mean blocking time Y401C channels (i.e., 1.32 ms) and that these short closures in Y401C/ E758C channels fully occlude the unitary current as in Y401C channels. Therefore, it seems plausible that the rapid flicker blocking observed in the double-cysteine mutant channel are associated with Cd^{2+} binding to the inserted cysteine at position 401. This assertion is further bolstered by the absence of subconductance levels in the presence of Cd^{2+} and by the measured mean unblocked-time histograms (i.e., open-time histograms). Specifically, Fig. 5 D shows that in the presence of only 5 μM Cd^{2+} the mean unblocked-time for the Y401C and Y401C/E758C channels was 1.32 ms (average 1.22 ± 0.24 ms, n = 3), respectively, while in the presence of 400 μM Cd^{2+} the mean unblocked-time for E758C channel was 1.37 ms (average 1.21 ± 0.13 ms, n = 3). These mean unblocked-times yield estimates of the second-order rate constants for Cd^{2+} binding to the channels; for Y401C, E758C, and Y401C/E758C channels the second order rate constants for Cd^{2+} binding to the pore were 2.44 x 10^8 $M^{-1}s^{-1}$

^{1}. 3.0×10^6 M^{-1}s^{-1}. and 2.1×10^8 M^{-1}s^{-1}, respectively. Thus it would appear that the rate of Cd^{2+} binding to the inserted cysteine at position 758 is too slow to contribute to the rapid blocking observed in Y401C/E758C channels exposed to 5 μM Cd^{2+}.

The very long average block-times (i.e.. 13.91 ms) observed in Y401C/E758C channel are never observed in either of the corresponding single-cysteine mutants. Therefore, it seems likely that these events represent a novel binding state of the channel and probably represent coordinated trapping of the Cd^{2+} ion by simultaneous binding to C401 and C758 residues. Single-channel analysis on Y401C, E758C, and reduced Y401C/E758C channels reveals the probable kinetic events involved in simultaneous Cd^{2+} binding to the two pore cysteine side-chains: Cd^{2+} binds multiple times (i.e.. average 3.4 times) to a single-cysteine residue (probably Y401C) for short durations followed occasionally by Cd^{2+} trapping as a result of simultaneous binding to C401 and C758 residues. Thus these observations provide direct information on the frequency of the interaction of these two residues within the pore in the process of trapping a Cd^{2+} ion and demonstrate that models describing Cd^{2+} interactions with pairs of cysteine residues must consider both independent and simultaneous Cd^{2+} binding to the available sulfhydryls.

3.4.4 *Relationship of P-loop flexibility to channel function*

While the data in Figure 3.4 suggests P-loop flexibility, the functional importance of pore motion on channel behavior, as previously postulated (Lauger, 1987; Eisemnan and Hom, 1983; Eisenman. 1984), remains speculative. The presence of cross-linkages for a number of double cysteine mutants provides a unique opportunity to further investigate the significance of pore motion. Indeed, we expect cross-linked channels to have reduced pore flexibility and motion compared to the same channels following reduction with DTT. As an example, Figures 3.6A and 3.6C show raw current traces following depolarization to -10 mV from a holding potential of -120 mV for E403C/D1532C and E403C/A1529C before (□, O) and after (■, ●) disruption of the disulfide linkage with DTT. DTT application caused about a 2-fold and 6-fold increase

Figure 3.6

Effect of cross-linking on conductance and selectivity properties of double-cysteine mutants.

(A) Raw current traces following depolarization to -10 mV from a holding potential of -120 mV for E403C/D1532C channels expressed in oocytes before (□) and after (■) reduction with DTT. Note the nearly 2-fold increase in current after reduction at this voltage.

(B) The corresponding current-voltage relationships for E403C/D1532C. In this particular mutant, there is little change in the channel's conductance (161 µS before and 156 µS after DTT), estimated from the slope of the current-voltage curve at voltages above 0 mV, but the reversal potential is shifted by 19 mV to the right following reduction with DTT.

(C) Raw traces for E403C/A1529C before (○) and after (●) the application of DTT. The current increased more than 6-fold following reduction with DTT.

(D) The current-voltage relationship for E403C/A1529C mutants shows a 5-fold increase in slope at voltages above 0 mV (22 AS before and 97 AS after DTT) while the reversal potential is only slightly shifted rightward (7 mV) by reduction with DTT.

A

E403C/D1532C

2 μA

2 ms

B

□ Oxidized
■ Reduced

I (μA)

8

4

-4

-8

V (mV)

-60

-30

30

60

C

E403C/A1529C

2 μA

2 ms

D

○ Oxidized
● Reduced

I (μAj

2

-2

-4

-6

V (mV)

-60

-30

30

60
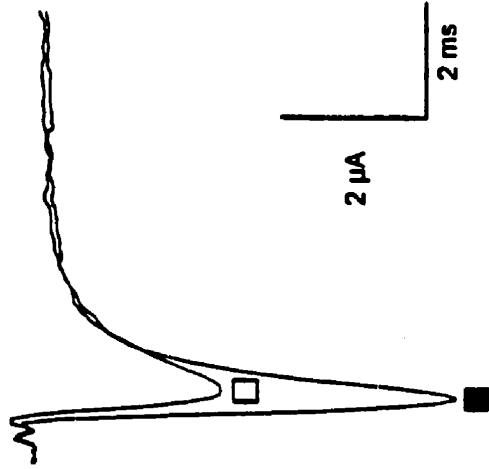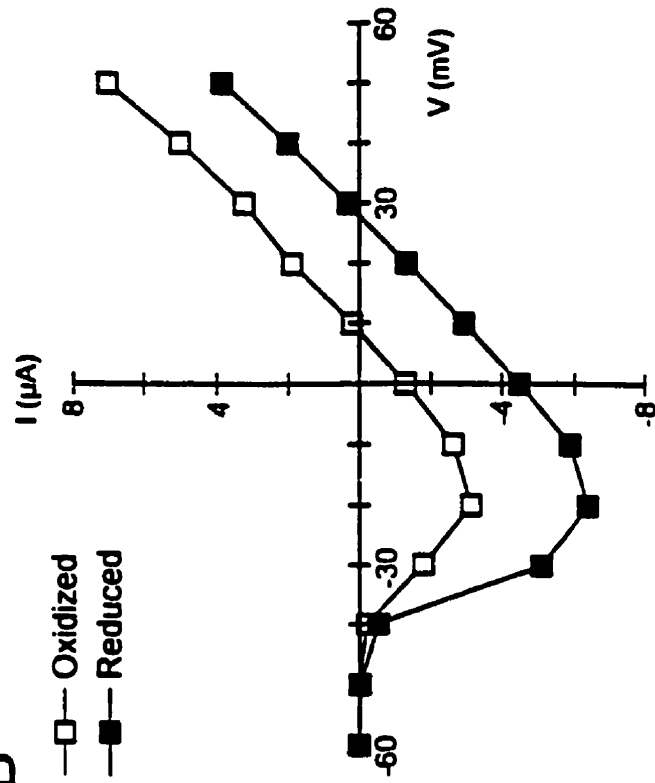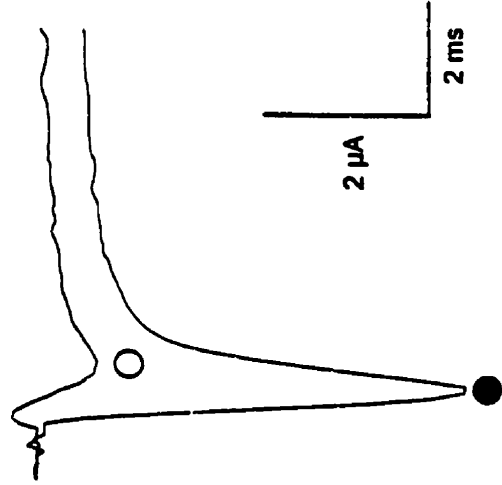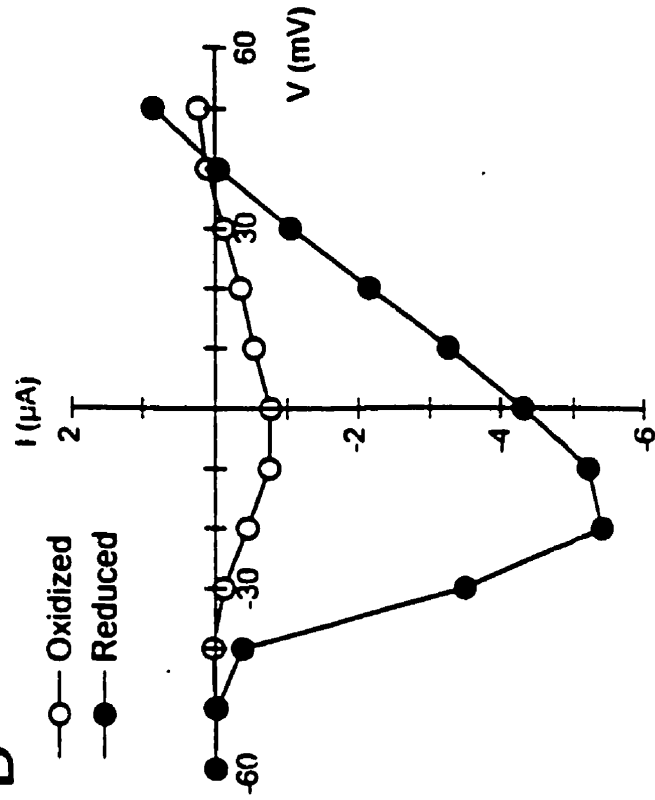
TABLE 3.3

The changes in the reversal potential before and after treatment with 10 mM DTT in cross-linked double-cysteine mutant channels

Channels	E_{rev} (-DTT)	E_{rev} (+DTT)	Observations
Wild-type	55.7 ± 3.6 mV	55.2 ± 2.9 mV	6
Y401C/E758C*	36.9 ± 7.5 mV	54.3 ± 8.5 mV	3
E403C/A1529C*	31.1 ± 4.9 mV	40.5 ± 4.2 mV	4
E403C/G1530C*	11.7 ± 6.7 mV	42.1 ± 7.4 mV	3
E403C/D1532C*	12.6 ± 6.1 mV	31.1 ± 6.6 mV	5

* significantly different before and after DTT application ($p < 0.05$)

in peak current for E403C/D1532C and E403C/A1529C respectively. indicating that these double-mutant channels are less capable of conducting current in the oxidized, cross-linked state versus the reduced state. The increase in whole-cell current following DTT exposure is not solely due to subtle changes in channel gating as illustrated in Figures 3.6B and 3.6D which shows the current-voltage relationships for the corresponding mutants before (□, O) and after (■, ●) the application of DTT. Not only is the peak of the current-voltage relationship significantly affected by DTT but the reversal potentials were also shifted: from 8 mV to 27 mV for E403C/D1532C and from 34 mV to 41 mV for F403C/A1529C following DTT application. Average shifts in reversal potential for 4 double-cysteine mutants studied are summarized in Table 3.3. Significant rightward shifts in reversal potential were observed in all cross-linked double mutants. in which it was studied. following reduction with DTT indicating that the channels are less selective when channel motion is reduced by cross-linking. Furthermore after reduction. the measured reversal potential closely matched the reversal potential observed in the least selective of the corresponding single-cysteine mutants. Changes in selectivity following reduction could not be studied in cross-linked double mutant channels involving cysteine replacements at position W1531 since W1531C channels are non-selective by themselves (Tsushima et al., 1997). Finally, the increase in whole-cell current for the cross-linked double-mutants shown in Figure 3.4 ranged from 1.8-fold to 8-fold following DTT exposure (data not shown). These results illustrate that both ionic selectivity and conductance for double-mutant channels are strongly influenced by the relative flexibility of the P-loops. The potential importance of dynamic pore relaxation in channel function is further supported by the observation that mutations in domain IV. which appears to be the most flexible domain. changes selectivity properties, compared to wild-type channels. more profoundly than other domains (see Chapter 4). It is interesting that the P-loop in D-IV. which appears to be the most flexible (Figure 3.4), has two glycines (Figure 3.1) which are the most permissive residues for backbone flexibility (Creighton. 1993). Alternatively, cross-linking of cysteine pairs could cause sufficient distortion of the P-loop structure to interfere with ion selectivity and permeation.

3.5 Discussion

3.5.1 Differences in Cd^{2+} binding affinity of single cysteine mutants and structural implications of the pore

Many previous studies have assessed side-chain accessibility and local secondary structure of pore-forming regions in channels using cysteine-scanning mutagenesis by examining the pattern of accessibility of residues to reaction to sulfhydryl probes (Akabas et al., 1992; Gross and MacKinnon, 1995; Kurz et al., 1995; Pascual et al., 1996). In our experiments, all the single-cysteine mutant channels created, except W756C, (Figure 3.1) showed enhanced sensitivity to block by extracellular application of Cd^{2+} when compared to wild-type channels. The enhancement of Cd^{2+} sensitivity in the single-cysteine mutants relative to WT channels ranged from no enhancement for Y401C channels. The basis for the variation in Cd^{2+} sensitivity between different single-cysteine mutant channels can be traced to differences in Cd^{2+} binding rates, unbinding rates or both. For example, Y401C is about 50-fold more sensitive to Cd^{2+} block than 758C, which results from a 100-fold faster Cd^{2+} binding rate (Figure 3.5D) and a 2-fold faster Cd^{2+} unbinding rate (Figure 3.5C) for Y401C compared to E758C channels. Alternatively, the difference in the Cd^{2+} binding affinity between Y401 and W402C can be traced primarily to a 40-fold increase in the Cd^{2+} unbinding rate form W402C channel compared to Y401C (Tomaselli et al., 1995). Generally, we found that both on- and off-rates for Cd^{2+} binding to the pore varied between different single-cysteine mutants as reported previously (Chiamvimonvat et al., 1996). The underlying molecular basis for these differences could relate to a number of factors such as variations in the dehydration/hydration rate, differences in the coordination of Cd^{2+} binding between mutants or varying degrees of exposure of the reactive sulfhydryls to the aqueous phase of the pore.

All single-cysteine mutant channels (except W756C) reacted with externally applied MTSEA which reduced, or eliminated, the enhanced Cd^{2+} sensitivity relative to WT channel. MTSEA application reduced the measured whole-cell current by varying

amounts (i.e.. 0.5- fold to 4-fold) in a time-dependent fashion for all the single-cysteine mutants except W756C. The rate of current reduction following MTSEA application varied between mutants, but the current invariably reached steady-state in less than 3 min. Thus all residues accessible to Cd^{2+} could be readily modified by MTSEA.

Our results confirm that multiple consecutive residues in the P-loops of all four domains have their side-chains exposed to the Na^+ channels pore (Chiamvimonvat et al.. 1996; Perez-Garcia et al., 1996). At first glance. these findings suggest that the secondary structure of these P-loops are not α-helices or β-strands as concluded by previous studies in Na^+ (Perez-Garcia et al.. 1996) and K^+ channels (Gross and MacKinnon. 1995; Kurz et al.. 1995; Pascual et al.. 1995; Soman et al.. 1995). However. conclusions based on cysteine-scanning studies have often implicitly assumed that the pore is a static structure which, as discussed below, may not the case for P-loops in Na^+ channels.

3.5.2 *Double-cysteine mutagenesis reveals a flexible pore*

Identification of interacting pairs of inserted cysteines in distinct P-loops of the Na^+ channel pore revealed a pattern which cannot be explained by static pore structures. Regardless of the secondary structure of P-loops in Na^+ channel pores, geometric and steric constraints prevent side-chains of three or four consecutive residues in a given P-loop from simultaneous coordinately binding Cd^{2+} with a single residue in another P-loop without backbone motion and flexibility (Creighton, 1993). The amount of movement required to account for our observations depends on the local secondary structure assumed but, for extended loop structures. requires residues to translate a minimum of 7 Å over-and-above that allowed by side chain motion. These estimates were obtained from simulations of random coils structures using the program HyperchemTM (Hypercube Inc., Waterloc. Canada), where the minimal distance which sulfur atoms on cysteine side-chains of four consecutive residues are required to translate in order to interact with a single point was examined. Therefore, our double-cysteine substitution

experiments in Na⁻ channels establish that, on the time-scale of Cd^{2-} binding and coordination shown in Figure 3.5, (i.e., several milliseconds), the P-loops are flexible structures, particularly for the P-loops in D-I and D-IV. As a results, experiments with single cysteine mutant Na⁻ channels, using techniques involving irreversible modification of inserted cysteines (which occurs on a time-scale of milliseconds), makes it difficult to make definitive conclusions regarding the secondary structure or membrane-sideness of pore-forming domains since some residues side-chains could be exposed to both faces of the channel for varied periods of time with flexible P-loops. These limitations a e expected to be particularly serious when using aqueous-soluble covalent modifiers of free sulfhydryls since these agents could irreversibly trap the channel in a subset of reactive conformational states available to the channel pore which might not reflect the average or important conformations available for normal channel function. The above reasoning might also provide an alternative explanation for the ability of sulfhydryl reagents applied to the outer or inner face of the channel to modify cysteine-substituted P-loop residues in cyclic nucleotide-gated channels (Sun et al., 1996).

Another related limitation of our experimental approach using single- and double-cysteine replacements as a strategy for unraveling pore structure, imposed by the existence of P-loop flexibility, is the possible existence of induced fits. For example, Cd^{2-} binding to single-cysteine mutant channels, coordinated Cd^{2-} binding within the pore of double-cysteine mutant channels and disulfide linkages are expected to energetically induce conformations which distort the normal molecular channel architecture of the pore required for normal ion permeation and selectivity thereby misrepresenting actual significant structures necessary for ion permeation and selectivity. This distortion is anticipated, despite the similarity between the ionic size between Na and Cd^{2-} for the inserted free sulfhydryls. However, it is equally possible that Cd^{2-}-trapped configurations of the channel reflect pore conformations, which are important for ion permeation and selection. Such Cd^{2-}-bound conformations, resulting from P-loop flexibility, might be equivalent to the induced fit required by many enzymes for specific substrate binding and catalysis (Creighton, 1993). In addition, cross-linked channels still produce functional

channels suggesting that the overall normal organization of the pore is not unduly distorted by such trapped channel conformations. Finally, pore flexibility could also promote induced fitting of channel pores when tightly binding to toxins thereby complicating the interpretation of experiments designed to examine relationships between pore residues using interactions with high affinity toxins (Gross and MacKinnon, 1995; Hidalgo and MacKinnon, 1995; Naranjo and Miller, 1996; Ranganathan et al., 1996).

Following reduction of double-cysteine mutant channels with DTT, channel currents were invariably increased (Figure 3.6). In principle, the rate of re-oxidation could be used as a measure of the proximity of the inserted cysteine pairs (Careaga and Falke, 1992; Benitah et al., 1996; Krovetz et al., 1997). However after DTT washout, currents did not decrease noticeably over periods lasting greater than 10 min in the presence of ND96 solutions for any of double mutant channels. In addition, the Cd^{2+} dose-response curves, which routinely took greater than 20 min to record, could be adequately fit with a binding equation assuming a single binding site. Had partial re-oxidation taken place during the time-course of these experiments under our recording conditions, the Cd^{2+} dose-response curves should show evidence for the existence of two types of binding sites, one for oxidized channels and one for reduced channels, which was not observed. Recently, Benitah et al (1997) examined the rates of disulfide formation of double-cysteine engineered Na^+ channels in the presence of the redox catalyst copper phenanthroline [$Cu(phen)_3$] to reflect thermal motions of the inserted cysteines and demonstrated that disulfide bonding between these residues is wide-spread within the channel pore yet in a spatial-specific manner. Moreover, disulfide formation is highly temperature-dependent implying bond formation is indeed the result of molecular collision between the cysteinyl thiols, which is a dynamic process. They conclude from these experiments that extensive motion exists within the P-segments thereby further reinforcing our model.

The mechanism of Cd^{2+} coordination as illustrated in Figure 3.5 reveals that Cd^{2+} trapping by a pair of cysteines does not occur each time the Cd^{2+} ion enters the pore. In

the case of the Y401C/E758C channel. it appears that Cd^{2+} binds in bursts followed by long-lived closure events. It seems probable that the bursts involve Cd^{2+} binding to single cysteines inserted in the pore while the long-lived blocking events reflect coordinated trapping of the Cd^{2+} ion by the two inserted cysteines. Therefore. the kinetic model which best explains coordinated Cd^{2+} binding in our double-cysteine experiments is:

$$O_{401}:O_{758} + Cd^{2+} \leftrightarrow O_{401} - Cd:O_{758}$$

$$\updownarrow \qquad\qquad \updownarrow$$

$$O_{401}:O_{758} - Cd \leftrightarrow O_{401} - Cd:O_{758}$$
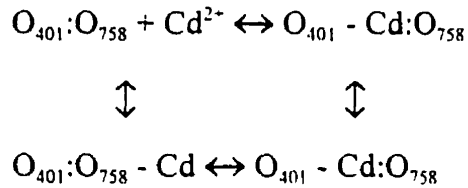
Where $O_{401}:O_{758}$ is unblocked channel. $O_{401}-Cd:O_{758}$ is the channel with a Cd^{2-} bound to the Y401C position. etc. Our experimental results demonstrate that $O_{401}:O_{758}$ – Cd is rarely formed. as suggested by the absence of subconductance blocking events because the rate constant for Cd^{2+} binding to the E758C channels is about 100-fold slower than for Y401C channels. From these observations it is clear that Equation 3.2. which is the correct dissociation constant for the formation of state $O_{401}-Cd:O_{758}$, does not correctly predict the experimentally observed dissociation constant for Cd^{2+} binding to the double-cysteine mutants as assayed by examining Cd^{2+} block of the whole-cell current.

3.5.3 Pore flexibility and channel functions

The previous discussion highlights some practical experimental limitations which arise as a result of P-loop flexibility in Na^+ channels, but is flexibility important for Na^- channel pore function (i.e.. conductance and selectivity properties)? In other words. is flexibility observed in double-cysteine experiments relevant on the time-scale of ions permeating the Na^- channel? The active sites of many well-studied enzymes. including diffusion-limited enzymes. are comprised of intrinsically flexible random coils or loop structures which have intrinsically more flexibility than more ordered secondary structures like α-helices or β-strands (Branden and Tooze, 1991; Stone et al., 1992:

Creighton. 1993; Wade et al., 1993; Arnold et al., 1994). Flexibility is essential for catalytic activity by influencing substrate binding. specificity. and sequestration (Welch et al., 1982; Branden and Tooze. 1991; Tanaka et al., 1992; Cottrell et al., 1995; Lan et al., 1995; Larson et al., 1995) as well as stabilization of intermediate transitional states (Fresht. 1985). Indeed. computer modeling and dynamic measurements of the active sites in numerous enzymes and peptides have identified critical dynamic motions in flexible loop structures of large amplitudes occurring on picosecond to nanosecond time-scales (Stone et al., 1992; Wade et al., 1993; Arnold et al., 1994) which is considerably faster than ion permeation in channels. By analogy the flexible P-loops in Na^+ channels might play similar roles. The possibility of pore flexibility is consistent with dynamic models of channel pores. used previously to describe gramicidin (Eisenman and Horn. 1983) and acetylcholine channels (Eisenman. 1984). wherein ion permeation requires motion of both channel pores and ions (Lauger, 1987). Dynamic behavior could also explain "multi-ion" behavior of Ca^{2+} channels (Lauger, 1987), which appear to have only a single cation binding-site (Ellinor et al., 1995). The potentially important role of flexibility in pore function is supported by a number of observations: (a) current decreased by as much as eight-fold whereas selectivity for Na^+ versus K^+ was impaired in many cross-linked channels (Table 3.3). (b) mutations in domain IV. which appear to be the most flexible. changed selectivity properties more profoundly than other domains (Tsushima et al., 1997). and (c) inspection of amino acid sequence of P-loops reveals that the P-loop in D-IV (i.e., GWDG) has a very high probability of forming a relatively flexible β-turn loop structure (Creighton. 1993).

From statistical thermodynamic theory, it is clear that the magnitude of structural fluctuations depends directly on the time-scale of the observations, the likelihood of observing energetically unfavorable, large structural fluctuations depends directly on the length of the observation period. Indeed, large amplitude excursions and long-range collective motions have been previously observed in ordered α-helical structures in proteins with known crystal structures (Careaga and Falke, 1992) using a similar double-cysteine strategy where rates of disulfide (i.e., seconds to minutes time-scale) were used

114

as measures of motion and flexibility. Since Cd^{2+} binding in our experiments occurs on a time-scale which is three-orders of magnitude slower than ion permeation, relatively large fluctuations in energy, and thus structure, will be surveyed by our Cd^{2+} coordination studies. However, channel flexibility (and therefore frequency of side-chain interactions) is probably under-estimated in our experiments because disulfide formation and coordinated Cd^2 binding require very restricted geometry (Torchinsky, 1981; Balaji et al. 1989; Careaga and Falke, 1992) and require many molecular collisions for reactions to occur (Careaga and Falke, 1992). Nevertheless, the kinetics of cross-linking (Torchinsky, 1981; Careaga and Falke, 1992) and Cd^{2+} coordination are too slow in comparison to the permeation process (sub-microsecond time-scale) (Hille, 1992) to allow direct conclusions regarding the role of channel flexibility in ion permeation and selectivity.

Finally, P-loop flexibility might reflect or be related to gating-dependent changes since channel gating usually occurs on a millisecond time-scale as does Cd^{2+} coordination. Indeed, movement in the pore of voltage-gated K^+ channels occurs during C-typed inactivation (Yellen et al., 1994). More recently P-loop motion has been directly measured in voltage-gated K^+ (Liu et al., 1996) and cyclic nucleotide-gated channels (Sun et al., 1996) using sulfhydryl modification. However, in our studies, the gating properties of cross-linked double-mutant channels was not noticeably altered compared to reduced or SkM1 channels.

3.5.4 K^+ channel pore versus Na^+/Ca^{2+} channel pores

Doyle et al (1998) have recently reported a crystallographic picture of the pore of a primitive K^+ channel which comprises of two transmembrane seg..ents supporting a rigid pore as proposed in the original molecular sieve model. The picture shows that the pore is constructed of an inverted teepee with the selectivity filter, of 12 Å in length, held at its wide end. They have also demonstrated, using electron density maps obtained from Rb^+ and Cs^+-containing solutions, that the selectivity filter contains an inner and an outer ion binding sites located at opposite ends of the filter about 7.5 Å apart These results

provide the first direct physical evidence that multiple ions can dwell in the K⁻ channel pore (i.e. multi-ion pore). Strong electrostatic interactions between ions in the filter thereby allow rapid ion conduction. Furthermore. these data suggest that the K⁻ selectivity filter is lined by carbonyl oxygen atoms from the signature sequence to provide multiple closely spaced sites for dehydration of the permeating ions with very limited stretch. These results are in full support of the classical biophysical views of ion permeation through the K⁻ channels.

The question that remains is whether the same architecture of the K⁻ channel pore is applicable in their Na⁻ and Ca^{2-} channel counterparts. There are several factors that need to be considered to answer this question. Firstly, Na⁻ and Ca^{2-} channels might employ different mechanisms for ion permeation than K⁺ channels. For example, it has been demonstrated that it is the carboxylate side chains of each of the four glutamate residues provided by multiple internal repeats of the Ca^{2-} channel α_1 subunits that form the dehydration site for permeating Ca^{2-} ions (Yang et al.. 1993) while K⁻ channels contain the carbonyl oxygens from the GYG signature sequence (Doyle et al., 1998). Moreover, each of the four glutamates contribute differently to ion permeation suggesting an asymmetrical arrangement of this ring of residues (Kim et al., 1993; Yang et al., 1993; Yatani et al., 1994: Ellinor et al., 1995) similar to that of the Na⁻ channel (Chiamvimovat et al., 1996). This is obviously not the case for the K⁻ channels, which display a clear four-fold symmetry arise from identical homomeric subunits (Doyle et al., 1998; Kreusch et al., 1998). In addition, though multi-ion behavior observed in K⁺ channels is clearly the result of multiple ion occupancy in the channel pore as demonstrated in crystallography (Doyle et al., 1998), no such evidence has yet been demonstrated in the Na⁻ and Ca^{2-} channels which also display apparent multi-ion behavior (Degenisich, 1987; Friel and Tsien. 1989; Yue and Marban, 1990; Rosenberg and Chen, 1991). In other words, other mechanisms may be responsible for such observed multi-ion behavior in the latter channels. For example, a single high affinity site for only one permeating ion which is also capable of interacting weakly with a second incoming ion can explain the phenomena (Armstrong and Neyton, 1992; Kuo and Hess, 1993). Alternatively, a high

affinity binding site for the permeating ion flanked by two low-affinity binding sites, with or without electrostatic interactions between these sites, is equally well to explain many of the observed so-called multi-ion behavior (Dang and McCleskey, 1998).

At first glance, it seems difficult to reconcile the high throughput rates of channel pores with such single high-affinity binding sites since as affinity for an ion increases, the ion's exit rate is expected to decrease in the same proportion to the increased occupancy of the site (Bezanilla and Armstrong, 1972). However, rapid rates of ion entry and exit from a pore can also be achieved by stepwise dehydration and rehydration of the permeating ions as a result of stepwise replacement of the chemical groups from the channel responsible for ion coordination (i.e. the glutamate carboxyls in the case of the Ca^{2+} channels). This scenario is in turn consistent with our flexibility model of the Na^+ channel pore and that proposed for the glutamate residues of the Ca^{2+} channels (Yang et al., 1993; Ellinor et al., 1995).

Also consistent with these theories, multi-ion behaviors of Na^+ and Ca^{2+} channels may not arise from pores composed of multiple discrete high-affinity ion binding sites which require mutual electrostatic repulsion between these sites to propel rapid ion permeation as previously proposed (Hess and Tsien, 1984; Almers and McCleskey, 1984; Tsien et al., 1987; Begenisich, 1987) because if multiple sites exist, single mutations of certain residues (e.g. glutamates of Ca^{2+} channel; lysine and tryptophan of Na^+ channel) are expected to shift only ion's affinity or reduce selectivity but not entirely abolished as observed (Yang et al., 1993; Kim et al., 1993; Ellinor et al., 1995; Sun et al., 1997). Furthermore, as demonstrated in the Ca^{2+} channels, Ca^{2+} ions bind at the same location of the pore whether it arrives from the outside or the cytoplasmic side as judged from the voltage dependence of Ca^{2+} block (Kuo and Hess, 1993) also supports a single binding site. Single binding site in turn requires flexibility to promote rapid ion conduction.

Lastly, Na^+ and Ca^{2+} channels are likely to exclude unwanted ions by involving mechanisms more than a simple molecular sieve, if itself does play a role. For example,

as demonstrated in the Na⁺ channel, mutations of residues comprise of the putative selectivity filter (i.e. DEKA locus, see also Chapter 4 for details) are expected, from the molecular sieve theory, to introduce a "big hole" within the channel pore thereby allowing permeation of bigger molecules otherwise impermeable. However, the selectivity mutants, while permeating big organic molecules such as tetramethyammonium (TMA), dimethylammonium (DMA) and methylammonium (MA), etc., are also blocked by the small guanidinium toxin tetradotoxin (TTX), which shares similar chemical structure as the above mentioned compounds and is expected to permeate through the channel if the filter is a simple molecular sieve (Sun et al., 1997). Another piece of evidence against a simple molecular sieve theory is that the bigger TMA permeates better than other smaller molecules such as DMA and MA which are all of the same basic chemical geometry but differ only in the size of their side chains. This again argues that relative permeability is not inversely related to the molecular size in a simple fashion and permeation of these molecules are likely to involve other interactions with the channel (Sun et al., 1997). Recent structural analysis of the DEKA locus using double-cysteine mutagenesis and cross-linking strategy, as we employ in this chapter, to probe proximity between these residues have further confirmed that these amino acids do not form a molecular sieve (Bennitah et al., 1997). Overall, it is likely that combinations of the above mentioned theories are responsible for ion permeation in Na⁺ and Ca²⁺ channels. Crystallography and further functional studies of these channels will be required to prove or disprove these hypotheses.

3.5.5 Conclusion

Our studies demonstrate that P-loops in Na⁺ channels are flexible structures on the time-scale of Cd²⁺ coordination of double-cysteine mutant channels. Clearly, nonstatic behavior of Na⁺ channel pores must be considered in evaluating structure-function studies using cysteine substitutions combined with sulfhydryl reactive probes. Further studies will be required to assess the contribution of pore flexibility to channel properties like ion permeation, selectivity, and channel gating.

3.6   *Acknowldegements*

I would like to thank Dr. Peter Backx for preparing the original manuscript published in *J. Gen. Physiol.* 110:59-72, Dr. Robert Tsushima for his numerous assistance during the entire course of this study, and Dr. Camie Chan for editing some of this chapter.

CHAPTER 4

THE ROLE OF P-LOOP RESIDUES IN IONIC SELECTIVITY

4.1 *Abstract*

Knowing that the Na⁺ channel pore is highly flexible and that flexibility may be important for selective translocation of Na⁺ ions, we next seek for correlation between channel flexibility and ion permeation by examining the influence of P-loop residues on the properties of ionic selectivity using single cysteine Na⁺ channel pore mutants. Selectivity sequence of WT and mutant channels was determined and compared by measuring current ratios of whole-cell currents in *Xenopus* oocytes in the presence of various monovalents and divalents as the only extracellular cations. WT rSkM1 channels displayed an ionic selectivity sequence Na⁺>Li⁺>NH₄⁺>>K⁺>>Cs⁺ and were impermeable to divalent cations. Replacement of residues in domain IV showed significantly enhanced current and permeability ratios of NH₄⁺ and K⁺, resulting in negative shifts in the reversal potentials recorded in the presence of external Na⁺ solutions when compared to WT and cysteine mutants in domains I, II and III (except K1237C). Mutants in domain IV showed altered selectivity sequences: W1531C (NH₄⁺>K⁺>Na⁺≥Li⁺≈Cs⁺), D1532C and G1533C (Na⁺>Li⁺≥NH₄⁺>K⁺>Cs⁺). Conservative replacement of the aromatic residue in domain IV (W1531) with phenylalanine or tyrosine retained Na⁺ selectivity of the channel while the alanine mutant (W1531A) reduced ion selectivity. A single mutation in domain III (K1237C) dramatically altered the selectivity sequence of the rSkM1 channel (NH₄⁺>K⁺>Na⁺≥Li⁺≈Cs⁺), and was permeable to divalent cations having the selectivity sequence Ca²⁺≥Sr²⁺>Mg²⁺>Ba²⁺. Sulfhydryl modification of K1237C, W1531C or D1532C with methanethiosulfonate derivatives that introduce a positively-charged ammonium group, large trimethylammonium moiety or a negatively-charged sulfonate group within the pore was ineffective in restoring Na⁺ selectivity to these channels. Selectivity of D1532C mutants could be largely restored by increasing extracellular pH suggesting a change in the ionized state at this position influences selectivity. These data suggest that K1237 in domain III and W1531, D1532 and G1533 in domain IV play a critical role in determining

the ionic selectivity of the Na⁺ channel. While mutations of domain IV residues displayed more pronounced effects in selectivity than residues from other domains. DIV is also the most flexible domain. This coincidence suggests a possible correlation between pore motion and ion selectivity.

4.2   *Introduction*

Voltage-gated Na⁻ channels are critical in the excitability of muscle and nerves They conduct Na⁻ ions across membrane bilayers at a rate of over 10^6 ions per second while still being able to selectively discriminate between Na⁻ ions and other physiological cations such as K⁻ and Ca^{2-} (Hille. 1992). This property is crucial for generating the electromotive forces required for electrical signaling. Even though several regions of the channel protein that control ion current have been identified, the underlying molecular basis for selectivity remains obscure.

The cloning of various ion channels and the development of site-directed mutagenesis has allowed examination of the molecular structure of the channel protein. Many voltage-gated ion channels are comprised of four homologous domains, each consisting of six transmembrane spanning regions (Catterall. 1995). The four domains merge to form a barrel-like structure with pore-forming region extending into the membrane (Catterall, 1995). The pore region was first shown to be located between the fifth and sixth transmembrane regions in K⁻ channels (Hartmann et al., 1991; Yellen et al., 1991; Yool and Schwartz, 1991). Further studies revealed that the conduction pathway of the Na⁻ channel was located in the same region (Backx et al., 1992; Heinemann et al., 1992). Regardless of this similarity, Na⁻ channels differ from other voltage-gated ion channels in their high selectivity for Na⁺ (Hille, 1992). Systematic mutations of residues within the pore region have revealed residues important for selectivity and permeation of voltage-gated K⁻ channels (Yool and Schwartz. 1992; Heginbotham et al., 1992; Taglialatela et al., 1993) and the L-type Ca^{2-} channel (Kim et al., 1993; Mikala et al., 1993; Yang et al., 1993). Similar studies in the rat brain II Na⁻ channel have suggested four amino acids (aspartate,

121

glutamate, lysine and alanine), one in each of the four pore segments, form the putative selectivity filter (Terlau et al., 1991; Heinemann et al., 1992). Neutralization of the negatively-charged aspartate and glutamate residues in the first and second repeat, respectively, drastically reduced Na^+ flux (Terlau et al., 1991), while conversion of the lysine and alanine residues in the third and fourth domain, respectively, to glutamate resulted in a channel that was more selective for Ca^{2+} over Na^+ (Heinemann et al., 1992). However, the involvement of other residues within the Na^+ channel pore to Na^+ selectivity and permeation has not been extensively examined.

In the previous chapter, I have demonstrated that the Na^+ channel pore is highly flexible and that flexibility may be important for selective translocation of Na^+ ions (cf. Figure 3.6 & Table 3.3). Here we looked for correlations between channel flexibility and ionic selectivity by examining the influence of amino acids within the pore region on the properties of ionic selectivity using cysteine scanning mutagenesis. In brief, we have identified three other residues (W1531, D1532 and G1533), all in the fourth domain, that significantly alter Na^+ selectivity but are not part of the proposed putative selectivity filter (D400, E755, K1237, A1529). Coincidentally, domain IV is the most flexible domain based on the double cysteine mutant data that I presented in Chapter 3. These results suggest that other residues, especially the ones in domain IV, are important in determining the ionic selectivity of the Na^+ channel and further implicate that channel flexibility may correlate ionic permeation and selectivity.

4.3   *Materials and Methods*

4.3.1   *Electrophysiology*

The control recording solution was ND96 (section 2.7). For examining the ionic selectivity of the rSkM1 and mutant channels, NaCl was replaced with equimolar monovalent (Cs^+, K^+, Li^+, NH_4^+) or divalent cation (Ba^{2+}, Ca^{2+}, Mg^{2+}, Sr^{2+}) (as the Cl^- salt) adjusted to pH 7.6 with the corresponding hydroxide salt or Tris. Substitution of NaCl with

122

equimolar divalent cation salts results in an increase in hypertonicity of the solution. Adjustments were not made to account for this change. To prevent endogenous Ca^{2+}-activated Cl^- current activity, either niflumic acid (1 mM) was included in the extracellular divalent solutions to block the Cl^- currents or the oocytes were injected with 1 mM BAPTA. All recordings were made within the first 10 min after initially voltage clamping the oocyte to the holding potential of -120 mV

Sulfhydryl modification by the methanethiosulfonate (MTS) derivatives (Toronto Research Chemical Co., Toronto, Canada), MTSEA (MTS-ethylammonium), MTSES (MTS-ethylsulfonate), MTSET (MTS-ethyltrimethylammonium) or MTSEB (MTS-ethylbenzoate; gift from Dr. A. Wooley) was performed by exposing the cysteine mutants to 1 mM MTS-X for 3 min followed by a 5 min washout. Modification of the cysteinyl sulfhydryl side-chain was irreversible (Akabas et al., 1992) and verified by examining the altered Cd^{2+} sensitivity. The MTS derivatives were prepared daily and dissolved in the recording solution.

To examine the effects of extracellular pH, the external bath solution consisted of (in mM) 96 NaCl, 1 BaCl$_2$, 1 MgCl$_2$ and 5 HEPES, Tris or MES (adjusted with NaOH or HCl to the desired pH).

4.3.2 *Determination of Current and Permeability Ratios*

Current ratios were determined by the ratio of peak inward current in the presence of extracellularly applied tested cations to the peak inward current in the presence of Na^+. Permeability ratios (P_X/P_{Na}) for a given cation were calculated using a modified Goldman-Hodgkin-Katz equation (Hille, 1992):

$$E_X - E_{Na} = k \ln (P_X [X]_{outside} / P_{Na} [Na]_{outside}) \qquad \text{Equation 4.1}$$

where E_X and E_{Na} are the reversal potentials observed with the tested cation (X) and Na⁻. respectively. k = RT/zF where z is the valence of the tested cation, and R is the gas constant (8.314 V C K⁻¹ mol⁻¹). T is the temperature in Kelvin and F is the Faraday's constant (9.648*10⁴ C mol⁻¹). Both current and permeability ratios can provide equivalent interpretations of ion selectivity (Eisenman and Horn, 1983). Reversal potentials and slope conductance were calculated by fitting the current-voltage relationship to a Boltzmann distribution function:

$$I = [(V_t - V_{rev}) * G_{max}]/[1 + exp((V_t - V_{1/2})/k)] \qquad \text{Equation 4.2}$$

where I is the peak I_{Na} at the given test potential V_t. V_{rev} is the reversal potential. G_{max} is the maximal slope conductance. $V_{1/2}$ is the half-point of the relationship and k (=RT/zF) is the slope factor.

Data presented are the means ± SEM. Statistical significance was determined using an unpaired Student's *t* test with p<0.05 representing significance.

4.4   *Results*

Although Na⁻ channels are highly selective for Na⁻, they permit permeation of other cations (Hille, 1992). We examined the relative ionic selectivity of the wild-type rat skeletal muscle Na⁺ channel (rSkM1) expressed in *Xenopus* oocytes to varying monovalent and divalent cations. Figure 4.2A shows whole-cell recordings of rSkM1 in the presence of equimolar Na⁻, Li⁻, NH₄⁻, and K⁺ containing solutions with the corresponding current-voltage relationship shown in Figure 4.2B. The rSkM1 Na⁻ channel was highly permeable to Na⁻ and Li⁻, exhibiting substantial inward currents (Figure 4.2A) compared with NH₄⁻ and K⁻. Since we are unable to control the intracellular ionic milieu of the oocyte, we are uncertain of the ionic species responsible for the outward current. No detectable inward currents were observed in the presence of Cs⁻ or the divalent cations (data not shown). These data give a selectivity sequence of Na⁻>Li⁺>NH₄⁻>>K⁺>>Cs⁺ based on current ratios.

Figure 4.1

Structural topology of the Na⁻ channel α subunit. The shaded area within the pore-forming domains denotes the region mutated in the present study. The putative amino acid alignment sequence for the four pore regions as shown by the single letter amino acid code is given below. The residues in capital letters were mutated to cysteine. The location of each residue within the primary sequence of the rSkM1 Na⁻ channel is shown below each amino acid letter.
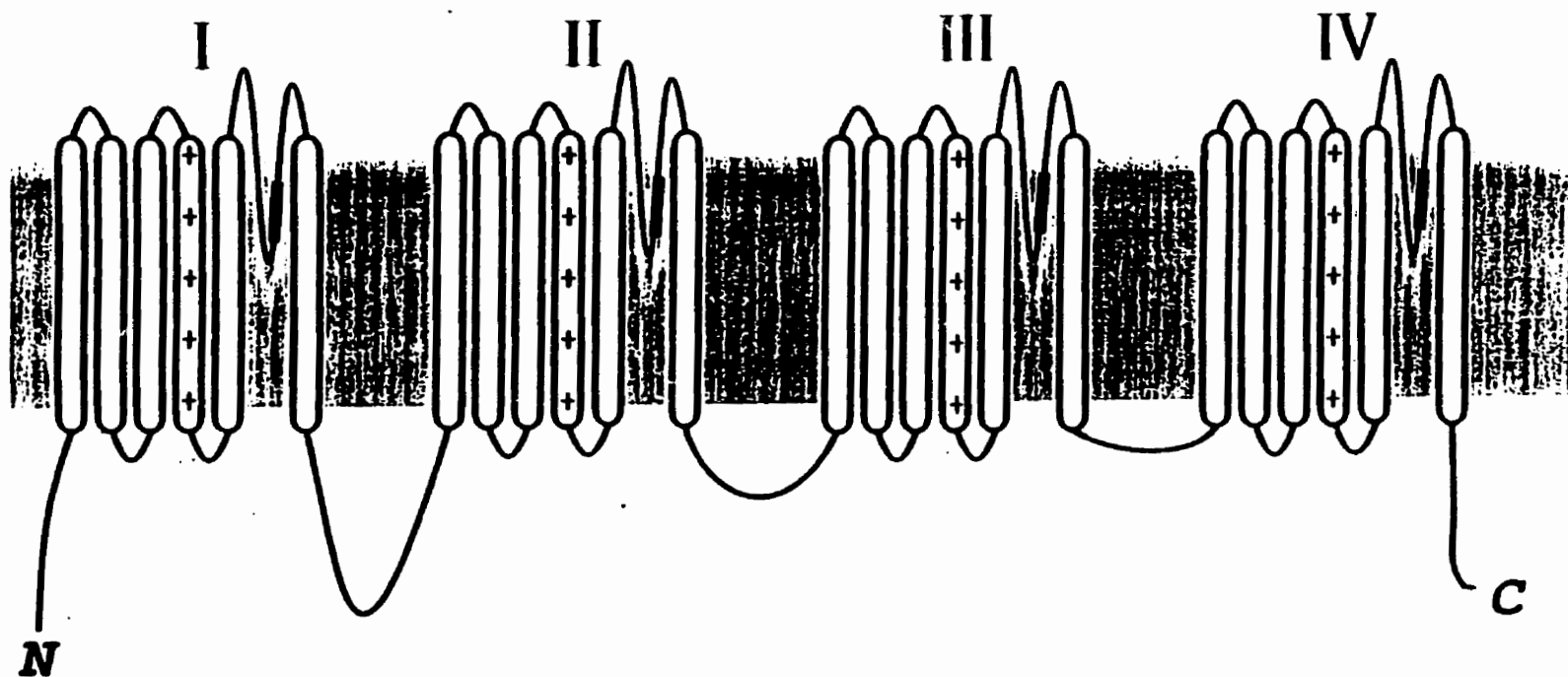
Domain I   q *D Y W E* n
              400 401 402 403

Domain II g *E W I E* t
              755 756 757 758

Domain III f *K G W M D*
              1237 1238 1239 1240 1241

Domain IV s *A G W D G*
              1529 1530 1531 1532 1533

Figure 4.2.

Ion selectivity of the rSkM1 Na⁻ channel.

A) Whole-cell recordings of the rSkM1 Na⁻ channel in the presence of 96 mM NaCl, LiCl, NH₄Cl and KCl solutions. Oocytes were depolarized between -60 to +50 mV from a holding potential of -120 mV. Currents traces displayed are from -50 to +40 mV in 10 mV increments. Currents were corrected for leak and capacitance current. B) Current-voltage relationship of the same oocyte shown in A) for Na⁻ (square), Li⁻ (circle), NH₄⁻ (diamond) and K⁻ (triangle). The data were fit to a Boltzmann distribution as described in the Methods.
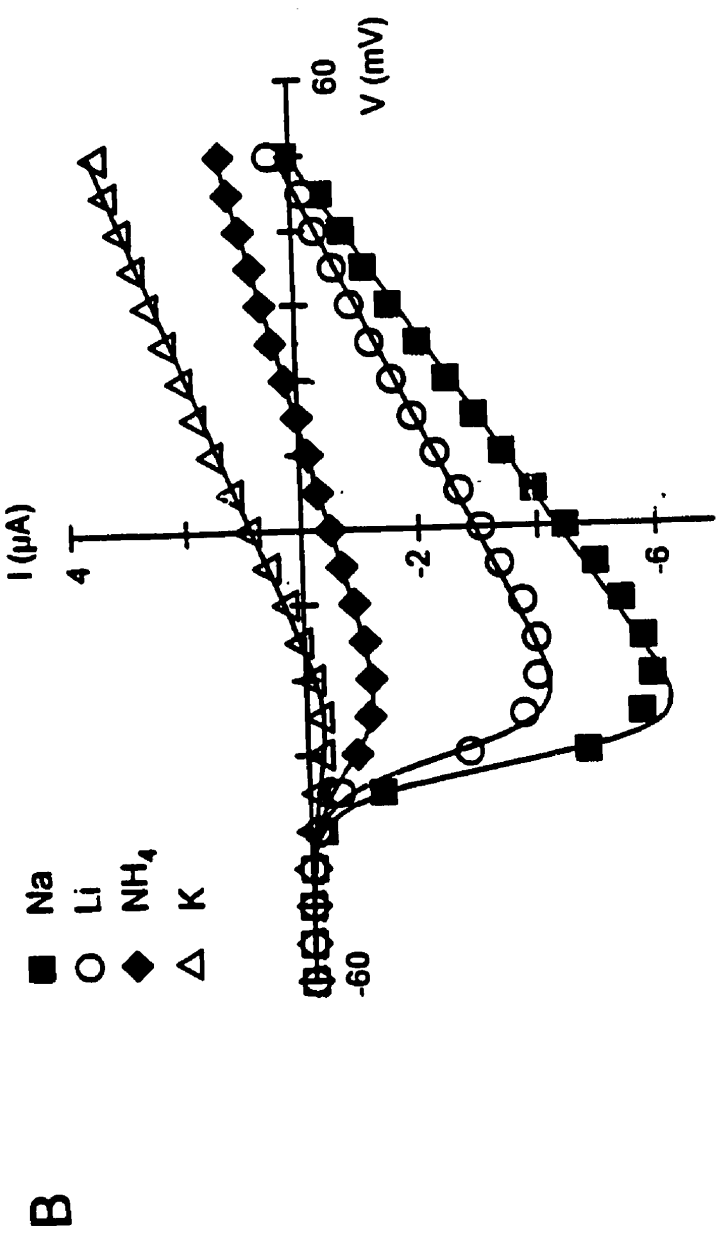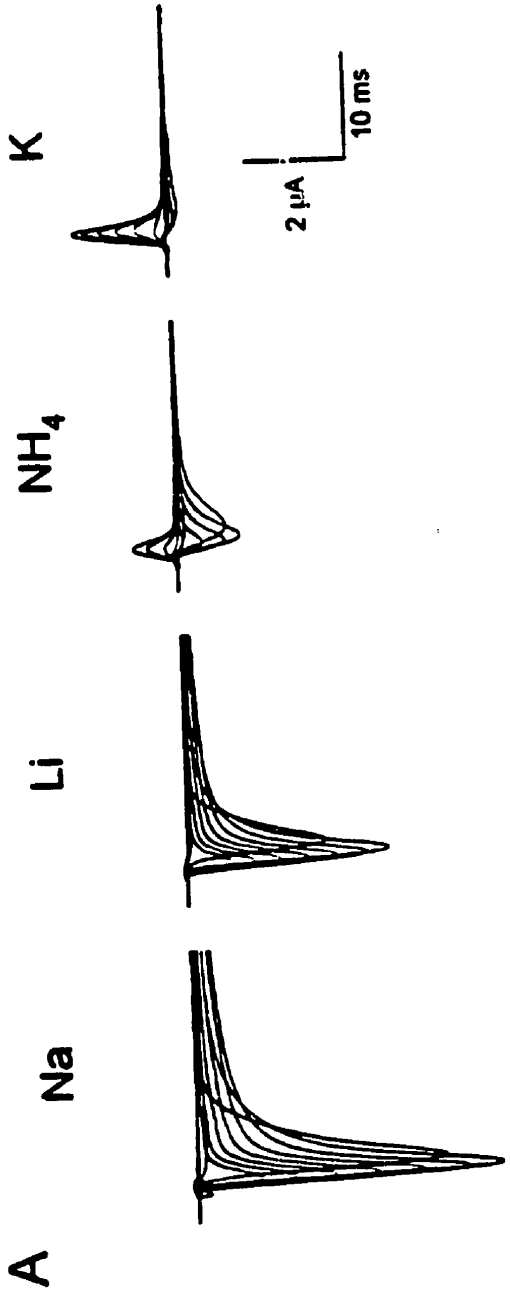
TABLE 4.1

Ionic Current and Permeability Ratios of rSkM1. Ionic current and permeability ratios of rSkM1 for Li^+, NH_4^+, K^+ and Cs^+. Current ratios were calculated from peak inward currents in the presence of tested cation normalized to the peak current in Na^+ solution. Permeability ratios were calculated from reversal potentials using a modified Goldman-Hodgkin-Katz equation as described in the Section 4.2. Values represent the mean ± SEM from 5 oocytes.

	Current Ratio	Permeability Ratio
P_{Li} / P_{Na}	0.79 ± 0.07	0.97 ± 0.06
P_{NH4} / P_{Na}	0.16 ± 0.07	0.17 ± 0.02
P_K / P_{Na}	0.03 ± 0.01	0.05 ± 0.01
P_{Cs} / P_{Na}	< 0.01	0.02 ± 0.01

These findings are very similar to those reported for native Na⁻ channels (for review, see Hille, 1992) and heterologously expressed Na⁻ channels (Heinemann et al., 1992; Chiamvimonvat et al., 1996a,b) using either current ratio or permeability ratio measurements. Current and permeability ratio measurements for rSkM1 gave comparable values and the same relationship regarding ion selectivity of rSkM1 (Table 4.1).

4.4.1 Ionic selectivity of cysteine mutants

We next examined the contribution of the pore-forming residues to ionic selectivity. The amino acids at the carboxyl end (SS2) of the four pore regions were mutated to cysteine (Figure 4.1). We chose to mutate the amino acids to cysteine because of the small size and intermediate polarity (Creighton, 1993), but more importantly, it allows the determination of the spatial orientation of the residues within the pore using Cd^{2+} or sulfhydryl modifying agents as probes (Akabas e. al., 1992; Kürz et al., 1995; Pascual et al., 1995; Li et al., 1996; Pérez-García et al., 1996). All cysteine mutants expressed functional channels with the exception of G1238C in domain III, suggesting no major structural changes to the channel protein. We implicitly assumed that only those residues which face into the aqueous pore region, and thereby are able to interact directly with the permeating ion, will be able to influence ion selectivity. It is possible that the carbonyl backbone of the protein or side-chains not facing into the aqueous pore environment may also influence selectivity. However, we are unable to distinguish these changes from side-chain effects per se. Initially, we measured the current ratios of the cysteine mutants to determine possible residues which influence ion selectivity. Figure 4.3 illustrates the current ratios for Li⁻, NH₄⁺ and K⁻ for rSkM1 and the cysteine mutants. All cysteine mutants were equally permeable to Li⁻ as rSkM1 with the exception of W402C, E758C and .!529C which had Li⁻ current ratios significantly larger than rSkM1 channels (Figure 4.3A).

Mutants in domains I, II and III (except E755C and K1237C) showed selectivity to NH₄⁺ and K⁻ statistically identical to wild-type rSkM1 channels (Fig 4.3). Similarly residues in these domains did not show significant alterations in reversal potentials (Table

130

Figure 4.3

Current ratios for A) Li$^-$, B) NH$_4^-$ and C) K$^-$ of the rSkM1 and cysteine mutant channels. Current ratios were determined from the ratio of the peak inward current in the presence of the test cation to the peak inward current in the presence of Na$^-$. Data represent the mean $\pm$ SEM of 3-5 oocytes. *n.e.* denotes no expression. The P values are * < 0.05 and ** < 0.01.
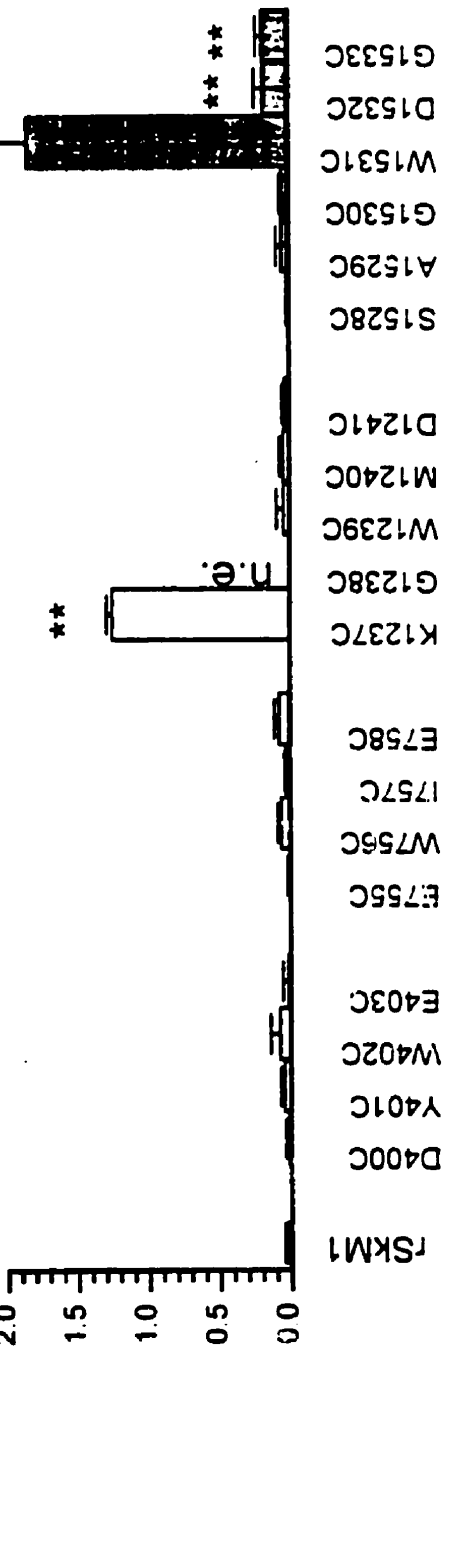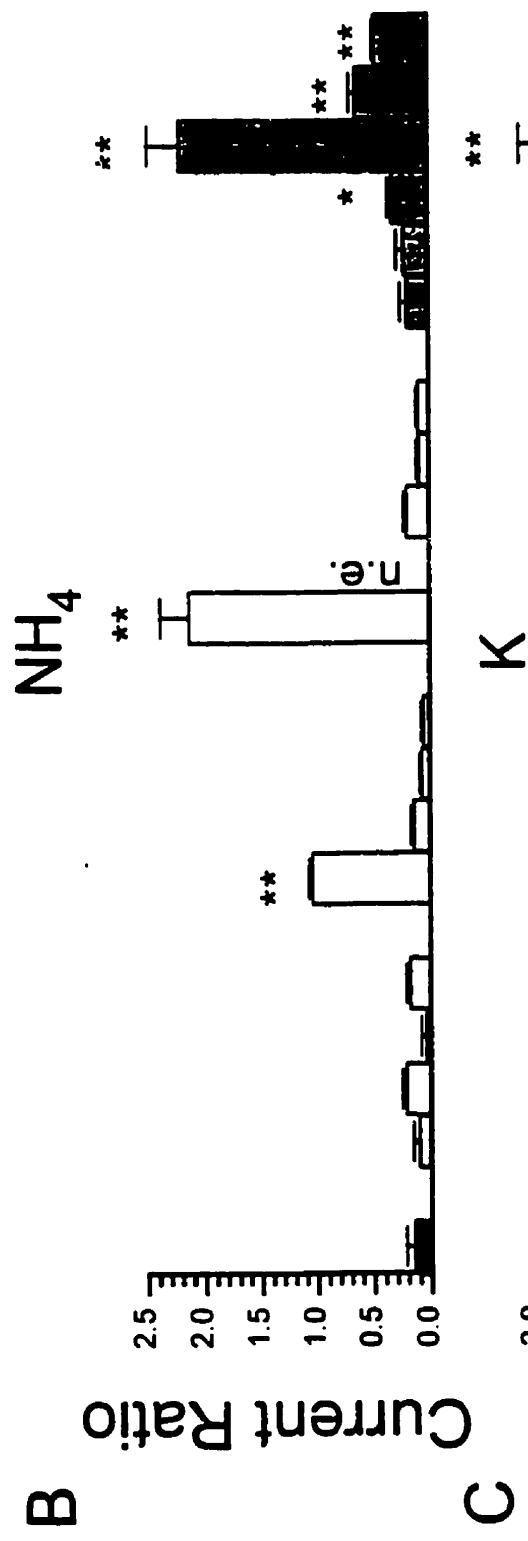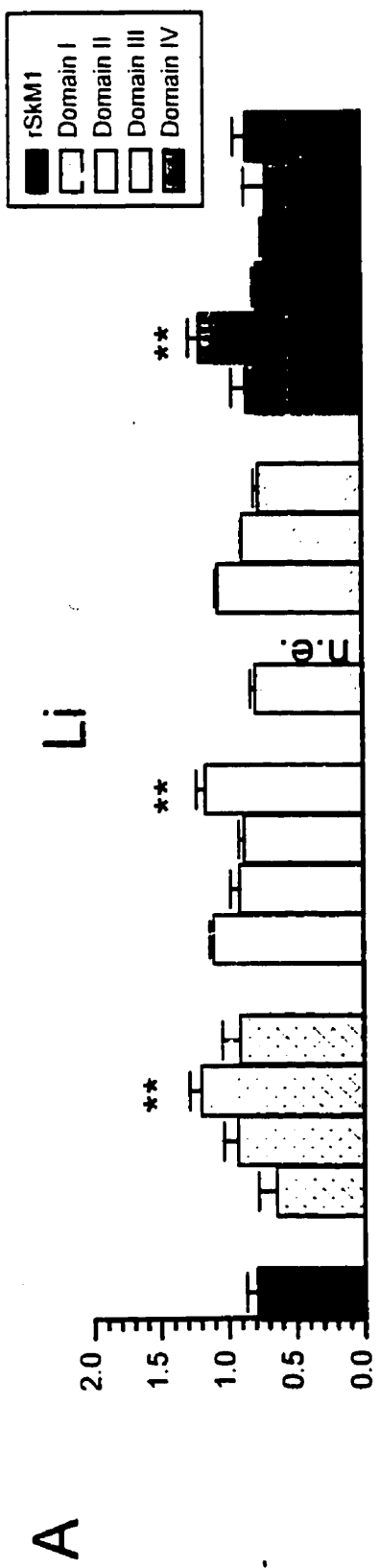
TABLE 4.2

Reversal Potentials of rSkM1 and Cysteine Mutants. Values represent the mean ± SEM. * and ** respectively denote $p<0.05$ and $p<0.01$ with respect to WT values.

	E_{Na} (mV)	n
RSkM1	54.4 ± 2.7	10
Y401C	50.7 ± 2.1	6
W402C	52.1 ± 2.3	6
E403C	51.0 ± 2.7	7
E755C	28.8 ± 2.2**	7
W756C	51.6 ± 1.9	6
I757C	53.4 ± 1.0	7
E758C	54.0 ± 3.9	7
K1237C	-1.3 ± 1.2**	9
W1239C	49.7 ± 2.1	6
M1240C	50.2 ± 3.9	5
D1241C	54.4 ± 2.0	6
A1529C	50.0 ± 1.1	7
G1530C	41.3 ± 2.9*	5
W1531C	1.6 ± 1.7**	12
D1532C	36.1 ± 2.4**	9
G1533C	35.9 ± 3.6**	4

4.2). On the other hand W1531C. D1532C and G1533C mutants in domain IV showed a statistically significant enhanced selectivity towards NH_4^- and K^- as measured using current ratios (Fig 4.3). In each of these domain IV mutants (W1531C. D1532C and G1533C). there was a corresponding significant shift in the reversal potential of the peak current versus voltage curve compared to rSkM1 channels. In addition. G1530C channels also showed significant shifts in reversal potential (Table 4.2) despite a lack of change in current ratio to K^- compared to rSkM1. These results establish that residues in domain IV more profoundly influence ion selectivity with respect to NH_4^- and K^- than residues in the other three domains (except E755C and K1237C).

4.4.2   *Loss of Na$^-$ selectivity by K1237C. W1531C and D1532C*

Relative to other cysteine mutants. K1237C. W1531C. D1532C and G1533C most profoundly affected the ionic selectivity compared to rSkM1 channels. Since two of these mutants (K1237C and D1532C) were substitutions for strongly hydrophilic charged residues and W1531C involved the replacement of a large aromatic residue. we therefore further characterized the nature of the changes in selectivity in these three mutants. Figure 4.4 shows the whole-cell Na$^-$ current recordings of K1237C. W1531C and D1532C in the presence of equimolar Na$^-$ or K$^-$. and their corresponding current-voltage relationship. K1237C and W1531C channels displayed marked alterations in ionic selectivity towards the monovalent cations tested (Fig 4.4A and 4.4B). The ionic selectivity sequences of both K1237C and W1531C was $NH_4^->K^->Na^-\geq Li^-\approx Cs^-$. Neither K1237C nor W1531C supported permeation by the quaternary ammonium compound. tetramethylammonium (data not shown). The marked alteration of channel selectivity by W1531C. which is not shared by the other tryptophan mutants in domain I-III (Figure 4.3). suggests that this residue and K1237 are important in regulating the selectivity of the rSkM1 Na$^-$ channel.

The present findings with W1531C suggest that the presence of an aromatic group in domain IV may be critical for Na$^-$ selectivity. To address this, we constructed two conservative mutants. W1531Y and W1531F, as well as the non-conservative mutant

Figure 4.4

Altered ion selectivity of K1237C, W1531C and D1532C. Whole-cell currents of A) K1237C, B) W1531C and C) D1532C recorded in a 96 mM NaCl or 96 mM KCl solution. Current recordings were measured from oocytes held at -120 mV and depolarized from -60 to +50 mV. Current traces shown are from -50 to +50 mV in 10 mV increments. Records were corrected for leak and capacitance current. The corresponding current-voltage relationship from the same oocytes shown below, recorded in Na$^+$ (square), NH$_4^+$ (triangle) and K$^+$ (circle) solutions. Values were normalized to the maximal peak inward current for Na$^+$. Data were fit to a Boltzmann distribution as described in Fig. 4.2.
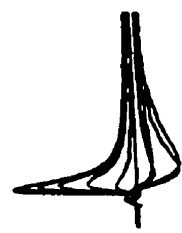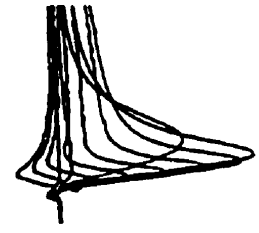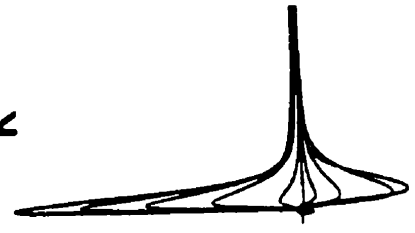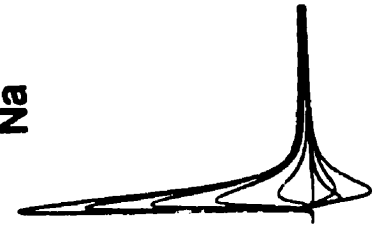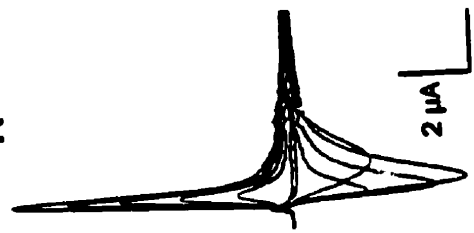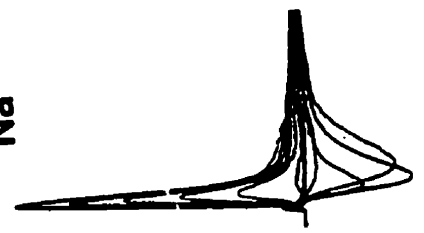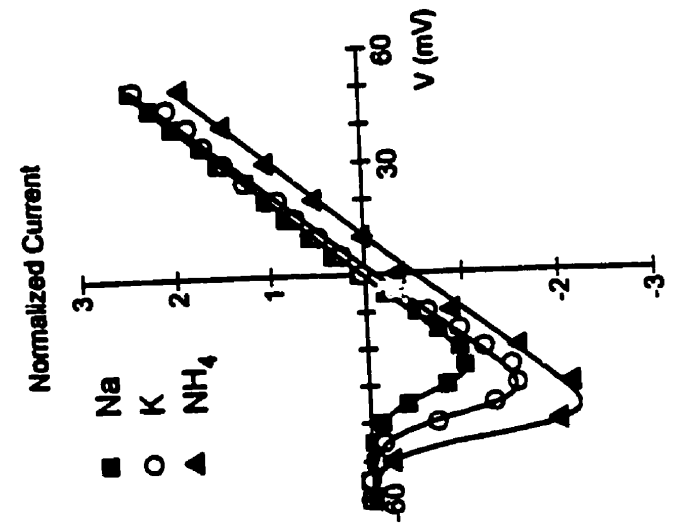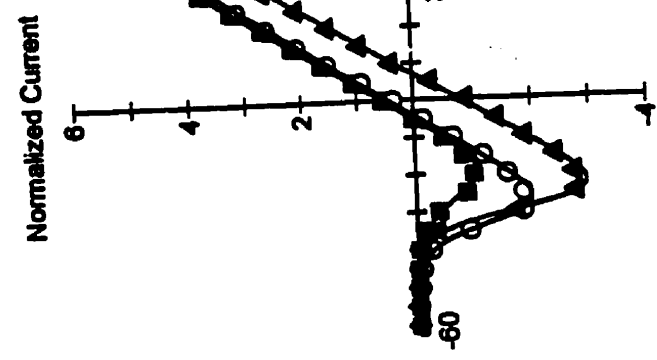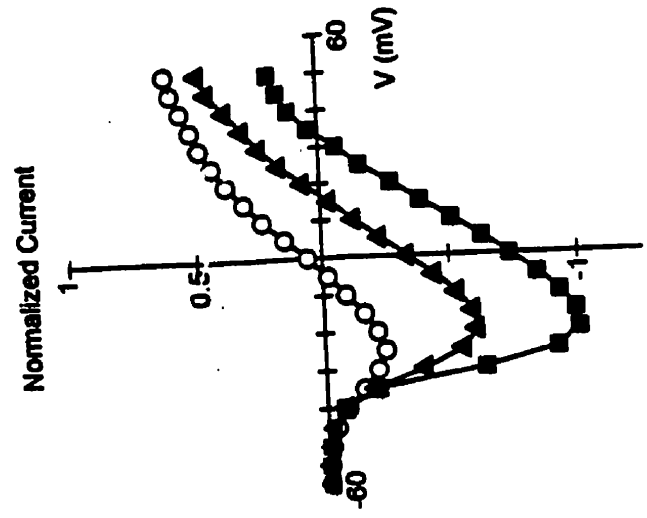
W1531A. Figure 4.5 illustrates the current ratio of rSkM1 and the tryptophan mutants. W1531C, W1531A, W1531F and W1531Y were equally permeable to Li^- as rSkM1. A larger difference was observed with NH_4^- and K^- current ratios. W1531A channels had NH_4^- and K^- current ratios greater than rSkM1 channels but surprisingly much less than W1531C channels (Figure 4.5). Alterations in ion selectivity with W1531A were as also reflected in a less positive reversal potential (+39.1 $\pm$ 2.9 mV, n = 6; p<0.05) measured in Na^- solutions. The conservative mutant, W1531Y, displayed NH_4^- and K^- current ratios similar to rSkM1. We were unable to detect any measurable inward currents in the presence of NH_4^- or K^- solutions with W1531F. Preservation of an aromatic residue in domain IV retained Na^- selectivity, and the results with W1531A suggest that the hydrophobic character is an important determinant of Na^- selectivity in rSkM1 channels.

A less dramatic but significant alteration in the selectivity of the rSkM1 Na^- channel was observed with the aspartate to cysteine mutation in domain IV (D1532C) (Figure 4.4C). This mutation resulted in a channel that was significantly more permeable to NH_4^- and K^- in comparison to the wild-type channel. Surprisingly, other negatively-charged amino acids in the other pore regions (D400C, E403C, E758C and D1241C) had very little effect on selectivity (Figure 4.3) with the exception of E755C which was significantly more permeable to NH_4^-, but interestingly not to $K^.$.

4.4.3 Divalent permeation of K1237C

Heinemann and colleagues (1992) demonstrated that replacing the lysine with glutamate in domain III (K1422E in the rat brain II Na^- channel) supported Ca^{2+} and Ba^{2+} permeation. We further examined this finding by replacing the equivalent residue with cysteine (K1237C). Exposure of K1237C to Ca^{2+} or Sr^{2+} solutions resulted in inward currents comparable to when Na^- was the permeant charge carrier, and rightward shifts in the current-voltage relationship (Figure 4.6A and B). Interestingly, replacement of Na^- in the external bath solution with Mg^{2+} also resulted in inward currents with a similar voltage-dependent shift in activation while replacement with Ba^{2+} resulted in barely detectable

137

Figure 4.5

Current ratios for tryptophan mutants. Current ratios were calculated as described in Figure 4.3. Values represent the mean ± SEM of 5-7 oocytes. The p values are * < 0.05, ** < 0.01.
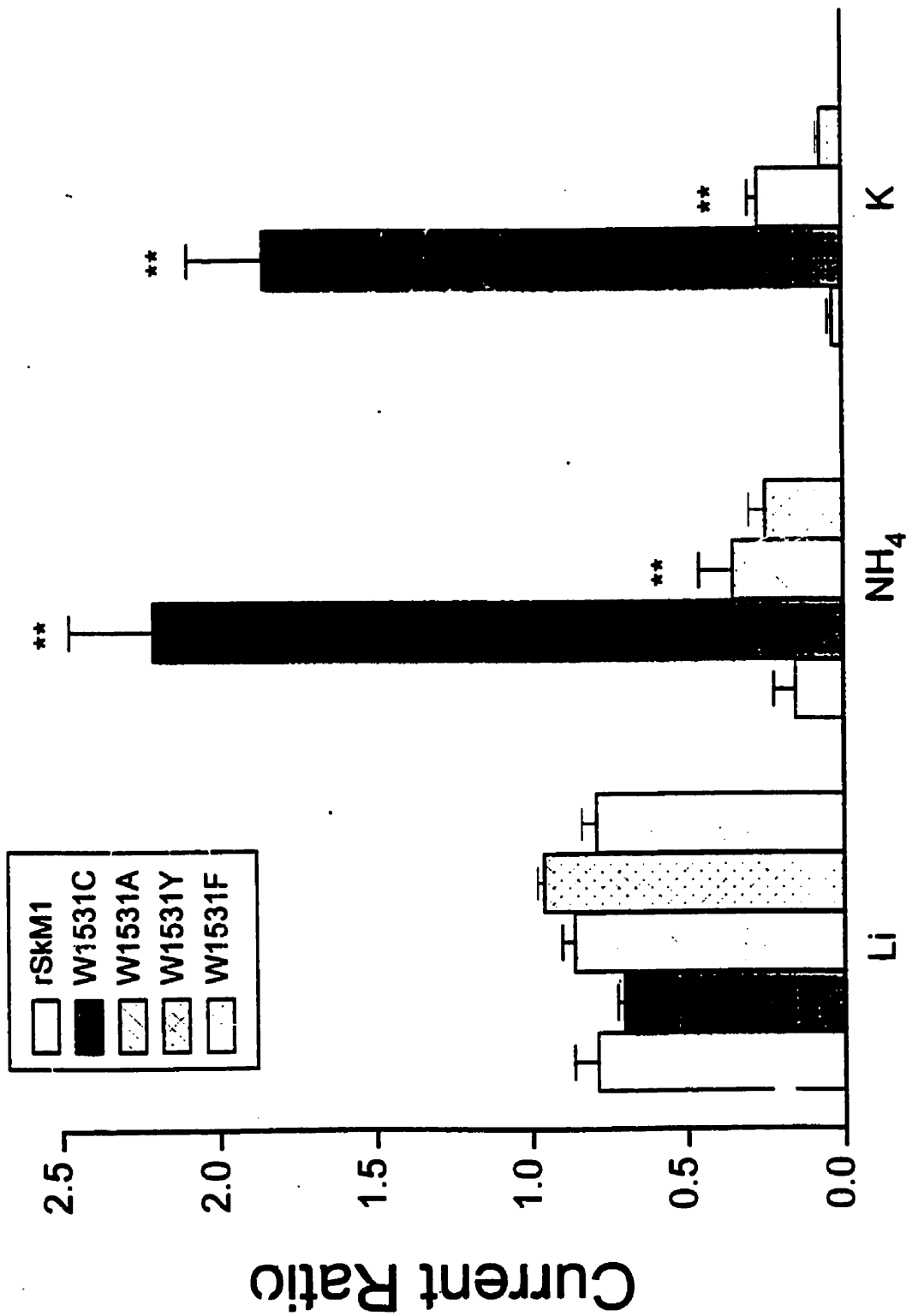
Figure 4.6

Divalent permeation of K1237C.

A) Current recordings of K1237C in the presence of 96 mM Na^+, Ca^{2+}, Sr^{2+}, Mg^{2+} and Ba^{2+} solutions. Currents were recorded as described in Fig. 4.4.

B) Corresponding current-voltage relationship from the same oocyte shown in panel A. Data were fit as described in Fig. 4.4.

C) Conductance-voltage relationship of K1237C in the presence of Na^+ and the divalent cations. Symbols are the same as denoted in panel B. Data were normalized to the maximal Na^+ conductance and fit to a Boltzmann distribution function. Values represent the mean ± SEM of 5 oocytes.

A

Na   Ca   Sr   Mg   Ba

2 μA | 5 ms

B

Na ■
Ca ○
Sr ▲
Mg ▽
Ba ◆

I (μA)

V (mV)

C

Relative Conductance

V (mV)
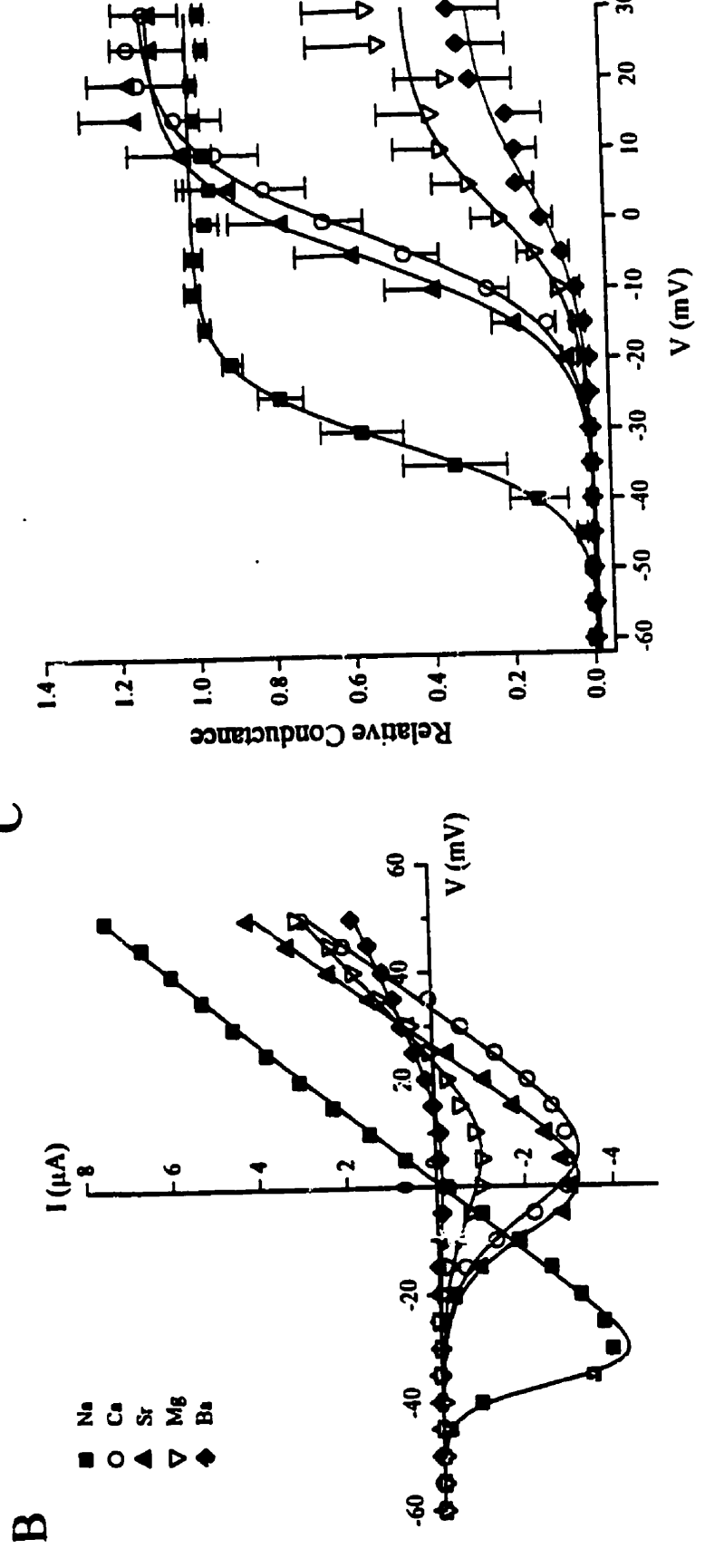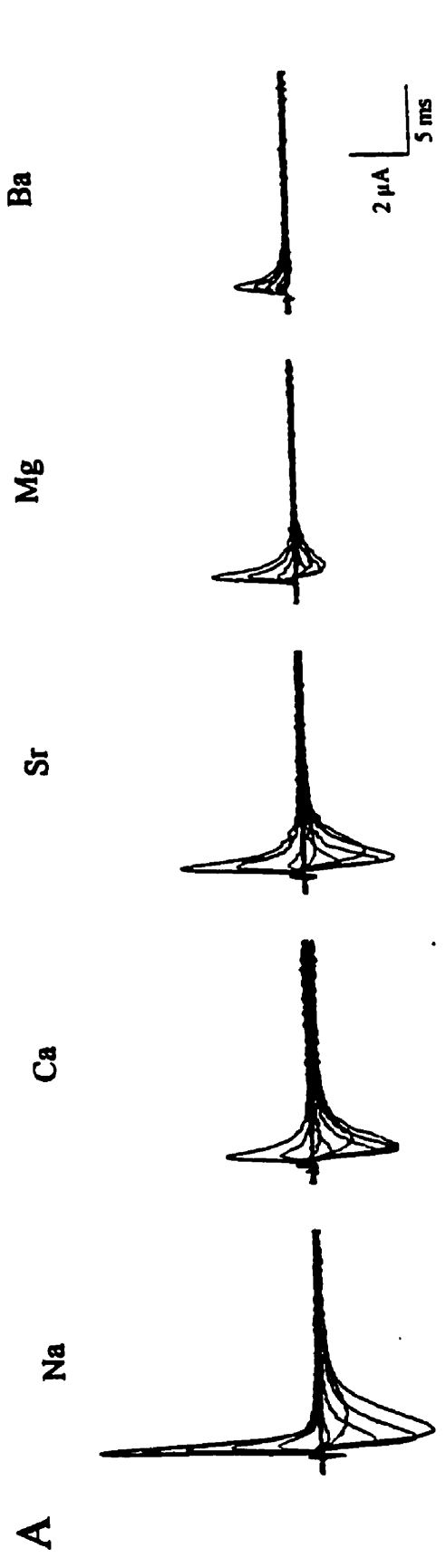
inward currents (Figure 4.6A and B). These results establish that replacement of K1237 with a residue not identical to that found at the homologous location in Ca^{2+} channels also support currents by divalents. K1237C channels were equally permeable to Ca^{2+} and Sr^{2+} compared to Na^- as measured using maximum conductance measurements (Fig 4.6C).

Since Cd^{2+} binds with high affinities to free sulfhydryls. we and others have used this cation as a biophysical probe to determine the spatial orientation of the amino acid side-chains by examining the Cd^{2+} sensitivity of the cysteine mutated channels (Chiamvimonvat et al.. 1996a; Li et al.. 1996; Pérez-García et al.. 1996). rSkM1 is relatively insensitive to Cd^{2+} block (K_d = 1.8 ± 0.4 mM. n=7) and whole-cell currents are unaffected by methanethiosulfonate (MTS) derivatives. Furthermore. there is no change in the Cd^{2+} sensitivity of rSkM1 after MTSEA exposure (K_d = 1.9 ± 0.3 mM. n=3). K1237C. W1531C and D1532C all appear to have their side-chain residues accessible to the aqueous pore environment as revealed by the modification by the MTS derivatives which modify free sulfhydryl groups. and the enhanced sensitivity of these cysteine mutants to Cd^{2+} block compared to rSkM1 (Figure 4.7). This enhanced Cd^{2+} sensitivity could be reversed by MTS modification (Figure 4.7). These findings suggest that the alteration in selectivity result from changes in the interaction between the permeating ion and the channel. and not due to structural transformations of the channel protein.

4.4.4   Can sulfhydryl modification reconstitute Na^+ selectivity?

A simple interpretation of the above data suggests that removal of the positively charged lysine side-chain. the aromatic moiety of tryptophan or the negatively charge carboxylate residue may be responsible for the alterations in ionic selectivity. We hypothesized that chemically reintroducing similar groups into the pore region would restore Na^- selectivity to the channel. We used the membrane-impermeant MTS derivatives to examine this question. To restore ionic selectivity to K1237C. W1531C and D1532C. we used the positively-charged (MTSEA. MTSET) or negatively-charged (MTSES) compounds, respectively.

Figure 4.7

Effect of methanethiosulfonate (MTS) modification on the current-voltage relationship (left panel) and Cd^{2+} sensitivity (right panel) of A) K1237C. B) W1531C and C) D1532C. Currents were recorded as described in Fig. 4.4 in the absence and presence of 1 mM MTS derivative denoted. Fractional whole-cell currents (I/I_o) measured at -10 mV were plotted as a function of Cd^{2+} concentration and fit to the Hill equation $I/I_o = 1/(1 + [Cd^{2+}]/K_d)$ assuming a single binding site. The K_d for Cd^{2+} block for rSkM1 was 1865 ± 386 μM for rSkM1 (n = 7). The K_d for Cd^{2+} block prior to and after modification by the MTS derivative was A) K1237C 124 ± 22 μM (solid square, n = 3) and 2154 ± 182 μM (open square, n = 3); B) W1531C 55 ± 7 μM (solid circle, n = 6) and 1980 ± 176 μM (open circle, n = 3); C) D1532C 583 ± 70 μM (solid triangle, n = 6) and 2325 ± 287 μM (open triangle, n = 3), respectively. Values represent the mean ± SEM.

A
K1237C
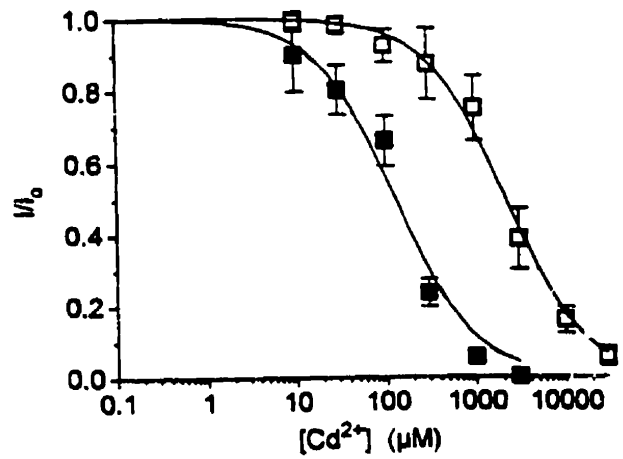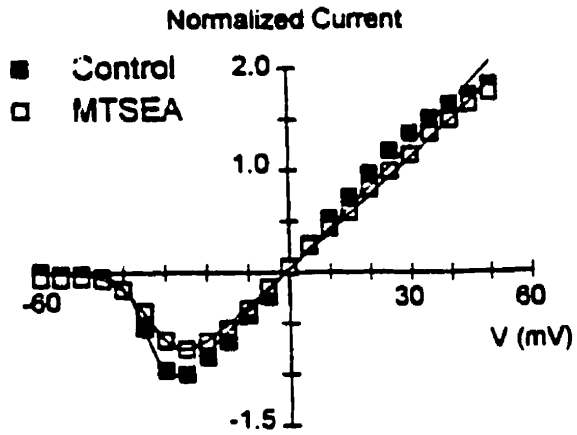
B
W1531C
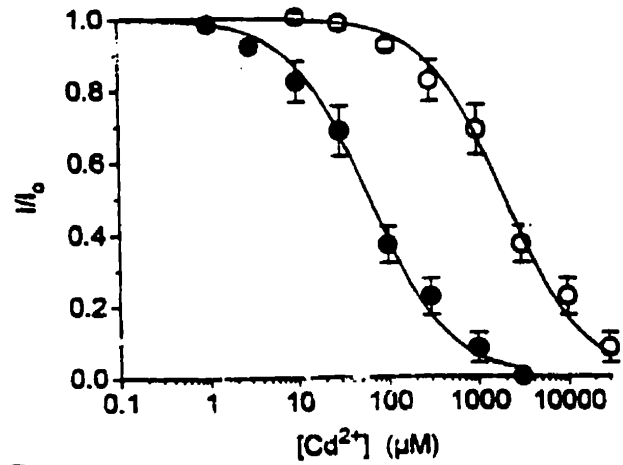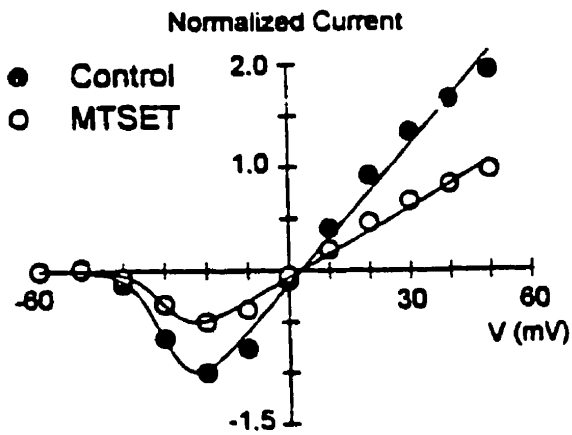
C
D1532C
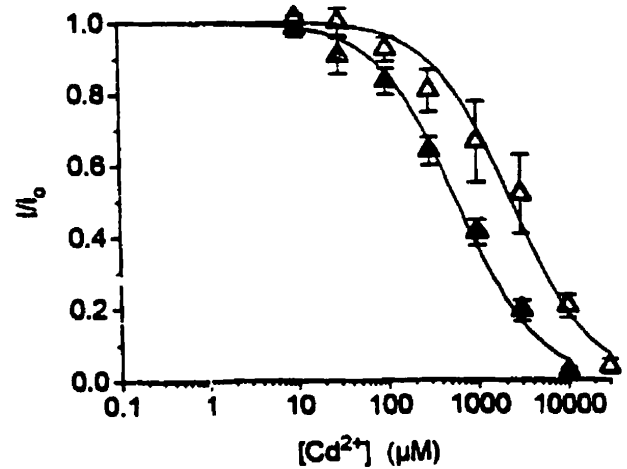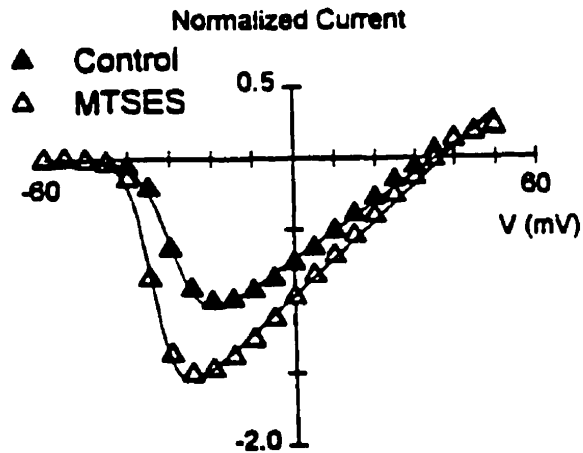
The effects of sulfhydryl modification of K1237C with 1 mM MTSEA are illustrated in Figure 4.8A. MTSEA resulted in a reduction in peak inward current which may result from an obstruction of the conduction pathway (Figure 4.7A). Sulfhydryl modification by MTSEA was irreversible since the reduction in peak current persisted even after washout of the agent, as has been shown by other investigators (Akabas et al., 1992; Kirsch et al., 1994; Kürz et al., 1995). Modification was also confirmed by the reduced sensitivity of the channel to Cd^{2+} block (Figure 4.7.; Li et al., 1996). Both the reduced peak inward current and the reduced sensitivity to Cd^{2+} could be restored following the application of dithiothreitol (data not shown). MTSEA modification did not reconstitute Na^+ selectivity to the K1237C mutant since this mutant remained nonselective towards the monovalent cations as demonstrated by the high degree of permeation by NH_4^+ and K^+ (Figure 4.8A) and by the lack of change in the permeability ratios of K1237C after sulfhydryl modification (Table 4.3). MTS-modified K1237C channels remained permeable to divalent cations. These data demonstrate that sulfhydryl modification of K1237C by MTSEA could not restore rSkM1-like monovalent or divalent cation selectivity to these channels.

Similar studies were performed with W1531C (Figure 4.8B) and D1532C (Fig 4.8C). Modification of W1531C with 1 mM MTSET, which introduces a bulky trimethylammonium group into the pore, reduced peak inward current but had no effect on selectivity as perceived by the lack of change in the NH_4^+ and K^+ current and the permeability ratios (Fig 4.8B, Table 4.3). We also examined the effects of the aromatic MTS derivative, methanethiosulfonate-ethylbenzoate (MTSEB), which would introduce the more appropriate phenolic group into the pore. However, attempts to chemically modify the cysteine residue with MTSEB failed since there was no change in the Cd^{2+} sensitivity of W1531C after MTSEB exposure. Failure of MTSEB to modified this channel mutant may be due to the inaccessibility of this reagent to the site within the pore. Lastly, replacement of a negative charge into D1532C channels using MTSES modification resulted in an

Figure 4.8

Effect of sulfhydryl modification of A) K1237C, B) W1531C and C) D1532C on ionic selectivity. Whole-cell currents were recorded in the presence of 96 mM NaCl or KCl solutions as described in Fig. 4.4. The corresponding current-voltage relationships of the cysteine mutants in the presence of Na^- (square), K^- (circle) and NH_4^- (triangle) are shown below. K1237C, W1531C and D1532C were modified with 1 mM of MTSEA, MTSET and MTSES, respectively.

?

A   K1237C   B   W1531C   C   D1532C

Na   K   Na   K   Na   K

10 ms   10 ms   10 ms

4 µA   1 µA   5 µA

I (µA)   I (µA)   I (µA)

12   4   12

6   2   8

4

-6   -2   -12

V (mV)   V (mV)   V (mV)

30   30   60

60   60

-60   -60   -60
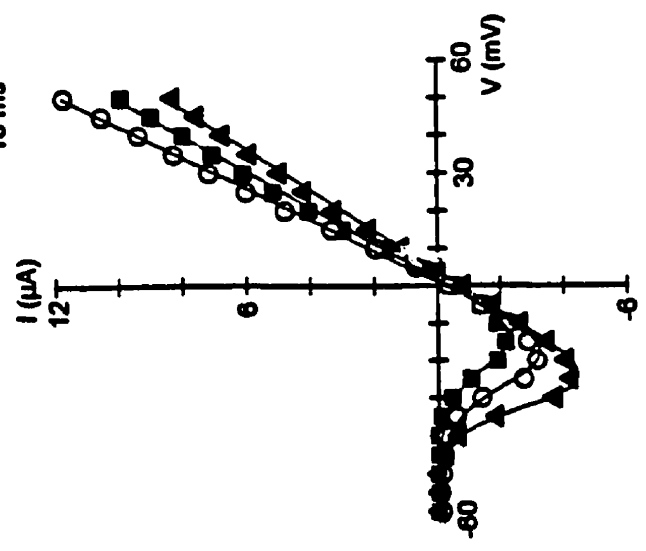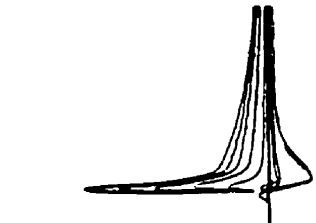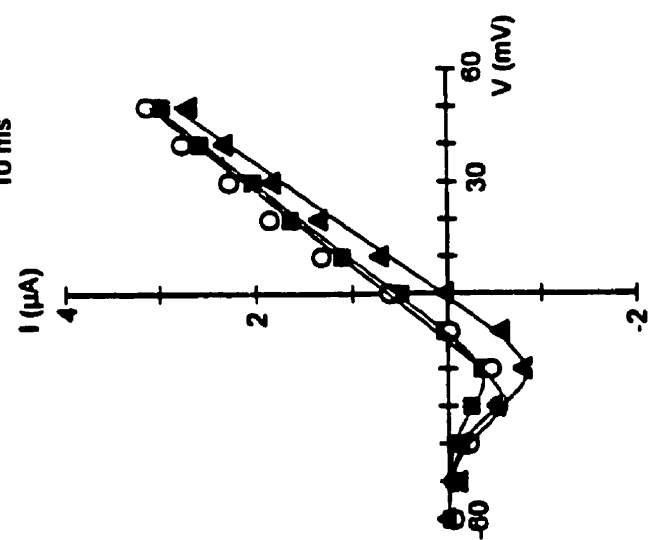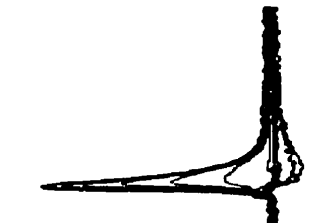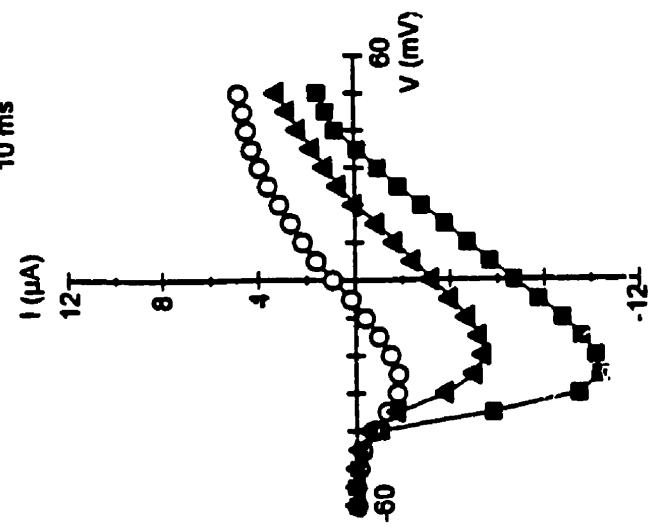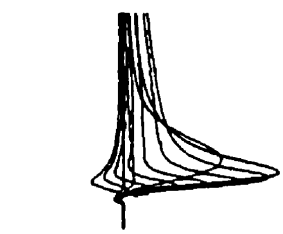
TABLE 4.3

Effect of Sulfhydryl Modification on Permeability Ratios of rSkM1. K1237C. W1531C and D1532C: Channels were modified with 1 mM of the corresponding MTS derivative. Values represent the mean ± SEM of 3-5 experiments.

	P_{Li}/P_{Na}	P_{NH4}/P_{Na}	P_K/P_{Na}	P_{Cs}/P_{Na}
rSkM1	0.97 ± 0.06	0.17 ± 0.02	0.05 ± 0.01	0.02 ± 0.01
K1237C	1.00 ± 0.03	1.19 ± 0.04	1.01 ± 0.06	0.87 ± 0.03
K1237C + MTSEA	1.01 ± 0.02	1.15 ± 0.05	1.02 ± 0.03	0.86 ± 0.02
W1531C	1.01 ± 0.01	1.24 ± 0.01	1.03 ± 0.02	0.89 ± 0.05
W1531C + MTSET	1.03 ± 0.02	1.23 ± 0.02	0.99 ± 0.01	0.90 ± 0.01
D1532C	0.88 ± 0.07	0.56 ± 0.04	0.20 ± 0.03	0.11 ± 0.01
D1532C + MTSES	0.96 ± 0.04	0.54 ± 0.06	0.22 ± 0.04	0.07 ± 0.03

enhancement of current (Figure 4.7C) but again did not restore channel selectivity (Figure 4.8C).

These data suggest that a simple reintroduction of a positively-charged group, bulky hydrophobic moiety or negatively-charged group into the pore of K1237C, W1531C or D1532C, respectively is not sufficient to reestablish selectivity. However, these findings do not negate the importance of the side-chains of these residues for selectivity since not only the charge or size of the side-chain may be important, but the localization of these groups within the pore may influence selectivity. Modification of the cysteine mutants with the MTS derivatives most likely do not localize the replaced group within the same vicinity because of their attachment to the ethyl alkyl chain.

4.4.5   Effects of extracellular pH on the selectivity of D1532C

To determine whether the localization of the negatively-charged group is critical for determining ionic selectivity, we examined the effects of extracellular pH on D1532C mutant channels. We reasoned that alteration in extracellular pH will affect the ionized state of the cysteinyl sulfhydryl side-chain (pK_a cysteine 8.5) thereby reintroducing a negative charge. Figure 4.9 illustrates the effects of changing extracellular pH on the current-voltage relationship of the rSkM1 and D1532C Na^+ channel. Decreasing the extracellular pH from 7.6 to 5.6 resulted in a reduction in peak inward current and a rightward shift in the current-voltage relationship of the rSkM1 Na^+ channel (Figure 4.9A). These effects have been previously attributed to proton block of the channel and screening of negative surface charges (Woodhull, 1973). Elevating the pH from 7.6 to 9.6 produced a modest increase in peak current of rSkM1. Increasing the extracellular pH had two effects on D1532C. There was a there was a large increase in peak inward current at pH 9.6 (Figure 4.9A). Secondly, there was a positive shift in the reversal potential as extracellular pH was made more basic (Figure 4.9A). This effect is more clearly illustrated in Figure 4.9B where the reversal potential (E_{Na}) is plotted as a function of the extracellular pH. There was a shift in the reversal potential from +33.2 ± 2.2 mV (pH 5.6) to +41.3 ± 1.6 mV (pH 9.6) (n = 5) which tended to converge towards the rSkM1 curve. Changes in pH did

Figure 4.9

Effect of extracellular pH on rSkM1 and D1532C.

A) Effect of pH 5.6 (circle), 7.6 (square) and 9.6 (trinagle) on the current-voltage relationship of rSkM1 and D1532C. Currents were recorded as described in Fig. 4.4.

B) Effect of extracellular pH on the reversal potential (E_{Na}) of rSkM1 (n) and D1532C (¡). Data represent the mean ± SEM of 4-5 oocytes.

A

D1532C

rSkM1

○ pH 5.6
■ pH 7.6
△ pH 9.6

B
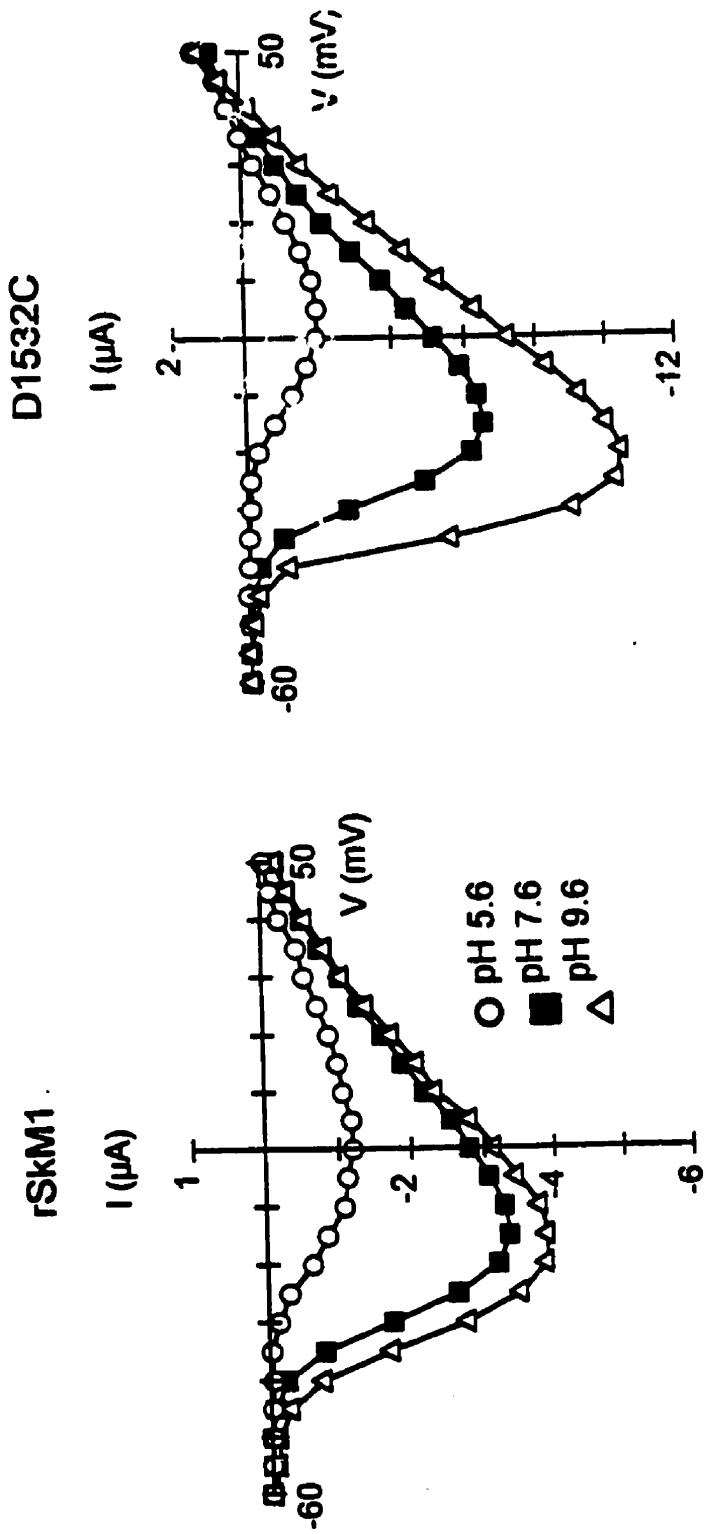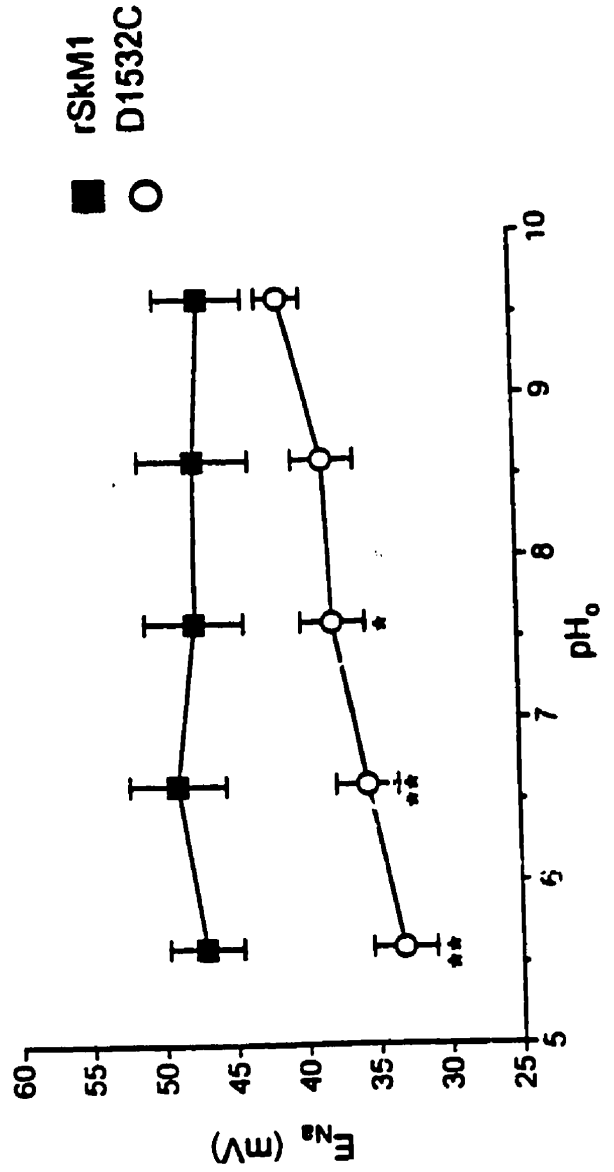
■ rSkM1
○ D1532C

not influence E_{Na} of rSkM1 (E_{Na}: +47.1 ± 2.6 mV - pH 5.6; +46.9 ± 3.1 mV - pH 9.6; n = 4). As observed with rSkM1, inward currents of D1532C were reduced and there was a depolarizing shift in activation at pH 5.6 (Figure 4.9A). These data suggest that not only the charge but the location of the negatively-charged group is critical for influencing ionic selectivity.

4.5 Discussion

Mutagenesis studies have revealed critical residues important for a number of intrinsic properties of the Na⁺ channel including activation and inactivation (Stühmer et al., 1989; West et al., 1992) and ionic selectivity (Heinemann et al., 1992). We have further used mutagenic strategies to probe the spatial orientation of the pore-forming residues of the rat skeletal muscle Na⁺ channel (Li et al., 1996). Most of the residues mutated were exposed to the aqueous pore environment. We have extended these studies and examined the contribution of these pore-forming residues to ion selectivity. Cysteine mutations within the pore appear to have localized effects since all but one cysteine mutant (G1238C) expressed functional channels with relatively little effect on channel gating.

4.5.1 Alterations in Selectivity Revealed by Cysteine Mutations

The present study demonstrated that four residues markedly influence ion selectivity of the rSkM1 Na⁺ channel: K1237, W1531, D1532 and G1533. Three of these residues (W1531, D1532 and G1533) have not been implicated before now in forming the selectivity filter of the Na⁺ channel. Studies with the rat brain II Na⁺ channel (Terlau et al., 1991; Heinemann et al., 1992) have suggested four amino acids (aspartate, glutamate, lysine, alanine), one in each of the four pore regions form the selectivity filter. This DEKA locus is absolutely conserved in all other Na⁺ channel subtypes known (except in jelly fish where the locus is DKEA (Anderson et al., 1993)) and also functions in molecular filtration as well as selectivity for organic and inorganic cations by determining the ionic cutoff diameter of the channel pore (Sun et al., 1997). The locus also plays a role in external Ca^{2+} and H^+ block

of the wild-type channel (Sun et al.. 1997). More notably. the lysine and alanine residues in domain III and IV had the most influence on Na^+ selectivity (Heinemanr. et al.. 1992; Favre et al.. 1996; Schlief et al.. 1997; Chen et al.. 1997; Sun et al., 1997). Mutating both of these residues to glutamate. which are found at the equivalent positions in the Ca^{2+} channel. conferred Ca^{2+} channel characteristics to the Na^+ channel. The single lysine to glutamate mutation alone had a large effect on ion selectivity of the channel such that the channel was relatively nonselective towards the monovalent cations tested. similar to the loss of selectivity we observed with K1237C. Furthermore. as observed with the lysine to glutamate mutant. our K1237C mutant showed appreciable inward currents in the presence of divalent cations.

The selectivity sequence of K1237C for divalent cations based on conductance and reversal potential measurements was $Ca^{2+} \geq Sr^{2+} > Mg^{2+} > Ba^{2+}$. However. the selectivity sequence of K1237C for the alkaline earth cations cannot be inferred from measurements of atomic radii ($Ba^{2+} > Sr^{2+} > Ca^{2+} > Mg^{2+}$) or hydration energies ($Mg^{2+} > Ca^{2+} > Sr^{2+} > Ba^{2+}$) (Hille. 1992). as it can be for the L-type Ca^{2+} channel using single-channel conductance ($Ba^{2+} > Sr^{2+} \sim Ca^{2+}$) or reversal potentials ($Ca^{2+} > Sr^{2+} > Ba^{2+}$) (Hess et al.. 1986). L-type Ca^{2+} channels are impermeable to Mg^{2+}. The permeation of Mg^{2+} through the K1237C channel is quite surprising since Mg^{2+} does not permeate many ion channels since the rate of dehydration is $>10^3$ s^{-1} slower than other alkali or alkaline earth metals (Diebler et al.. 1969). Therefore. dehydration of the ion may not play a significant role in Mg^{2+} permeation through this channel. The finding that Ba^{2+} is weakly permeable through the K1237C channel is also unexpected since Ba^{2+} has a higher dehydration rate than the other divalent cations tested (Diebler et al.. 1969) and a similar atomic radius as the permeant K^+ ion (Hille. 1992). therefore we would have expected a greater degree of Ba^{2+} permeation than Mg^{2+}. The presence of a positively-charged residue at position 1237 in domain III appears to be critical in preventing divalent permeation since the mutation K1237R abolished Ca^{2+} conductance. however. still rendered the channel non-selective towards monovalent cations (Favre et al.. 1996). In addition to exclusion of divalent entry. it has also been proposed that K1237 may play a functional role analogous to the Ca^{2+} (Sun et al., 1997) that resides in a

153

high affinity binding site in the Ca^{2-} channels which controls selectivity for inorganic cations and prevents permeation of large organic cations (Sather et al., 1994).

Negative-charged residues have a strong influence on ion selectivity and permeation of Na^- channels (Terlau et al., 1991; Heinemann et al., 1992; Chiamvimonvat et al., 1996a,b) and Ca^{2-} channels (Kim et al., 1993; Mikala et al., 1993; Yang et al., 1993; Ellinor et al., 1995), whereas for voltage-gated K^- channels, less hydrophilic residues contribute more so to K^- selectivity (Yool and Schwarz, 1991; Taglialatela et al., 1993; Heginbotham et al., 1994). It has been speculated that the conserved tyrosine residue within the pore of the voltage-gated K^- channels is important for coordinating cation-p interactions between the permeating K^- ion and the channel protein (Heginbotham and MacKinnon, 1992; Kumpf and Dougherty, 1993; Lü and Miller, 1995) and furthermore, may form part of the selectivity filter of the channel (Durell and Guy, 1992). It is intriguing that mutating the hydrophobic tryptophan residue in domain IV to cysteine (W1531C) but not the other tryptophan residues in the domains I-III rendered the channel unable to discriminate against the monovalent cations tested. Furthermore, maintaining an aromatic group at this position (W1531F and W1531Y) retained selectivity similar to that of the wild-type channel. The alterations observed with W1531C strongly suggests that size and chemical nature of the residue at this position is a critical determinant in conferring Na^- selectivity to rSkM1.

D1532C showed prominent inward current with both NH_4^- and K^-. Mutating the negatively-charged residues in the domains I-III (D400C, E403C, E755C, F758C and D1241C) did not have as a dramatic effect on selectivity as D1532C. The importance of negative-charged residues in the pore has been attributed to electrostatic focusing or binding of the permeant ions and determinants of ion translocation for the voltage-gated Na^- channel (Hille, 1972; Terlau et al., 1991; Chiamvimonvat et al., 1996b). Our data further supports this notion and that the negatively-charged residue in domain IV plays a critical role in Na^- permeation. These data and the results with W1531C also suggest that each domain does not contribute equally to the property of ion selectivity. Such asymmetry in the conduction pathway has been recently described for the Na^- (Chiamvimonvat et al.,

1996a,b) and Ca^{2+} channel (Kim et al., 1993; Mikala et al., 1993; Yang et al., 1993; Ellinor et al., 1995).

Both glycine residues in domain IV (G1530C and G1533C) disrupted selectivity. Glycines allow for high degree of protein backbone flexibility and furthermore, are major constituents of β hairpin turns within proteins (Creighton, 1993). It may be possible that the two glycine residues are involved in allowing for the coordination of a Na^- ion with the channel protein, through cation-p interactions with W1531 (Dougherty, 1996) or electrostatic interactions with D1532 (Chiamvimonvat et al., 1996), as has been suggested for the glycine residues located in the "signature sequence" of the voltage-gated K^- channel (Heginbotham et al., 1994) and in the Ca^{2+} channel (Kim et al., 1993).

Heinemann and colleagues (1992) demonstrated the importance of the lysine residue in domain III in conferring Na^- selectivity to the Na^- channel and suggested that it comprised part of the selectivity filter. A more recent study further examined the role of this residue on selectivity and demonstrated the importance of the chemical nature at this locus in domain III for determining Na^- selectivity over K^- and Ca^{2+} (Favre et al., 1996). The present study supports these findings and furthermore demonstrates that the residues in domain IV influence ion selectivity more so than the residues in the other domains. The unique characteristic of this region may be associated with the high degree of flexibility within the pore region of domain IV, as I have demonstrated in Chapter 3. This property of the channel may be important for ion coordination, selectivity and permeation.

4.5.2 *Effect of Sulfhydryl Modification on Selectivity*

The development of the methanethiosulfonate compounds have been provided a unique probe to examine the tertiary nature of the pore-forming residues in ion channels when combined with cysteine scanning mutagenesis (Akabas et al., 1992). We (Li et al., 1996) and others (Akabas et al., 1992; Kürz et al., 1995; Pascual et al., 1995; Pérez-Garcia et al., 1996) have used these compounds to study the topology of the pore residues in a

number of ion channels. We have further employed these probes to determine whether ion selectivity can be restored by reintroducing specific groups into the pore to mimic the mutated residue. Modification of K1237C, W1531C and D1532C with specific methanethiosulfonate derivatives which reproduce the positive charged, bulky moiety or negative charged side-chains did not restore selectivity suggesting that a simple replacement is not sufficient for reconstituting selectivity of the channel. Furthermore, the presence of the positively-charged ammonium group within the pore of K1237C did not prevent divalent permeation. This is unlike the finding with K1237R which exhibited no Ca^{2+} permeation (Favre et al., 1996). Recently, Marban and colleagues demonstrated that the loss in selectivity of rSkM1 with D1532C could be partially restored by 10 mM MTSES as measured by whole-cell flux and single-channel permeability ratios (Chiamvimonvat et al., 1996b). Although we used 1 mM MTSES to modify D1532C channels, we observed a similar 50% increase in peak current (Figure 4.8C) as observed with 10 mM MTSES (Chiamvimonvat et al., 1996b) suggesting that differences in the degree of channel modification cannot explain the discrepancy in results.

4.5.3 *Extracelluar pH Influences Selectivity*

It should be noted that conservative replacements of pore-forming amino acids do not ensure conservation of selectivity and vice versa, as has been demonstrated for the L-type Ca^{2+} channel (Ellinor et al., 1995) and voltage-gated K^- channels (Taglialatela et al., 1993; Heginbotham et al., 1994). Side-chain length, charge and polarity may all influence selectivity of the channel. In this regard, although we have tried to preserve charge and polarity using the MTS compounds, the localization of the desired groups is confounded by their attachment to an ethyl alkyl chain. To overcome this problem, we changed the extracellular pH to alter the ionized state of the sulfhydryl side-chain of D1532C to maintain side-chain length, charge and polarity. D1532C became more selective as we changed the cysteinyl sulfhydryl side-chain to a thiolate derivative as extracellular pH increased. This further supports our findings that this negatively-charged residue is important for ion selectivity.

4.5.4 *Summary*

We have demonstrated that four residues (K1237, W1531, D1532 and G1533) in the pore of the rat skeletal muscle Na⁻ channel play an important role in ion selectivity. Three of these residues have not been previously reported to influence ion selectivity. Given the degree cf nonselectivity observed when the residue W1531 is mutated to cysteine, it is reasonable to suggest that this residue also forms part of the selectivity filter. We speculate that this residue may directly interact with the positively-charged lysine group in domain III or with the permeating Na⁻ ion through cation-π interactions which have been recently ascribed to be important for a number of biological interactions (Dougherty, 1996). Since mutations of domain IV residues produced more pronounced effects in ionic selectivity than residues from other domains and, coincidentally, DIV is the most flexible domain. Our results suggest a possibility that pore motion may correlate ion permeation and selectivity. Further studies will be required to verify this hypothesis.

4.6 *Acknowledgements*

CHAPTER 5

THE ROLE OF P-LOOP RESIDUES IN TOXIN BINDING

5.1 *Abstract*

Toxins whose 3-dimensional structures are known have been useful probes for studying the molecular structure of ion channels. We studied μ-conotoxin (μ-CTX) block of rat skeletal muscle sodium channel (rSkM1) in which single amino acids within the pore (P-loop) were substituted with cysteine. Among 17 cysteine mutants studied, 7 showed significant alterations in sensitivity to μ-CTX compared to wild-type rSkM1 channel (IC_{50}=17.5±2.8 nM). E758C and D1241C were less sensitive to μ-CTX block (IC_{50}=220±39 nM and 112±24 nM respectively) whereas the tryptophan mutants W402C, W1239C, and W1531C showed enhanced μ-CTX sensitivity (IC_{50}= 1.9±0.1, 4.9±0.9 and 5.5±0.4 nM respectively). D400C and Y401C also showed statistically significant, yet modest, changes in sensitivity to μ-CTX block compared to WT ($p<0.05$). Application of the negatively-charged sulfhydryl reactive compound, MTSES, enhanced the toxin sensitivity of D1241C (IC_{50}=46.3±12 nM) while having little effect on E758C mutant channels (IC_{50}=199.8±21.8 nM). On the other hand, the positively charged MTSEA completely abolished the μ-CTX sensitivity of E758C (IC_{50}>1mM) and increased the IC_{50} of D1241C about 2-fold. Applications of MTSEA, MTSES and the neutral MTSBN (benzyl methanethiosulfonate) to the tryptophan-to-cysteine mutants partially or fully restored the wild-type μ-CTX sensitivity, suggesting that the bulkiness of the tryptophan's indole group is a determinant of toxin binding. In support of this suggestion, the blocking IC_{50} of W1531A (7.5±1.3nM) was similar to W1531C while W1531Y showed wild-type sensitivity (14.6±3.5nM). Our results demonstrate that charges at positions 758 and 1241 are important for μ-CTX toxin binding and further suggest that the tryptophan residues within the pore in domain I, III and IV influence toxin-channel interaction. We also tested several current models of the Na⁻ channel pore with these data. Overall, our results are in favor of an asymmetrical pore.

5.2   *Introduction*

Knowing that the P-loops of Na⁻ channels are flexible structures (Chapter 3) and may correlate ionic selectivity (Chapter 4), we moved on to examine their contributions in the pharmacology of Na⁻ channels. Channel pores are invariably the targets of numerous channel blockers and drugs (see 1.6). Understanding the molecular actions of these agents and their interactions with the channel will not only shed light on the structures of their binding or receptor sites but potentially will also help understand the mechanisms underlying channel function and improve design of new therapeutic agents.

Toxins such as AgTX. TTX. STX and μ-CTX whose 3-dimensional structures are known have been useful probes for studying the molecular structure of ion channels. I will first describe in this chapter the roles of pore residues in binding of the blocker μ-conotoxin (μ-CTX), a class I Na⁻ channel toxin (see 1.10.1 for classification), to the rSkM1 Na⁻ channels. Several current models of the Na⁻ channel pore were tested with these data. In the next chapter, I will then discuss the contribution of P-loop residues in lidocaine (a class I antiarrhythmic, see also 1.10.2) binding.

Conotoxins (CTXs) are a group of toxins isolated from the venom of the piscivorous sea snail *Conus geographus* (Cruz et al.. 1985: Gray et al., 1988: Olivera et al.. 1990). Many of these toxins have specific actions on ion channels and neurotransmitter receptors. The μ-conotoxins (μ-CTX) are a class of conotoxins which selectively block ion flux through voltage-gated skeletal muscle and electric eel sodium channels with high affinity compared to the brain, heart or peripheral nerve isoforms (Cruz et al.. 1985). μ-CTXs are peptides with 22 amino acids including 6 cysteine residues (Nakamura et al., 1983; Gray et al., 1988: Olivera et al., 1990) which form 3 disulfide linkages making the toxins very rigid (Cruz et al.. 1985; Moczydlowski et al.. 1986; Ohizumi et al.. 1986; Yanagawa et al.. 1986; Chen et al., 1992). At neutral pH. μ-CTXs are very hydrophilic and carry a net positive charge of either 6 or 7 depending on the subtype. Rigid peptide inhibitors have previously been used to study the molecular structures of receptors and ion

159

channels (Park and Miller, 1992; Goldstein et al, 1994; Stampe et al; 1994; Hidalgo and MacKinnon, 1995). Consequently, rigid μ-conotoxins should be useful molecular probes for testing various molecular models of Na⁻ channel pore structure (Hille, 1992; Dudley et al., 1995; Stampe et al, 1994; Gross et al; 1996) since the molecular structure of μ-CTXs has been determined at very high resolution (Lancelin et al., 1991; Sato et al., 1991; Wakamatsu et al., 1992; Hill et al., 1996). Recently, French and colleagues (1996) have further used the activation shifts resulting from partial blockade of sodium single-channel current by the derivative R13Q of μ-CTX to implicate movements of the S4 voltage sensor (French et al, 1996). In addition to its rigidity, μ-CTX binds to skeletal muscle Na⁻ channels with a 10³-fold higher affinity compared to cardiac and nerve Na⁺ channels (Cruz et al, 1985), making these toxin useful probes for identifying structural differences between different Na⁺ channel subtypes.

Based on mutagenesis studies of the toxin, it has been suggested that the positively charged guanidinium group of Arg13 of μ-CTX is directly involved in the binding to sodium channels (Sato et al., 1991; Becker et al., 1992; Chahine et al., 1994). To further identify residues of the channel pore which might contribute to high-affinity μ-CTX binding, we constructed 17 cysteine pore mutants of the rat skeletal muscle Na⁻ channel (rSkM1). All mutations (except E1524C) were constructed in the ascending portion (SS2) of the P-loop in the four homologous domains (DI-DIV). Cysteine mutants were initially tested for Cd²⁺ sensitivity to assess their side chain accessibility and then tested for μ-CTX sensitivity. These studies therefore allowed us to identify pore-lining residues which influence the toxin binding to the pore.

In this report, we located 7 residues (D400, Y401, W402, E772, W1239, D1241, W1531) in the pore that significantly affected the binding of μ-CTX to Na⁻ channels. These results are discussed in relationship to previous models of Na⁻ channel pore structure.

5.3   *Methods and Materials*

5.3.1   *Toxin and sulfhydryl modifier application*

The recording solution used was ND 96 (section 2.7). For examining the Cd^{2+} and μ-CTX sensitivity of rSkM1 and mutant channels, appropriate amounts of $CdCl_2$ (Sigma, Mississauga, ON, Canada) and GIIIB homolog of μ-CTX (Biomol, Plymouth, PA, USA) were added to the bath recording solution from a 1M and 100 mM stock respectively. The purity of the toxin as provided by the supplier was 75% peptide content. Sulfhydryl modification by the methanethiosulfonate (MTS) derivative (Toronto Chemical Co., Toronto, Canada) MTSEA (MTS-ethylammonium), MTSES (MTS-ethylsulfonate) or MTSBN (benzyl methanethiosulfonate) was performed by exposing the cysteine mutants to 1 mM MTS-X for 3-10 min followed by a 5 min washout. Modification of the cysteinyl sulfhydryl side chain was reversed by adding 1 mM DTT (Fischer, Madison, USA). The MTS-X derivatives and DTT were prepared daily and dissolved in the recording solution.

5.3.2   *Statistical Analysis and Curve fitting*

Individual IC_{50} values were determined by fitting dose-response data, using the Marquardt-Levenberg algorithm in a non-linear least-squares procedure, to the binding equation:

$$I_B / I_O = 1 / (1 + [blocker] / IC_{50})$$ Equation 5.1

where I_B and I_O represent measured Na^+ currents respectively in the presence and absence of μ-CTX or Cd^{2+}, and IC_{50} is the [blocker] at which $I_B = 0.5\ I_O$. In cases where incomplete substate blocks were observed, a modified form of the binding equation was used to accomodate the steady-state component at relatively high blocker concentrations. Such an equation is given as follows:

161

$$I_B / I_O = (1-(I_B / I_O)^x) / (1+ [blocker] / IC_{50}) + {}_x I_B / I_O)^x \qquad \text{Equation 5.2}$$

where $(I_B / I_O)^x$ represents the fraction of current remaining at very high [blocker]. All mean values presented were calculated by taking the average of at least three individual IC_{50} values of each mutants. Data presented are the means $\pm$ SEM. Statistical significance was determined using an unpaired student's t-test with $p<0.05$ representing significance.

5.4   *Results*

5.4.1   *Pore-lining residues become Cd^{2+} sensitive after cysteine substitution*

Single cysteine mutants were created and initially probed with Cd^{2+} and the sulfhydryl reactive agent MTSEA in order to assess side-chain accessibility of putative P-loop residues that line the pore. All single cysteine mutants expressed functional channels except G1238C which did not express after at least 10 rounds of injection. Table 5.1 summarizes the half-blocking concentration (IC_{50}) for Cd^{2+} of each of the mutants before and after MTSEA modification. All mutants except W756C showed elevated Cd^{2+} sensitivity ($p<0.001$) when compared with the wild type (rSkM1) and were modified by MTSEA. All Cd^{2+} sensitive mutants became Cd^{2+} insensitive after MTSEA modification (Table 5.1) further supporting side-chain accessibility to the aqueous phase and establishing that the free inserted cysteine sulfhydryl was responsible for the elevated Cd^{2+} sensitivity of the single mutants.

5.4.2   *μ-Conotoxin sensitivity of rSkM1 and single cysteine mutants*

We initially examined the μ-CTX sensitivity of wild-type rSkM1 channels expressed in *Xenopus* oocytes to block by μ-CTX. Figure 5.1A shows a typical whole-cell current recording from an oocyte coexpressing the rSkM1 α-subunit with 5-fold excess of the rat brain β1 suburit. The currents were recorded using a 2-electrode voltage-clamp in the absence and presence of 30 nM μ-CTX following depolarization to -10 mV from a

Figure 5.1

A) Representative records of raw current traces of rSkM1 with (left panel) and without (right panel) co-expression with the rat brain $\beta 1$ subunit recorded in the absence and presence of 30 nM μ-CTX as indicated by arrows. Lack of $\beta 1$ co-expression resulted in slower inactivation kinetics but did not significantly affect the toxin binding.

B) The dose-response relationship for μ-CTX binding to rSkM1 Na⁻ channels with (solid square) and without (open circle) co-expression with $\beta 1$. Normalized peak Na⁺ currents at -10 mV were plotted as a function of extracellular μ·CTX concentrations. The curve fitted with the binding equation allows estimation of the IC_{50} for μ-CTX block (see 5.3). Data are plotted as mean $\pm$ S.E.M.. IC_{50} values estimated were : 17.4 $\pm$1.5 nM (n=5) with $\beta 1$ and 27.9 $\pm$1.8 nM (n=4) without $\beta 1$.

A

rSkM1+ ß1

rSkM1

30 nM μ-CTX
0 nM μ-CTX

30 nM μ-CTX
0 nM μ-CTX

1 μA

5 ms

1.5 μA

10 ms

B

I_B / I_o at -10 mV

[μ-CTX] (nM)
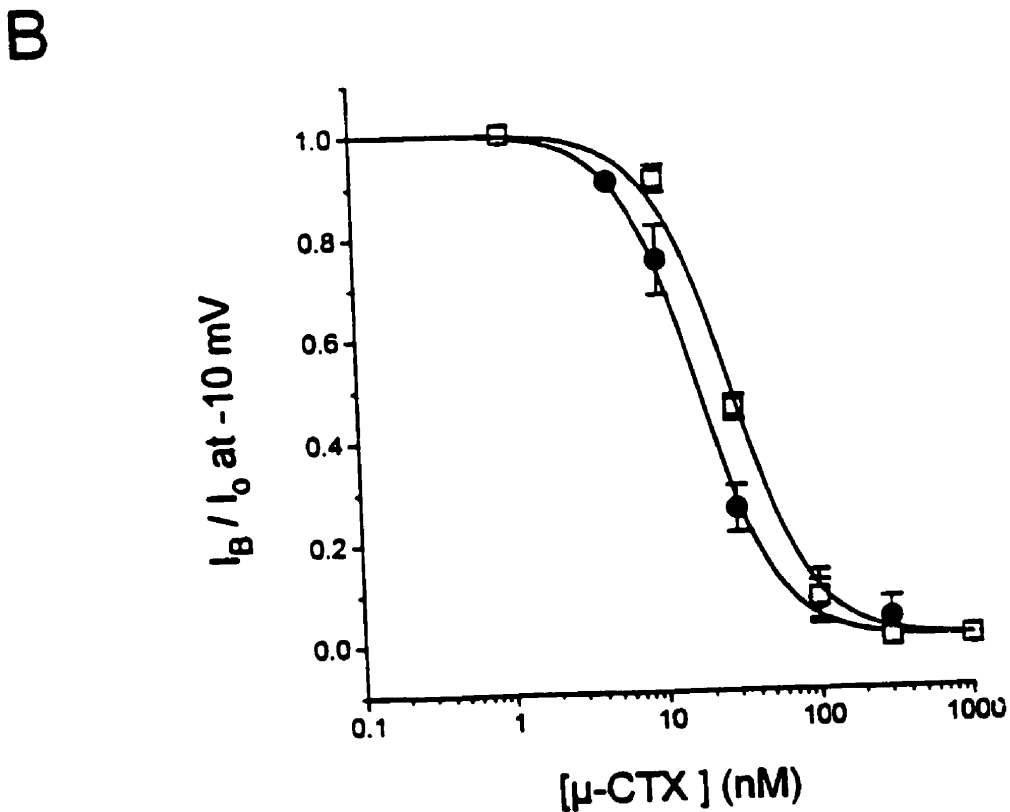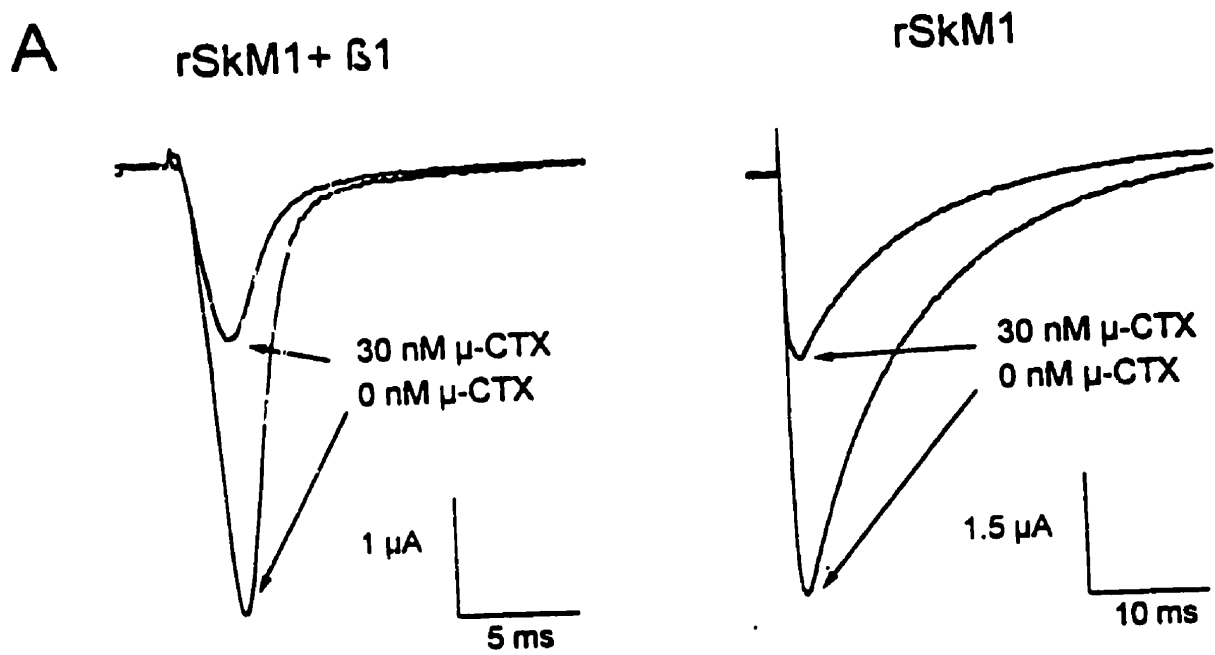
holding potential of -120 mV. The IC_{50} estimated from the binding curve fit to the data (solid circles) shown in Figure 5.1C was 17 4±1.5 nM (n=5) which falls within the range of 5 - 150 nM reported previously for expressed rSkM1 channels (Chen et al.. 1992; Stephan et al.. 1994; Dudley et al.. 1995). While the wide range of IC_{50} values measured previously could originate from differences in toxin purity, it is also conceivable that the level of co-expression with the rat brain β1 Na⁺ channel subunit could contribute to, or be responsible for these differences. To address this question, we examined the effects of μ-CTX block on rSkM1 channels without co-expressing β1. The representative current trace in Figure 5.1A (right panel) shows the expected slowing of inactivation kinetics when the rSkM1 α subunit is expressed alone (Krafte et al. 1988; Zhou et al. 1991; Cannon et al. 1993; Nuss et al. 1995) (cf compare with Figure 5.1A. left panel). In spite of these changes in channel gating, Figure 5.1B shows that β1 subunits did not significantly (P>0.05) effect the sensitivity for μ-CTX block (IC_{50} = 27.9 ± 1.8 nM. n=4 without β1).

All single cysteine substitution in the P-loops of the four internal repeats of rSkM1 expressed functional channels except G1238C. Furthermore, all mutant channels except W756C were sensitive to externally applied Cd^{2+} and MTSEA suggesting these residues line the extracellular face of the pore (Tsushima et al.. 1997a.b) and thereby might influence toxin interaction with the channel.

Figure 5.2 summarizes the estimated IC_{50} values for μ-CTX binding to our single cysteine mutants with significant differences from wild-type indicated by asterisks. All mutant channels were co-expressed with β1. Most cysteine substitutions did not significantly alter sensitivty to block by μ-CTX compared to rSkM1. However, the negative charge substitution mutants E758C (IC_{50} = 220±39 nM, n=5) and D12-₁C (IC_{50} = 112±24 nM, n=6) were about 15- and 6-fold less sensitive to μ-CTX block than rSkM1. In contrast, the tryptophan substitution mutants W402C (IC_{50} = 1.9±0.1 nM, n=4), W1239C (IC_{50} = 4.9±0.9 nM, n=5) and W1531C (IC_{50} = 5.5±0.4 nM, n=5) were about 10-, 4- and 3-fold more sensitive to μ-CTX block compared to rSkM1 channels. The estimated IC_{50} values for

Figure 5.2

Summary of the changes in μ-CTX sensitivities: plot of the half-blocking concentration (IC_{50}) for μ-CTX block of each of the single cysteine mutants. Roman numerals denote the corresponding domain numbers. All mutants formed functional channels except G1238C which showed no expression (n.e.). Data represent at least three individual IC_{50} determinations for each of the mutants. The abscissa represents the wild-type sensitivity to μ-CTX block. The left ordinate axis measures the ratio of the IC_{50} for mutant channels to the IC_{50} for rSkM1 channels on a logarithmic scale. The right ordinate represents the absolute IC_{50} (nM) plotted on a logarithmic scale. Mutants with IC_{50} values that are statistically different (p<0.05) from WT are marked with asterisks. D400C. Y401C. E758C and D1241C were less sensitive to μ-CTX block than WT whereas W402C. W1239C and W1531C were more sensitive.

I

100 — 10 — 1 — 0.1 — 0.01

1000 — 100 — 10 — 1 — 0.1

* * W402C E403C

D400C Y401C *

II

100 — 10 — 1 — 0.1 — 0.01

1000 — 100 — 10 — 1 — 0.1

*

E755C W756C I757C E758C

$IC_{50,Mutant} / IC_{50,WT}$

$IC_{50} (nM)$

III

100 — 10 — 1 — 0.1 — 0.01

1000 — 100 — 10 — 1 — 0.1

n.e. W1239C *

K1237C G1238C M1240C D1241C *

IV

100 — 10 — 1 — 0.1 — 0.01

1000 — 100 — 10 — 1 — 0.1

G1530C W1531C

A1529C D1532C *
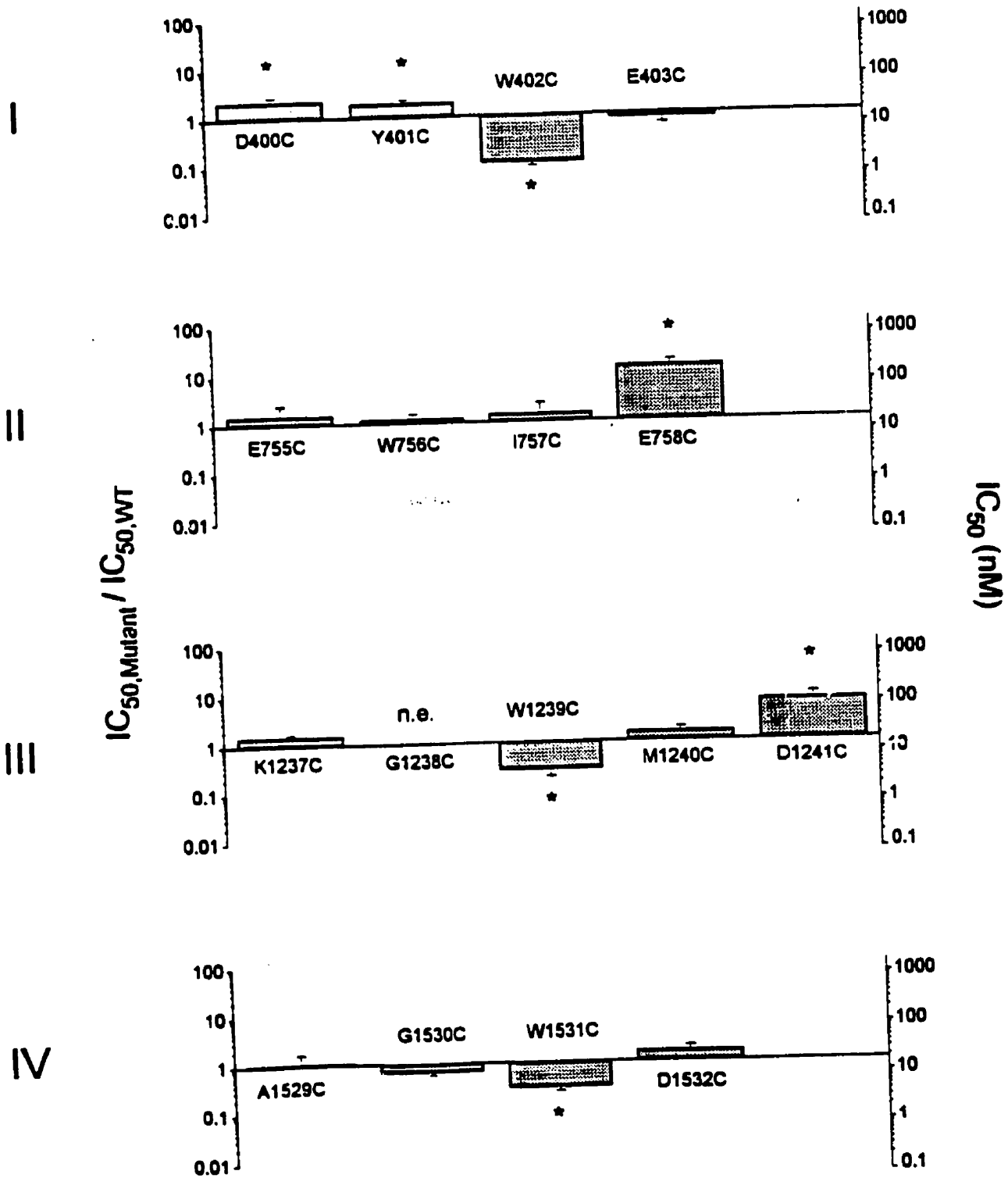
μ-CTX binding to D400C (38.8±4.5 nM, n=4) and Y401C (32.9±2.1 nM, n=3) were only modestly, yet significantly (p < 0.05), different from rSkM1 channels.

5.4.3 Effects of charge replacements on μ-CTX sensitivity of charged mutants

One simple explanation for the reduced potency to μ-CTX block of E758C and D1241C mutant channels is the loss of negative charge disrupts the electrostatic interactions with positively-charged toxins. If electrostatic interactions are important, introduction of a positive charge to the cysteine sulfhydryl might further destabilize toxin binding while replacing a negative charge should strengthen toxin binding. Methane thiosulfonate derivatives MTSEA (positively-charged) and MTSES (negatively-charged), which have been used for many functional studies of ion channels (Akabas et al., 1992, 1994a,b; Kurz et al., 1995; Pascual et al., 1995; Li et al., 1996; Perez-Garcia et al., 1996), were chosen to introduce positive and negative charges to the pore of the cysteine mutants. In these experiments 1 mM MTSEA and MTSES were applied for 3-10 minutes and subsequently washed out prior to the application of μ-CTX. The duration of application was chosen to be sufficient to ensure complete modification of all channels. Complete charge insertion was established using two independent methods.

First, following application and washout of MTSEA and MTSES, the peak current recorded in response to depolarizing pulses changed irreversibly (Perez-Garcia et al., 1996). As an example, Figure 5.3A depicts the peak current-voltage relationship recorded in E758C channels before (solid square) and after modification with 1mM MTSEA (left) and MTSES (right) applied for 5 minutes. Reductions in peak current by MTSEA and the increase in peak current by MTSES recorded in E758C channels were reversed following treatment with 10 mM DTT (open triangle) applied for 10 minutes.

Sulfhydryl modification was further verified by examining the sensitivity to Cd^{2+} block before and after treatment with MTSEA and MTSES. Since these agents react with free sulfhydryls by forming disulfide bonds (Akabas et al., 1992) and since Cd^{2+} binds with

Figure 5.3

The effects of MTS-X modifications on E758C.

A) The current-voltage relationships of E758C before and after MTSEA (left panel) and MTSES (right panel) modifications. MTS-X modifications were irreversible in the absence of reducing agents and persisted even after prolonged washout. Both MTSEA and MTSES modifications could however be reversed by adding 1 mM DTT in the recording solution. Other single mutants also showed similar results.

B) Current traces of E758C in the absence (solid line) and presence (broken line) of 300 mM Cd^{2+} before (left panel) and after MTSEA (middle panel) and MTSES (right panel) modifications. Current records have been scaled such that the peak currents at the baseline are equal. The vertical scale bar represents 1.2, 0.8 and 1.3 mA for control, after MTSEA and MTSES respectively.

C) Dose-response curves of the normalized peak Na^+ currents as a function of extracellular Cd^{2+} concentrations. MTSES (diamond, n=3) and MTSEA (triangle, n=3) shifted the Cd^{2+} binding curve of E758C channels (circle, n=4) to the right. Note the presence of a Cd^{2+} resistant plateau at high Cd^{2+} concentrations suggesting that these channels were blocked by Cd^{2+} to a subconductance state. A modified version of the binding equation was used in order to accomodate for these steady-state components (see Materials and Methods).

A

MTSEA

MTSES

B

E758C

E758C
(MTSEA modified)

E758C
(MTSES modified)

C
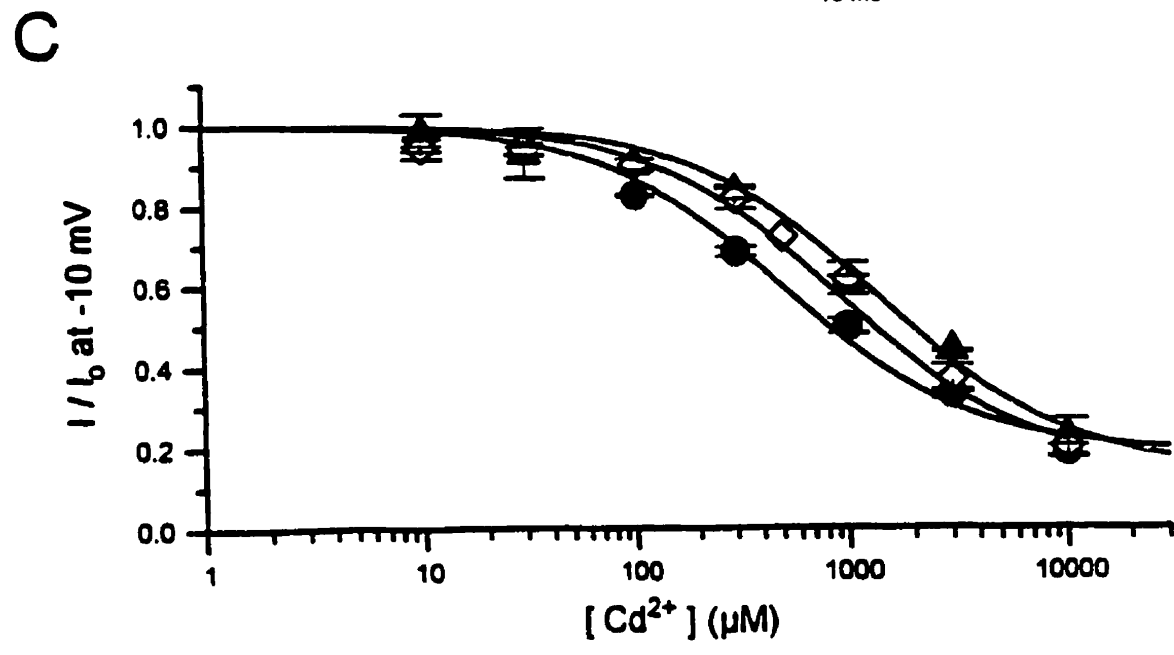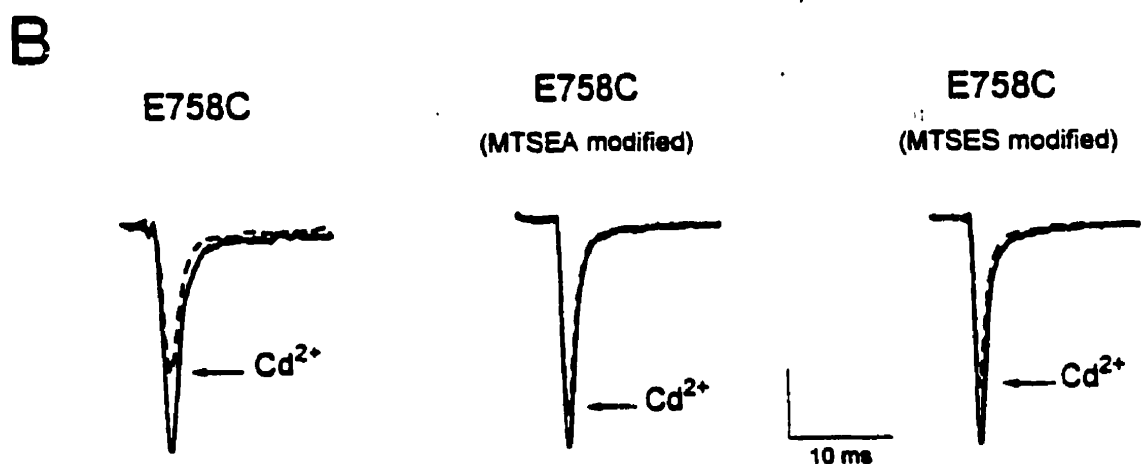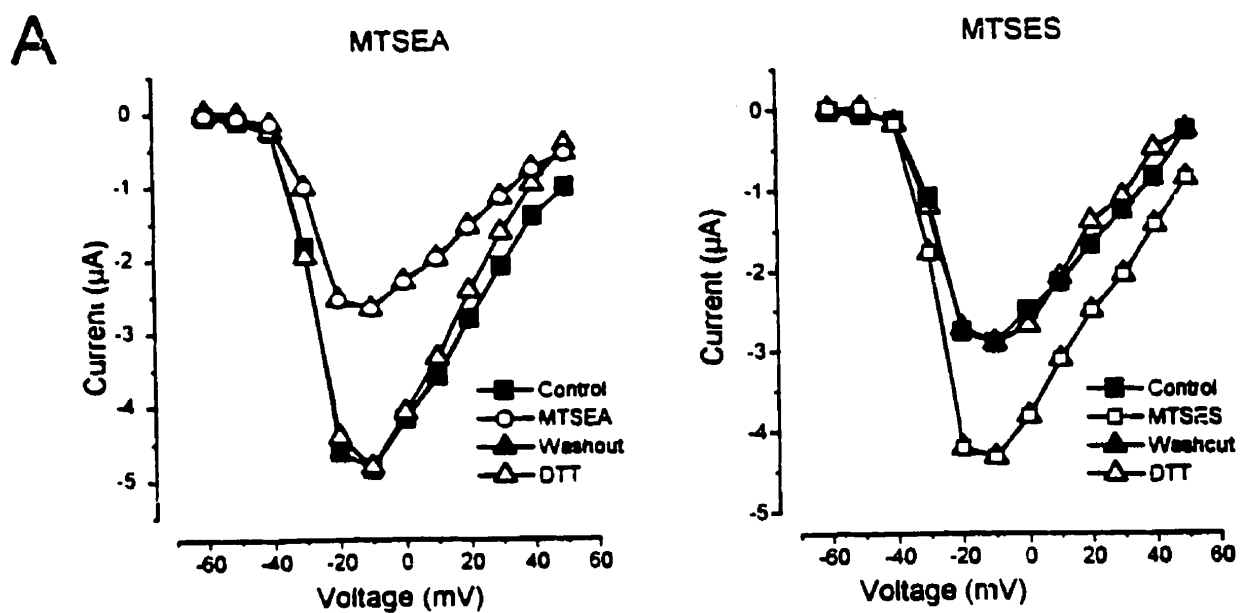
much higher affinity to free sulfhydryls compared to disulfide-linked sulfhydryls (Torchinsky, 1981), successful modification of our cysteine mutant channels by MTSEA and MTSES should result in reductions in Cd^{2+} binding affinity. As an example, Figure 5.3B shows whole-cell current traces recorded in oocytes expressing E758C channels following depolarization to -10 mV from a holding potential of -120 mV before (solid lines) and after (broken line) the application of 300 mM Cd^{2+} in the absence (left panel) and presence of sulfhydryl agents (MTSEA, middle panel and MTSES, right panel). Clearly, following the introduction of MTSEA and MTSES, only a small fraction of the current was blocked by 300 mM Cd^{2+}. This observation is quantified in Figure 5.3C showing the fraction of peak current recorded with E758C channels expressed in oocytes following depolarization to -10 mV as a function of extracellular $[Cd^{2+}]$ current: the average estimated IC_{50} (see methods) for Cd^{2+} from Figure 5.3C was increased from 493.3 ± 34.2 µM (n=4) to 1054 ± 112 µM (n=3) by MTSEA and to 1120 ± 224 µM (n=3) by MTSES application. Notice that the IC_{50} estimated following the application of MTSEA and MTSES are not statistically different (p > 0.05) from WT channels (i.e. 1250 ± 224 µM). Similar analyzes were used for all the cysteine mutants studied to ensure successful sulfhydryl modification by the methanethiosulfonate derivatives (See Table 5.1).

Careful inspection of Figure 5.3C demonstrate that E758C channels are not fully blocked by high $[Cd^{2+}]$. Similar results were also observed in E403C channels. Single-channel recordings reveal that incomplete blockade at high $[Cd^{2+}]$ results from the incomplete block of unitary current to a subconductance level, rather than a full conductance closure (Tsushima et al, 1997b). Nevertheless, the presence of incomplete block did not interfere with our ability to establish complete modification of the inserted cysteine by MTSEA and MTSES.

Having confirmed that the cysteine mutant channels could be successfully modified by methanethiosulfonate derivatives, we next examined the effects of charge insertions using MTSEA and MTSES on µ-CTX binding (Figure 5.4). MTSEA and MTSES application did not significantly affect our estimates of IC_{50} for µ-CTX block in wild-type,

Table 5.1

Half-blocking concentrations (IC_{50}) for Cd^{2+} of WT and mutant Na^+ channels before and after MTSEA modification Abbreviations: n.a.=not available, n.e.=no expression.

Mutants	IC_{50} (mM)	IC_{50} (mM) after MTSEA modification
WT (Skm1)	1250 ± 224	1340 ± 250
D400C	880 ± 102	n.a.
Y401C	13.0 ± 2.5	1581 ± 86
W402C	199 ± 9	1235 ± 146
E403C	283 ± 20	1176 ± 227
E755C	55 ± 12	720 ± 120
W756C	1081 ± 62	n.a.
I757C	200± 23	858 ± 74
E758C	493 ± 34	1054 ± 112
K1237C	159 ± 23	1150 ± 152
G1238C	n.e.	n.e.
W1239C	37 ± 10	323 ± 25
M1240C	569 ± 30	1209 ± 125
D1241C	454 ± 46	1910 ± 262
A1529C	297 ± 58	800 ± 58
G1530C	68 ± 9	1722 ± 168
W1531C	46 ± 5	1625 ± 250
D1532C	602 ± 70	2325 ± 287
G1533C	33 ± 5	n.a.

Figure 5.4

A) Na⁻ current tracings of E758C and D1241C mutant channels in response to depolarization to -10 mV from a holding potential of -120 mV in the absence (solid line) and presence (broken line) of 300 nM μ-CTX before and after MTSES and MTSEA modifications. Current amplitudes were normalized to the peak current for each mutant in the absence of μ-CTX. The vertical scale bar represents 1.5, 0.9 and 1.3 mA for E758C, E758C after MTSEA and 0.8, 1.1 and 1.3 μA for E758C after MTSES, D1241C, D1241C after MTSEA and D1241C after MTSES, respectively.

B) Bar graphs summarizing the half-blocking concentrations (IC_{50}) for μ-CTX of WT (rSkM1), E403C, E758C, D1241C and D1532C before and after MTSES and MTSEA modifications. μ-CTX sensitivities of WT, E403C and D1532C were not significantly altered by applications of MTS-X ($p > 0.05$). E758C and D1241C became less susceptible to μ-CTX block after MTSEA modification. MTSES increased the μ-CTX sensitivity of D1241C but had no effect on toxin binding to E758C. The data presented are the mean ± SEM from 3 to 6 oocytes.
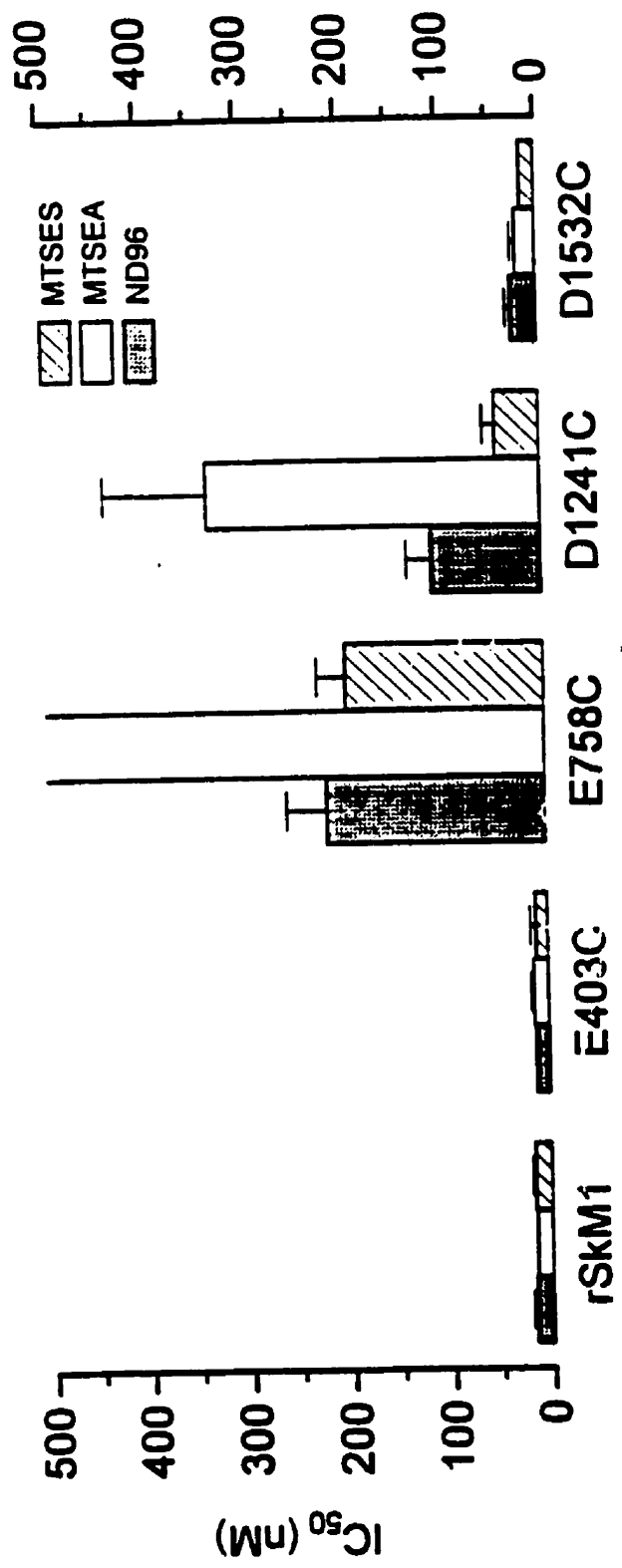
Figure 5.5

Dose-response curves of the normalized peak Na$^-$ currents at -10 mV as a function of extracellular μ-CTX concentrations before (open square) and after MTSEA (circle) and MTSES (triangle) modification. MTSEA completely abolished μ-CTX sensitivity of E758C while MTSES did not significantly affect μ-CTX binding to these channels. Data were fit to a Hill equation assuming n=1.
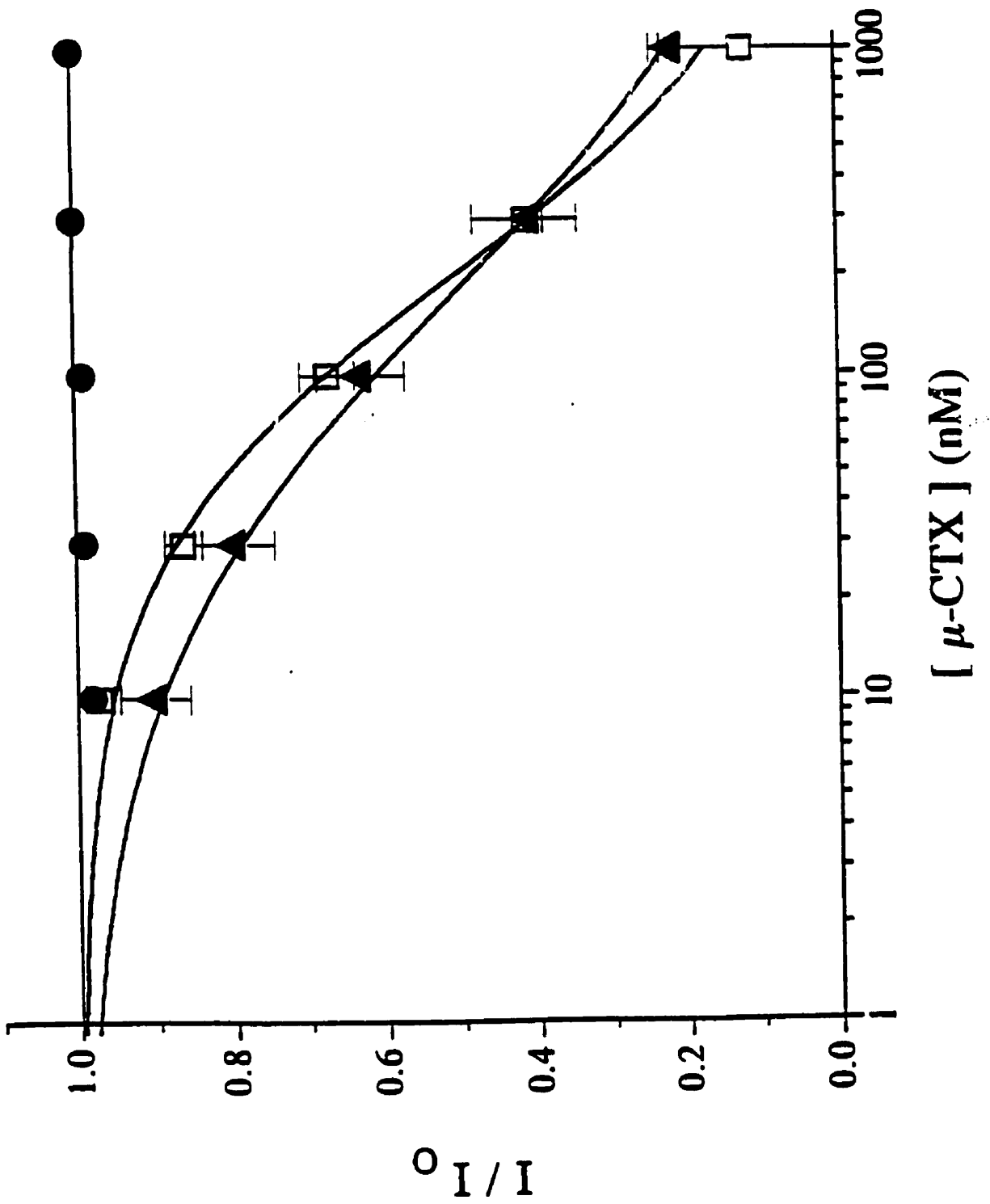
E403C or D1532C. These observations are anticipated for rSkM1 channels due to the absence of free sulfhydryls in the pores of these channels (Backx et al.. 1992) and for E403C and D1532C channels since toxin block of these channels were not different from rSkM1 channels despite the change in charge after modification.

By comparison. Figure 5.4 shows that MTSEA application to D1241C channels further destabilized toxin binding thereby increasing the IC_{50} for μ-CTX block to 334 ± 103 nM (n=3, p<0.05) while MTSES increased the μ-CTX sensitivity to 46 ± 12 nM (n=3 p<0.05) suggesting that charge at position 1241 is a determinant of toxin binding. More dramatic changes were observed with E758C: MTSEA modification completely abolished μ-CTX block even at μ-CTX concentrations as high as 1 mM (Figures 5.4 & 5.5) while MTSES treatment did not significantly affect μ-CTX sensitivity (IC_{50} = 199.8 ± 21.8 nM, n=4 for MTSES compared to IC_{50} = 220 ± 39 nM. n=5 for control). These results combined with the results in Figure 5.2. suggest that the charge at position 758 plays an important role in μ-CTX binding. However. the effects of MTSEA and MTSES are clearly disproportionate. That is. insertion of a positive charge has an enormous effect on toxin binding while negative charge replacement causes no significant change. despite the similarity in molecular size and shape of MTSEA and MTSES. This observation demonstrates that factors other than just charge magnitude also critically influence toxin binding.

5.4.4 *Competitive binding between Cd^{2+} and μ-CTX in E758C and D1241C channels*

To further test the role of charge and charge localization at positions E758 and D1241 in μ-CTX binding, we examined the ability of 1.0 mM Cd^{2+} to modify μ-CTX binding affinities. Since specific Cd^{2+} binding to cysteine sulfhydryls (Li et al. 1996: Perez-Garcia et al. 1996) will introduce a local positive charge, we anticipate that μ-CTX binding to E758C and D1241C channels might be more destabilized than to rSkM1 in the presence of Cd^{2+}. Furthermore, the location of the added charge . due to the lack of an ethyl alkyl

chain, should differ from the site of the positive charge introduced by MTSEA. However, rSkM1 and E758C channels became about 2-fold less sensitive to μ-CTX in the presence of 1.0 mM Cd^{2-} (31.76±2.59 nM, n=4 and 458±150 nM, n=4 respectively) while the IC_{50} for μ-CTX binding to D1241C was only modestly increased to 158±29 nM (n=6). Clearly, MTSEA and Cd^{2-} had differential effects on the sensitivities of E758C and D1241C channels to μ-CTX block. Nevertheless, these results are not inconsistent with the importance of charges at these positions on toxin binding. These differences might reflect the dynamic binding and unbinding of Cd^{2-}. Unlike MTSEA, Cd^{2-} dynamically binds and unbinds to the pore. As a result, the kinetics of Cd^{2-} binding in relationship to μ-CTX binding could influence their interaction. Assuming no dramatic alterations in channel structure following Cd^{2-} binding, these observations suggest that μ-CTX binds to the channel pore.

5.4.5 Modification of -CTX binding to W402C, W1239C and W1531C using sulfhydryl modification

In order to investigate the nature of toxin-channel interaction at positions 402, 1239 and 1531, we added MTSEA, MTSES and MTSBN to W402C, W1239C and W1531C channels. Despite their opposite charges, both MTSEA and MTSES increased the IC_{50} tor μ-CTX block for the three tryptophan-to-cysteine mutants (Figure 5.6). After MTSEA modification, the IC_{50} values of W402C, W1239C and W1531C increased from 1.9±0.1 nM (n=4), 4.9±0.9 nM (n=5) and 5.5±0.4nM (n=5) to 12.5±1.2nM (n=4), 15.1±1.9nM (n=5) and 12.2±3.4nM (n=4) respectively, while with MTSES the IC_{50} values changed to 7.0±1.3nM (n=4), 8.2±0.5nM (n=4) and 11.8±3.1nM (n=4). Since both MTSEA and MTSES decreased μ-CTX sensitivity, it appears that electrostatic interactions at these positions are not important components of μ-CTX binding. Therefore, we hypothesized that the presence of any additional side chain bulk at these positions will decrease toxin binding. To test this hypothesis, we applied the agent MTSBN (benzyl methanethiosulfonate), which attaches a neutral benzyl group resembling the tryptophan side-chain to the inserted cysteine sulfhydryl. In accordance with our postulate, MTSBN modification fully restored the lower
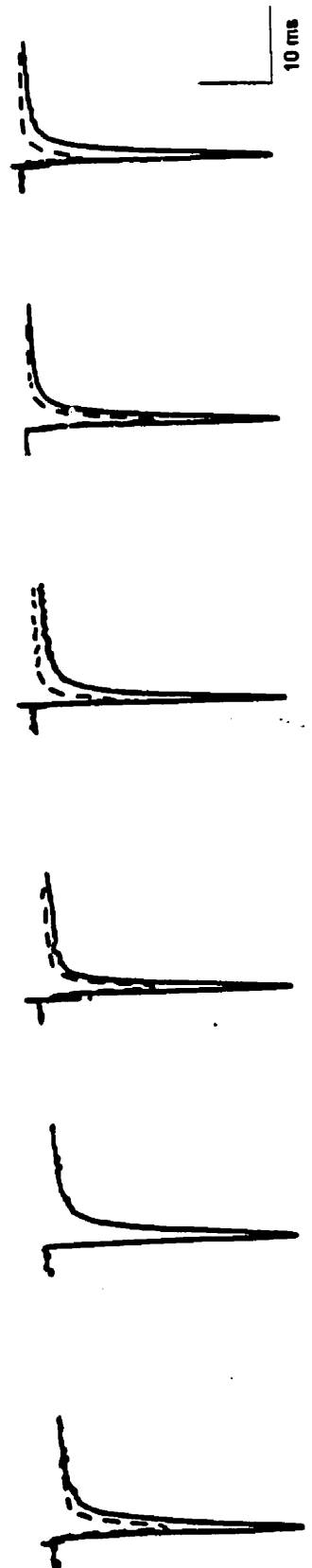
Figure 5.6

A) Na⁺ current tracings of W402C, W1239C and W1531C mutant channels in response to depolarization to -10 mV from a holding potential of -120 mV in the absence (solid line) and presence (broken line) of 10 nM µ-CTX before and after MTSES, MTSEA and MTSBN modifications. Peak control currents have been normalized to the same magnitude. Vertical scale bar represents currents range from 0.6 to 2.2 mA.

B) Bar graphs summarizing the half-blocking concentrations (IC_{50}) for µ-CTX of WT (rSkM1), W402C, W1239C and W1531C before and after MTSES, MTSEA and MTSBN modifications. All three agents were capable of partially or fully restoring WT µ-CTX sensitivity to W402C, W1239C and W1531C. WT channel sensitivity to µ-CTX block were not modified by MTSEA, MTSES and MTSBN.

179
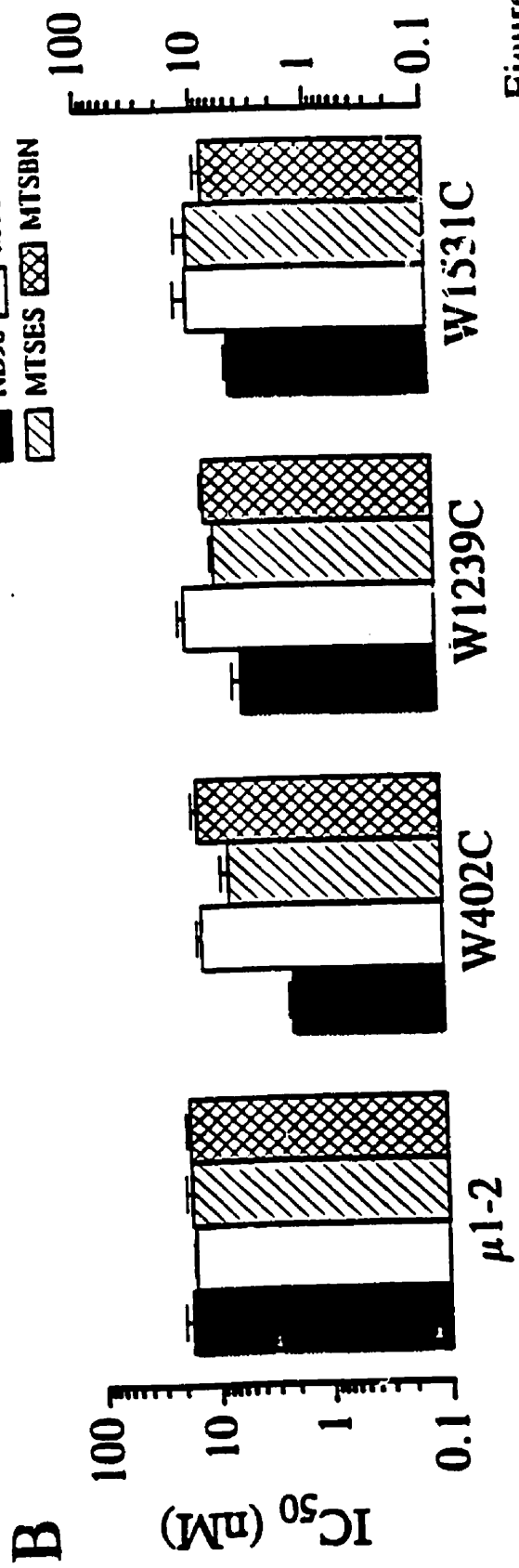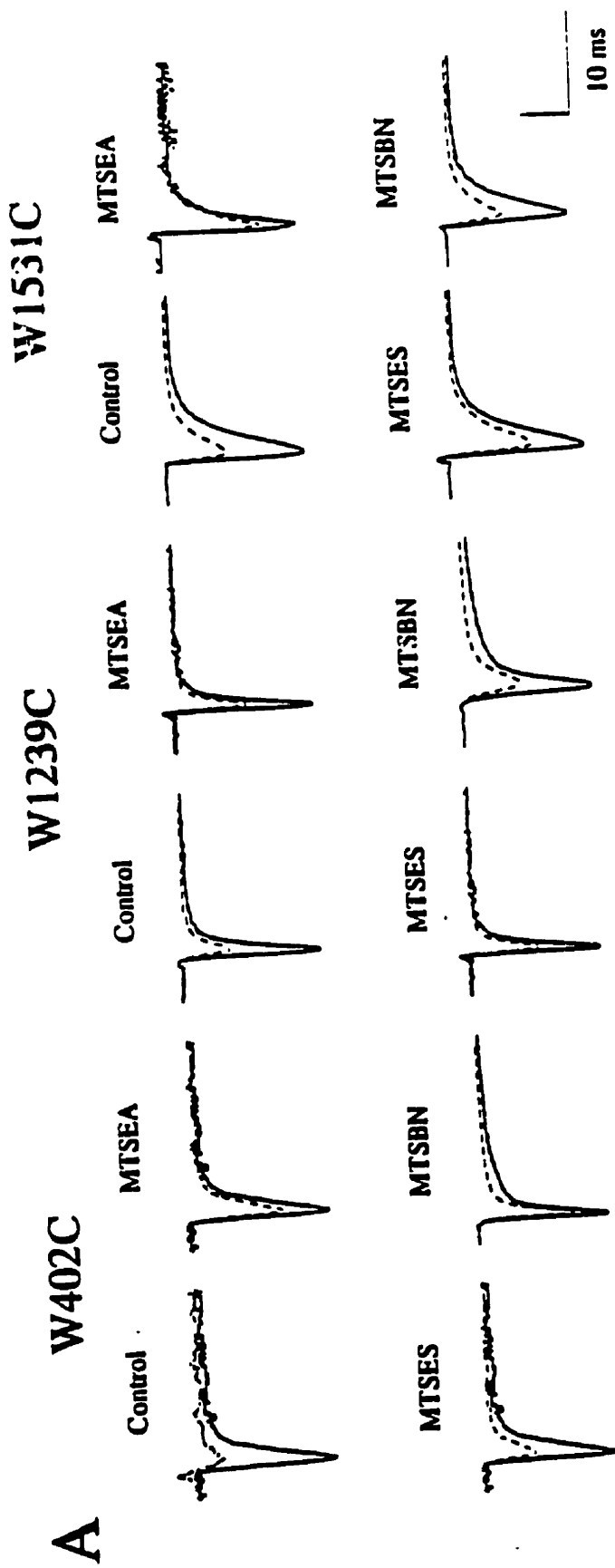
Figure 6

wild-type μ-CTX sensitivity in W402C (12.7±2.0 nM, n=4) and W1239C (17.75±0.6 nM, n=5) while largely restoring the sensitivity of W1531C (8.5±1.2 nM, n=4). The incomplete restoration for W1531C may be attributed to the distant attachment of the benzyl group by an ethyl alkyl chain. Nevertheless, these observations suggest that side chain bulkiness at these positions influences μ-CTX binding.

5.4.6 *E1524C shows wild-type sensitivities to Cd^{2+} and μ-CTX block*

All P-loop residues studied above, except Y401C, are conserved between cardiac, nerve and skeletal muscle Na^+ channels despite much stronger binding of μ-CTX to skeletal muscle Na^+ channels. Previous results using chimeric exchanges of domains of cardiac and skeletal muscle Na^+ channels established that domains I and IV were primarily responsible for the differences observed in μ-CTX sensitivity in these Na^+ channel subtypes (Chen et al, 1992, Chahine, et al; 1996). In the descending portion of the P-loop in domain IV, skeletal muscle Na^+ channels have a glutamate at position 1524, that is conserved at the equivalent position in electric eel Na^+ channels while being a neutral glutamine in heart and brain Na^+ channel subtypes. Since E1524 is negatively charged and is only found in the μ-CTX-sensitive Na^+ channels, we speculated that this residue might be crucial for the high affinity toxin binding of the skeletal muscle and electric eel subtypes. Similar to all other cysteine mutants, E1524C channels were first probed with Cd^{2+} and then tested for μ-CTX sensitivity. This mutant channel showed the wild-type sensitivity to Cd^{2+} block (1120±129 mM, n=5) suggesting that the side chain of this glutamate residue does not lie within the permeation pathway. In spite of the lack of Cd^{2+} sensitivity for this mutant, it is still conceivable that it may play a role in isoform-specific binding of μ-CTX. However, E1524C showed wild-type sensitivity to μ-CTX block (22.4±5.8 nM, .'=4) demonstrating that this residue does not play a significant role in the specific high affinity block of μ-CTX to the skeletal muscle Na^+ channels.

181

5.5   *Discussion*

In the present study, we used cysteine mutagenesis to identify P-loop residues in the four internal repeat domains of rat skeletal muscle Na channels that are important for binding μ-CTX since this strategy enables identification of pore-lining residues and allows sulfhydryl-specific chemical modifications in charge and size at the residues under examination. Most cysteine replacements of P-loop made in our studies (except G1238C) produced functional channels with relatively normal macroscopic channel kinetics (Li et al. 1996; Perez-Garcia et al.1996) suggesting preserved pore structure. Furthermore, all P-loop residues replaced by cysteine appeared to line the pore as assessed by Cd^{2+} block and sulfhydryl modification. Our results identify seven pore lining residues that significantly influenced μ-CTX binding to rSkM1 channels: D400, Y401, W402, E758, W1239, D1241 and W1531 (Figure 5.2).

Expected and unexpected results were obtained with negative charge replacement mutants like E403C, E758C, D1241C and D1532C channels. Modification of E403C and D1532C with MTSEA and MTSES had no affect on toxin binding, as expected from the identical μ-CTX binding of E403C, D1532C and rSkM1 channels; apparently these residues do not participate in μ-CTX binding. Similarly, MTSEA modification of E758C and D1241C channels, whose IC_{50} values for μ-CTX binding were 15-fold and 6-fold higher than rSkM1, further increased the IC_{50} for μ-CTX binding with E758C channels becoming completely resistant to block by concentration up to 1 mM (see Figure 5.5). On the other hand, MTSES treatment of D1241C enhanced the toxin sensitivity to a value approaching wild type channels whereas MTSES modification had little effects on toxin binding to E758C channels. Taken together, these results are consistent with electrostatic interactions between the charges at position 758 and 1241 and μ-CTX. However, simple charge substitution at position 758 did not produce expected effects; restoring the negative charge using MTSES in E758C had modest effects on toxin binding while insertion of a positive charge by MTSEA completely eliminated toxin binding. One potential explanation for these unexpected findings is that the inserted charged groups are not localized to

equivalent molecular positions with MTSES and MTSEA due to their attachment via an ethyl alkyl chain (Akabas et al. 1992). Alternatively, modification by methanethiosulfonate compounds could induce local structural changes to the P-loops thereby altering toxin binding.

To further test the role of charge and its localization within the channel pore on μ-CTX binding, we examined the effects of Cd^{2+} on toxin binding to E758C and D1241C channels. Similar competitive binding studies between Zn^{2+} and STX have previously been performed in cardiac Na^+ channels (Schild and Moczydlowski, 1991; Doyle et al. 1993). μ-CTX block was only slightly reduced in E758C and D1241C channels in the presence of Cd^{2+} compared to MTSEA treatment possibly reflecting either the dynamic nature of the interaction of the channel with Cd^{2+} compared to irreversible channel modification by cysteine modifying agents or the differences in charge distribution and localization. Since μ-CTX block of rSkM1 was also impaired in the presence of Cd^{2+}, our results are consistent with μ-CTX binding to the channel pore.

Our data generally support previous hypotheses that electrostatic interactions between negatively charged residues within the channel pore and the positively charges μ-CTX are important factors for high affinity μ-CTX binding (Becker et al. 1992; Stephan et al. 1994; Dudley et al. 1996). However, negatively charged residues at equivalent locations in the four internal repeat domains do not contribute equally to this interaction. Indeed, E403C and D1532C mutant channels showed wild-type behavior with respect to μ-CTX block while E758C and D1241C channels were far less sensitive to μ-CTX block than rSkM1 channels. Therefore our results establish that these negatively charged residues do not contribute equally to toxin binding. The non-equivalence of the negatively charged residues located at equivalent alignment position could reflect a non-symmetric arrangement of the residues within the pore (Chiaminovat et al., 1996). Alternatively, the toxin might interact with a symmetric pore in an off-axis fashion (Gross et al, 1996) similar to that observed for AgTx binding to the *Shaker* K^+ channels.

The large reductions in affinity for μ-CTX observed in E758C and D1241C are consistent with the suggestion that Arg13 of μ-CTX interacts with the negatively charged groups of glutamate and aspartate side chains within the pore (Becker et al: 1992; Dudley et al, 1995). Becker and co-workers (1992) suggested that glutamate residues within the pore interact with Arg13 of μ-CTX, which has been shown to be an essential residue for the toxin binding to the channel since mutations of this toxin residue dramatically reduced the toxin binding affinity (Sato et al., 1991; Becker et al., 1992; Chahine et al., 1994). The potency of μ-CTX to block is related to the positive charge of the guanidinium group of Arg13 since replacement with lysine or ornithine had only moderate effects on affinity compared to less conservative substitutions using alanine, glutamine and arginine (Sato et al., 1991; Chahine et al., 1994; Chang et al., 1998). These observations support the hypothesis that interactions between positive charges on the toxin with negative charges within the channel pore are essential for high affinity toxin binding. This electrostatic hypothesis is consistent with our observation that E758C had the largest effect on μ-CTX binding. Our finding is also consistent with the model proposed previously by Dudley and colleagues (1995) in which E758 interacts with the N-H moiety of the guanidinium group of Arg13 (Dudley et al., 1995). In fact, reversal of charges at E758 of the channel and Arg13 of the toxin (i.e. the E758K / R13D pair) which partially restores wild-type block further confirms a pure electrostatic interaction between these two locations of opposite charges (Chang et al., 1998). In addition, our observations of a modest decrease by 2.2-fold in μ-CTX binding to D400C channels and no change in toxin binding to E755C channels (P>0.05) compared to rSkM1 (Figure 5.2) are also consistent with a revised Lipkind-Fozzard model of μ-CTX binding which proposes that Arg-13 of the toxin interacts only with the outer vestibule but does not reach deeply into the pore to the putative selectivity filter (i.e. D400, E755, K1237 and A1529) because of its bulk (Chang et al., 1998). Mutation of E403 also showed little effect on μ-CTX binding consistent with the suggestion that the aliphatic portion of Arg-13 may face E403 (Stephan et al., 1994).

Interestingly, the tryptophan-to-cysteine mutants (W402C, W1239C and W1531C) were more sensitive to μ-CTX block. Since both MTSEA and MTSES decreased μ-CTX

sensitivity to about the same extent in spite of their opposite charges, we speculated that reintroduction of large side groups at those positions would influence toxin binding. Consistent with this suggestion, modification of channels with MTSBN (which attaches an ethylbenzene side group to the inserted cysteine sulfhydryl), largely restored wild-type μ-CTX binding affinities to these mutants. Furthermore, we found that the sensitivity of W1531A (7.5±1.3nM, n=4) to μ-CTX block was similar to W1531C while that of W1531Y (14.6±3.5nM, n=5) was indistinguishable from wild-type.

Sequence alignment analysis of the voltage-gated Na channels reveal a high homology within the four pore forming regions, with very few nonconservative differences in amino acid composition. Two such notable differences are Y401 and E1524. The tyrosine at position 401 of rSkM1 is critical for TTX/STX sensitivity (Backx et al., 1992) while phenylalanine at the equivalent position in brain Na$^-$ channels also confers high affinity TTX/STX binding to the channel (Heineman et al., 1992b). Substitution of the Tyr or Phe residues for cysteine, which is the residue found in the TTX/STX resistant cardiac isoform at the equivalent position (Satin et al., 1992), abolishes TTX sensitivity of both skeletal muscle and brain Na$^-$ channels while enhancing their sensitivity to Cd^{2-} block by 200-fold (Backx et al. 1992; Heinneman et al, 1992). This residue ,however, cannot account for the 10^3-fold differences in sensitivity to μ-CTX between cardiac and skeletal muscle Na$^-$ channels since Y401C reduced μ-CTX binding by only 2-fold (Chen et al., 1992 and Chahine et al., 1995). Though TTX/STX competitively bind with μ-CTX to the Na$^-$ channel, it is not uncommon that mutations that significantly affect TTX/STX binding only have slight or no effects on the affinity of μ-CTX (Chahine et al., 1995; Chen et al., 1992; Stephan et al., 1994; Chahine et al., 1998). These observations suggest that binding of the bulkier μ-CTX to its receptor certainly involves interactions with other regions of the channel despite the binding sites for these toxins may overlap. Similar to Y401, mutation of E1524 to cysteine had no effect on toxin sensitivity suggesting this residue is also not responsible for the differences in toxin affinity between the μ-CTX sensitive skeletal and μ-CTX insensitive cardiac channel subtypes. Nevertheless, recent chimeric studies between rSkM1 and hH1 Na$^-$ channels have revealed the order of influence for toxin binding by the

185

four domains as D2>D1>D4 (Chahine et al., 1998). Swapping D2 of rSkM1 with that of hH1 renders the chimeric construct insensitive to μ-CTX block with $IC_{50}>10.000$ nM (Chahine et al., 1998). However the exact structural elements underlying these subtype differences at the molecular level still remain to be determined.

In summary, our results support models wherein μ-CTX interacts with E758 in skeletal muscle Na⁻ channel pore. Our results further suggest that the D-III residue D1241 is also an important determinant of toxin binding. The fact that the tryptophan mutants (W402C, W1239C and W1531C) are more sensitive to μ-CTX block suggests that these large uncharged residue side-chains appear to inhibit or weaken the toxin-channel interaction in WT channels. Finally, the differences in μ CTX binding between cardiac and rat skeletal muscle Na⁺ channels do not originate from absolutely conserved differences at position 401 (i.e. Y401C) or 1524 (i.e. E1524Q).

CHAPTER 6

Na⁺ CHANNEL PORE & LOCAL ANESTHETIC BINDING

6.1   *Abstract*

Voltage-gated Na⁻ channels are responsible for initiating action potentials in excitable cells and are the targets of local anesthetics. The local anesthetic binding site has previously been shown to reside on the cytoplasmic face of Na⁻ channel but the exact constituents remain unresolved. Cysteine mutagenesis reveals that certain P-loop residues also affect local anesthetic block. Mutation of the W1531 residue in rat skeletal muscle Na⁻ channel (rSkM1), located within the ascending portion (SS2) of the P-loop in Domain IV, to cysteine abolished use-dependent blockade and voltage-dependent shifts of channel availability by lidocaine. W1531C channels also eliminated drug block when assayed using the slow drug-dependent component of recovery from inactivation. Studies with QX-314 also showed reduced block of W1531C channels without changing access to the local anesthetic binding site. W1531Y exhibited blocking properties not unlike WT channels while W1531A channels showed an intermediate phenotype. Mutation of the analogous residue (i.e. W1712) in the human heart Na⁻ channel clone (i.e. hH1) produced effects similar to rSkM1 channels on lidocaine block. These results suggest that aromaticity and hydrophobicity of the tryptophan residue in the P-loop of domain IV of both cardiac and skeletal muscle Na⁻ channels plays an important role in local anesthetic block.

6.2   *Introduction*

Voltage-gated Na⁻ channels are responsible for the initial rapid rising phase of action potentials in excitable tissues such as cardiac, nerve and muscle cells. Mutations in Na⁻ channels are responsible for inherited cardiac arrhythmia and muscle paralysis, often as a result of altered channel inactivation (Goldin, 1994; Hudson et al., 1995; Cannon, 1996; Keating, 1996). Antiarrhythmic drugs such as lidocaine as well as some anticonvulsants

exert their clinical effects by selectively inhibiting Na$^-$ currents particularly during periods of excessive activity and abnormal depolarizations (Courtney, 1975; Hille, 1977; Hondeghem and Katzung, 1977). This selective drug action results largely from preferential binding of these agents to the activated and inactivated states of the channel (Hille, 1977; Hondeghem and Katzung, 1977; Bean et al., 1983).

According to the modulated receptor hypothesis, affinity of Na$^-$ channels for local anesthetic (LA) binding depends on the conformational state of the channel (Hille, 1977). Allosterically, the drug receptor is in a low-affinity conformation when the channels are in resting closed states and transforms into a high-affinity conformation when the channels are open or inactivated (Hille, 1977; Hondeghem and Katzung, 1977). In addition to these changes in binding affinity, access to the binding site is also state-dependent with both hydrophobic and hydrophilic pathways available depending on the drug's hydrophobicity (Hille, 1977; Hondeghem and Katzung, 1977; Schwartz et al., 1977). Hydrophobic LA compounds appear to bind and unbind freely to Na$^-$ channels (Hille, 1977) while permanently charged LAs such as QX-314 and GEA-968 block Na$^-$ channels by interacting via hydrophilic pathways which are available only when the channels open (Strichartz, 1973; Courtney, 1975; Hille, 1977). Amphiphilic polar LAs like lidocaine and mexiletine can access the local anesthetic binding site via both pathways. These pathways affect LA block by determining the rates of drug binding and unbinding from the local anesthetic binding site (LABS) and can be modified by mutations independent of drug binding energetics. Therefore, binding of local anesthetics depends on both the intrinsic binding affinity of the LABS and drug access to this receptor site.

Cardiac Na$^-$ channels are more sensitive to local anesthetics than their skeletal muscle and nerve counterparts. It remains controversial whether the enhanced LA sensitivity of the cardiac subtype is due to predomination of inactivated states under physiological conditions (Wright et al., 1997) or whether the heart channels intrinsically bind local anesthetics with a higher binding affinity (Nuss et al., 1995; Wang et al., 1996). Despite these differences, the receptor for local anesthetic binding in Na$^-$ channels

has been localized to the cytoplasmic side of the pore (Hille, 1992) Previous studies have demonstrated that replacements of pore-lining residues located in the S6 segment of domain IV (i.e. IVS6) altered binding affinities of local anesthetics to Na⁻ channels (Ragsdale et al., 1994; Qu et al., 1995; Ragsdale et al., 1996; Wang et al., 1998; Sunami et al., 1998) and could alter drug access to the local anesthetic binding site (LABS). Moreover, the residues shown previously to strongly affect local anesthetic are conserved between the different Na⁻ channel homologues leaving open the possibility that other residues may also play a role in local anesthetic binding. However, the role of other residues have not been extensively described.

The fractional electrical distance (δ) for LA block is 0.7-0.8 from the inside (Gingrich et al., 92) while $\delta = 0.2$ from the outside for block by Cd^{2+} (which binds to the P-loop in D1) (Backx et al., 1992). Therefore, it seems possible that the P-loops may participate in local anesthetic binding to the pore. Recently, Sunami and colleagues (1997) have demonstrated that mutations of the putative selectivity filter (DEKA) in rat skeletal muscle (rSkM1) Na⁻ channel affect local anesthetic binding by modifying drug access to the LABS. The roles of other P-loop residues however have not been examined. In this report, we used cysteine mutagenesis to investigate the role of pore-lining residues in local anesthetic binding to rSkM1 Na⁻ channels and their potential candidacy as part of the LABS. We find that a number of pore mutations did affect LA block. Replacement of a tryptophan residue in the P-loop of domain IV strongly influences lidocaine block of both skeletal muscle and human heart Na⁻ channels.

6.3   Materials and Methods

6.3.1   Site-Directed Mutagenesis

For construction of the rat skeletal muscle Na⁺ channel (rSkM1) mutants and the human heart Na⁻ channel (hH1) mutants (i.e. W1712C and W1712A), a 1.9 kb BamH1-SphI or a 2.5 kb Sph I-Kpn I fragment of rSkM1 and a 3.2 kb Kpn I-Xba I fragment of hH1

were subcloned into pGEM-7f (Promega. Madison. WI). Site-directed mutagenesis was performed using oligonucleotides containing the appropriate base substitutions. Mutants were phenotypically selected using the Kunkel's method (1985). All mutations were confirmed by dideoxynucleotide sequencing (Sanger et al., 1977) prior to final subcloning into the expression vector. For rSkM1 mutants. the cassettes carrying the mutations were subcloned into the expression vector pGW1H (British Biotechnologies. Oxford. UK) containing the full length WT rSkM1 Na⁻ channel clone. For hH1 mutants. the mutational cassettes were subcloned into pcDNA3 (Invitrogen Co., San Diego, CA) carrying the full length hH1 clone. All subcloned mutants were re-sequenced to ensure that the desired mutations were present.

6.3.2 Heterologous Expression

Xenopus laevis oocytes were isolated as described in 2.4. For WT and mutant (i.e. W1712C and W1712A) hH1 channels, only 50 nL of the corresponding α subunit cDNA (0.1 μg/μL) was injected. Injected oocytes were incubated at room temperature (22-22°C) for 24-48 hr to allow for protein expression prior to electrical recording.

6.3.3 Macropatch Recording

For macropatch recordings, injected oocytes were first tested for expression using the two-electrode voltage clamp technique as described. Oocytes expressing current ≥ 20 μA were chosen for macropatch recording. The vitelline membrane was mechanically removed with a pair of fine forceps after incubation in a hypertonic stripping solution (see below) for 5 minutes. Electrodes were fabricated from 1.5 mm outer diameter thin-walled borosilicate glass pulled on a Sutter puller and heat polished to yield a final resistance of about 1 MΩ. Na⁻ currents were measured in excised inside-out configuration using an Axopatch 200B amplifier (Axon Instruments, Foster City, CA, USA). Data were sampled at 10 kHz and low-pass filtered (4-pole Bessel. -3 dB at 2 kHz). The membrane patch was mechanically ripped out by pulling the pipette electrode away from the cell after a giga-

Ohm seal was formed in the cell-attached configuration.

6.3.4 *Drug application*

Drug solutions were applied extracellularly to oocytes in the two-electrode voltage clamp experiments by superfusion. When the drug concentrations were changed, the solutions were equilibrated for 5 minutes prior to recording currents. Intracellular application of QX-314 to oocytes was performed by injecting 100 nL of a 2 mM drug solution (dissolved in dH_2O) 10 minutes before voltage-clamping the cells. Assuming an oocyte volume of 1 µL (Ragsdale et al., 1994; Qu et al., 1995), the final QX-314 concentration applied intracellularly was estimated to be about 200 µM.

For macropatch experiments, QX-314 solution was rapidly perfused to the intracellular face of the excised patch using a custom made electronic fast-flow system (BMT Research Services Inc., Calgary). The system consists of a syringe containing the drug solution connected to a glass pipette whose opening and closing of its tip is controlled by an electronic device. The pipette tip was placed immediate to the excised patch such that solution exchange could take place rapidly. In single channel recordings, lidocaine was applied extracellularly by including it in the pipette solution. Control and lidocaine data were obtained from different patches.

6.3.5 *Electrophysiological Protocols*

Use-dependent block was induced by applying a continuous train of 20 ms step depolarizations to -10 mV from rest at a stimulation frequency of 10 Hz in the presence of lidocaine for both rSkM1 and hH1 wild-type and mutant channels. Test potentials for K1237C, W1531C and W1531A mutants were -20 mV because the reversal potentials for these channels were close to 0 mV (Tsushima et al, 1997a). Holding potentials were -100 mV and -120 mV for rSkM1 and hH1 channels respectively.

191

Channel availability curves (i.e. fast-inactivation curves) were obtained by normalizing the peak current recorded in test pulses to -20 mV for 50 ms after 500 ms prepulses to various voltages (-120 mV to -20 mV in 10 mV increments).

Recovery from inactivation of WT and mutant channels was examined using a two-pulse protocol in which a 500 ms depolarizing pulse to -20 mV was followed by repolarization to -100 mV for rSkM1 channels for a varying period (i.e. the repolarization time) prior to a second depolarizing "test" pulse to -20 mV. The holding potential was -100 mV. The first conditioning pulse resulted in channel inactivation and allowed drug binding to the channels without inducing significant slow-inactivation (Balser et al., 1996). The peak current evoked during the test depolarizing pulse assays the fraction of channels that recover from the inactivated state to the closed state during the period spent in the hyperpolarized potential (Bean et al., 1983; Bennett et al., 1995).

6.3.6 Data Analysis, Statistics and Curve Fitting

For Figure 6.1, use-dependent block by lidocaine at steady state was assessed as $1 - I_{pulse\ 15} / I_{pulse\ 1}$ where $I_{pulse\ 1}$ and $I_{pulse\ 15}$ respectively represent the peak currents measured during the 1st and 15th pulse respectively at a frequency of 10 Hz from rest with lidocaine.

Inactivation curves were obtained by fitting data with a Boltzmann function using the Marquardt-Levenberg algorithm in a non-linear-least-squares procedure:

$$h_{\infty} = 1 / \{1 + \exp[(V_t - V_{1/2}) / k]\}$$

where V_t is the test potential, $V_{1/2}$ is the half-point of the relationship, k (=RT/zF) is the slope factor. h_{∞} was measured as the ratio of the peak current in response to depolarization to -20 mV following 500 msec prepulses to various voltages (from -120 to -20 mV by 10 mV increments) to the peak current recorded from a holding potential of -120 mV. Shifts of midpoint (i.e. $\Delta V_{1/2}$) caused by the application of lidocaine were measured as $V_{1/2,\ lidocaine} - V_{1/2,\ control}$ where $V_{1/2,\ control}$ and $V_{1/2,\ lidocaine}$ represent the midpoints measured in the absence and presence of lidocaine respectively.

Tonic block of WT and tryptophan mutant channels were characterized using the following binding isotherm equation:

$$I_{drug} / I_0 = 1 / (1 + [drug]^n / IC_{50}^n)$$

where I_{drug} and I_0 represent the measured Na^- currents in response to 50 ms depolarizations from a holding potential of -120 mV at 0.25 Hz stimulation in the presence (I_{drug}) and absence of drug (I_0), IC_{50} is the concentration of drug that results in 50 % reduction of peak I_{Na} and n is the Hill coefficient. n is assumed to be 1 for binding without cooperativity

Recovery from inactivation data were fit with a bi-exponential function. in experiments designed to assay drug binding to the inactivated state. the same binding equation described above was used except I_{drug} and I_0 represent the amplitudes of the slow component of recovery from inactivation in the presence and absence of drug respectively

Single-channel recordings were idealized using the 50% amplitude criterion to identify channel openings and closings (Colquhoun and Sigworth. 1983). The mean number of opening per depolarization was derived from at least 50 consecutive depolarizations excluding the blank sweeps. Idealized channel openings were used to generate open-time density distribution histograms. Mean open-times were estimated by fitting open-time density histograms to a mono-exponential function using a non-linear least-squared algorithm. The slope of the current-voltage plot of single channels gives the channel conductance (g). Data were fit by least squares linear regression. Probability of channel openings (P_{open}) was determined as the ratio of number of depolarizations that elicited at least one channel opening to the total number of depolarizations. For patches containing more than one channel, data were corrected for the number of channels using the equation $P_{close} = (1 - P_{open})^n$ where P_{close} is the probability of channel being closed and is depicted as the ratio of number of blank sweeps to the total number of depolarizing pulses and n is the number of channels present in the patch. Only patches containing no more than 3 channels were used in our studies. All patches studied were stable for at least 800 sweeps.

All data were obtained from at least 3 cells and combined for statistical analysis. Data presented are the means ± SEM. Statistical significance was determined using the student-t test with p<0.05 representing significance.

6.4 Result

6.4.1 Screening of cysteine pore mutants for lidocaine sensitivity

To examine for the effects of pore mutations on local anesthetic block, we constructed a total of 12 cysteine pore mutants. Three rings of residues were selected for examination: the inner putative selectivity filter (D400, E755, K1237, A1529), the tryptophan ring (W402, W756, W1239, W1531) and the outer charge ring (E403, E758, D1241, D1532). These residues were chosen since the charged residues may interact electrostatically with the hydrophilic amine group of lidocaine while the tryptophans may interact with the aromatic moiety of the drug via hydrophobic interactions. We initially screened for changes in local anesthetic block of these pore mutants in comparison with WT rSkM1 channels by examining use-dependence and shifts of mid-points of channel availability curves by 300 µM lidocaine. The data for both WT and mutant rSkM1 channels are summarized in Figure 6.1. Several of these pore mutants displayed significant changes in lidocaine block compared to WT channels (p<0.05). For example, reduced use-dependent block ($1-I_{Pulse\ 15}$ / $I_{Pulse\ 1}$) was observed in W402C (25.1±3.0 %, n=3) and W1239C (25.3±2.0 %, n=3) channels while enhancement was seen in D400C (52.5±3.2 %, n=3), E403C (80.2±3.0 %, n=3), E755C (65.1±3.0 %, n=3), E758C (62.2±2.6 %, n=3) and D1241C (72.5±4.2 %, n=3) channels relative to WT channels (36.9±5.0 %, n=4). In addition, the shift in channel availability with lidocaine application was also significantly altered in W402C ($\Delta V_{1/2}$=-12.2±2.5 mV, n=3), E755C (-13.5±3.1 mV, n=4), E758C (-12.6±2.1 mV, n=4), K1237C (-10.6±1.9 mV, n=4), W1239C (-12.5±3.2 mV, n=4), A1529C (-11.3±1.8 mV, n=4) and D1532C (-13.3±2.4 mV, n=4) compared to WT (-16.5±2.5 mV, n=4, p<0.05). Though these changes displayed

Figure 6.1.

Effects of lidocaine on the midpoints of channel availability curves and use-dependence of cysteine pore mutants. The inner charge (D400, E755, K1237, A1529), tryptophan (W402, W756, W1239, W1531) and outer charge (E403, E758, D1241, D1532) rings were examined. Roman numerals denote the corresponding domain numbers. The left ordinate axis represents shifts of midpoint of channel availability curve of the corresponding channel by 1 mM lidocaine measured as $\Delta V_{1/2} = V_{1/2, \text{control}} - V_{1/2, \text{lidocaine}}$. Midpoints were estimated from channel availability curves recorded under control conditions and in the presence of 1 mM lidocaine using the fast inactivation protocol and Boltzmann fits(see Materials and Methods). The right ordinate represents the degree of use dependent block of each channel by 300 μM lidocaine measured as $1 - I_{\text{pulse } 15} / I_{\text{pulse}}$ where $I_{\text{pulse } 1}$ and $I_{\text{pulse } 15}$ respectively represent the peak currents measured during the 1st and 15th pulse during a continuos train of depolarization to –20 mV from –120 mV at 10 Hz in the presence of 300 μM lidocaine. All data represent at least 3 individual determinations for each mutants and are presented as mean ± S.E.. Asterisks and double asterisks denote values that are statistically different ($p < 0.05$ and $p < 0.01$ respectively) from WT.

195
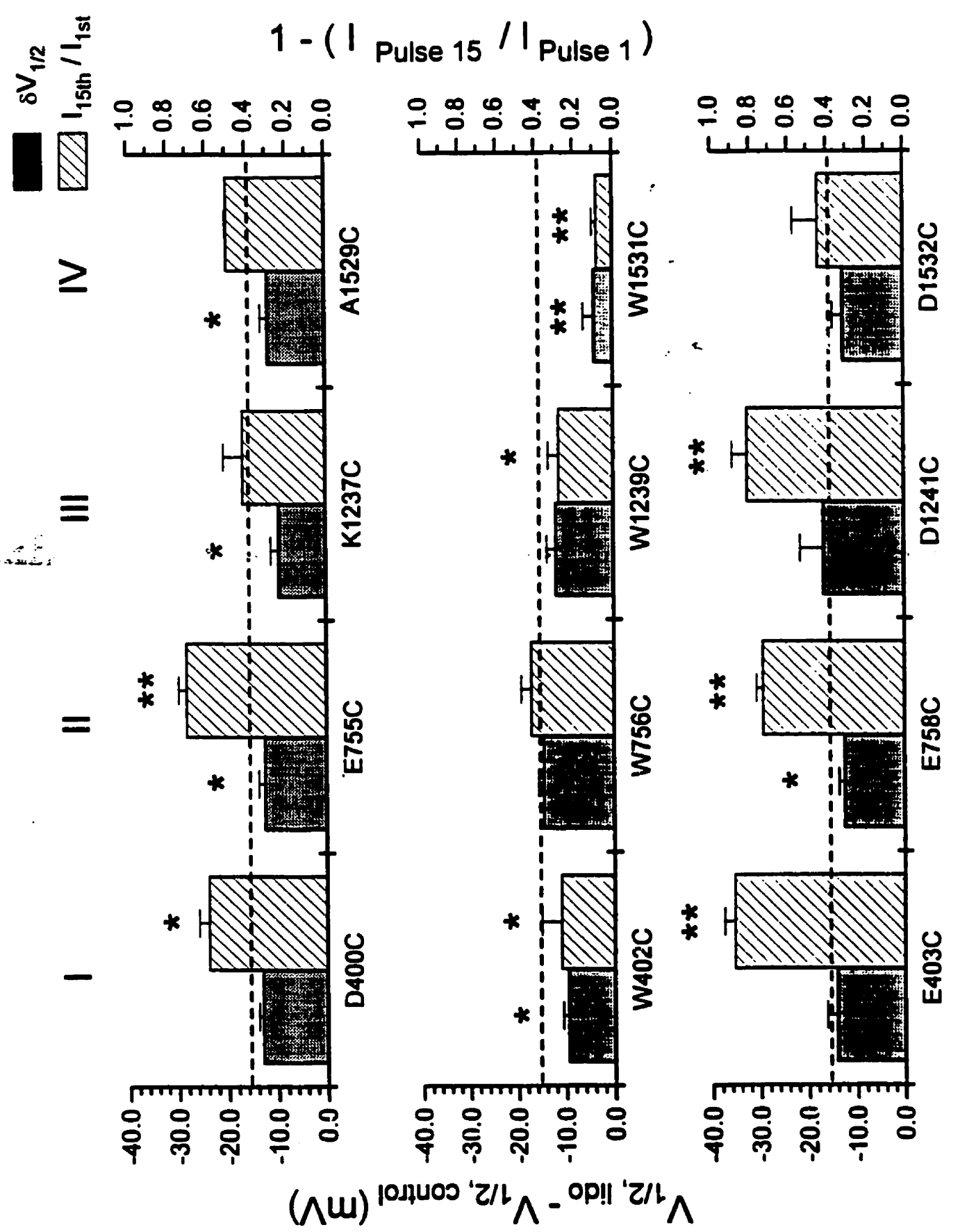
statistical significance, they were however modest. Distinct from the above mutations, W1531C channels showed virtually no use-dependence (3.0±0.3 %, n=4. p<0.01) and shift in $V_{1/2}$ with 300 µM lidocaine ($\Delta V_{1/2}$=-3.9±1.0 mV, n=4, p<0.01). Having observed these dramatic changes in drug blocking properties, we therefore went on to investigate the mechanisms underlying this mutation.

6.4.2   Use-dependent block of W1531C, W1531A and W1531Y by lidocaine

The drastic changes observed with W1531C channels suggest that aromaticity and hydrophobicity at position 1531 in DIV may be critical for lidocaine modification of rSkM1 channels. To address this hypothesis, we created also the mutations W1531A and W1531Y. These channels were first examined for use-dependent block by lidocaine in comparison to WT channels. Figure 6.2 shows the effect of lidocaine on WT and mutant rSkM1 Na⁺ currents during a train of 20 ms depolarizing pulses to -10 mV applied at a stimulation frequency of 10 Hz from a holding potential of -100 mV. The inset shows raw traces of Na⁺ currents recorded from WT. W1531C, W1531A and W1531Y channels during the 1st and 15th depolarizing pulse in the absence and presence of 100 and 300 µM lidocaine. Without lidocaine, WT currents elicited during the 1st ($I_{Pulse\ 1}$) and 15th ($I_{Pulse\ 15}$) pulse were not significantly different in size ($I_{Pulse\ 15}$ / $I_{Pulse\ 1}$ = 98.4 ± 0.6 %, n=4, p>0.05). On the other hand. 100 µM lidocaine induced progressive reduction in WT currents following subsequent stimulations with the ratio $I_{Pulse\ 15}$ / $I_{Pulse\ 1}$ significantly reduced to 88.3 ± 3.0 %, n=4 in steady state (p<0.05). Application of 300 µM lidocaine further reduced the steady-state current (i.e. $I_{Pulse\ 15}$) to 63.1 ± 5.0 % (n=4) of $I_{Pulse\ 1}$ (p<0.05). In contrast to WT channels, $I_{Pulse\ 15}$ / $I_{Pulse\ 1}$ was 95.2 ± 1.2 %, n=4 for W1531C channels without lidocaine while addition of 100 µM and 300 µM lidocaine did not significantly change this ratio (92.6 ± 1.3 %, n=4 and 92.3 ± 2.0 %, n=4 respectively, p>0.05). Thus, the mutation W1531C appeared to completely abolish use-dependent block of rSkM1 channels by lidocaine. For W1531A channels, $I_{Pulse\ 15}$ / $I_{Pulse\ 1}$ was 90.4 ± 1.1 %, n=4 under drug-free conditions while application of 100 µM and 300 µM lidocaine caused modest yet significant use-dependent block with the ratio reduced to 84.5 ± 1.4 %, n=4 and 76.6

Figure 6.2.

Time-course of development of use-dependent block of rSkM1, W1531C, W1531A and W1531Y channels by lidocaine. Peak Na^+ currents were normalized to that mesaured during the first pulse and plotted against the pulse number. Use-dependent blocks were induced by depolarizing cells to -10 mV for 50 ms from rest at a holding potential of -100 mV at 10 Hz. The concentrations of lidocaine shown were 100 μM (open circle) and 300 μM (open triangle). The decrease in current magnitude was fitted with a mono-exponential function. Data shown represent mean ± S.E. of 5-10 individual cells. Use-dependent block was completely abolished in W1531C and significantly reduced in W1531A channels. Use-dependent block of W1531Y channels was not statistically different from WT.

W1531C

HP=-100 mV
10 Hz

■ Control
○ 100 μM Lidocaine
△ 300 μM Lidocaine

W1531Y

rSkM1

W1531A

Normalized Current
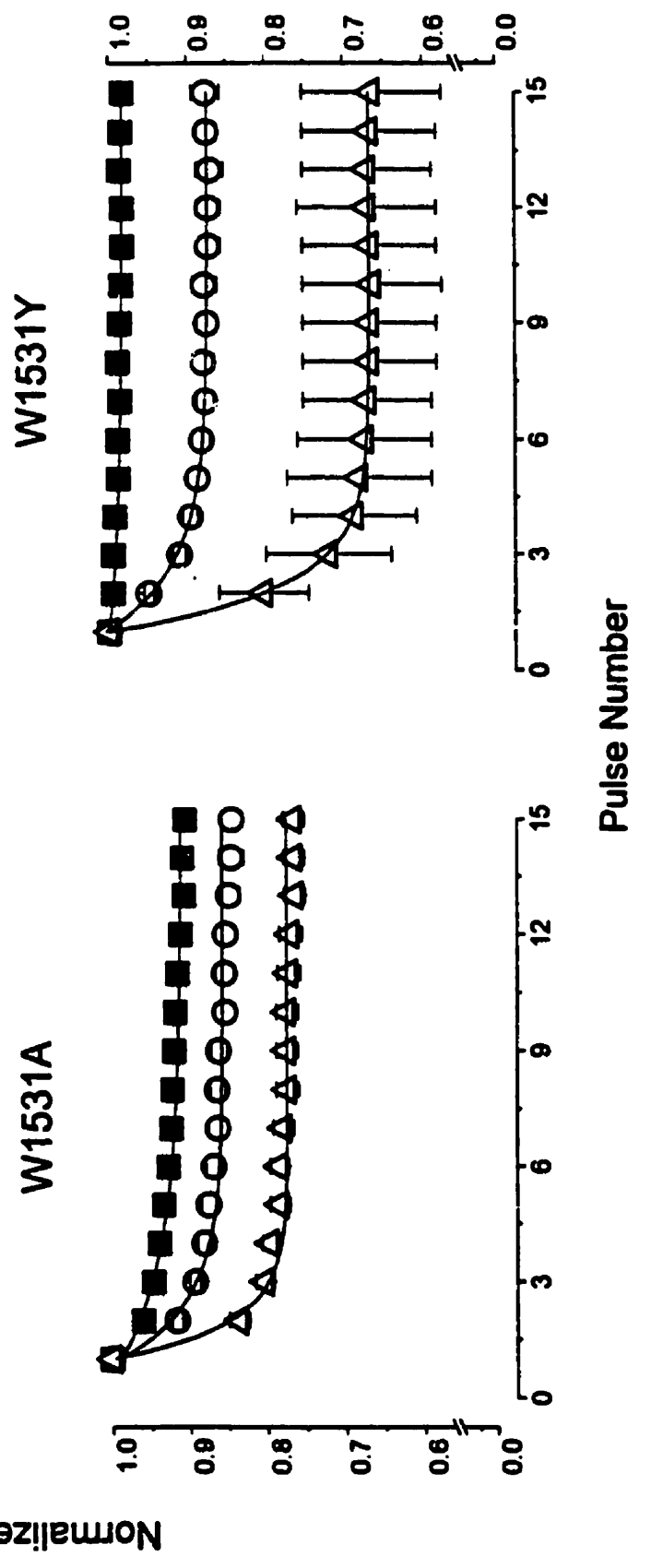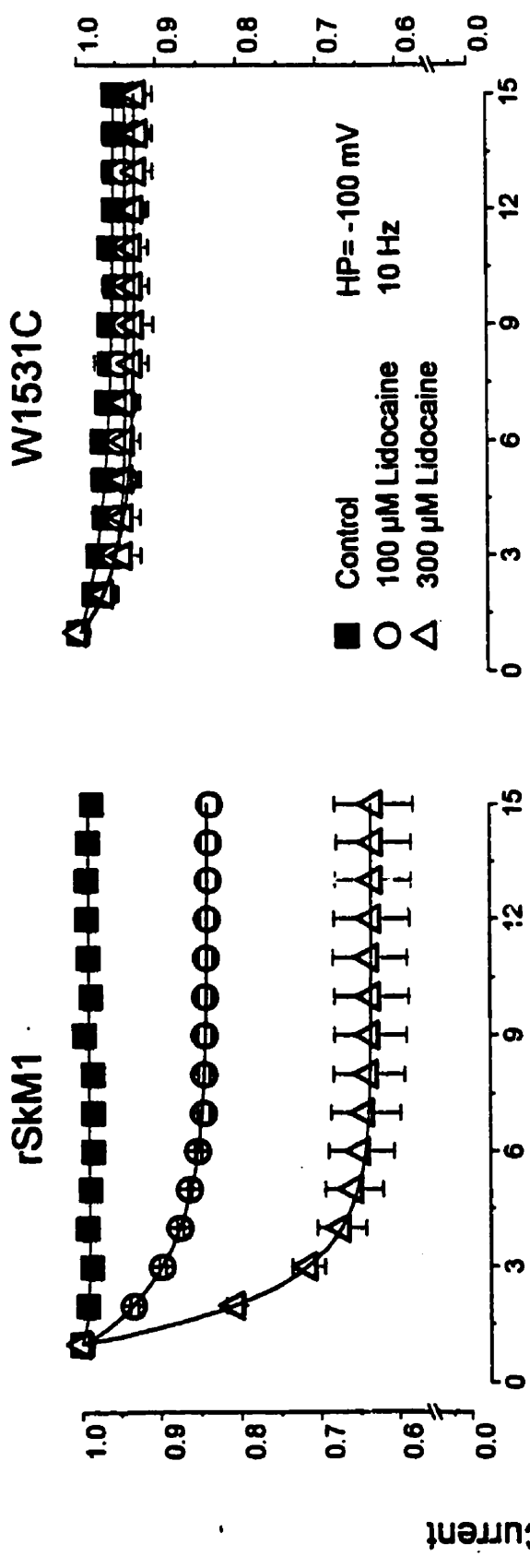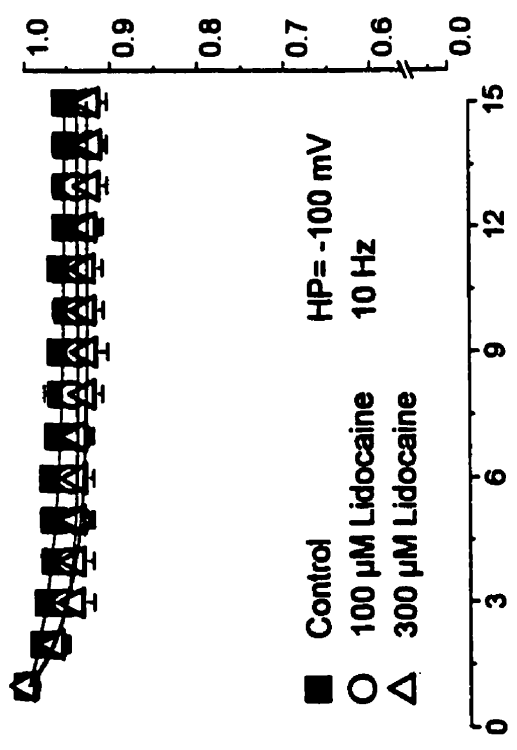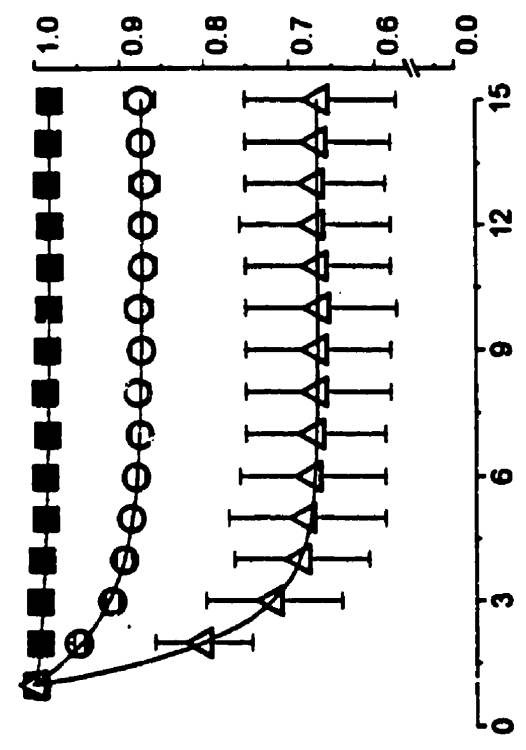
Pulse Number

± 1.3 %, n=4 respectively (p<0.05). These ratios were significantly bigger than those of WT but smaller than W1531C's (p<0.05) suggesting that use-dependent block of W1531A channels by lidocaine was intermediate between WT and W1531C channels. Use-dependence of W1531Y channels were however not different from WT (control: 98.2 ± 0.5 %, n=3; 100 μM: 87.5 ± 1.8 %, n=3; 300 μM: 66.3 ± 8.8 %, n=3) (p>0.05). Since use-dependent block by lidocaine follows the sequence WT~W1531Y>>W1531A>W1531C, these results suggest that aromaticity and hydrophobicity of the residue at position 1531 influence lidocaine block of rSkM1 channels.

6.4.3 The effects of lidocaine on the voltage-dependence of channel availability

Several mechanisms can result in changes in local anesthetic block. Mutations could modify use-dependent lidocaine block by disrupting inactivation since local anesthetics bind preferentially to this conformation of the channel (Hille. 1977; Hondeghem and Katzung, 1977; Bean et al.. 1983). Alternatively, mutations could modify the drug binding and unbinding rates with or without affecting the energetics of binding thereby altering use-dependence. Changes in the rates of binding and unbinding could occur if access of drug to the binding site has been altered as described previously for selected mutations in S6 of domain IV of neuronal Na⁻ channels (Ragsdale et al.. 1994; Qu et al., 1995). Third, the amount of drug block can also be modified by changes in the intrinsic binding affinity of drug to the channels.

Examination of the raw current traces in Figure 6.6A shows that both W1531C and W1531A channels completely inactivate within 50 ms suggesting no disruption of inactivation. This lack of inactivation disruption is further tested in Figure 6.3A by measuring the voltage-dependence of channel availability in rSkM1 and W1531 mutant channels using fast-inactivation curves. Data points were fit with a Boltzmann equation (see Materials and Methods). Parameters estimated from these fits are summarized in Table 6.1. Note that the values of $V_{1/2}$ for W1531C and W1531A were negatively shifted compared to

Table 6.1

Effects of 100 µM lidocaine on the voltage-dependence of channel availability of WT rSkM1, W1531C, W1531A and W1531Y channels.

Data represent the mean ± SEM. * denotes entries statistically (P < 0.05) different from control values of the corresponding channels.

Channel	Control		300 µM lidocaine	
	$V_{1/2}$ (mV)	k	$V_{1/2}$ (mV)	k
WT	-51.1 ± 0.4 (3)	4.6 ± 0.5 (3)	-65.6 ± 1.5 (4)*	4.6 ± 0.3 (4)
W1531C	-73.3 ± 3.9 (3)	8.7 ± 1.1 (3)	-76.7 ± 4.2 (3)	8.7 ± 1.7 (3)
W1531A	-66.4 ± 0.8 (4)	6.1 ± 0.3 (4)	-77.6 ± 1.1 (4)*	6.1 ± 0.5 (3)
W1531Y	-51.6 ± 1.8 (3)	4.8 ± 0.5 (3)	-70.9 ± 3.0 (3)*	4.6 ± 0.5 (3)

WT channels (p<0.05) confirming that the inactivated states of these mutant channels were not destabilized.

Since leftward shift of channel availability is expected for preferential drug binding to the inactivated state with addition of lidocaine (Courtney, 1975; Hille, 1978), we next examined for changes in drug binding energetics by measuring shifts in $V_{1/2}$ by 300 μM lidocaine. Figure 6.3A and Table 6.1 show summarized data for these experiments. For WT rSkM1 channels, $V_{1/2}$ was shifted significantly in the hyperpolarizing direction with lidocaine application consistent with the above hypothesis (p<0.05). In contrast, W1531C channels showed no measurable shift in $V_{1/2}$ after addition of lidocaine (p>0.05) suggesting disruption of drug binding to the inactivated channels. Again, W1531A channels showed intermediate shifts while W1531Y channels were unaltered with respect to shifts in $V_{1/2}$ by lidocaine. The slopes of all channels, however, were not significantly changed by lidocaine (p>0.05).

We also examined the concentration dependence of the shift of mid-points by lidocaine. Figure 6.3B plots the magnitudes of the change in the mid-point of channel availability (i.e. $\Delta V_{1/2}$) as a function of the applied lidocaine concentrations. As expected, the magnitude of $\Delta V_{1/2}$ increased with elevated lidocaine concentrations in all channels except W1531C which showed no significant shifts (p>0.05). However, changes with W1531A channels were less concentration dependent than WT and W1531Y channels.

6.4.4 *Change in recovery from inactivation with W1531 mutants*

The results above suggest that the affinity of lidocaine binding to W1531C and W1531A channels is reduced compared to rSkM1 channels. To further bolster this conclusion, we next examined their rates of recovery from inactivation in the absence and presence of lidocaine. A typical two-pulse protocol was used (see Materials and Methods) and the holding and recovery potentials were -100 mV. Figure 6.4A shows that rSkM1 channels recovered from inactivation with two time constants. The fast component

Figure 6.3.

Lidocaine-dependent shifts in the voltage dependence of channel availability for rSkM1, W1531C, W1531A and W1531Y channels.

A) Channel availability curves of rSkM1, W1531C, W1531A and W1531Y in the absence (solid symbols) and presence (open symbols) of 300 μM lidocaine. Depolarizing pulse duration was chosen to be 500 ms to allow equilibration of drug binding to channels. The maximum current amplitudes of both inactivatior curves under control conditions and with drug were normalized to 1.0 to allow easier comparison of the shifts by lidocaine. Data points were fitted by the modified Boltzmann function (see Materials and Methods).

B) Plot of the shifts in midpoint for half-maximal inactivation ($\Delta V_{1/2}$) as a function of lidocaine concentration for rSkM1 and tryptophan mutant channels. Not only the mid-points of W1531C and W1531A channels were less shifted but their lidocaine concentration-dependence were also reduced when compared to WT channels. W1531Y behaved not differently than WT. $\Delta V_{1/2}$ was determined from $V_{1/2, \text{lidocaine}} - V_{1/2, \text{control}}$ using $V_{1/2}$ values obtained from fits of the data as described in A. Data plotted are shown as $\Delta V_{1/2} \pm$ SEM as a function of lidocaine concentration.

203

A

rSkM1

W1531C

W1531A

W1531Y

■ Control
○ 300 µM Lidocaine

Normalized Current

Voltage (mV)

B

$V_{1/2, control} - V_{1/2, lido}$

[Lidocaine] (µM)

■ rSkM1
○ W1531C
△ W1531A
▽ W1531Y
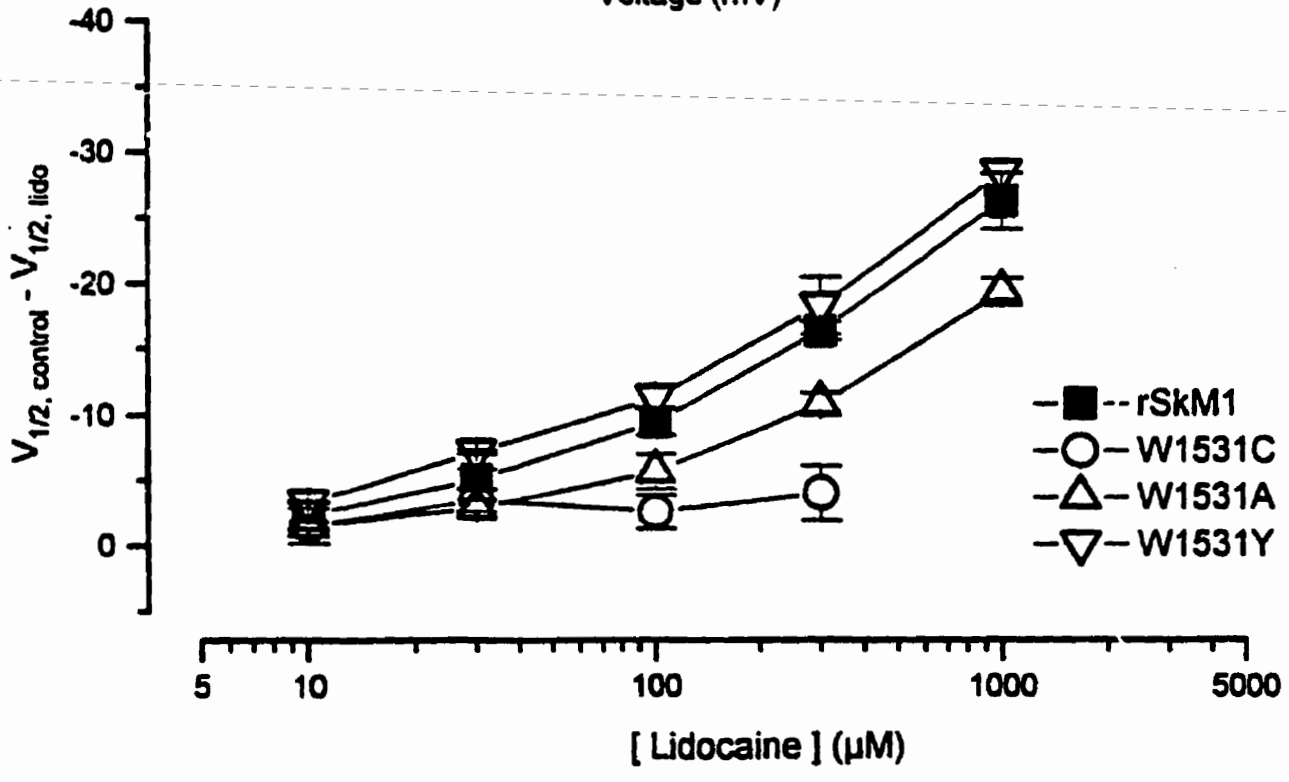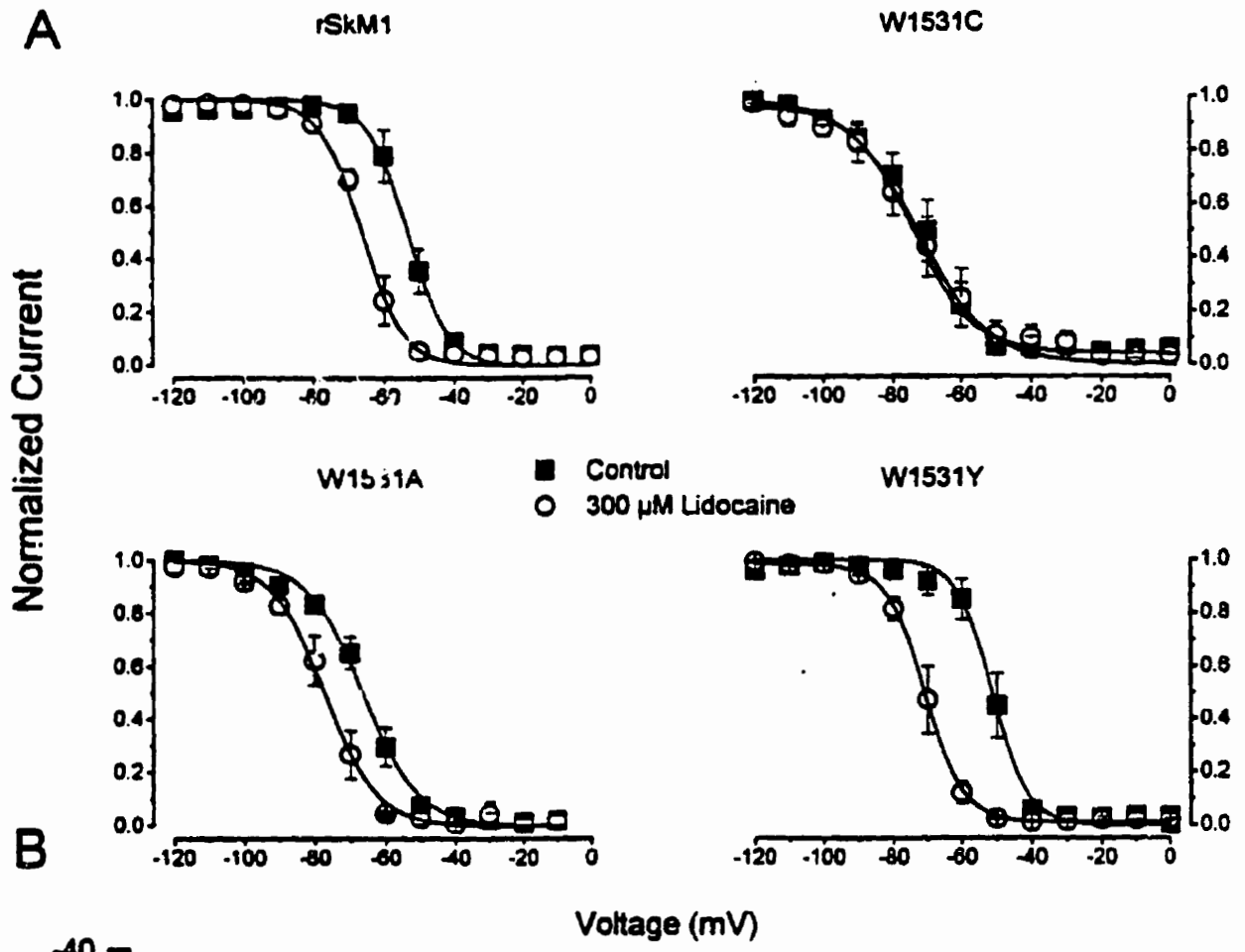
accounted for the majority of the total recovery with a time constant ($\tau_{fast, con}$) of 1.8 ± 0.2 ms (n=4) while the minor slow component ($A_{slow, con} = 6.4 \pm 1.4$ %, n=4) recovered with a time constant ($\tau_{slow, con}$) of 1026 ± 703 ms (n=4). The slow component probably reflects channels recovering from the slow inactivated states in response to 500 ms depolarizations (Featherstone et al., 1996). Nevertheless, its relatively small amplitude indicates that the degree of slow-inactivation was minor in our experiments. In the presence of 100 μM lidocaine, the proportion of channels recovering quickly is substantially reduced ($\tau_{fast, lido} = 2.9 \pm 0.1$ ms, $A_{fast, lido} = 17.7 \pm 4.9$ %, n=4). However, $\tau_{fast, lido}$ is very similar in magnitude to $\tau_{fast, con}$ (p>0.05) consistent with this component measuring the fast recovery of drug-free channels (Bean et al., 1983). On the other hand, $\tau_{slow, lido} = 300.0 \pm 43.6$ ms, n=4 gives a measure of the rate of lidocaine unbinding from channels blocked during the depolarizing prepulse. Therefore, $A_{fast, lido}$ and $A_{slow, lido}$ give a measure of the proportion of drug-free and drug-bound channels respectively during the 500 ms conditioning prepulse (Bennett et al., 1995).

Figure 6.4A also shows the effect of 100 μM lidocaine on the recovery from inactivation for W1531C, W1531A and W1531Y channels. Under control drug-free conditions, the recovery of W1531C channels from inactivation displayed two distinct phases. In contrast to WT channels, the proportion of W1531C channels recovering slowly ($\tau_{slow, con} = 330.7 \pm 50.1$ ms, n=5) made up a much larger component ($A_{slow, con} = 44.7 \pm 5.1$ %, n=5) of the total recovery. However, application of 100 μM lidocaine neither significantly (p>0.05) altered the time constant ($\tau_{slow, lido} = 224.7 \pm 15.6$ ms, n=5) of this slow component nor its amplitude ($A_{slow, lido} = 55.8 \pm 3.9$ %, n=5). Moreover, the kinetics of the rapid phase ($\tau_{fast, lido} = 9.1 \pm 2.4$ ms, n=5) was also approximately the same as that in the absence of drug ($\tau_{fast, con} = 5.8 \pm 1.7$ ms, n=5) (p>0.05). Similar to W1531C, W1531A channels also displayed two recovery components ($\tau_{fast, con} = 3.4 \pm 0.6$ ms, $A_{fast, con} = 77.9 \pm 1.6$ %; $\tau_{slow, con} = 159.2 \pm 73.5$ ms, $A_{slow, con} = 22.1 \pm 1.6$ %, n=4) under drug-free conditions. Compared to WT, the increase in the proportion of channels recovering slowly with lidocaine application was substantially smaller ($A_{slow, lido} = 68.5 \pm 5.1$ %, n=4). Moreover, drug unbinding was accelerated as reflected by its 3 times faster slow component ($\tau_{slow, lido} = 114.7 \pm 16.2$ ms,

Figure 6.4.

Effects of lidocaine on the recovery from inactivation of rSkM1, W1531C. W1531A and W1531Y channels.

A) Recovery from inactivation in the absence (solid square) and presence (open circle) of 100 μM lidocaine. A two-pulse protocol was used and data points were fit with a bi-exponential function (see Materials and Methods). Recovery of WT channels was slowed by 100 μM lidocaine and displayed clearly two distinct time constants (see text). Application of 100 μM lidocaine however did not affect recovery of W1531C channels and only modestly slowed recovery of W1531A channels. W1531Y behaved not differently from WT.

B) Plot of fractional recovery at 50 ms in the presence of lidocaine, normalized to that measured under control drug-free conditions, against lidocaine concentration. Data were fitted with a binding isotherm equation (see Materials and Methods) to estimate the binding affinity of lidocaine to the inactivated states of these channels.
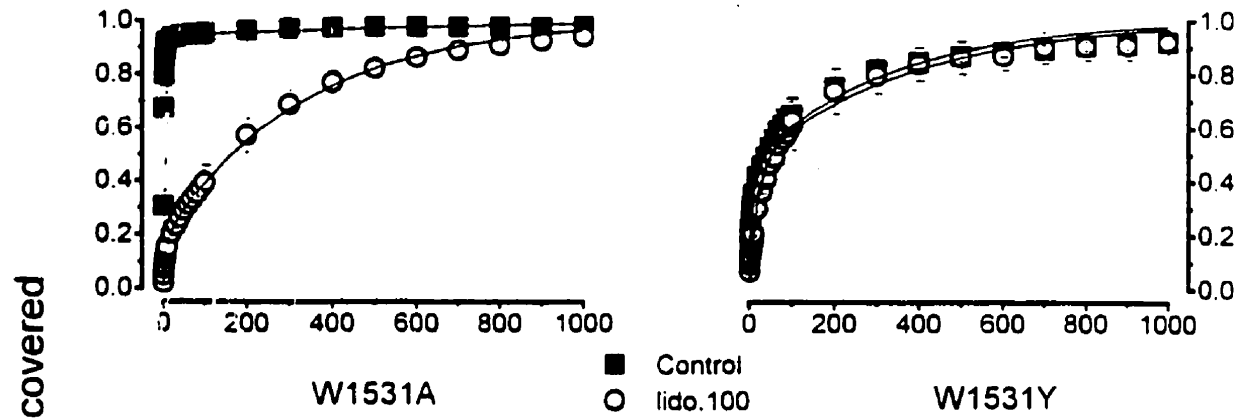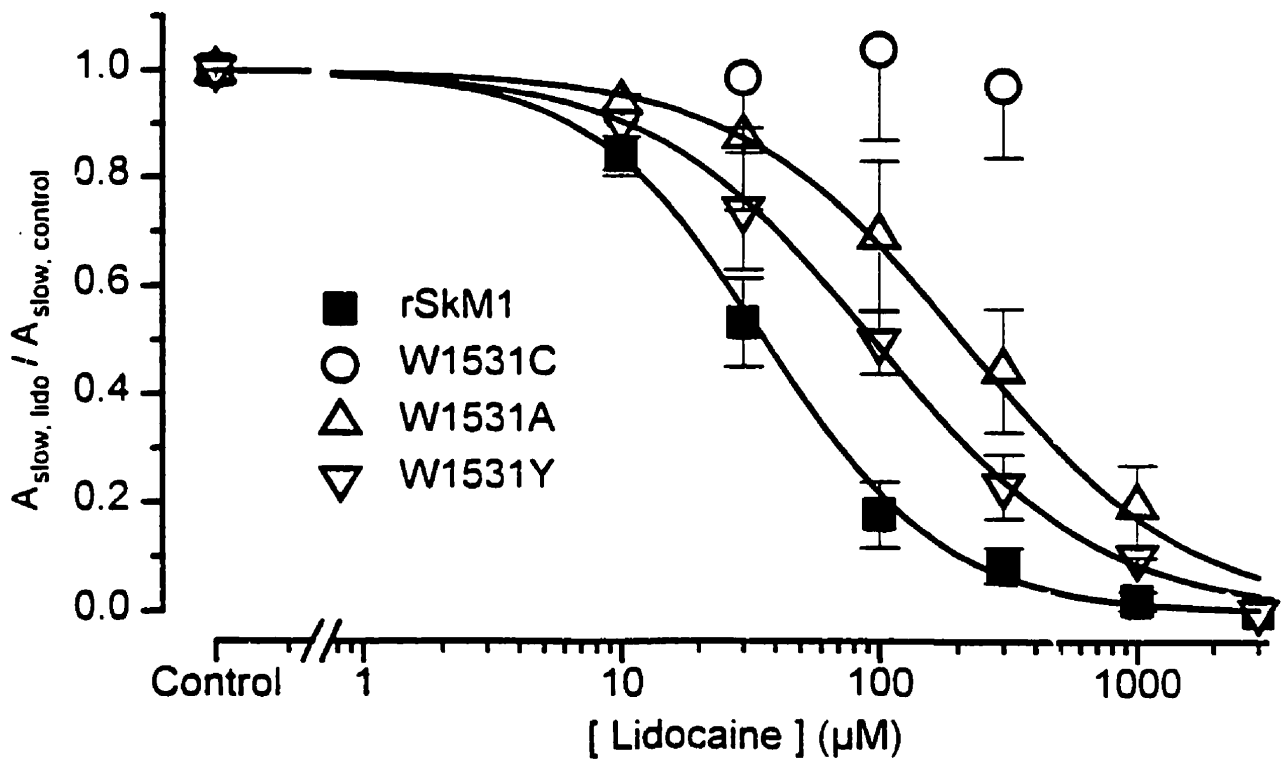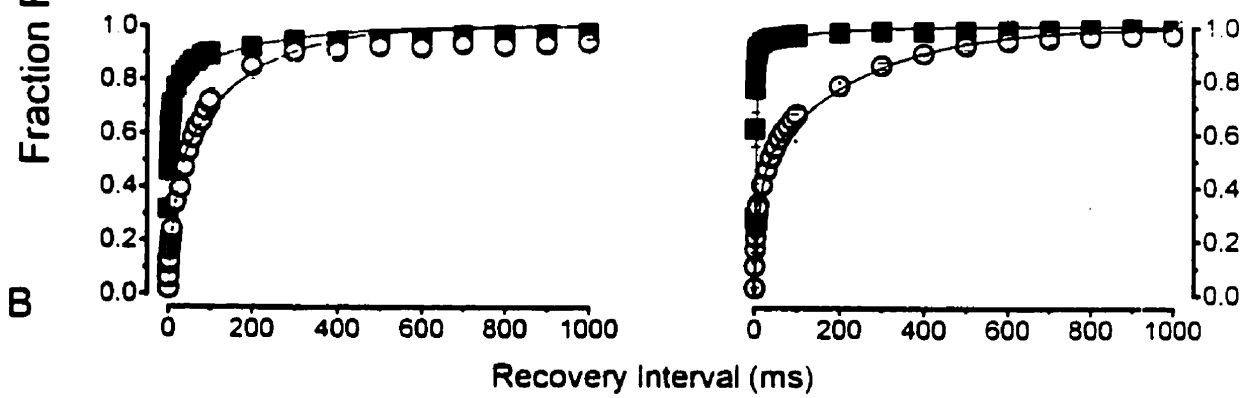
n=4) with drug. Nevertheless, the fast constants with $(\tau_{fast, lido} = 3.7 \pm 0.4$ ms, n=4) and without drug were approximately the same (p>0.05) indicating the kinetics of drug-free channels were unchanged. For W1531Y channels, both the kinetics and proportion of the slowly recovering drug-bound channels with lidocaine were intermediate (control: $\tau_{fast} = 1.9 \pm 0.3$ ms, $A_{fast} = 93.1 \pm 2.9$ %; $\tau_{slow} = 2375.5 \pm 1619$ ms, $A_{slow} = 6.9 \pm 2.9$ %, n=3; 100 μM lidocaine: $\tau_{fast} = 2.84 \pm 0.1$ ms, $A_{fast} = 36.2 \pm 2.4$ %; $\tau_{slow} = 191.5 \pm 12.1$ ms, $A_{slow} = 63.8 \pm 2.4$ %, n=3) suggesting this mutation did not seriously alter lidocaine binding. These recovery data are summarized in Table 6.2.

To quantity drug binding to the inactivated state of these channels, Figure 6.4B plots the amplitude of the slowly recovering component (i.e. A_{slow}) as a function of drug concentration. Data were fitted with a binding isotherm equation assuming n=1 (see Materials and Methods). The lidocaine concentration required for 50% reduction of current (i.e. IC_{50}) was 52.5 ± 4.5 μM (n=4) for rSkM1 channels which agrees reasonably well with previous studies of lidocaine affinity of fast-inactivated channels in rSkM1 (Nuss et al., 1995, Balser et al., 1996) and native cardiac (Bean et al., 1983) Na^- channels. Drug binding to inactivated W1531C channels was entirely abolished over the range of lidocaine concentrations examined as demonstrated by a flat dose-response relationship. For W1531A channels, the estimated IC_{50} was 455 ± 12 μM (n=4) while being 135 ± 7.2 μM (n=3) for W1531Y channels.

6.4.5 Block by internal and external QX-314

The data above suggests a drastic reduction in lidocaine binding affinity of the inactivated states of W1531C and W1531A. To explore further whether drug access to the LABS was also modified in these mutant channels in addition to changes in drug binding energetics, we used the permanently positively charged membrane-impermeant quaternary lidocaine derivative, QX-314 which binds to the same receptor as lidocaine (French et al. 1996). QX-314 was applied internally at about 200 μM by injecting 100nL of 2 mM QX-314 into *Xenopus* oocytes at least 10 minutes before recording currents (Ragsdale et al..

Table 6.2

Effects of 100 μM lidocaine on the recovery from inactivation of WT rSkM1, W1531C, W1531A and W1531Y channels.

Recovery data were fit with a bi-exponential function (see Materials and Methods). $A_{fast} = 100\% - A_{slow}$. Data represent the mean ± SEM. *

denotes statistical significance ($P < 0.05$) with respect to control values of the corresponding channels.

Channel	Control			100 μM lidocaine		
	τ_{fast} (ms)	τ_{slow} (ms)	A_{slow} (%)	τ_{fast} (ms)	τ_{slow} (ms)	A_{slow} (%)
WT	1.8±0.2 (4)	1026±703(4)	6.4±1.4 (4)	2.9±0.1 (4)	300.0±43.6(4)*	82.3±4.9 (4)*
W1531C	9.1±2.4 (5)	330.7±50.1 (5)	44.7±5.1 (5)	5.8±1.7 (5)	224.7±15.6 (5)	55.8±3.9 (5)
W1531A	3.4±0.6 (4)	159.2±73.5 (4)	22.1±1.6 (4)	3.7±0.4 (4)	114.7±16.2 (4)	68.5±5.1 (4)*
W1531Y	1.9±0.2 (3)	2376±1619 (3)	6.9±2.9 (3)	2.8±0.1 (3)	191.5±12.1 (3)*	63.8±2.4 (3)*

1994; Qu et al., 1995; Sunami et al., 1997). In the absence of QX-314, WT and mutant rSkM1 channels showed no use-dependence when a train of 100 ms depolarizing pulses was applied at 1 Hz (data not shown). Figure 6.5A shows that application of ≈ 200 μM intracellular QX-314 induced significant ($p < 0.05$) use-dependence in WT rSkM1 channels by blocking progressively $84.5 \pm 2.6\%$ (n=3) of peak I_{Na} at steady-state. In contrast, significantly less block was observed with the same concentration of internal QX-314 in W1531C ($15.1 \pm 4.5\%$, n=4) and W1531A ($45.5 \pm 7.6\%$, n=3) channels. The degree of block observed in W1531Y ($89.7 \pm 3.8\%$, n=3) in steady state was not different from WT ($p > 0.05$).

Figure 6.6 shows the recovery of Na$^-$ current amplitude from internal QX-314 block. In these experiments, channels were blocked to steady-state by applying a train of 60 depolarizations each of 100 msec in duration followed by hyperpolarization to -140 mV for various intervals to allow channels to recover from block. Representative traces for Na$^-$ currents recorded from WT rSkM1, W1531C, W1531A and W1531Y channels before ($I_{Pulse\,1}$) and after ($I_{Pulse\,60}$) internal QX-314 block and after 1 min of hyperpolarization for recovery from block ($I_{Pulse\,1}^{min}$) are shown in Figure 6.6A. The time course of recovery from block was obtained by plotting the ratio of differences between the 1st and 60th pulses before and after recovery (i.e. ($I_{Pulse\,1}^- - I_{Pulse\,60}^-$) / ($I_{Pulse\,1} - I_{Pulse\,60}$) where I$^-$ represents the current elicited after a particular interval of hyperpolarization) against the duration of hyperpolarization at -140 mV. Consistent with previous reports, recovery from internal QX-314 block of WT rSkM1 channels was extremely slow (Strichartz, 1973; Yeh and Tanguy, 1985; Sunami et al., 1997). In rSkM1 channels, less than 5% of the blocked current recovered during a 4 minute hyperpolarization period, consistent with strong drug binding or trapping of the charged drug within the channel (Strichartz, 1975; Yeh and Tanguy, 1985, Starmer et al., 1986). In contrast, $86.3 \pm 6.6\%$ (n=3) and $83.3 \pm 7.2\%$ (n=3) of the currents of W1531C and W1531A respectively recovered within 5 seconds. Complete recovery from block of both mutant channels occurred after 15 seconds. The time constants for recovery were 2.1 ± 0.1 s (n=4) and 2.2 ± 0.4 s (n=4) respectively for W1531C and W1531A channels. While being ≈ 60-fold slower than W1531C and W1531A, the rate of recovery from block ($\tau = 127 \pm 34$ s,

Figure 6.5.

Effects of mutations W1531C, W1531A and W1531Y on block by extracellular and intracellular QX-314.

A) Normalized Na^+ current plotted against exposure time. Exposure of WT, W1531C, W1531A and W1531Y channels to 500 μM external QX-314 by superfusion to oocytes expressing the corresponding channels resulted in no detectable reduction in current in all channels.

B) Use-dependent block by intracellular QX-314 in rSkM1 (solid square), W1531C (open circle), W1531A (open triangle) and W1531Y (open diamond). Xenopus oocytes expressing the desired channels were microinjected with 100 nL of 2 mM QX-314 10 minutes before recording. Internal QX-314 block of W1531C and W1531A channels were attenuated. Steady-state block of W1531Y channels was not different from WT.
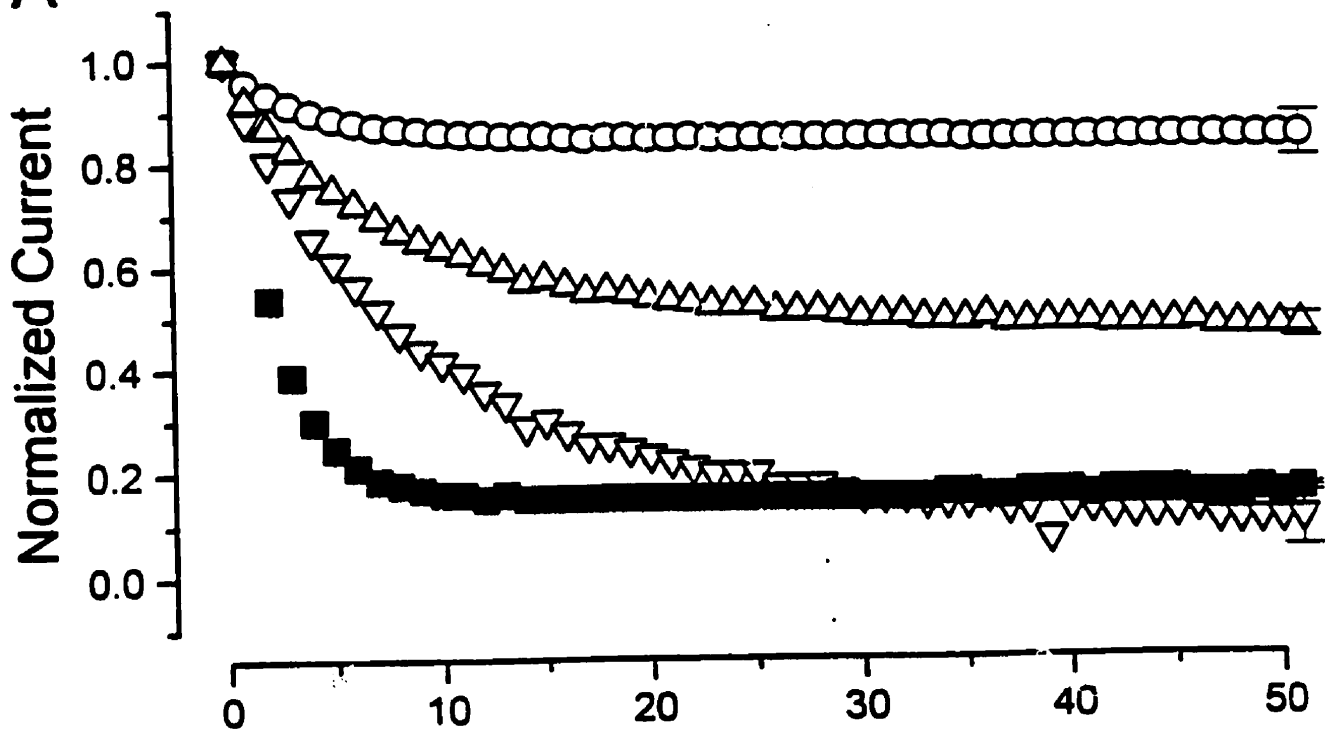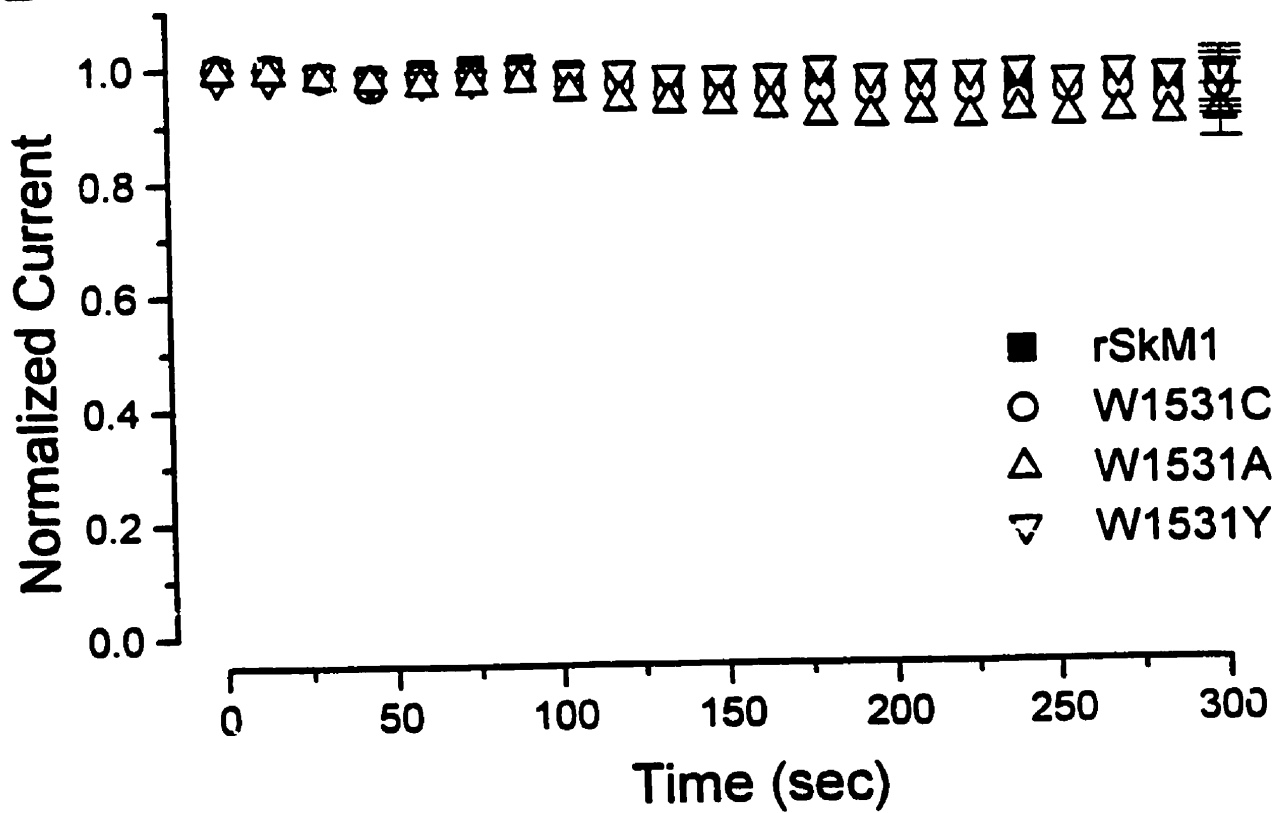
Figure 6.6

Recovery of WT rSkM1, W1531C W1531A and W1531Y channels from use-dependent block by intracellular QX-314.

A) Current traces normalized to the 1st pulse such that peaks at the baseline are equal. The numbers 1, 2 and 3 respectively indicate the 1st and 60th pulses of the 1 Hz train and the current recovered from block after holding at -140 mV from 1 minute. The peak currents shown were 4.8, 4.2, 4.3 and 4.5 μA for rSkM1, W1531C. W1531A and W1531Y respectively.

B) Recovery from use-dependent block by intracellular QX-314. Ratios of $(I_1' - I_{60th}')$ / $(I_{1st}-I_{60th})$ are plotted against duration of hyperpolarization at -140 mV where I_{1st}' and I_{60th}' respectively represent the current elicited by the first and 60th pulses after a particular interval of hyperpolarization. Recovery data were fitted with a mono-exponential function to estimate for the time constants for recovery from block.

213

rSkM1   W1531C   W1531A   W1531Y

2
3
1

2
3
1

2
1, 3

2
3
1

10 ms
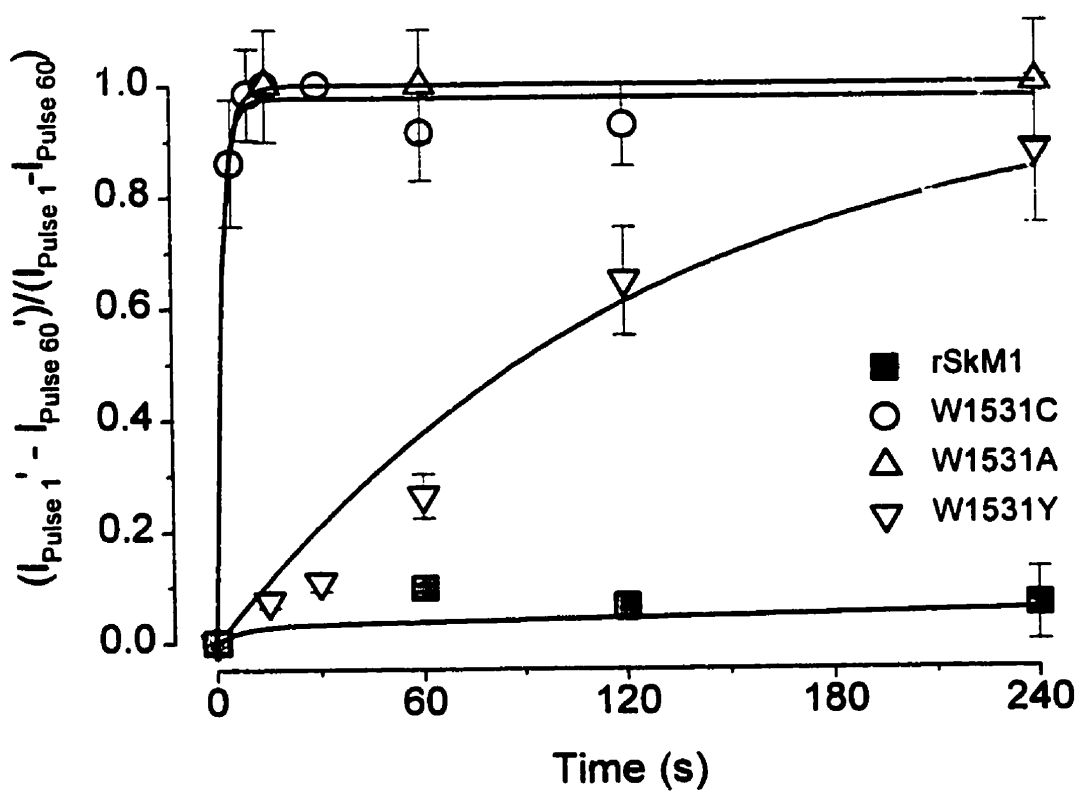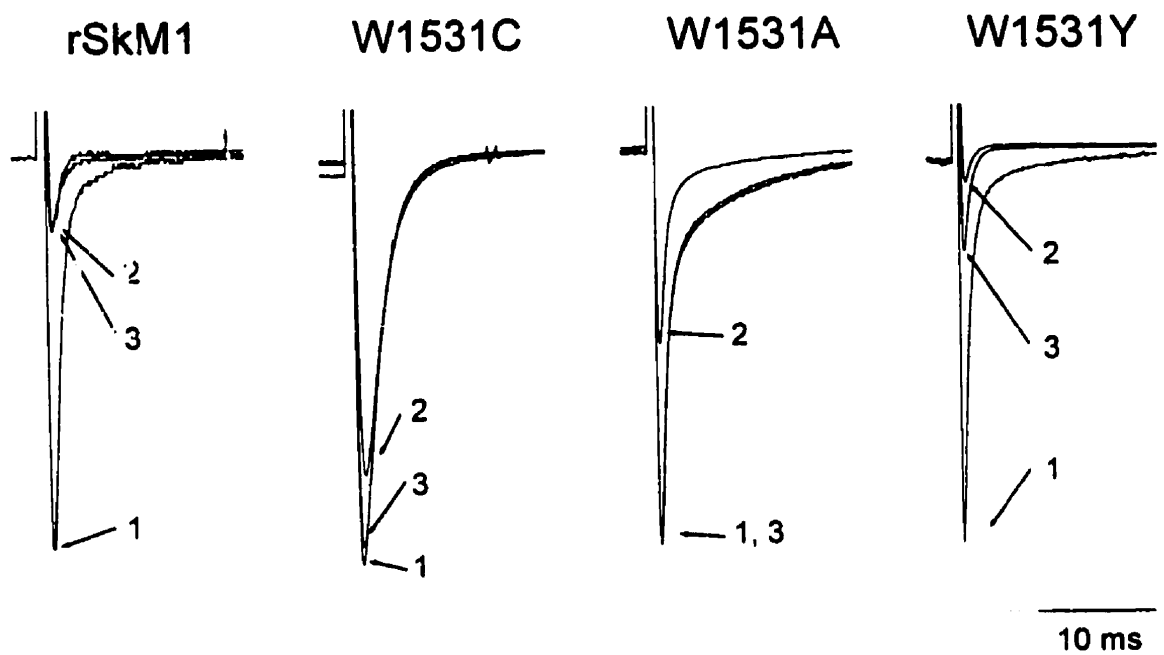
n=3) of W1531Y channels was still significantly (p<0.05) faster than WT rSkM1 consistent with a modest reduction in lidocaine binding affinity (Figure 6.3B).

Reduction of use-dependent block by intracellular QX-314 and the more rapid rate of recovery of W1531C and W1531A mutants compared to WT channels are consistent with a disruption or destabilization of the drug-channel complex. Alternatively, these differences could result from alterations in drug access to the binding site (Ragsdale et al., 1994; Qu et al., 1995). While lidocaine can bind to its receptor via both hydrophilic and hydrophobic pathways, the permanently charged membrane impermeant QX-314 can only take the hydrophilic route making it an ideal probe for assessing drug access to the intracellular local anesthetic binding site via an extracellular pathway (Frazier et al., 1970; Strichartz, 1973; Alpert et al., 1989). Consistent with previous studies, extracellular application of 500 μM QX-314 to WT rSkM1 channels did not result in significant block of Na^+ current 5 minutes after drug application (I_{QX} / $I_{Control}$ = 96.7 ± 1.3 %, n=3, p>0.05) (Figure 6.5B). Similarly, 500 μM QX-314 did not significantly block W1531C (96.6 ± 1.9%, n=5), W1531A (96.7 ± 2.1 %, n=3) and W1531Y (98.2 ± 1.2 %, n=3) channels from the outside over the same period of time (p>0.05, Figure 6.5B) suggesting these tryptophan replacements did not create a low energy pathway between the LABS and the extracellular solution for drug binding and unbinding.

6.4.6 Does QX-314 block resting and inactivated W1531C channels without requiring them to open?

To determine whether access to the LABS from the inside was altered in W1531C channels, we examined the ability of QX-314 to bind to inactivated channels. The protocols used are shown in the inset of Figure 6.7. Channels were prepulsed from a holding potential of -120 mV to -55 mV for a variable period of time from 1 ms to 10 s to induce channel inactivation without opening them (Lawrence et al., 1991). At -55 mV, more than 90 % of the channels enter the fast-inactivated state at steady-state (Figure 6.3A). This prepulse was followed by a hyperpolarizing interval of 300 ms at -120 mV to allow channels to recover

Figure 6.7

QX-314 did not bind to the inactivated states of W1531C channels until they opened.

Inset shows the electrophysiological protocol used in these experiments. Channels were prepulsed to -55 mV for a variable period of time from -120 mV to induce inactivation without opening. An interval of hyperpolarization to 300 ms was given to allow recovery from fast-inactivation. Under control conditions (solid square), the reduction of cuurent after 100 ms was due to accumulation of slow inactivation. Oocytes were then injected with 100 nL of 2 mM QX-314 as described in Figure 6.5. The onset of current reduction with intracellular QX-314 (open circle) was not different from control suggests that QX-314 did not bind to the inactivated states of these channels.
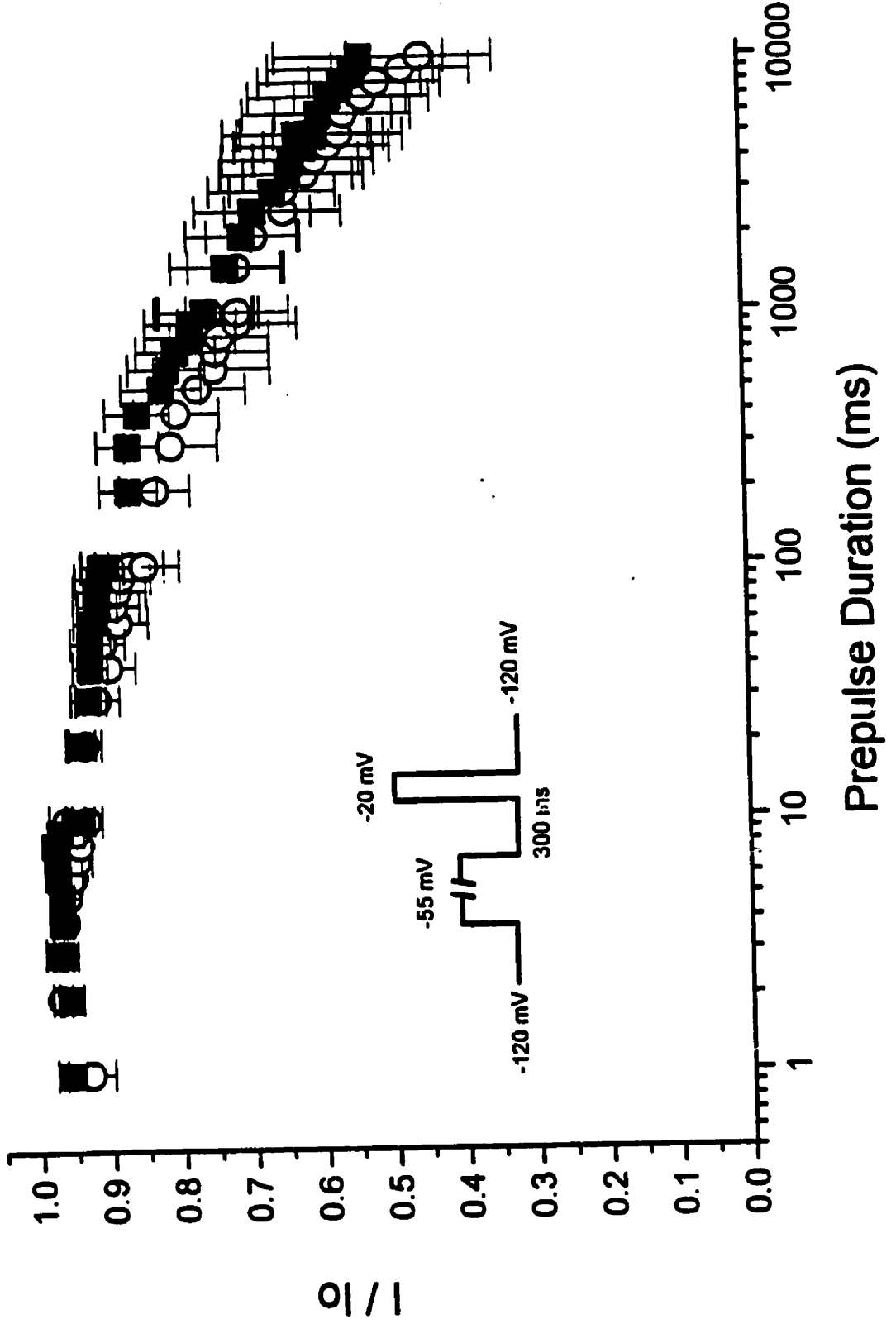
from fast-inactivation. Figure 6.7 shows control data obtained from oocytes without QX-314 (solid square). The small reduction of current following depolarizing prepulses longer than 100 ms probably reflects accumulation of slow inactivation (Featherstone et al.. 1996). The same oocytes were then injected with 100 nL of 2 mM QX-314 and the same protocol was repeated 10 minutes later. Data were collected every 25s to ensure all channels recovered from open channel block by internal QX-314 (Figure 6.6). If QX-314 is able to gain access to the local anesthetic binding site when channels are inactivated, then accumulated block is expected. However, the onset of current reduction after injecting QX-314 (open circle, Figure 6.7) was not different from the control. Unfortunately, similar studies in WT rSkM1 channels were not possible due to the extremely slow recovery of this channel from internal QX-314 block (Figure 6.6B; Strichartz, 1973; Yeh and Tanguy, 1985; Sunami et al.. 1997).

To further confirm that QX-314 is accessible to the LABS only when the channels open and that the internal access pathway for drug binding and unbinding has not been modified, we performed excised inside-out macropatch recordings on both WT rSkM1 and W1531C channels. The protocol used is shown in Figure 6.8A. Na⁻ currents were elicited by depolarizing channels to -10 mV for WT rSkM1 and -20 mV for W1531C for 20 ms from a holding potential of -150 mV at 1 Hz to measure the magnitude of the control current ($I_{Control}$). Channels were then held at -150 mV, at which channels were essentially in the resting closed state, while 250 μM QX-314 was constantly perfused to the intracellular face of the patch. Pulsing at 1 Hz was started again 15 sec after drug perfusion. Any QX-314 binding to its receptor while the channels were closed during the 15 sec hyperpolarization period should be reflected as a reduction of current (i.e. $I_{QX. Pulse 1}$) compared to $I_{QX. control}$ upon restoration of pulsing. Both WT rSkM1 and W1531C did not show any clear evidence for drug binding to the resting state since the $I_{QX. Pulse 1}$ / $I_{QX. control}$ ratios were very close to 1 (WT: 1.0 ± 0.1, n=4; W1531C: 0.9018, n=1). Figure 6.8C shows that continuous pulsing at 1 Hz in typical macropatches of WT rSkM1 and W1531C channels exposed to 250 μM internal QX-314 resulted in use-dependent block ($84.7 \pm 8.6\%$, n=4 and $15.0 \pm 2.5\%$, n=2 respectively) similar to those obtained from QX-314

Figure 6.8

Excised inside-out macropatch experiments demonstrating QX-314 did not bind to the resting states of rSkM1 and W1531C channels until they opened.

A) Electrophysiological protocol. Na+ current was elicited by depolarizing channels to -10 mV (-20 mV for W1531C) from a holding potential of -150 mV in the absence of QX-314 to measure the size of the control current ($I_{control}$). Channels were then held at -150 mV for 15 s while constantly being perfused with 250 μM QX-314. Continuous pulsing at 1 Hz was applied again 15 s after drug perfusion. Current elicited during the 1st pulse ($I_{QX, Pulse\ 1}$) after application of QX-314 was compared with the control current to assess the degree of block of resting channels by QX-314. The bar indicates the period of application of 250 μM QX-314 in the bath solution.

B) Current elicited upon the first depolarization after perfusion of 250 μM QX-314 for 15 s ($I_{QX, Pulse\ 1}$) while channels were being held at -150 mV was normalized with the current elicited before perfusion of QX-314 ($I_{Control}$). Both WT rSkM1 and W1531C channels did not show any significant QX-314 binding to their resting states as the ratios were not statistically different from 1 (p > 0.05).

C) Use dependent block of WT and W1531C channels by QX-314. The graph shows typical example for WT and W1531C cnannels. 250 μM QX-314 when applied to the cytoplasmic side in excised inside-out configuration resulted in 84.7 $\pm$ 8.6%, n=4 block of WT rSkM1 current at steady-state while the same concentration blocked only 15.0 $\pm$ 2.5%, n=2 of W1531C current.

219

A

250 μM QX-314

$I_{control}$ $I_{QX, pulse 1}$

-20 mV

-150 mV

15 s   1 s

B

$I_{QX, pulse 1} / I_{Control}$

rSkM1   W1531C

C

I / Io

Time (s)
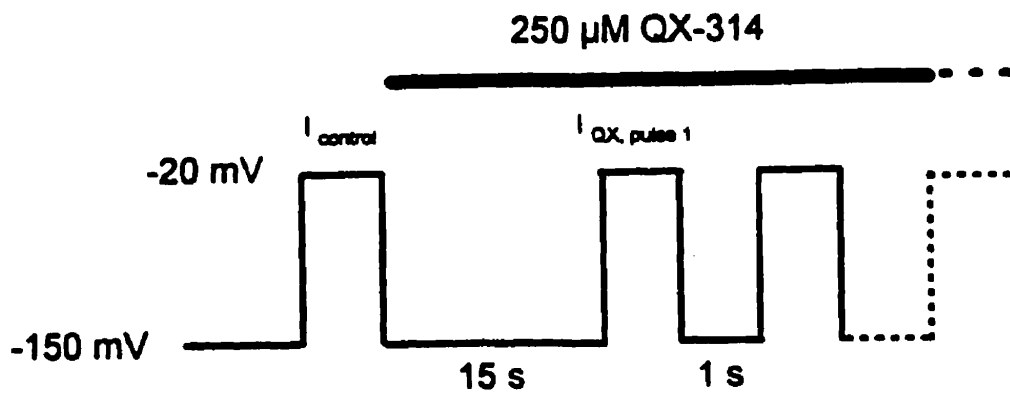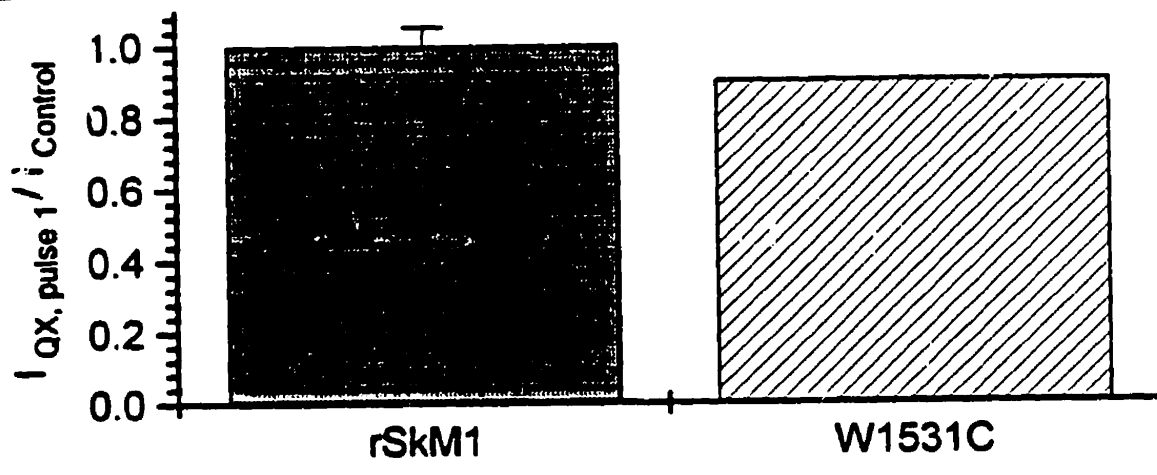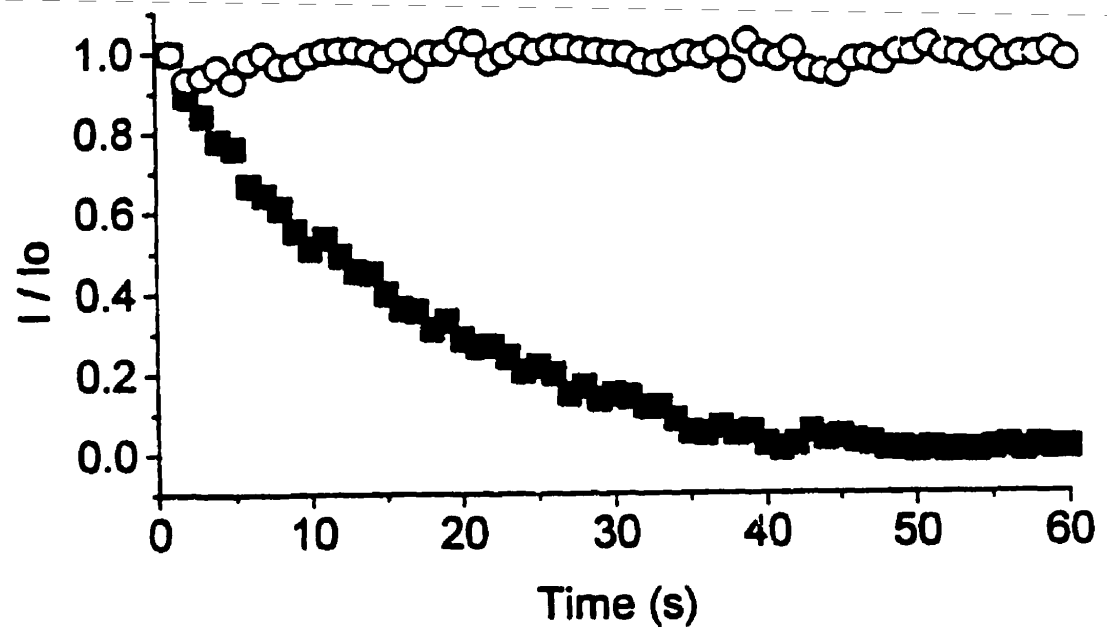
injected oocytes (Figure 6.5A).

Taken together, our results show that the local anesthetic binding site of W1531C channels is inaccessible to intracellular QX-314 when the channels are in the resting or inactivated states or when the drug was applied extracellularly.

6.4.7   *W1712 in the human heart Na$^+$ channel (hH1) is also critical for lidocaine block*

The Na$^+$ channel pore sequence is highly conserved among different Na$^+$ channel subtypes (Fozzard, 1996). The residue analogous to W1531 in rSkM1 is absolutely conserved in other cloned Na$^+$ channels. To investigate if this pore tryptophan in domain IV also plays a similar role in lidocaine block of human heart Na$^+$ channels (i.e. hH1), we replaced the equivalent tryptophan (i.e. W1712) with cysteine and alanine. Figure 6.9 shows use-dependence of hH1, W1712C and W1712A channels using the same protocol used in rSkM1 channel in the absence and presence of lidocaine. For WT hH1 channels, $I_{Pulse\ 20}$ was modestly reduced to 91.8 ± 1.9 %, n=4 compared to $I_{Pulse\ 1}$ under control drug-free conditions while following application of 100 μM lidocaine the degree of reduction was reduced to 45.0 ± 6.7 %, n=4 (p<0.05) which is far greater than for rSkM1 channels as described previously (Nuss et al., 1995; Wang et al., 1996; Wright et al., 1997). Interestingly, no measurable current (<1 μA) was initially observed in oocytes injected with W1712C cDNA. However, following the application of 10 mM dithiothreitol (DTT), a sulfhydryl reducing agent, the current amplitude was increased about 10-fold (data not shown) consistent with reduction of a disulfide bond in the pore as observed previously in rSkM1 double-cysteine mutant channels (Tsushima et al., 1997b). A disulfide bridge was probably spontaneously formed between the introduced (i.e. W1712C) and the native (i.e. C373) cysteines in the pore because of their spatial proximity (Tsushima et al., 1997b). For DTT reduced W1712C channels, 100 μM lidocaine induced substantially less use-dependent block in W1712C channels ($I_{Pulse\ 20}$ / $I_{Pulse\ 1}$ = 98.1 ± 0.4 %, n=3 without and 87.4 ± 5.0 %, n=4 with lidocaine) than in WT hH1 channels (p<0.05). Similar to W1712C, the mutation W1712A also significantly reduced use-dependence by 100 μM lidocaine (91.7 ±

221

Figure 6.9

Use-dependent block of WT hH1, W1712C and W1712A by lidocaine.

A) Representative current records of each of the WT hH1, W1712C and W1712A channels in the presence of 100 μM lidocaine elicited in 1st, 2nd, 5th and 15th pulse as indicated. Peak currents were normalized to the first pulse. Use-dependent blocks were induced by giving a 10 Hz train of depolarizations to -10 mV each of 20 ms duration from a holding potential of -120 mV. W1712C channels were recorded under reducing conditions in the presence of 10 mM DTT due to the presence of disulfide bond formed between the inserted and native cysteines in the pore. Peak currents were 2.1, 1.7 and 1.8 μA for hH1, W1712C and W1712A respectively.

B) Peak currents were normalized to that mesaured during the first pulse and plotted against the pulse number. The concentration of lidocaine used was 100 μM. Data shown represent mean $\pm$ SE. Use-dependent block was significantly reduced ($p < 0.05$) in both W1712C (n=3) and W1712A (n=3) channels compared to WT channels (n=3) suggesting this tryptophan residue in the pore is also critical for lidocaine binding to hH1 channels.

hH1   W1712C   W1763A

15
5
2
1

15
5
2
1

15
5
2
1

10 ms

Normalized Current

1.0
0.9
0.8
0.7
0.6
0.5
0.4
0.0

1.0
0.9
0.8
0.7
0.6
0.5
0.4
0.0

■ Control   HP=-120 mV
O 100 µM Lidocaine   10 Hz

0   5   10   15   20
0   5   10   15   20
0   5   10   15   20
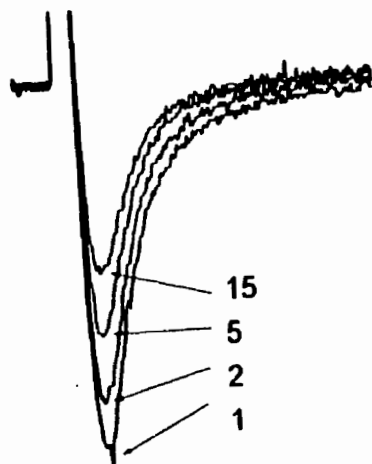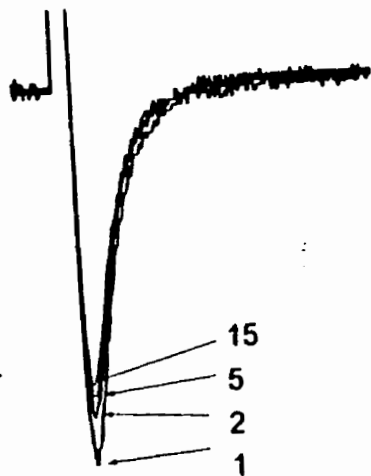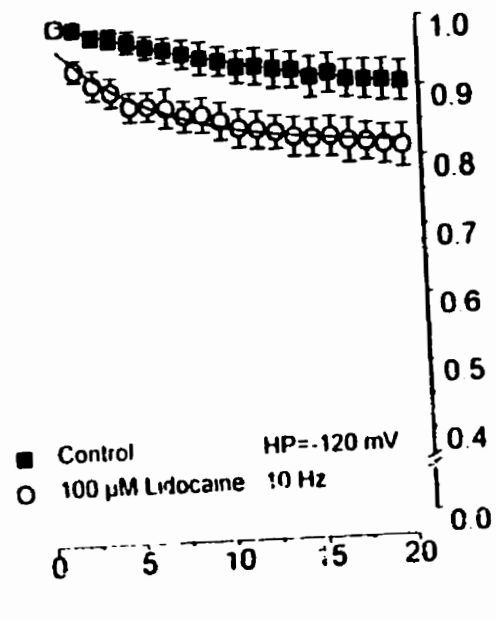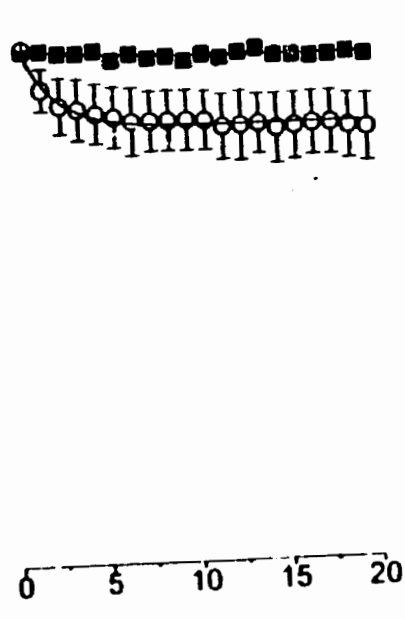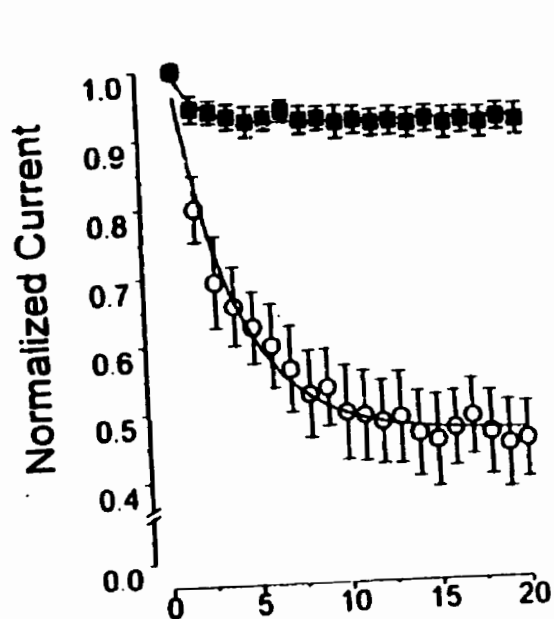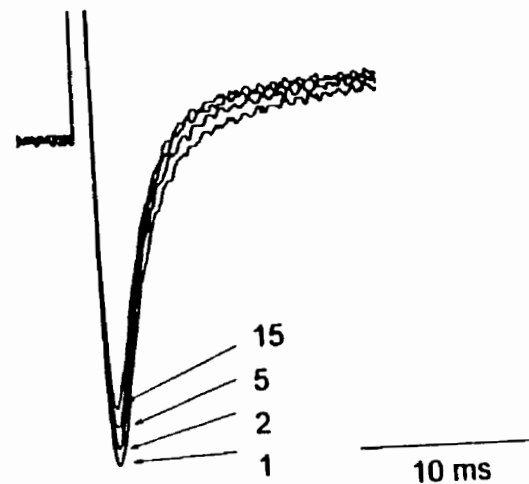
Pulse Number

2.9%, n=3 without and 82.9 ± 2.6%, n=3 with lidocaine) compared to WT hH1 channels (p<0.05%). These results indicate that the residue W1712 in hH1 Na⁻ channels plays a similar critical role in lidocaine block as W1531 does in rSkM1 channels.

6.4.8 Tonic block by lidocaine of rSkM1, W1531C, W1531A and W1531Y

While local anesthetics bind preferentially to the inactivated state of Na⁻ channels, they can also bind to the resting or open states thereby producing tonic block (Hille, 1977; Hondeghem and Katzung, 1977). Assessment of tonic block was accomplished by comparing the peak Na⁻ current amplitude (recorded following step depolarizations from a holding potential of -120 mV at a low stimulation rate of 0.25 Hz) before and after application of various concentrations of lidocaine. Since almost 100 % of WT and mutant rSkM1 channels are closed when held at -120 mV in the presence of all lidocaine concentrations examined (Figure 6.3A and unpublished data), reductions in peak current at such low stimulation rates cannot be attributed to shifts of the voltage-dependence of channel availability or entry into the inactivated state. Such reduction of current by LA is referred to as tonic block (Hille, 1977; Hondeghem and Katzung, 1977). Figure 6.10A shows the effects of 300 μM lidocaine on macroscopic whole-cell currents of rSkM1 W1531C, W1531A and W1531Y channels. Figure 6.10B plots the fraction of current remaining after drug application as a function of extracellular lidocaine concentration. The half-blocking concentrations (i.e. IC₅₀) for tonic block estimated using binding isotherm fits for WT rSkM1, W1531C, W1531A and W1531Y mutant channels were 1395 ± 315 μM (n=4), 445 ± 53 μM (n=5), 532 ± 91 μM (n=4) and 1413 ± 215 μM (n=4) respectively. Despite such significant (p<0.05) changes in IC₅₀ values observed in W1531C and W1531A channels relative to WT rSkM1 channels, all channels (with rSkM1 and W1531Y inclusive) showed 1:1 drug binding as expected from previous studies (Bean et al., 1983; Nuss et al., 1995; Balser et al., 1996).

Figure 6.10.

Tonic block by lidocaine for rSkM1, W1531C, W1531A and W1531Y.

A) Representative Na^+ current traces recorded in the absence and presence of $300\mu M$ lidocaine. Currents were elicited by depolarizing cells to -10 mV for rSkM1 and W1531Y and -20 mV for W1531C and W1531A for 50 ms from -120 mV. Currents have been scaled such that the peaks of these channels in the absence of lidocaine are the same. The vertical bar represents 5.5, 4.4, 4.2 and 4.7 μA for rSkM1, W1531C, W1531A and W1531Y respectively.

B) Dose-response relationships for tonic block by lidocaine of WT and tryptophan mutant channels. The degrees of tonic block indicated as normalized currents were plotted as a function of lidocaine concentration for WT (solid square), W1531C (open circle), W1531A (open up triangle) and W1531Y (open down triangle) channels. Data were fitted to a binding isotherm equation to estimate for the values of IC_{50} for tonic block (see Materials and Methods). W1531C and W1531A were more sensitive than WT rSkM1 channels to tonic block by lidocaine as indicated by the leftward shifts of their binding curves. The IC_{50} for tonic block of W1531Y was not different from WT.

A

rSkM1

W1531C

1.1 uA
10 ms

1.25 uA
1.1 ms

W1531A

W1531Y

15 uA
10 ms

1.0 uA
10 ms

B

■ rSkM1
○ W1531C
△ W1531A
▽ W1531Y

Normalized Current
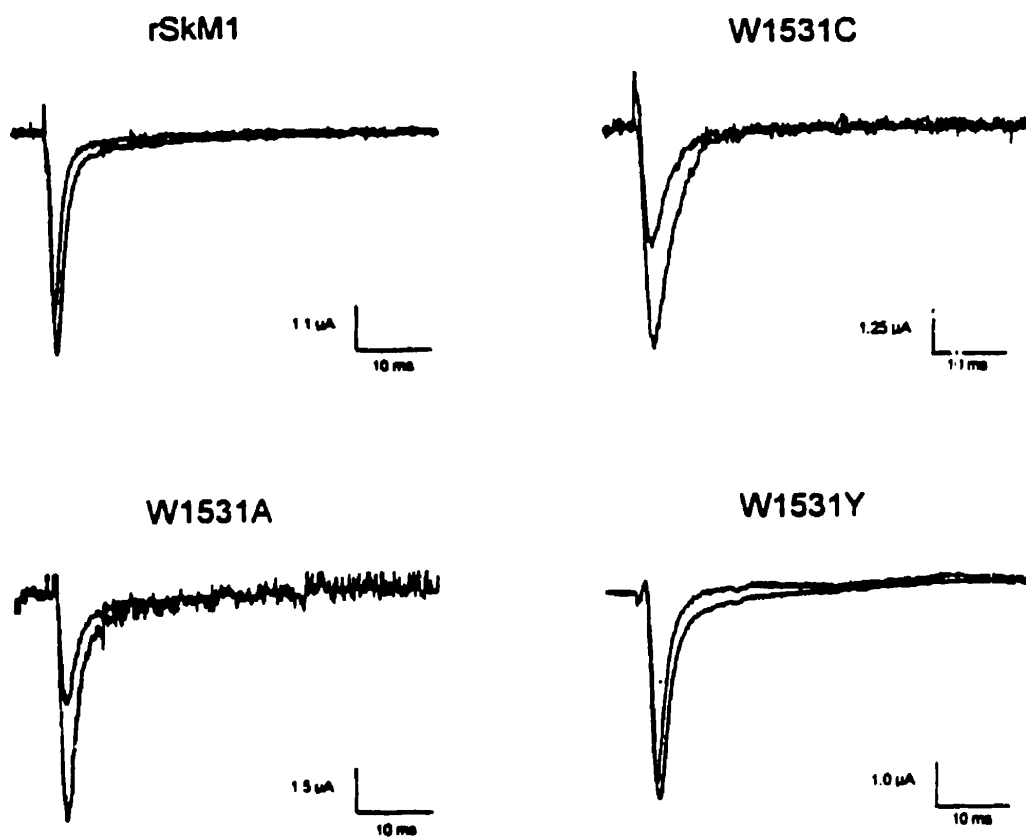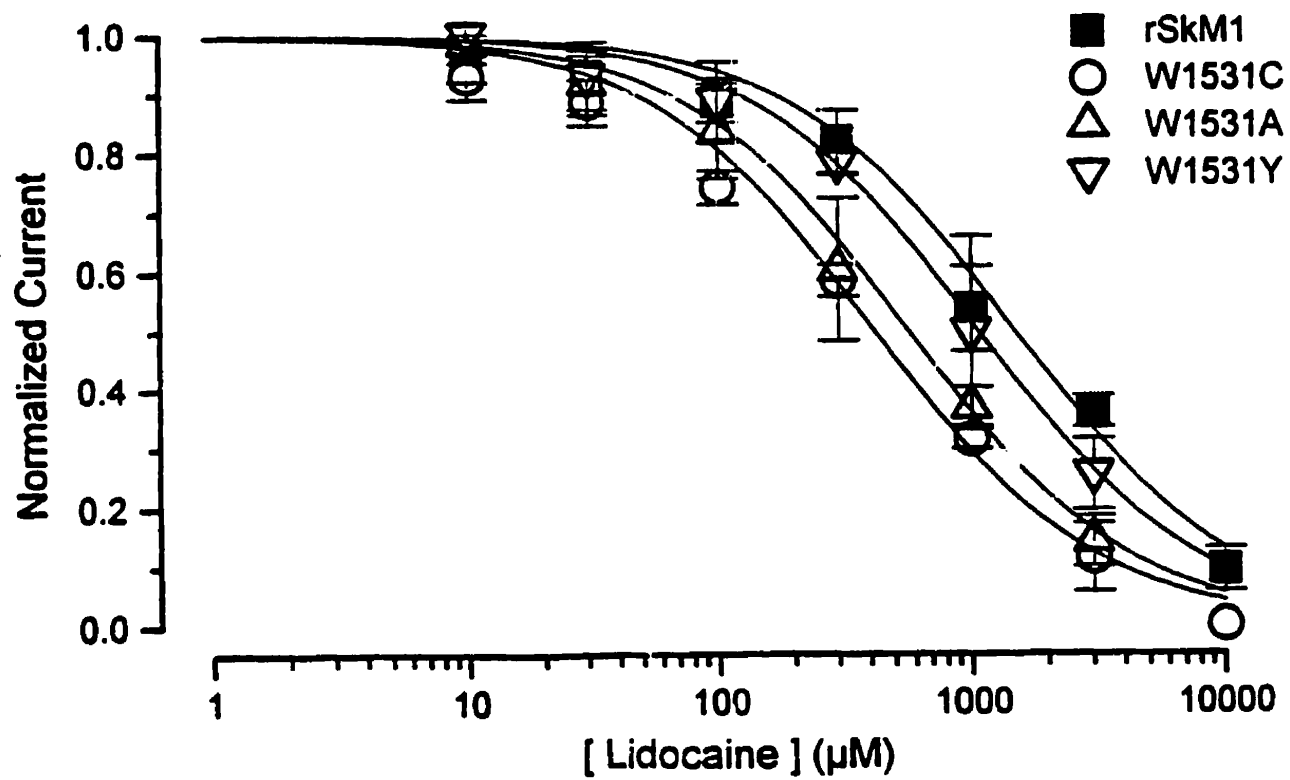
[Lidocaine] (μM)

6.4.9   Effects of lidocaine on single rSkM1 and W1531C channels

Interestingly, W1531C and W1531A channels were more sensitive to tonic block by lidocaine than WT channels despite the fact that drug block as assessed by use-dependence. shift in channel availability and the effects of drug on recovery from inactivation was reduced for these channels. To further elucidate the underlying mechanism responsible for the enhanced tonic block observed in W1531C channels, we performed cell-attached single channel recordings. Figure 6.11A shows typical traces of single channel currents recorded from patches containing WT rSkM1 and W1531C channels both in the absence and presence of 300 μM lidocaine. Currents were elicited by repeated depolarizations to – 20 mV for 50 ms from a holding potential of –120 mV. Lidocaine was applied extracellularly by including it in the pipette solution in patches separate from the control. Under drug-free conditions, both WT and W1531C single channels generally opened once briefly and their mean numbers of opening per depolarization were 1.04 ± 0.04. n=3 and 1.05 ± 0.06, n=3 respectively. These observations are consistent with absorbing inactivated states for these channels as expected from our whole-cell recordings (Figure 6.3 and 4) and further confirm that the changes in lidocaine block observed in W1531C channels were not effects secondary to destabilization of inactivation. Nevertheless, application of 300 μM lidocaine did not significantly affect the mean number of opening per depolarization of either WT (1.03 ± 0.03. n=3) or W1531C (1.04 ± 0.04. n=3) channels ($p>0.05$).

Figure 6.11B shows the ensemble average currents assembled from idealized single-channel records derived from the same patches shown in Figure 6.11A. Ensemble currents show that peak amplitudes for WT and W1531C channels in the presence of 300 μM lidocaine were reduced to 77.2 % (73.9 ± 13.3 %, n=3) and 40.0 % (33.6 ± 4.0 %, n=3) of pre-drug values respectively. These results are consistent with the corresponding tonic blocks observed at the whole-cell level with this concentration of lidocaine (Figure 6.10). Since $I_{Na} = N*P_{open}* i$, where I_{Na} is the total Na^- current, N is the total number of channels. P_{open} is the probability of channel opening and i is the unitary current of a single

Figure 6.11

Single channel recordings of WT rSkM1 and W1531C channels expressed in *Xenopus* oocytes. Typical single-channel currents of rSkM1 and W1531C channels recorded under control conditions and in the presence of 300 μM lidocaine as indicated. Lidocaine was applied in the pipette solution. Currents were elicited by repeated depolarizations to –20 mV for 50 ms from a holding potential of –120 mV at a stimulation frequency of 0.67 Hz. Both wild-type patches (control and lidocaine) contained 1 channel. The W1531C patches contained 2 (control) and 1 (lidocaine) channels.

rSkM1   W1531C

A
          Control   Control

1 pA
10 ms

          300 µM Lidocaine   300 µM Lidocaine

B
     Control   300 µM Lidocaine   Control   300 µM Lidocaine

                   0.1 pA   0.05 pA
                   10 ms   10 ms
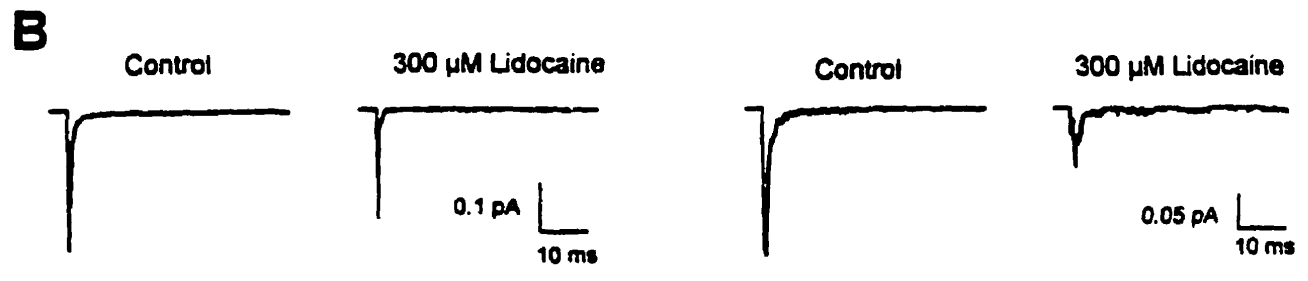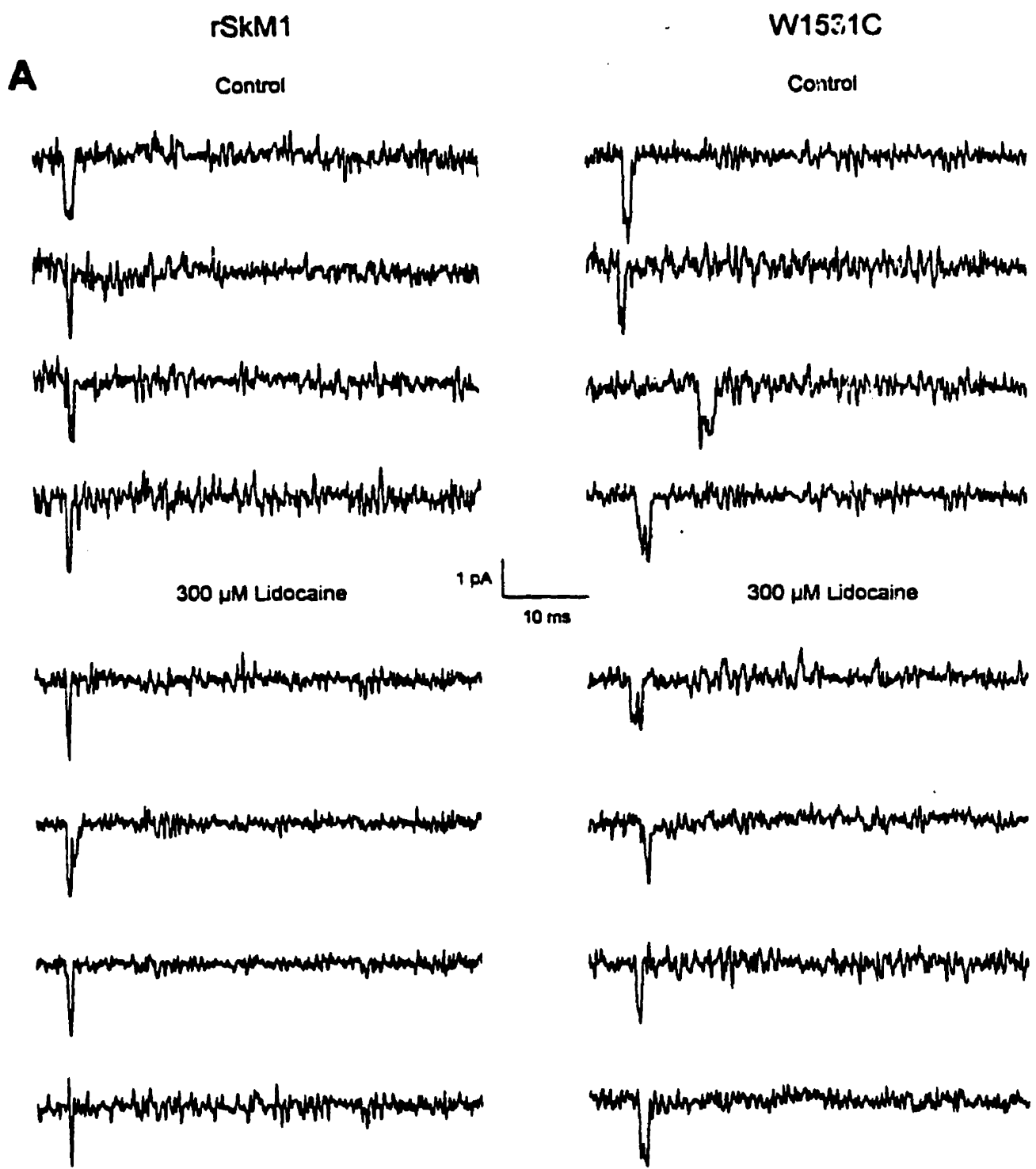
Figure 6.12

Effects of lidocaine on single channel current-voltage relationship, probability of channel opening and mean open time of WT rSkM1 and W1531C channels.

A) Current-voltage relationship of rSkM1 and W1531C single channels obtained with and without lidocaine. Unitary currents are plotted as a function of step membrane potential in the absence (solid square) and presence (open circle) of 300 μM lidocaine. Holding potential was -120 mV. Solid lines are best fits to the mean data by linear regression. Channel conductances (δ) were determined from the slopes of these fits. Data shown are the averages of 4 (control) and 8 (lidocaine) patches for rSkM1 channels and 5 patches (both control and lidocaine) for W1531C channels.

B) The effect of 300 μM lidocaine on the probability of channel opening (P_{open}). P_{open} was depicted as the ratio of number of depolarizations that elicited at least one channel opening to the total number of depolarizations during the experiments. Data shown are the average of 3, 3, 4 and 3 patches respectively.

C) The effect of 300 μM lidocaine on mean open time of channel openings. Open time histograms shown are derived from typical patches of rSkM1 and W1531C channels recorded in the absence and presence of 300 μM lidocaine at -20 mV from a holding potential of -120 mV. Solid lines are best fits of single exponentials. Mean open times of respective patches are indicated. See text for mean data.

rSkM1

W1531C

A

Voltage (mV)

-60 -50 -40 -30 -20 -10

$g_{control}$ = 32.5±2.8 pS

$g_{lidocaine}$ = 23.9±2.5 pS

0.0
-0.5
-1.0
-1.5
-2.0
-2.5
-3.0

Voltage (mV)

-60 -50 -40 -30 -20 -10

■ Control
○ 300 µM Lidocaine

0.0
-1.0
-2.0
-3.0
-4.0
-5.0

I (pA)

$g_{control}$ = 78.3±2.5 pS

$g_{lidocaine}$ = 46.6±6.5 pS

B

P_{open}

0.25
0.20
0.15
0.10
0.05
0.00

C

Number of Events

Control
t = 0.26 msec

100
80
60
40
20

0.5 1.0 1.5 2.0 2.5 3.0

Control
t = 0.32 msec

160
140
120
100
80
60
40
20

0.5 1.0 1.5 2.0 2.5 3.0

300 µM Lidocaine
t = 0.29 msec

60
50
40
30
20
10

0.5 1.0 1.5 2.0 2.5 3.0

300 µM Lidocaine
t = 0.31 msec

70
60
50
40
30
20
10

0.5 1.0 1.5 2.0 2.5 3.0

Time (ms)

Na$^-$ channel, and that N is fixed within the time frame of our experiments, reduction of I_{Na} by drug may result from either a reduction of P_{open} or i or combination of both.

Careful inspection of Figure 6.11A reveals that there was a reduction in unitary current at −20 mV in both rSkM1 (1.7±0.1 pA, n=4) and W1531C (1.7±0.1, n=5) patches when channels were exposed to 300 μM lidocaine (WT: 1 5±0.1 pA, n=8; W1531C: 1.1±0.2 pA, n=5) consistent with a rapid open-channel block by lidocaine. This rapid block has been suggested to be largely responsible by charged lidocaine molecules as the drug exists as a mixture of charged and neutral species in solution under neutral pH conditions (Hille, 1977; Nettleton and Wang, 1990). Figure 6 12A plots the unitary current amplitudes of WT rSkM1 and W1531C channels in the absence and presence of 300 μM lidocaine as a function of membrane potential. Under control conditions, single channel conductances of rSkM1 and W1531C channels estimated from linear regression analysis of the data in Figure 6.12A were 32.5±2.8 pS (n=5) and 78.3±2.5 pS (n=5), consistent with previous report (Chiamvimnovat et al. 1996). Application of 300 μM lidocaine significantly (p<0.05) reduced the single channel conductances of both WT and mutant channels to 23.9±2.5 pS (n=8) and 46.6±6.5 pS (n=5) respectively. These reductions in single channel conductances (i.e. unitary currents) match closely the changes in ensemble average currents as well as the tonic block of whole-cell macroscopic Na$^-$ currents, suggesting that enhanced rapid open channel block of W1531C channels underlies the enhanced tonic block. This interpretation is further bolstered by the observation that the probability of channel opening, P_{open}, in WT (0.21±0.05, n=3) and W1531C (0.14±0.02, n=3) channels were not significantly (p>0.05) affected by 300 μM lidocaine (WT = 0.20±0.05, n=3; W1531C = 0.14±0.01, n=3) suggesting tonic block of both WT and W1531C channels does not involve drug binding to some pre-open states of these channels. These results are pictorially presented in Figure 6.12B.

Intermediate (between fast and discrete) modes of open channel block which occur on the time scale of channel gating are expected to reduce channel mean open

times. We next examined if such modes of block exist, in addition to the rapid block, by examining changes in channel mean open time. Figure 6.12C shows typical open time histograms constructed from corresponding single channel patches with and without exposure to 300 μM lidocaine. Under control conditions, mean open time of W1531C channels (0.30±0.03 ms, n=3) was modestly prolonged when compared to WT channels (0.27±0.01 ms, n=3) when examined at −20 mV. Mean open times of both channels however were not significantly altered (p>0.05) by lidocaine at the concentration used (300 μM lidocaine: W1531C = 0.24±0.03 ms, n=3; WT = 0.26±0.02 ms, n=3) suggesting such intermediate mode of open channel block by lidocaine at 300 μM did not exist. These results are consistent with previous single channel recordings of Na⁻ channel with lidocaine (Grant et al., 1989) and the observations that lidocaine does not accelerate the rate of decay of macroscopic whole-cell current of rSkM1 channels (Wang et al., 1996; Sah et al., 1998).

6.5   Discussion

6.5.1 P-loop residues and lidocaine binding

In this study, we examined the changes in lidocaine block following mutations of three rings of pore-lining residues. We observed reduced use-dependence by lidocaine in W402C, W1239C and W1531C channels which could result from reduced hydrophobic or π-electron interactions of these residues with the aromatic moiety of lidocaine (Ragsdale et al., 1994). Neutralization of negative residues with cysteine was expected to weaken drug binding by reducing attraction of the positively charged drug molecules to the their binding site, but this is not observed. Indeed, we observed an enhanced use-dependent block when the negative residues were mutated to cysteine. Perhaps, as suggested for E755A channels which also involves neutralization of a negative charge but displays enhanced lidocaine block, these native negative charges in the pore attract the charged portion of lidocaine pulling the aromatic portion of the drug away from its optimal position for interacting with its binding site (Sunami et al., 1997). Loss of these

negative interactions therefore enhance drug binding by allowing better hydrophobic interactions. Overall. these pore mutations may affect lidocaine block by mechanisms such as modified intrinsic binding. altered drug access for binding and unbinding. and by alterations in channel gating since local anesthetics bind preferentially to the inactivated states of Na⁺ channel.

6.5.2 Mutations of W1531 alter the intrinsic binding affinity of lidocaine without affecting drug access

The major finding of our study was the observation that replacement of W1531. located in the ascending portion of the P-loop in Domain IV. with cysteine or alanine reduced use-dependence and the shifts in channel availability in the presence of lidocaine. These mutations also accelerated the rate of recovery from inactivation in the presence of lidocaine. While modification of drug access can affect use-dependence and recovery from inactivation by changing the rates for drug binding and unbinding. it predicts no change in steady-state channel availability curve which is determined by drug binding energetics (Bean et al.. 1983). The reduction of shifts in channel availability curves caused by lidocaine in W1531C and W1531A channels compared to WT channels (Figure 6.3) establishes that the lidocaine binding affinity was disrupted in these channels. The use of a 500 msec depolarizing pulse has previously been shown to allow drug binding to channels to reach steady-state (Balser et al.. 1996) without significantly inducing slow inactivation (Featherstone et al.. 1996) in rSkM1 channels. Though a longer prepulse duration might be required for the mutant channels to reach steady-state. our experiments nevertheless indicate that drug binding was seriously weakened in both W1531C and W1531A channels over the same interval when compared to WT. Furthermore. our experiments with QX-314 demonstrated that drug access from the extracellular and intracellular faces of the channel were not modified. In addition, changes in LA block secondary to changes in inactivation also seems unlikely since mutations of W1531 did not disrupt normal fast-inactivation as revealed by both whole-cell and single channel recordings. In fact, steady-state inactivation curves of both

W1531C and W1531A mutants were shifted in a hyperpolarized direction relative to WT channels while their rates of recovery from inactivation were actually slower than WT. These gating characteristics are expected to enhance drug block due to stabilization of the inactivated state rather than inhibiting it as observed. Taken together. mutations of W1531 appeared to alter the binding affinity of the drug to the channel without affecting drug access.

6.5.3 *Tonic block and single channel conductance*

Interestingly, the W1531C and W1531A mutations enhanced tonic block by lidocaine while reducing the effects of drug on use-dependence. shifts of channel availability and recovery from inactivation. Similar changes in the profile of drug modification have been observed previously in channels with residues replaced in S6 of domain IV (Ragsdale et al.. 1994). Bean et al. (1983) suggested that tonic block antagonizes use-dependent block at depolarized holding potentials since channels with drug bound to the closed or open state are not available for further drug binding to the inactivated state thus leading to an apparent reduced use-dependence. This possibility is unlikely in our case since tonic block was assessed from a holding potential (-120 mV) where all channels were essentially in the resting closed states. To fully elucidate the underlying mechanisms responsible for such enhanced tonic block observed in W1531C channels. we performed cell-attached single channel recordings. Two modes (fast and discrete-slow) of block by lidocaine and its analogue QX-314 have been previously observed in skeletal muscle and cardiac Na$^+$ channels at the single channel level (Gingrich et al.. 1993; Zamponi et al.. 1993). Under our experimental conditions, reductions in unitary current consistent with rapid open channel block was observed in both WT rSkM1 and W1531C channels. Examination of the current-voltage relationship revealed that the lidocaine block of WT channels was 50% of the block observed in W1531C channels which matched remarkably well the approximate 3-fold increase in tonic block of whole-cell W1531C currents by lidocaine. The absence of measurable changes in mean open times and probabilities of channel opening by lidocaine in W1531C channels suggests that the increase in tonic

block observed in W1531C channels primarily results from increased open channel blockade.

6.5.4 Molecular Interpretation

W1531 has previously been shown to be accessible from the extracellular face of the channel (Perez-Garcia et al., 1996; Chiamvimonvat et al., 1996; Li et al., 1997b; Tsushima et al., 1997a.b). At first glance, this might seem suprising since the LABS is thought to be located on the intracellular face of the channel pore (Hille, 1992). One explanation for this observation is that replacement of this residue causes a significant disruption of the channel pore structure. Consistent with this possibility, replacement of this residue creates channels unable to discriminate between different monovalent cations (Chiamvimonvat et al., 1996; Tsushima et al., 1997a). However, W1531C channels are impermeable to organic cations such as TMA (data not shown), which has a chemical structure similar to lidocaine.

Alternatively, the residue could undergo a translocation from the extracellular to the intracellular face of the channel either during the inactivation process or following drug binding which ultimately leads to intimate hydrophobic or π-electron interactions of the aromatic portion of the drug with W1531 and other residues (such as those in DIV S6) which comprise the LABS. Similar dynamic rearrangement of residues in the outer pore has been previously observed in voltage-gated K^+ and Na^+ channels (Liu et al., 1996; Balser et al., 1996) and would be consistent with our previous observation that the P-loop in domain IV is flexible compared to P-loops in the other domains (Tsushima et al., 1997b). This model is also consistent with a previous suggestion that low affinity rapid QX-314 block serves as an intermediate that catalyzes the formation of a high-affinity discrete-block complex (Gingrich et al., 1993). W1531 might be a critical residue for such transition. Nonetheless, we cannot rule out the possibility that W1531 may not participate directly in drug binding but the mutations modify LA block by interfering with the conformations required for wild-type drug-channel interactions through some

long-ranged effects. Further experiments are required to prove or disprove our hypothesis.

It is interesting that the mutations W1531C and W1531A mimic the effects of lidocaine in several respects: they both shifted the midpoint of channel availability curve and slowed recovery from inactivation in a manner similar to WT channels modified by lidocaine. Given these observations, one might argue that lidocaine application to these mutant channels did not display additive effects because the mutations already mimic normal drug-bound channels thereby saturating the drug effects. However, the analogous mutation in hH1 channels did not alter channel gating to the same extent as in rSkM1 channels but still rendered channels less sensitive to lidocaine block when assessed by use-dependence, shift of channel availability curve and the effects of drug on recovery from inactivation (Li and Backx, unpublished data). Therefore, it seems unlikely that the changes in drug block observed in these mutants result from effects secondary to gating changes.

The conclusion that W1531 forms a part of the LABS is appealing for a number of reasons. First, W1531 is an aromatic residue capable of hydrophobic or π-electron interactions and these interactions have previously been shown to be critical for high affinity blockade of Na⁻ channels (Sheldon et al., 1991; Ragsdale et al., 1994; Zamponi and French, 1993). Second, we have previously shown that W1531 also forms part of the selectivity filter (Tsushima et al., 1997) and it has long been thought that local anesthetics bind deep into the pore from the cytoplasmic side up to the selectivity filter region. Recently, residues that comprise the putative selectivity filter (i.e. DEKA) of rSKM1 Na⁻ channels have been shown to affect lidocaine binding (Sunami et al., 1997). Third, the electrical distance (δ) for LA block is 0.7-0.8 from the inside (Gingrich et al., 1993; Hille, 1977) while W1531 has $\delta \approx 0.25$ from the outside for block by Cd^{2+} (Chiamvimonvat et al., 1996) suggesting this P-loop region is structurally adjacent to the LABS and possibly forms the roof of the intracellular channel vestibule containing the LABS. Future experiments studying the relationships between W1531 and residues lining IVS6 in the binding of local anesthetics thus possibly further define the molecular basis of local

anesthetic action.

6.5.5 *Aromaticity is critical for Na$^+$ channel function and pharmacology*

Previous studies have demonstrated that mutations of certain residues lining DIVS6 disrupt inactivation and weaken local anesthetic binding (Ragsdale et al., 1994). We demonstrate in this report that replacement of a pore tryptophan in DIV of rSkM1 and hH1 Na$^-$ channels is also critical for lidocaine action. Interestingly, W1531 in rSkM1 Na$^-$ (Tsushima et al., 1997a) and its analogous residue in hH1 (Li & Backx, unpublished data) are both important in ionic selectivity. When the aromatic residue is replaced with cysteine or alanine, the channel allows permeation of monovalent cations such as K$^-$, NH$_4^-$ and Cs$^-$. W1531 is also an important determinant of the wild-type sensitivity of Na$^-$ channel to μ-CTX block (Li et al., 1997b). These changes in channel properties are largely prevented in W1531Y channels suggesting that the aromaticity at this location is critical for proper channel function and pharmacology (Tsushima et al., 1997a; Li et al., 1997).

Cardiac Na$^-$ channels are known to be more sensitive to local anesthetics than their skeletal muscle and nerve counterparts. Clinically, 5-20 μM lidocaine can effectively treat arrhythmias by blocking cardiac Na$^-$ channels whereas >100 μM doses are required to produce local anesthesia in nerve and skeletal muscle (Gianelly et al., 1967; Jewitt et al., 1968; Hille, 1978). Despite these differences in drug sensitivity between different Na$^-$ channel subtypes (Wright et al., 1997; Nuss et al., 1995; Wang et al., 1996), mutations of W1712 in DIV in hH1 Na$^-$ channels produced effects similar to those observed at the analogous position in rSkM1 channels (i.e. W1531) suggesting that this pore tryptophan is a common molecular determinant of local anesthetic action.

6.5.6 *Conclusion*

In summary, our study demonstrates that the pore tryptophan located at position

238

1531 within the ascending limb (i.e. SS2) of the P-loop in Domain IV of rSkM1 Na⁻ channel. which has previously been shown to be critical for ionic selectivity (Chiamvimonvat et al., 1996; Tsushima et al., 1997a) and μ-CTX binding (Li et al., 1997), also plays an important role in channel modification by lidocaine. Such changes in lidocaine block observed in W1531C and W1531A channels were not results due to modification of drug access or effects secondary to changes in channel gating. Mutations of the analogous residue in hH1 (i.e. W1712) also reduced lidocaine block suggesting that this pore tryptophan plays a similar role in LA block of cardiac Na⁻ channels.

6.6   *Acknowledgements*

CHAPTER 7

MAPPING THE SPATIAL RELATIONSHIP BETWEEN
THE PORE AND THE LOCAL ANESTHETIC BINDING SITE

7.1 *Abstract*

To map the spatial relationship between the pore and the local anesthetic binding site of Na⁻ channels. we have developed a novel local anesthetic agent (MTSBZ) by tethering benzocaine to the sulfhydryl reactive group, methanethiosulfonate. The application of MTSBZ modified both native rat cardiac Na⁺ channels and *Xenopus* oocytes expressed human heart (hH1) Na⁺ channels, whose pores contain a native cysteine. in a manner indistinguishable from the effects observed in the presence of benzocaine. Unlike benzocaine, these effects persisted after drug washout however. In contrast, MTSBZ modification of rat skeletal muscle (rSkM1) Na⁺ channels expressed in *Xenopus* oocytes was totally reversible upon washout but not in the mutant skeletal muscle Na⁺ channels containing a cysteine at the equivalent location as cardiac Na⁻ channels (Y401C) unless treated with dithiothreitol. These results suggest irreversible modification by MTSBZ requires the presence of a reactive cysteine in the channel pore. Furthermore, MTSBZ reduced the affinity of lidocaine for cardiac Na⁻ channels while mutating the phenylalanine residue (F1579A) known to be critical for local anesthetic binding abolished the effects of MTSBZ, suggesting that MTSBZ interacts with the local anesthetic binding site. Overall, these observations indicate that MTSBZ anchors specifically at a cysteine in the pore but is still able to maintain drug efficacy. Changing the linker length varied the degree of drug modification of hH1 Na⁻ channel thereby providing information on the spatial distance between the anchor site (⁻ the cysteine) in the pore and the local anesthetic binding site. Since only the cardiac channels but not other tissue subtypes contain a native cysteine in the pore, our strategy also provides a potentially useful method for developing a heart-specific local anesthetics.

7.2   *Introduction*

Knowing that mutations of certain pore residues of the Na⁻ channels affect lidocaine binding (Chapter 6), we next tried to map the spatial relationship between the pore and the local anesthetic binding site. To accomplish this goal, we developed a novel strategy which comprises of an Anchor, a Linker and an active Drug, referred to as ALD (Figure 7.1). The key to ALD is that the anchor serves to recognize a unique and distinct receptor thereby effectively delivering the active drug to the drug binding site via the linker. Drug efficacy of these ALD agents should depend critically on the linker length for reasons given below. When the linker is too short, drug efficacy will reduce because protein distortions will be needed before the drug moiety of an ALD can access to the binding site. On the other hand, collision time will increase when the linker is too long thereby reducing drug efficacy. Therefore, an optimal linker length should exist for maximum drug action. This optimal length better reflects the time-averaged distance between the anchor and the drug binding site because many proteins are flexible and dynamic in nature. In addition, our strategy also permits development of protein-specific drugs since the anchor can be chosen to recognize specific distinct regions of the protein of interest.

Previous studies have identified a unique cysteine within the external pore of cardiac Na⁻ channels (Noda et al, 1986; Rogart et al., 1989; Trimmer et al., 1989; Backx et al., 1992; Akopian et al., 1996) (Figure 7.1A). This pore cysteine results in an enhanced sensitivity to extracellular applied sulfhydryl modifying agents (Satin et al., 1992; Backx et al., 1992; Heinemann et al., 1992) and is not present in other Na⁻ channel subtypes such as neuronal, sympathetic or skeletal muscle (Auld et al., 1988; Frelin et al., 1986; Rogart et al., 1989; Satin et al., 1992). Based on these molecular differences, we took advantage of the presence of this native pore cysteine in the cardiac channels to probe the spatial distance between the Na⁻ channel pore and the local anesthetic binding site using our ALD strategy.

241

Figure 7.1

A) Sequence alignment of the pore forming region of Domain I of different rat Na⁺ channel isoforms. The numbers denote amino acid position within the primary sequence. The unique cysteine residue in the heart isoform is shown within the box.

B) Structure of benzocaine and methanethiosulfonate-benzocaine (MTSBZ).

C) Schematic diagram of local anesthetic drug targeting to cardiac Na⁻ channels. The local anesthetic moiety has access to the local anesthetic binding site on the channel protein.

A

Domain I - Pore

rat heart ^{366}LFRLMTQD $\boxed{\text{C}}$ WERLYQ^{380}
rat skeletal muscle ^{393}LFRLMTQD Y WENLFQ^{407}
rat brain II ^{377}LFRLMTQD F WENLYQ^{391}
rat peripheral nerve ^{338}LFRLMTQD S WERLYQ^{362}

B

Benzocaine

MTSBZ

C

= local anesthetic agent

local anesthetic binding site
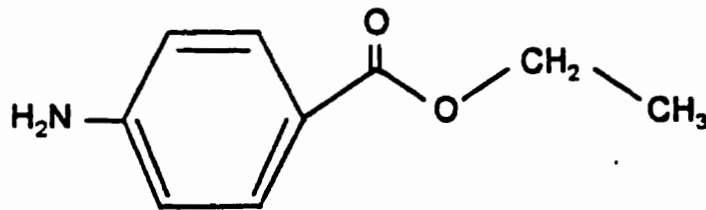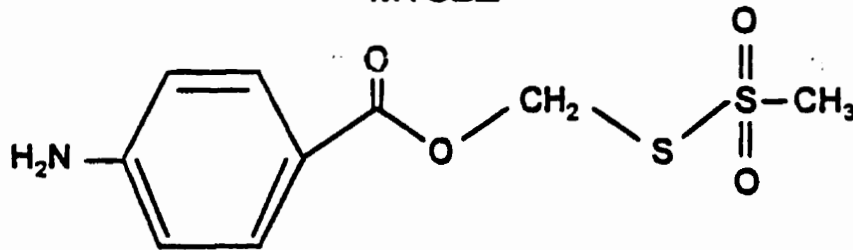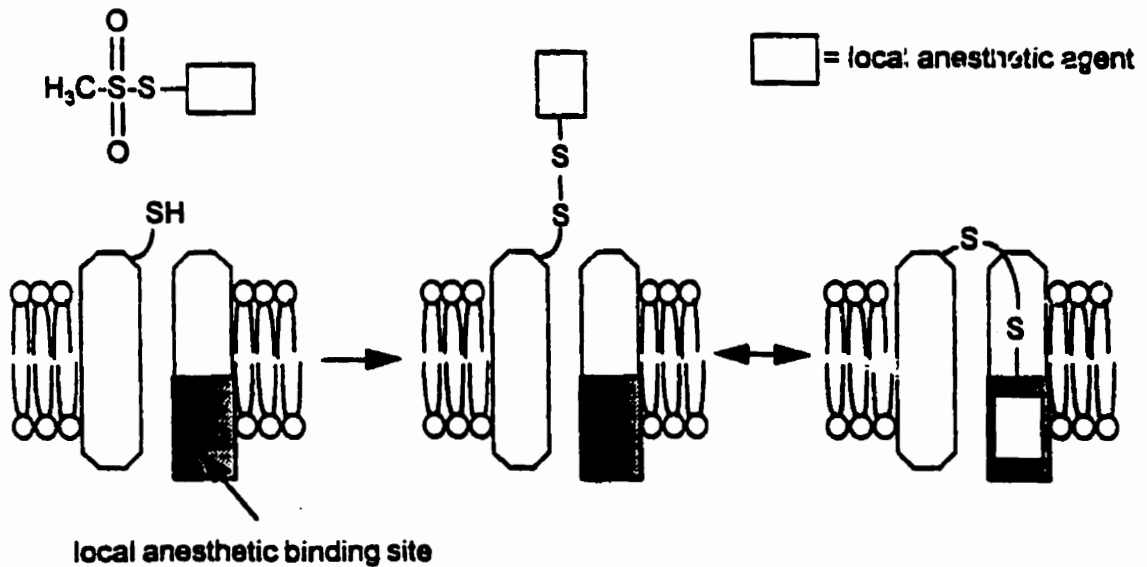
Specifically, we synthesized a novel local anesthetic agent by linking benzocaine to the sulfhydryl-reactive group, methanethiosulfonate via a hydrocarbon chain (methanethiosulfonate benzocaine, MTSBZ; Figure 7.1B). We used benzocaine since it is a prototypic hydrophobic class 1b agent with very rapid kinetics for channel binding (Butterworth and Strichartz, 1990; DeLuca et al., 1991; Grant, 1991; Hondeghem and Katzung, 1977) thus providing distinct effects on Na⁺ channel behaviour (Hille, 1992). We reason that MTSBZ will covalently react with the free sulfhydryl group within the human heart Na⁺ channel (hH1) pore thereby anchoring the local anesthetic to the pore and delivering the drug to the local anesthetic binding site (Figure 7.1). In fact, our results show that MTSBZ works as anticipated. By varying the linker length, we find that the optimal distance between the native pore cysteine (i.e. C373) and the local anesthetic binding site in hH1 channels is approximately 10Å.

Since MTSBZ binds irreversibly and specifically only to cardiac Na⁺ channels but not other subtypes lacking a reactive cysteine in the pore, our strategy further forms the basis for potentially developing a cardiac specific local anesthetic in addition to its application in biophysical studies. While this ALD paradigm is demonstrated here in the Na⁺ channel, it is of general utility and can be applied to any proteins and tissues.

7.3   Materials and Methods

7.3.1   Rat Venticular Myocyte Isolation and Patch-Clamp Recording

Rat ventricular cardiac myocytes were isolated as described previously (Wickenden et al, 1997). Briefly, male Sprague-Dawley rats (250-300 g) were heparnized (3000 U/kg) and anesthetized wit 150 mg/kg pentobarbital. Hearts were excised and retrogradely perfused for 5 min with a Krebs-Hensleit buffer consisting of (in mmol/L): 123 NaCl, 5.4 KCl, 1 CaCl₂, 1.2 MgSO₄, 1.2 NaH₂PO₄, 20 NaHCO₃, 5.6 glucose, gassed with a 95% O₂-5 % CO₂ mixture (pH 7.4) followed by a 5 min perfusion with calcium-free Krebs-Hensleit solution. Hearts were then perfused in with the

calcium-free solution containing collagenase (Type II, 0.6 mg/mL, Boehringer Mannheim) and protease (Type XIV, 0.05 mg/mL, Sigma) for 8 min. At the end of the digestion period, hearts were perfused for 5 min with an enzyme-free high K$^-$ solution (KB) consisting of (in mmol/L): 120 KCl, 1 MgCl$_2$, 0.5 K$_2$-EGTA, 10 glucose, 20 HEPES (pH to 7.4 with KOH). The hearts were dismounted, and the atria and aorta were removed. Ventricular tissue was cut into small pieces, and cells were mechanically isolated by trituration with a Pasteur pipette and filtering through nylon mesh. Cells were stored in KB solution until required. Only calcium-tolerant, rod-shaped, quiescent myocytes with clear cross striations were used for electrophysiological recordings.

Na$^-$ currents were recorded using the whole-cell patch-clamp configuration (Hamill et al, 1981) with an Axopatch 200A amplifier (Axon Instruments) (see 2.3 for details). Rat cardiac ventricular myocytes were placed in a 1 ml bath and perfused with extracellular solution with the following composition (in mmol/L): 135 tetramethylammonium chloride (TMA), 5 NaCl, 1 CaCl$_2$, 1 MgCl$_2$, 10 glucose, 10 HEPES (pH to 7.4 with TMA-OH). The intracellular solution consisted of (in mmol/L): 150 CsF, 10 EGTA, 10 HEPES (pH to 7.2 with CsOH).

7.3.2 *Experimental Protocols and Data Analysis*

Whole-cell Na$^-$ current-voltage relationships, steady-state inactivation and recovery from inactivation were recorded from oocytes or rat ventricular myocytes as described in previous chapters. Cells were exposed to methanethiosulfonate benzocaine (MTSBZ) or benzocaine (500 μM) for at least 10 minutes to allow for complete channel modification. Wash out of the drugs were performed for 5-10 minutes with recording solution. MTSBZ, benzocaine and MTSBN were dissolved in DMSO and diluted to the desired concentration. Lidocaine and MTSHE was dissolved in ND96. The final concentration of DMSO (0.01%) had no significant effect on any parameters measured. MTSBN and MTSHE were purchased from Toronto Research Chemicals Inc. MTSBZ and its analogues were a gift from Dr. David Dime (Toronto Research Chemicals).

.

Benzocaine and lidocaine were purchased from Sigma. Data were analyzed. mathematically fitted and statistically tested as described before.

7.4   *Results*

7.4.1   *A pore cysteine is required for specific interactions of MTSBZ*

We initially determined whether tethering benzocaine to the methanethiosulfonate group altered local anesthetic efficacy by comparing the effects of MTSBZ to benzocaine. Exposure of human heart (hH1) Na$^-$ channels expressed in *Xenopus* oocytes to 500 μM benzocaine resulted in a 43 $\pm$ 3 % (n = 5) reduction in peak current measured at -10 mV (Figure 7.2A). The effects on peak currents were completely reversed upon drug washout. MTSBZ (500 μM) elicited a similar 62 $\pm$ 8% (n = 7) reduction in peak hH1 Na$^-$ currents in comparison to benzocaine (Figure 7.2A). However, the reduction of peak current amplitude persisted after drug washout (50 $\pm$ 8%) suggesting that the channels were irreversibly modified by MTSBZ (Figure 7.2A). In contrast, application of MTSBZ (500 μM) to rat skeletal muscle Na$^-$ channels (rSkM1) lacking the pore cysteine, resulted in a completely reversible decrease in peak current magnitude (Figure 7.2A).

To establish whether MTSBZ interacted specifically with the cysteine pore residue in hH1 channels, we introduced an equivalent cysteine residue into the rSkM1 channel pore (Y401C) (Backx et al, 1992). Y401C channels resemble cardiac Na$^-$ channels in relation to block by tetrodotoxin and Cd^{2+}, and single channel conductance (Backx et al, 1992) but have similar inactivation properties as wild-type rSkM1 channels (see below). A 10 min exposure of Y401C channels to MTSBZ followed by a 5 min washout resulted in an irreversible reduction current amplitude at -10 mV, as observed with hH1 channels (Figure 7.2A). Longer washout periods did not restore peak current amplitude to predrug values. These data are consistent with a specific interaction of MTSBZ with a cysteine residue in the extracellular face of the pore, unlike the nonspecific modification normally observed with local anesthetics like benzocaine.

246

Figure 7.2

Effects of benzocaine on hH1 and MTSBZ on hH1. rSkM1 and Y401C channels.

A) Whole-cell Na⁻ currents recorded from *Xenopus* oocytes in the before. during and after washout of 500 μmol/L benzocaine (far left panel) or MTSBZ. Currents were elicited by a 50 ms depolarizing step pulse to -10 mV from a holding potential of -100 mV. Currents were normalized to peak currents in the absence of drug. Only the first 15 ms are shown. The dashed line indicates currents recorded after drug washout.

B) Voltage-dependence of steady-state inactivation in the presence and following washout of benzocaine and MTSBZ. Data were fit with a Boltzmann function.

C) Recovery from inactivation of hH1. rSkM1 and Y401C. Recovery was fit with a biexponential function (see Materials and Methods). Data represent the mean ● SEM of 4-8 experiments.

247

A

hH1   Y401C   rSkM1   Y401C

5 ms

B

- ■ Control
- ○ Benzocaine (500 μmol/L)
- △ Washout

- ■ Control
- ○ MTS-LO-BZ (500 μmol/L)
- △ Washout

Normalized Current

Conditioning Potential (mV)

C

Fraction Recovered

Recovery Interval (ms)
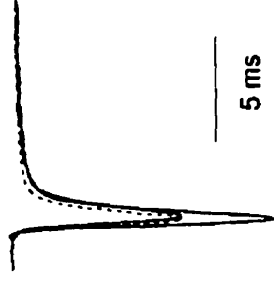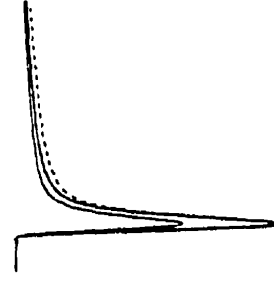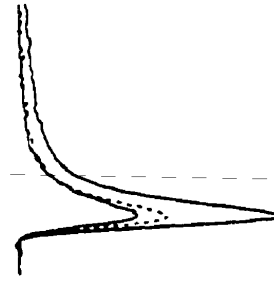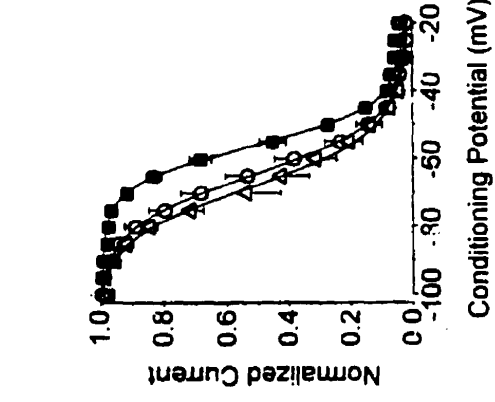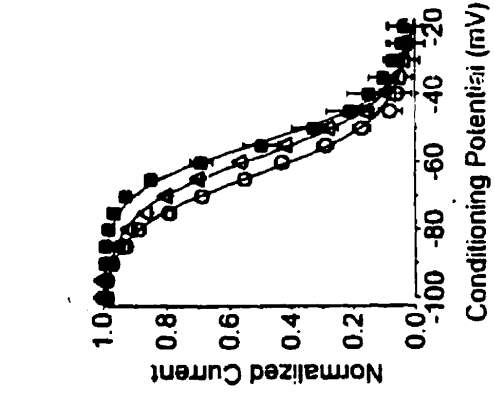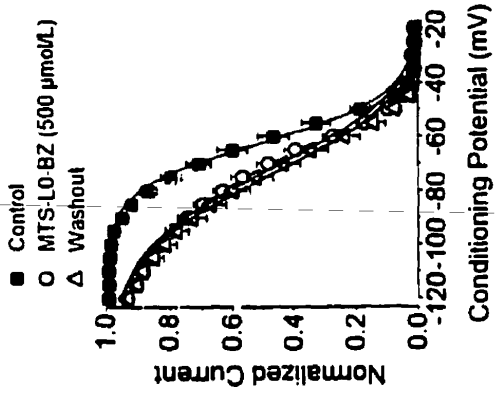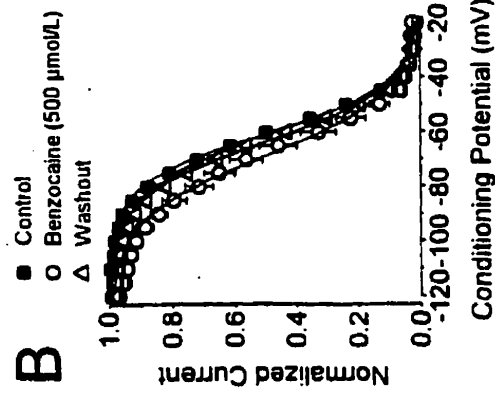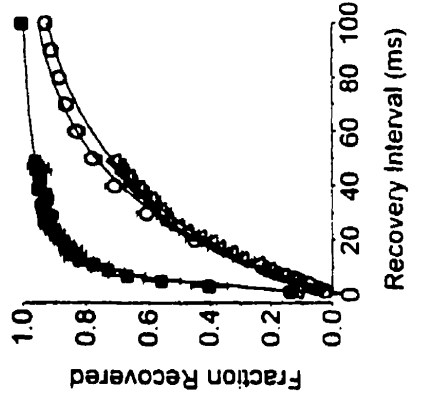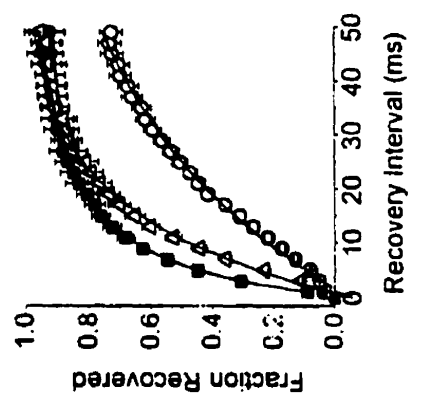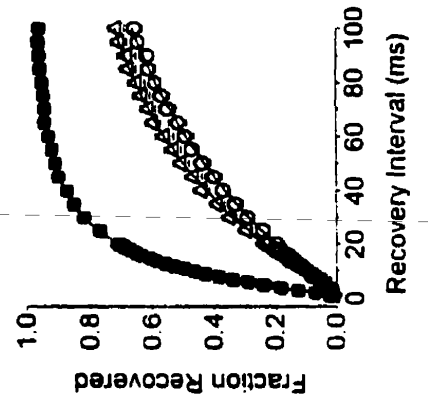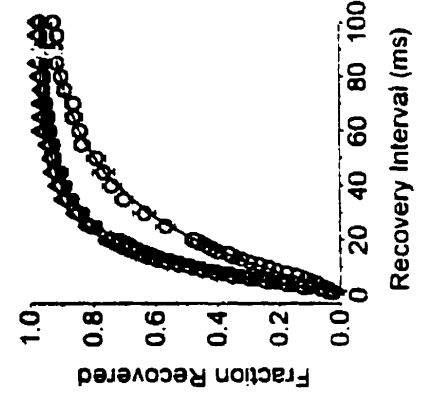
To further verify that MTSBZ reacted specifically with the cysteine pore residue in both hH1 and Y401C, we examined the effects of this drug on the Cd^{2+} sensitivity of the channels. Modification of hH1 and Y401C channels with the methanethiosulfonate compounds like MTSEA or MTSES is known to reduce sensitivity to block by Cd^{2+} and Zn^{2+} which react with high affinity with reduced free sulfhydryl groups (Kirsch et al. 1994; Chiamvimonvat et al., 1996; Tsushima et al., 1997). Modification with MTSBZ reduced the sensitivity of the channels to Cd^{2+} block (IC_{50}) from 50 ± 8 μM to 1552 ± 245 μM ($n = 3$; $P < 0.05$) and for Y401C channels from 16 ± 3 μM to 1081 ± 322 μM ($n = 5$; $P < 0.01$) (Figure 7.3C). The Cd^{2+} sensitivity of the MTSBZ modified Y401C channels is similar to that observed for the wild-type rSkM1 channel (Tsushima et al. 1997). The effects of MTSBZ were reversible upon exposure to the sulfhydryl reducing agent, dithiothreitol (DTT, 10 mM). For example, DTT application restored peak current amplitude (Figure 7.3A), the rate of recovery from inactivation (Figure 7.3B) and Cd^{2+} sensitivity of Y401C channels previously modified with MTSBZ (Figure 7.3C).

7.4.2 Effects of MTSBZ on Na^+ Channel Inactivation

Local anesthetic agents alter the inactivation properties of Na^+ channels leading to leftward shifts in the voltage-dependence of steady-state inactivation and a slowing in the rate of recovery from inactivation (Hille, 1977; Bean et al., 1983; Sanchez-Chapula et al. 1983; Nuss et al., 1995) These effects stem from high affinity binding of these compounds to the inactivated state of Na^+ channels resulting in a stabilization of the inactivated state (Hille, 1977; Bean et al, 1983). The receptor site for local anesthetics is accessible from the cytoplasmic side of the channel (Hille, 1977) and has been recently localized to the sixth transmembrane spanning region in domain IV of the Na^+ channel α subunit (Sanchez-Chapula et al, 1983).

We determined whether benzocaine anchored to an external pore residue on Na^+ channel can access to the local anesthetic binding site and thereby lead to an alteration

Figure 7.3

Reversibility of MTSBZ modification of Y401C channels.

A) Whole-cell Na⁻ currents of Y401C channels expressed in *Xenopus* oocytes. Currents were elicited as described in Figure 2. Channels were modified with 500 μM MTSBZ for at least 10 min followed by drug washout. The channels were then exposed to 10 mM DTT.

B) Recovery from inactivation of MTSBZ-modified channels and after DTT exposure. Data were fit to a biexponential function as described in Figure 7.2.

C) Cd^{2+} sensitivity of Y401C channels before and after MTSBZ modification and following sulfhydryl reduction of MTSBZ-modified channels by DTT. Data were fit with the Hill equation, $1/(1 + [Cd^{2+}]/IC_{50})$. Data represent the mean ● SEM of 3-5 experiments.

A

2 ms

Control

MTSBZ

DTT

B

Fraction of Recovery

1.0
0.8
0.6
0.4
0.2
0.0

0   10   20   30   40   50

Recovery Interval (ms)

■ Control
○ MTSBZ (500 µM)
△ DTT (10 mM)

C

I/I_o at -10 mV

1.0
0.8
0.6
0.4
0.2
0.0

0.1   1   10   100   1000   10000

[Cd^{2+}] (µM)
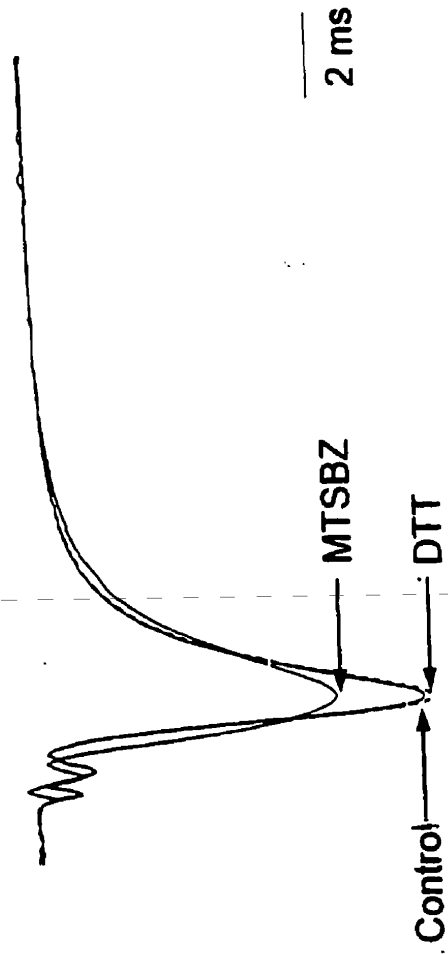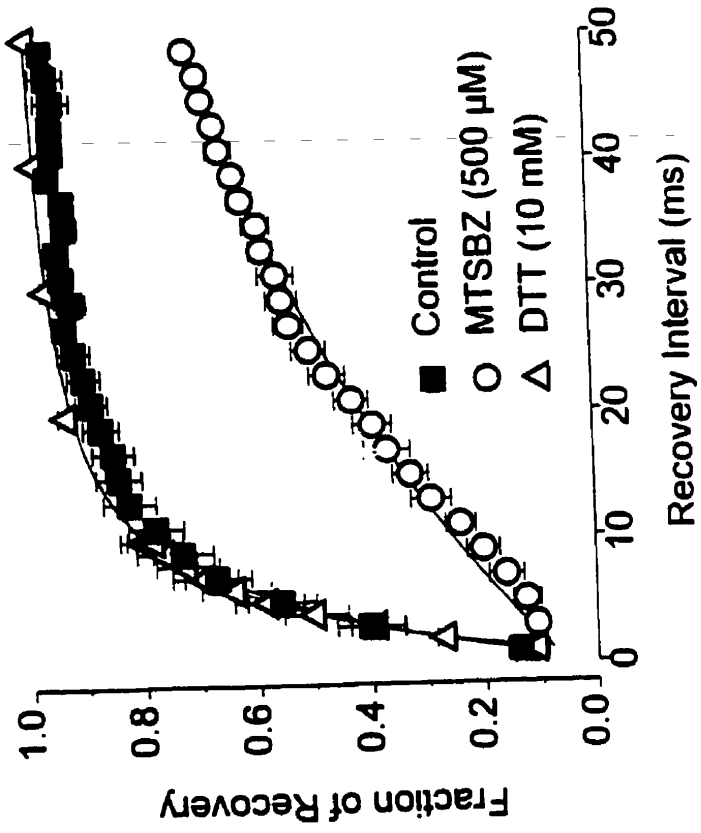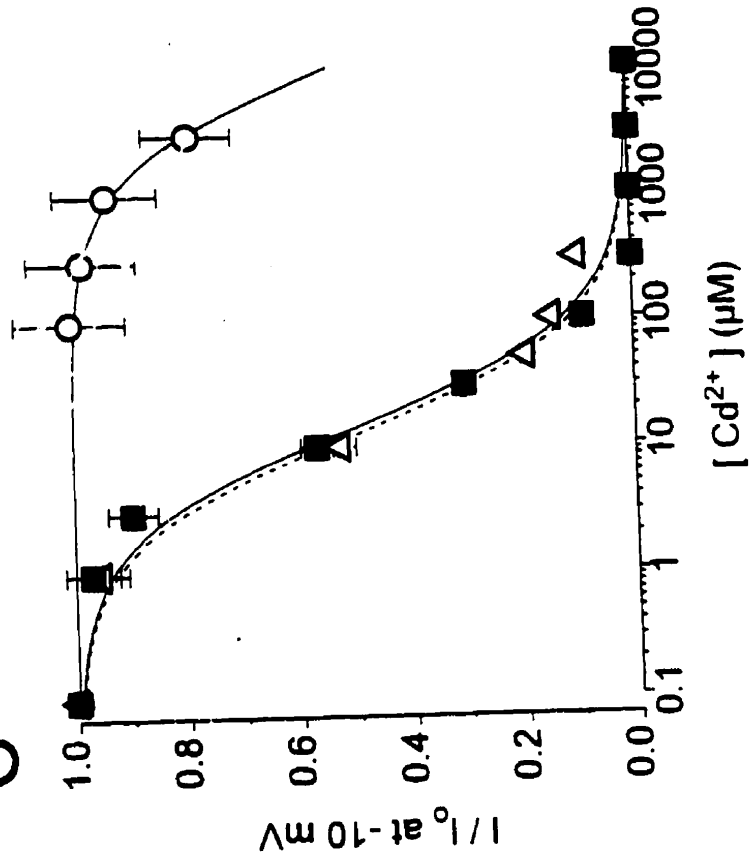
of channel inactivation as observed with other local anesthetics. The effects of MTSBZ on steady-state inactivation of hH1 channels were studied using a standard two-pulse protocol as summarized in Figure 7.2B. Channels were depolarized to various conditioning potentials for 50 ms from -100 to -20 mV from a holding potential of -100 mV followed by a 50 ms test pulse to -10 mV. The 50 ms conditioning pulse was sufficient to allow for equilibrium binding of benzocaine due to the fast kinetics of benzocaine binding to the channels (Hille, 1977; Wang et al., 1998).

MTSBZ shifted the steady-state inactivation curve of hH1 channels from -60.2 ± 1.7 mV to -71.7 ± 2.8 mV (n = 7; P < 0.01) which was not reversed upon washout (-75.7 ± 3.0 mV, n = 7; P < 0.01) (Figure 7.2B, Table 7.1). A similar shift of the steady-state inactivation curve was observed with 500 μM benzocaine (-61.4 ± 0.7 mV control vs. -74.2 ● 0.3 mV benzocaine; P < 0.01), however this was reversible upon washout of the agent (-65.4 ± 1.4 mV; n = 5) (Figure 7.2E). These results establish that the MTSBZ can stabilize the inactivated state of hH1 Na⁻ channels in a manner similar to that observed with benzocaine (Hille, 1977; Wang et al., 1998).

MTSBZ also produced leftward shifts of the steady-state inactivation curves in rSkM1 channels from -54.7 ± 0.7 mV to -61.2 ± 2.0 mV (n = 6; P < 0.05) which could be largely restored to predrug values upon washout of MTSBZ (-58.4 ± 1.0 mV) (Figure 7.2B). However, in Y401C mutant channels, the shift in the steady-state inactivation curve was irreversible upon washout of MTSBZ (-55.8 ± 1.2 mV control; -64.7 ± 3.8 mV MTSBZ; -67.3 ± 2.6 mV wash, n = 6).

To further examine the effects of MTSBZ on channel inactivation, we measured the recovery from inactivation which gives another measure of drug binding to Na⁻ channels by providing an index of the rate of exit from the inactivated state. The recovery from inactivation was measured using a standard two-pulse protocol. Identical 50 ms step depolarizations to -10 mV from a holding potential of -100 mV were separated by a varying recovery interval at -100 mV (Figure 7.2C). We initially

examined the effects of benzocaine on hH1 channels. The recovery from inactivation for hH1 channels was best fit with a biexponential function with fast (τ_{fast}) and slow (τ_{slow}) time constants of 15.9 ± 2.0 ms (86 ± 4 %) and 64 ± 16 ms (15 ± 5%) (n = 5), respectively (Figure 7.2C). Benzocaine (500 µM) significantly prolonged the fast (29.2 ± 3.9 ms, n = 5; $P < 0.05$) but not the slow time constant (104 ± 41 ms) for the recovery from inactivation or the fraction of channels recovering at the faster rate (95 ± 2%). The rate of recovery returned to control values upon drug washout (τ_{fast} 18.1 ± 1.9 ms, 89 ± 4%, n = 5). Similarly, MTSBZ significantly slowed the fast rate of recovery from inactivation (τ_{fast} 12.8 ± 1.1 ms to 51.9 ± 3.5 ms, n = 7; $P < 0.01$), but did not significantly alter the proportion of channels recovering at the fast time constant (88 ± 4 % control vs. 71 ± 6 % MTSBZ) or change τ_{slow} (120 ± 42 ms control, 195 ± 20 ms; n = 7) following modification and wash out (Figure 7.2C, Table 7.1). This data are also consistent with a stabilization of the inactivation state by MTSBZ anchored to the channels.

MTSBZ slowed the fast rate of recovery from inactivation of rSkM1 channels from 5.3 ± 1.0 ms to 18.3 ± 3.9 ms (n = 4; $P < 0.05$) which was reversible upon washout of the agent (8.2 ± 1.7 ms) (Figure 7.2C). However, in Y401C channels, MTSBZ slowed the fast recovery rate from 4.3 ± 0.9 ms to 26.5 ± 3.3 ms (n = 4; $P < 0.01$) which remained significantly prolonged (22.1 ± 3.5 ms, $P < 0.01$) after washout (Figure 7.2C).

7.4.3   Effect of MTSBN and MTSHE on hH1 Na⁺ Channels

Sulfhydryl modification of hH1 Na⁺ channels with the methanethiosulfonate derivatives, MTSEA, MTSET and MTSES, reduce peak current amplitude (Chiamvimonvat et al, 1996; Tsushima et al., 1997). However, the effects of sulfhydryl modification on inactivation properties of the channel have not previously been studied. To determine whether the effects of MTSBZ on Na⁺ channel inactivation results simply from nonspecific effects of the pore cysteine modification, effects of benzyl methanethiosulfonate (MTSBN) and 2-hydroxyethyl methanethiosulfonate (MTSHE) on hH1 channels were examined. MTSBN is similar to MTSBZ in that an aromatic group is

253

linked to the methanethiosulfonate moiety, whereas MTSHE mimics MTSBZ without the aminobenzyl group. Modification of hH1 channels with 500 μM MTSBN resulted in a 62 ± 3% (n = 4) reduction in peak current after modification and wash out of the drug (Figure 7.4A, Table 7.1). This was similar to the decrease in peak current observed with MTSBZ modification (50 ± 8%). As with MTSBZ, the reduction in current by MTSBN was irreversible. Furthermore, the voltage dependence of the steady-state inactivation relationship shifted leftward, the slope factor increased, and the fast recovery rate was prolonged after MTSBN modification (Table 7.1) which were very similar to the effects observed with MTSBZ. In contrast, MTSHE had no effect on any of the inactivation parameters measured and reduced peak currents to a lesser extent than either MTSBZ or MTSBN.

7.4.4 Effect of MTSBZ on the Local Anesthetic Binding Site

The results above suggest that attachment of the methanethiosulfonate moiety to benzocaine did not alter drug efficacy or the interaction of the benzocaine group with the inactivated state of the Na⁺ channel. Access to the local anesthetic binding site on the cytoplasmic face of the α subunit of the Na⁻ channel occurs through hydrophobic and hydrophilic pathways (Hille, 1977). Our results strongly suggest that benzocaine can interact with the local anesthetic binding site while anchored to an external pore residue.

Another method for further establishing whether anchored MTSBZ interacts with the local anesthetic binding site involves examining if MTSBZ can compete with the binding of other local anesthetics (Schmidtmayer et al., 1980). Exposure of hH1 channels to lidocaine elicited two distinct time components for the recovery from inactivation (data not shown). The fast component ($\tau < 20$ ms) reflects normal gating channels whereas the slow component ($\tau > 300$ ms) is indicative of lidocaine binding to the inactivated state of the channel (Hille, 1977; Bean et al., 1983). Increasing lidocaine concentrations enhances the fraction of slowly recovering channels without altering the time constant (Hille, 1977; Bean et al., 1983). Plotting the fraction of the hH1 channels recovering at

254

Figure 7.4

Effect of MTSBN and MTSHE on hH1 channels. hH1 channels were modified with 500 μmol/L MTSBN (left panel) or MTSHE (right panel) followed by drug washout.

A) Whole-cell currents recorded as described in Figure 2. The dashed line indicates current after drug washout.

B) Steady-state inactivation and C) recovery from inactivation of hH1 channels modified with MTSBN or MTSHE. Data represent the mean ± SEM of 4 experiments.

A

MTSBN

CH_2-S-S-CH_3 with O=S=O

MTSHE

HO-CH_2-CH_2-S-S-CH_3 with O=S=O

1 µA

5 ms

0.5 µA

5 ms

B

■ Control
○ MTSBN (500 µmol/L)
△ Washout

Normalized Current

Conditioning Potential (mV)

■ Control
○ MTSHE (500 µmol/L)
△ Washout

Normalized Current

Conditioning Potential (mV)

C

Fraction Recovered

Recovery Interval (ms)

Fraction Recovered

Recovery Interval (ms)
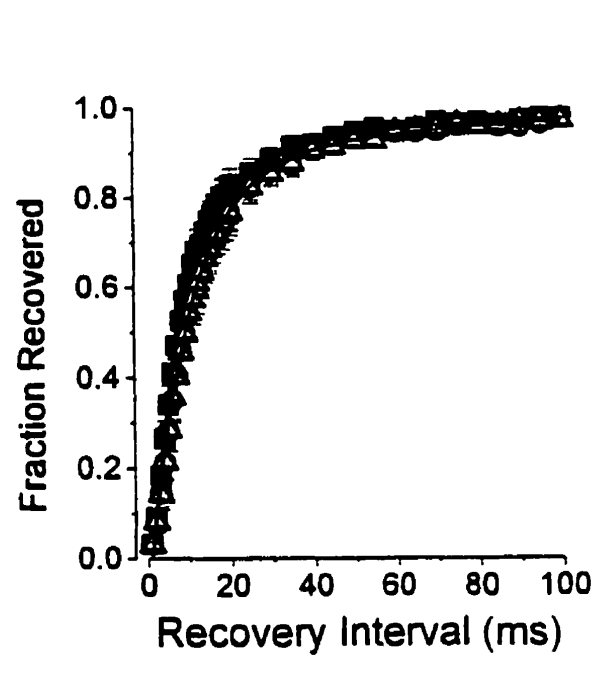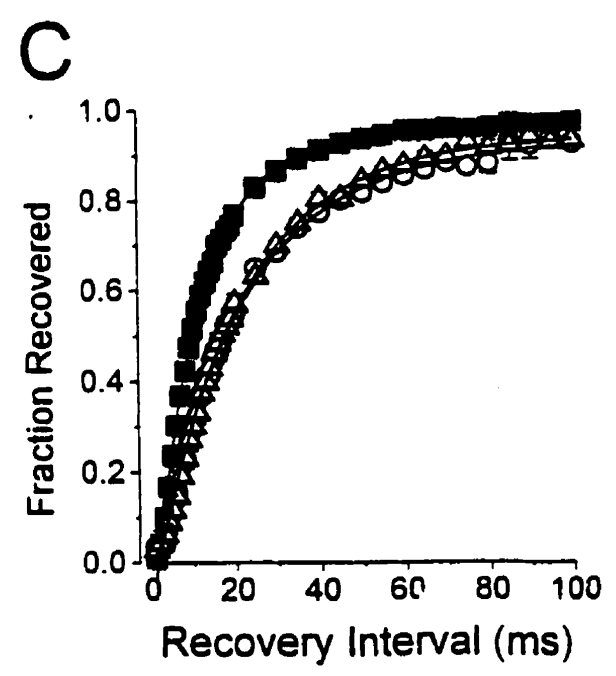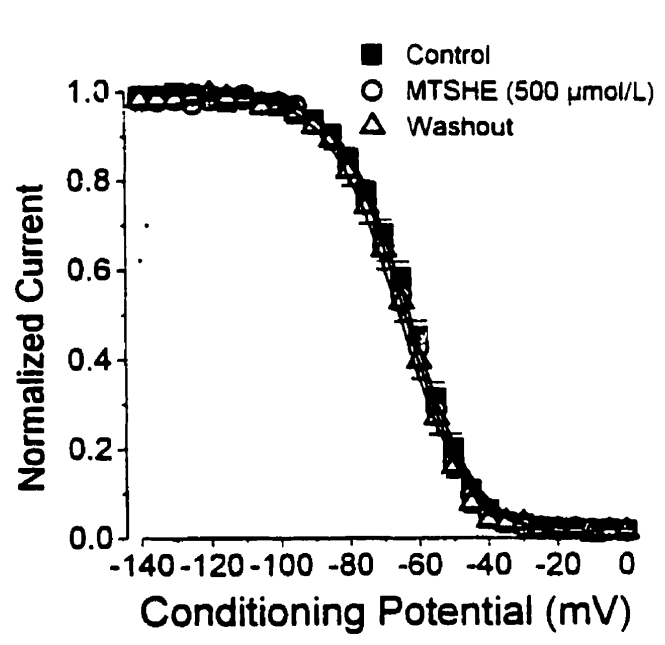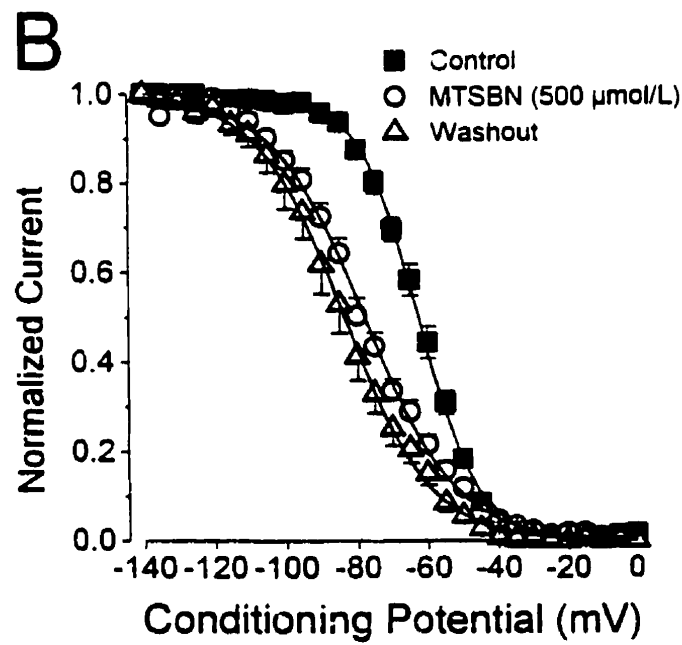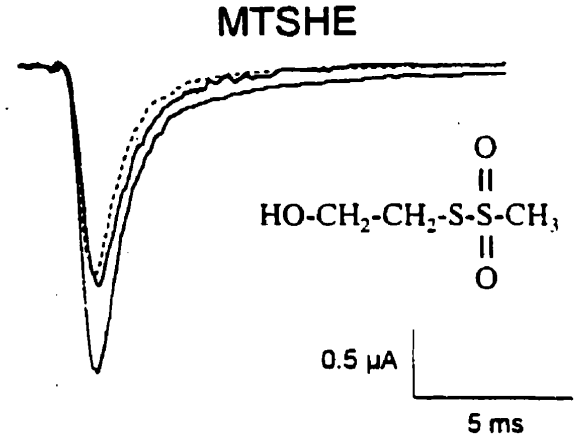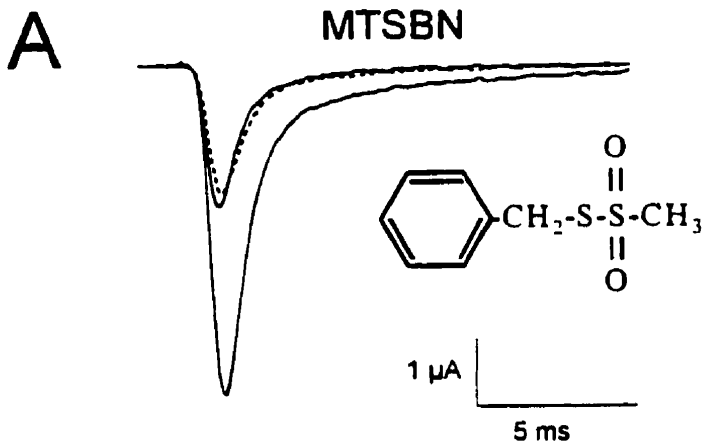
Table 7.1

Effect of MTSBZ, MTSBN and MTSHE on hH1 Channels

	% Peak Current at 0 mV	Steady-State Inactivation		Recovery from Inactivation	
		$V_{1/2}$ (mV)	k (mV)	τ_{fast} (ms) (% recovering at τ_{fast})	τ_{slow} (ms)
Control (n = 24)		-60.9 ± 1.0	8.1 ± 0.2	11.1 ± 0.6 (90 ± 1%)	205 ± 54
Benzocaine (n = 4)	50 ± 3 %	-68.8 ± 2.7**	11.3 ± 0.3**	28.2 ± 2.4** (91 ± 2%)	672 ± 157**
MTSBZ (n = 7)	50 ± 8 %	-75.7 ± 3.0**	13.3 ± 1.0**	67.4 ± 6.3** (71 ± 6%)	302 ± 43
MTSBN (n = 4)	63 ± 3 %	-83.5 ± 2.8**	11.6 ± 0.6**	20.8 ± 1.2** (93 ± 3%)	303 ± 39
MTSHE (n = 5)	27 ± 4 %	-64.8 ± 1.8	9.2 ± 0.4**	10.1 ± 1.1 (86 ± 5%)	85 ± 31

Values for benzocaine represent measurements after a 10 min exposure. hH1 channels were modified with 500 µmol/L for the methanethiosulfonate compound for 10 min followed by wash out of the drug. Data represent the mean ± SEM . ** denotes $P < 0.01$.

the slow time constant as a function of the lidocaine concentration allows estimation of the IC_{50} for lidocaine inhibition of Na⁺ current (Figure 7.5). We calculated an IC_{50} of 22 ± 3 µM (n = 5) which is very similar to those reported previously in native Na⁺ channels (9.7 µM)[4], and hH1 channels expressed in *Xenopus* oocytes (16 µM) (Nuss et al. 1995) or human embryonic kidney cells (21 µM) (Wang et al. 1996). As expected. the local anesthetic benzocaine (500 µM) shifted the affinity of lidocaine for the inactivated-state to 123 ± 13 µM (n = 4; $P < 0.01$) (Figure 7.5A) while irreversible modification of hH1 channels with MTSBZ resulted in a similar reduction in lidocaine sensitivity of the channel (167 ± 29 µM. n = 4; $P < 0.01$) (Figure 7.5B).

Recent mutagenesis studies have identified critical residues that influence local anesthetic binding to the rat brain Na⁺ channel (Ragsdale et al., 1994). These residues are located in the sixth transmembrane spanning region of domain IV of the Na⁺ channel α subunit. One residue in particular. F1764. when mutated to alanine resulted in near complete abolition of use-dependent and voltage-dependent block by local anesthetics (Ragsdale et al., 1994). Similarly, alanine substitution of the equivalent residue in rSkM1 (F1579A) has been shown to reduce local anesthetic sensitivity (Wang et al., 1998). Therefore. we examined the effects of MTSBZ on rSkM1 Na⁺ channels containing the F1579A mutation as well as the Y401C pore mutation to allow for covalent anchoring of the drug. In comparison to Y401C channels (Figure 7.2B), Y401C/F1579A mutant Na⁺ channels had a rightward shifted voltage midpoint of the steady-state inactivation relationship from -55.8 ± 1.2 mV (n = 5) to -44.8 ± 0.7 mV (n = 5) ($P < 0.01$) (Figure 7.6A) and an accelerated rate of recovery from inactivation from 4.30 ± 0.90 ms (n = 4) to 1.00 ± 0.04 ms (n = 5) ($P < 0.01$) (Figure 7.6A). Modification of Y401C/F1579A mutant Na⁺ channels by 500 µM MTSBZ had no significant effect on the voltage dependence of steady-state inactivation (Figure 7.6A). The voltage midpoint for the steady-state inactivation relationship was -43.3 ± 1.1 mV and -44.4 ● 1.4 mV (n = 5) during exposure and wash out of MTSBZ, respectively which was not significantly different from control values (-44.8 ± 0.7 mV). There was also a modest but significant slowing in the fast rate of recovery from inactivation from 1.00 ± 0.04 ms to 1.23 ± 0.06

Figure 7.5

Competition binding of lidocaine-benzocaine and lidocaine-MTSBZ. The relative amplitude of hH1 channels recovering from inactivation at the slow time constant as a function of lidocaine concentration in absence (■) and presence of A) 500 μmol/L benzocaine (O) or B) after irreversible modification by 500 μM MTSBZ (Δ). Data were fit with a Hill equation as described in Figure 3. Each point represents the mean ± SEM of 4-5 experiments.
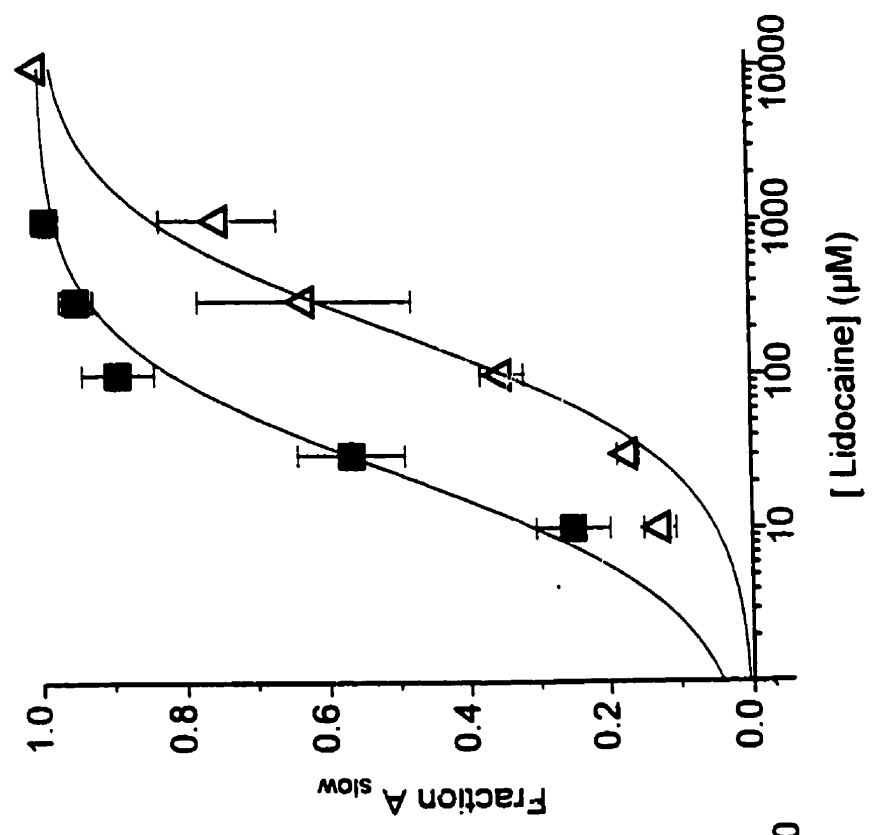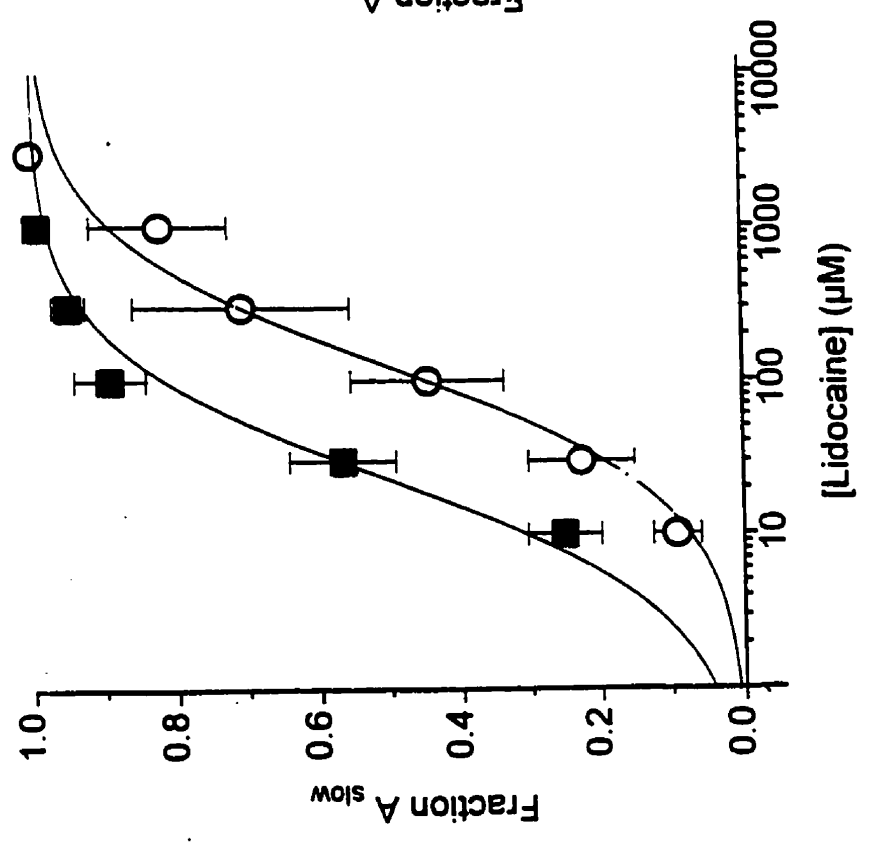
Figure 7.6

Effects of MTSBZ on Y401C/F1579A.

A) Current traces from Y401C/F1579A channels expressed in *Xenopus* oocytes. Current was elicited by a 50 ms step depolarization to -10 mV from a holding potential of -100 mV. Only the first 15 ms are shown. Note the non-inactivating pedestal current. Channels were modified with 500 μmol/L MTSBZ for 10 min followed by drug wash out.

B) Steady-state inactivation and C) recovery from inactivation of MTSBZ-modified Y401C/F1579A channels. Data were fit as described in Figure 2. Each point represents the mean ± SEM of 5 experiments.

A

B
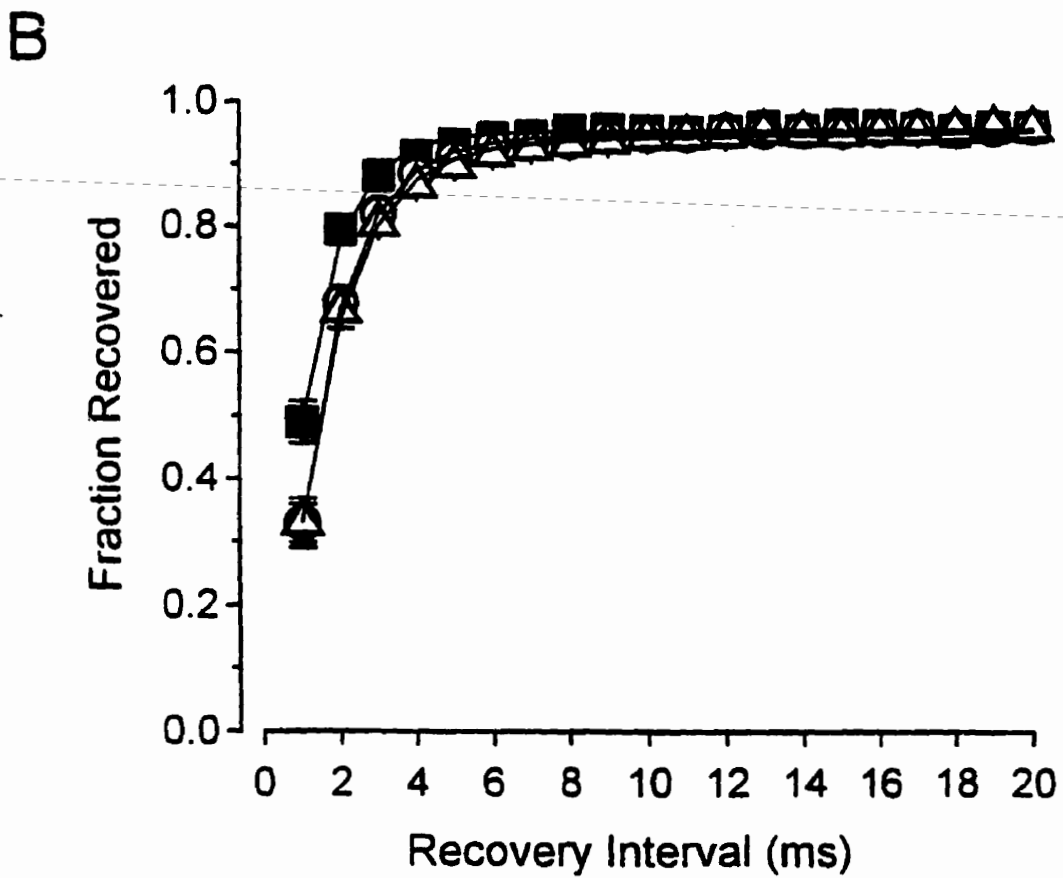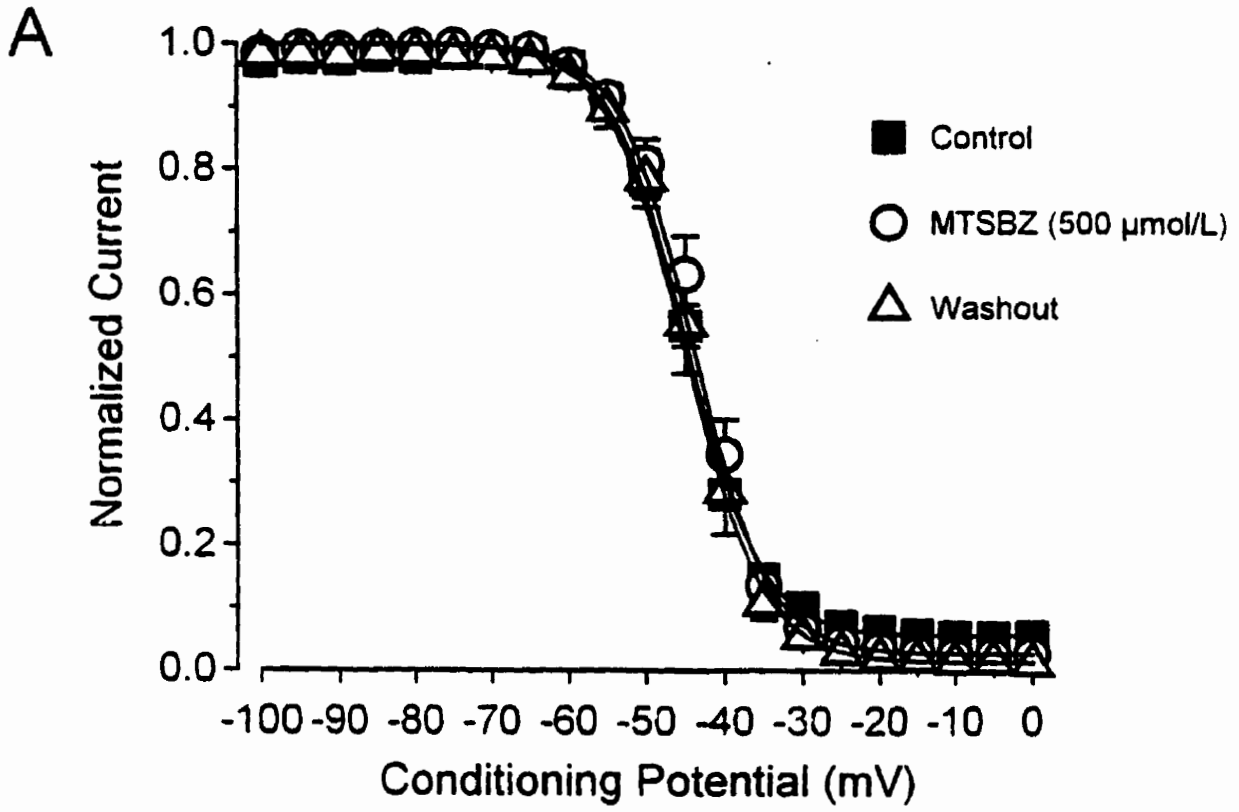
ms (n = 5; $P < 0.05$) with 500 μM MTSBZ present (Figure 7.6B) and 1.30 ± 0.06 ms ($P <$ 0.05) after drug washout. These data further suggest that MTSBZ modifies Na⁻ channel inactivation by binding to the local anesthetic receptor following anchoring to the external pore site.

7.4.5 Optimal Modification by Varying Linker Length

The results above establish that tethering benzocaine to the sulfhydryl reactive methanethiosulfonate group via an ethyl alkyl linker allowed irreversible modification of hH1 Na⁻ channels. Based on the structure of the local anesthetic MTSBZ, it is conceivable that varying the linker properties could influence drug action. Indeed, we hypothesized that excessively short linker length may prevent interaction of the anchored drug with the local anesthetic binding site thus reducing drug efficacy. Alternatively, very long linkers could increase diffusion times or produce steric effects that would also reduce drug efficacy. Moreover, the precise chemical properties of the linker may also have effects on drug modification and/or delivery. Therefore, altering the linker properties may affect the ability of the MTSBZ to modify Na⁻ channels. Initially, the linker length was increased with 3, 6 or 9 alkyl groups. However, increasing the alkyl linker length reduced the drug solubility and reduced the rate of anchoring to hH1 channels at low concentrations. For that reason, linkers were constructed using polyethylether units, $(-OCH_2CH_2-)_n$ (n = 1, 2, or 3) which markedly enhanced their solubility. Extending the single sulfide linker (-S-) in MTSBZ with an ethylether sulfide unit ($-O-CH_2-CH_2$)-S-increased the linker by 3 bond lengths which is referred to as MTSBZ-L3. Incorporation of 2 ethylether units ($-O-CH_2-CH_2-O-CH_2-CH_2$)-S- produced a linker 6 bond lengths longer and is referred to as MTSBZ-L6 and so forth. In contrast to the polyalkyl linker based drugs, the compounds with linkers created from polyethylether units were very water soluble and reacted readily with hH1 and Y401C but not rSkM1 Na⁻ channels. The application of polyethylether-based drugs with 3, 6 or 9 bond lengths did not enhance the reduction in peak hH1 Na⁻ current (Table 7.2) or produce a further leftward shift steady-state inactivation curves (Figure 7.7A, Table 7.2)

263

Figure 7.7

Effects of linker length of MTSBZ on hH1 Na⁺ channel modification.

A) Steady-state inactivation and B) recovery from inactivation were measured and fitted as described in Figure 2. Only the first 100 ms recovery period is shown in (B). Currents recovered fully within 1 sec. Fitted values are described in Table 2.

C) Use-dependence of the MTSBZ analogues on peak hH1 currents. Currents were elicited by 20 ms depolarizing step pulses to -10 mV from a holding potential of -100 mV at a stimulation frequency of 5 Hz. Oocytes were modified with the MTSBZ analogue for at least 10 min followed by drug wash out. Benzocaine data as shown in Figure 2 are plotted for comparison. Data represent the mean ± SEM of 24 experiments for control and 3-7 experiments for benzocaine and MTSBZ compounds.
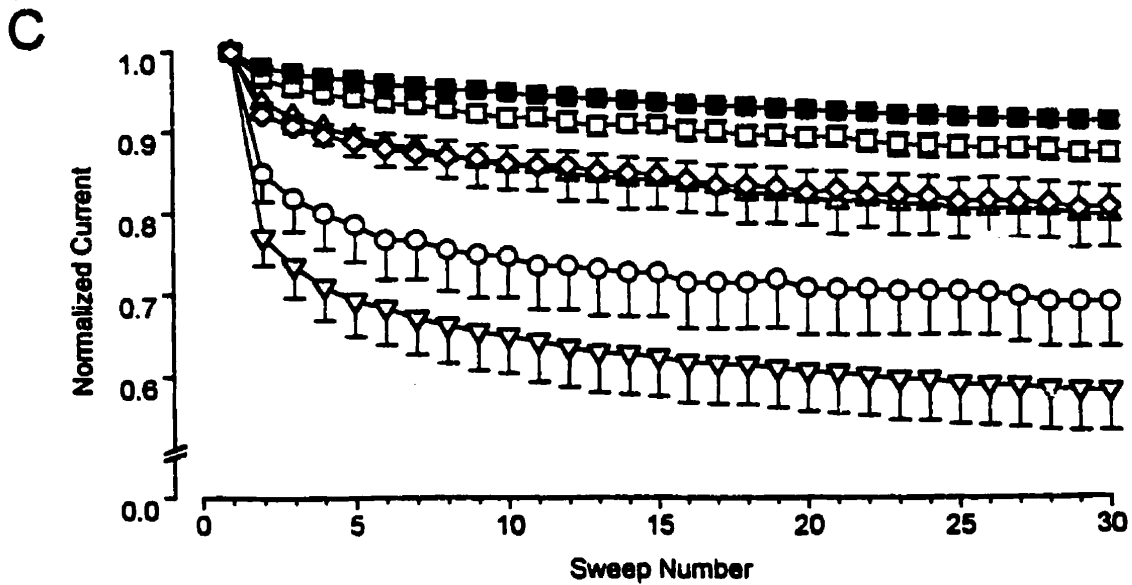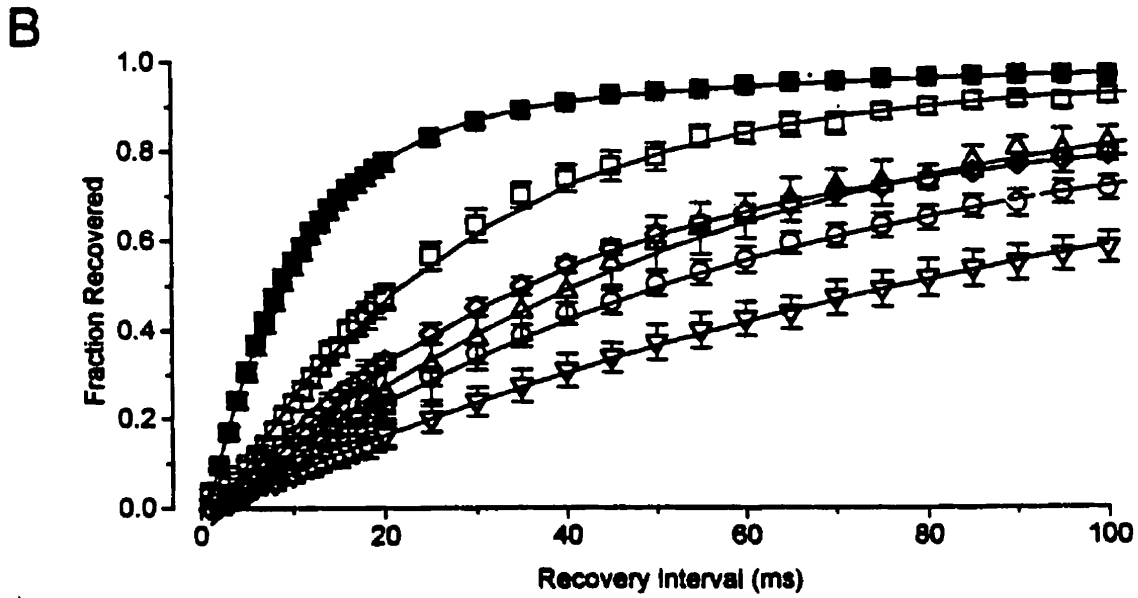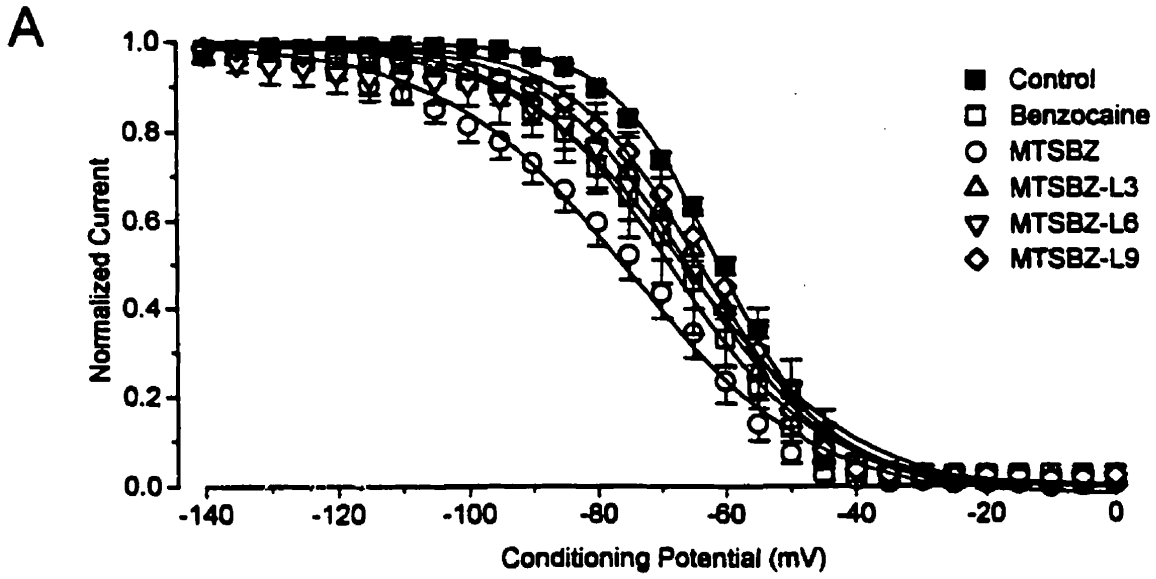
Table 7.2
Effects of Linker Length of MTSBZ on hH1

	Peak Current Reduction at 0 mV	Steady-State Inactivation		Recovery from Inactivation	
		$V_{\frac{1}{2}}$ (mV)	k (mV)	τ_{fast} (ms) (% recovering at τ_{fast})	τ_{slow} (ms)
Control (n=24)	-	-60.9 ± 1.0	8.1 ± 0.2	11.1 ± 0.6 (90 ± 1%)	205 ± 54
MTSBZ (n = 7)	49 ± 8%	-75.7 ± 3.0†	13.3 ± 1.0†	67.4 ± 6.3† (71 ± 6%)	195 ± 20
MTSBZ-L3 (n = 5)	41 ± 10%	-65.9 ± 1.2*	11.1 ± 1.0†	42.1 ± 3.9† (88 ± 2%)	598 ± 152†
MTSBZ-L6 (n = 5)	59 ± 3%	-68.9 ± 2.9†	15.9 ± 1.9†	92.7 ± 11.2† (86 ± 1%)	631 ± 52†
MTSBZ-L9 (n = 4)	50 ± 9%	-64.9 ± 3.9	8.9 ± 1.3	32.8 ± 3.5† (79 ± 4%)	261 ± 68

hH1 channels were modified with 500 μmol/L for the methanethiosulfonate compound for 10 min followed by wash out of the drug. Data represent the mean ± SEM. Symbols denote * $P <$ 0.05 and † $P <$ 0.01

when compared to MTSBZ (Figure 7.7A). Indeed. shifts in the steady-state inactivation curves with the extended linker compounds followed the sequence MTSBZ > MTSBZ-L6 = benzocaine > MTSBZ-L3 > MTSBZ-L9 (Figure 7.7A. Table 7.2).

A very different rank potency emerged when the effects of MTSBZ and the various linker lengths on recovery from inactivation were examined. MTSBZ-L6 prolonged the fast rate constant of recovery from inactivation more than MTSBZ or MTSBZ-L3 (Figure 7.7B. Table 7.2). Further lengthening of the linker to 9 bond lengths did not elicit any further modification. In fact. MTSBZ-L9 was less able to slow rate of inactivation compared to MTSBZ-L6 (32.8 ± 3.5 ms vs. 92.7 ± 11.2 ms. $P < 0.05$). The rank potency for slowing the rate of recovery from inactivation was MTSBZ-L6 > MTSBZ > MTSBZ-L3 = MTSBZ-L9 > benzocaine suggesting that a longer linker is more efficacious at modifying certain inactivation properties of hH1 channels.

In addition to the marked slowing in the recovery from inactivation with MTSBZ compounds. there were use-dependent reductions in peak current. hH1 channels depolarized to -10 mV for 20 ms (holding potential -100 mV) at a stimulation frequency of 5 Hz resulted in a 9 ± 1% reduction in peak current amplitude measured at the 30th pulse (n=18. Figure 7.7C). Application of 500 µmol/L benzocaine produced a modest but significant increase in use-dependence as compared to control ($13 ± 1$ %. $n = 4$. $P < 0.05$) (Figure 7.7C). All MTSBZ analogues tested resulted in a significant use-dependent reduction in peak current amplitude as compared to control (measured at the 30th pulse) as shown in Figure 7.7C. but only MTSBZ ($31 ± 5$%. $n = 3$) and MTSBZ-L6 ($42 ± 5$%. n = 5) resulted in a significantly greater use-dependence than benzocaine ($P < 0.01$). The same rank potency was observed for the use-dependent reduction in peak current with the MTSBZ compounds as compared to the sequence seen with the slowing in the recovery from inactivation.

7.4.6 Effect of MTSBZ on Native Cardiac Na⁺ Channels

To ensure that the isoform specificity of MTSBZ was applicable to native cardiac Na⁺ channels, we examined the effects of MTSBZ on native rat cardiac Na⁺ currents. Using the patch-clamp recordings, MTSBZ (500 μM) reduced peak rat cardiac Na⁺ current (Figure 7.8A) and shifted the voltage midpoint of the steady-state inactivation relationship leftward from -68.5 ± 1.3 mV to -92.8 ± 1.7 mV (n = 6; $P < 0.01$) (Figure 7.8B). As in expressed hH1 channels, this hyperpolarizing shift was maintained despite extensive washout of the drug (V½ -90.4 ± 5.0 mV, k 9.1 ± 1.1 mV) consistent with irreversible anchoring of MTSBZ to native cardiac Na⁺ channels. This notion is further supported by the irreversible slowing in the rate of recovery from inactivation at -120 mV (Figure 7.8C). MTSBZ prolonged the rate of recovery from 8.3 ± 1.5 ms to 46.1 ± 3.0 ms ($P < 0.01$) after drug modification and washout.

7.5 Discussion

I have demonstrated in this chapter a novel paradigm to map the spatial relationship between the Na⁺ channel pore and the local anesthetic binding site. Covalently anchoring benzocaine to an external pore residue using a linker with an approximate length of 3 Å appear to be sufficient to allow access to the local anesthetic site. While surprising, this result is not entirely unexpected since local anesthetic agents have access to their receptor binding site via hydrophobic pathways through the protein phase or hydrophilic pathways from the cytoplasmic face of the channel (Hille, 1977). Previous studies have suggested that the spatial distance between pore lining residues and the local anesthetic binding site are in close proximity or potentially adjacent to each other within the channel pore. Pore residues have an electrical distance (δ) of 0.2 - 0.3 (Backx et al., 1992) from the outside based on Cd²⁺ blocking studies while the local anesthetic blocking site has a δ of 0.7 (Gingrich et al., 1993) from the cytoplasmic side. Residues forming the putative selectivity filter of rSkM1 Na⁺ channels that are accessible by external sulfhydryl modifying agents can influence local anesthetic access and binding

Figure 7.8

Effect of MTSBZ on native rat cardiac Na⁺ channels.

A) Whole-cell currents of freshly isolated rat ventricular myocytes recorded at -10 mV before, during and after 500 μmol/L MTSBZ exposure. The holding potential was -120 mV.

B) Steady-state inactivation and recovery from inactivation (C) of rat cardiac Na⁺ channels in the absence, presence and wash out of MTSBZ. Data were fit as described in Figure 2. Each point represents the mean ± SEM of 4-5 experiments.

A

Washout ←→ MTSBZ

1 nA
2 ms

B

Control
MTSBZ (500 μM)
Washout

Normalized Current

Conditioning Potential (mV)

C

Fraction Recovered

Recovery Interval (ms)
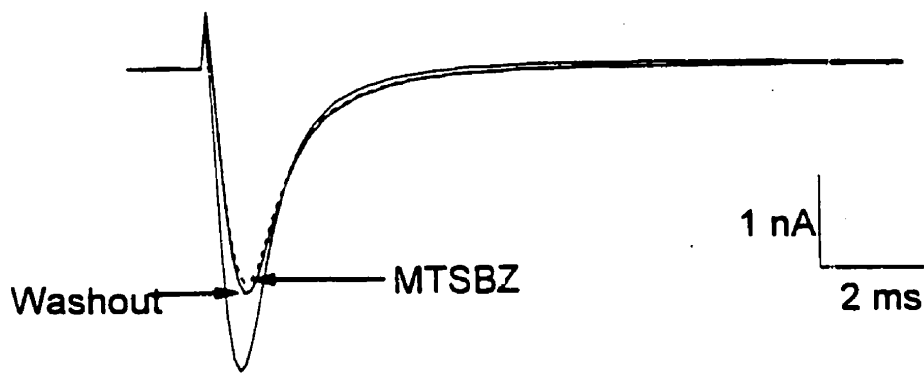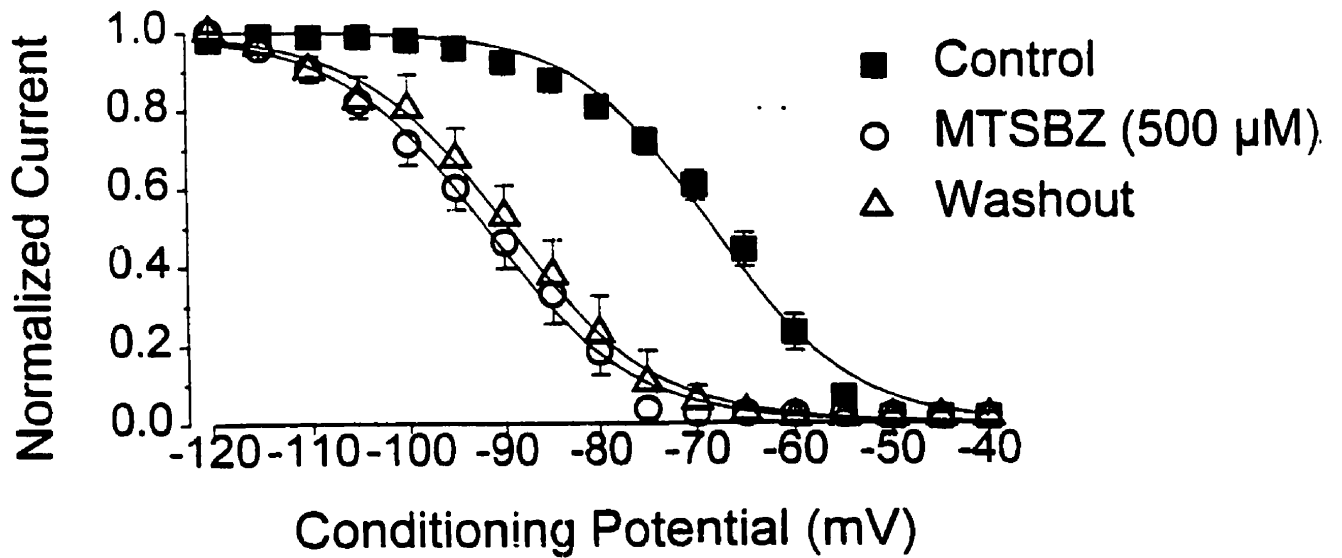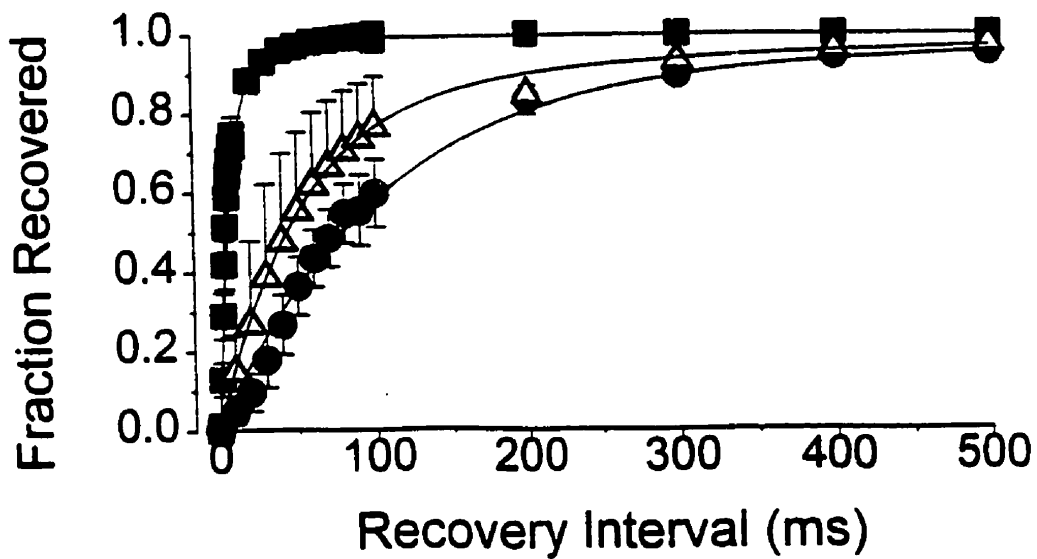
of the drug with its receptor (Sunami et al., 1997). We have observed that with a longer linker length of 6 Å. there is even a greater alteration in Na⁺ channel inactivation properties while a 9 Å linker reduces the effects of the drug on channel inactivation (data not shown). These results suggest that an optimal linker length exists for channel modification possibly by reducing mechanical strain required to allow energetically stable drug binding while longer linkers may result in slower diffusion times for drug interaction with the local anesthetic receptor.

The potency of the different MTSBZ and MTSBZ-L (3n) compounds depended on channel property studied. MTSBZ was the most effective at shifting the steady-state inactivation curve while MTSBZ-L6 slowed recovery from inactivation more and elicited greater use-dependent reductions in peak current than the other compounds tested. While steady-state inactivation conveys information on the properties of Na⁺ channel inactivation at equilibrium and gives a thermodynamic measure of the energetics of binding, recovery from inactivation reflect the kinetics of channel gating and drug binding. Therefore, it is not too surprising that the MTSBZ compounds can have different potencies depending on the assay used. The larger alterations observed with MTSBZ-L6 on the rates in recovery from inactivation and use-dependence may possibly be due to easier access of the benzocaine moiety to the local anesthetic binding site. This enhanced accessibility may be a result of less mechanical strain on the channel required to allow energetically stable drug binding or that the chemical nature of the shorter linker of MTSBZ-L3 may reduce access of the benzocaine moiety to its binding site. Longer linkers may result in slower diffusion times for drug interaction with the local anesthetic receptor. Indeed, extending the linker length from ~ 10 Å (MTSBZ-L6) to ~14 Å (MTSBZ-L9) attenuated the efficacy of the drug on channel inactivation. The greater modification of MTSBZ-L6 may be also related to the fact that the 6 bond length linker is in close proximity to the spatial distance between the pore anchor site and the local anesthetic binding region suggesting that the two sites are approximately 10 A apart. Alternatively, the interaction of the linker with the channel may be responsible for some of the differences observed between the different linker length drugs. However,

271

compounds comprised of the methanethiosulfonate attached to the polyethylether linkers without a local anesthetic agent did not produce notable changes on Na⁻ channel function (data not shown). Therefore. it appears that these compounds may also be used to determine the "distance" between residues and the local anesthetic binding site. We are currently investigating this possibility.

Remarkably. tethering benzocaine to the methanethiosulfonate group produced effects very similar to the alterations observed with 500μM benzocaine. One property that was changed however was the slope factors of the steady-state inactivation curves. Structure-function studies on local anesthetics have revealed chemical requirements for drug activity (Ehring et al.. 1988; Zamponi and French. 1994). Small changes in drug structure can influence state-dependent binding or potency (Ehring et al.. 1988: Zamponi and French. 1994). Anchoring benzocaine to the channel via a disulfide linkage did not prevent drug binding suggesting no significant alteration in drug interaction with the channel.

The effects of covalent sulfhydryl modification on channel inactivation was not the result of drug interaction with another region of the channel other than the local anesthetic binding site as can be observed in some circumstances (Yang et al.. 1995, 1996). Sulfhydryl modification of the channel MTSHE had no effect on inactivation. The observations that MTSBN can mimic the effects of MTSBZ are most likely due to the chemical interaction of the benzyl group with the local anesthetic binding site. Benzene (Elliott et al., 1987) and phenol (Zamponi and French. 1993) convey similar effects on Na⁻ channel function as lidocaine or benzocaine suggesting that the aromatic moiety of local anesthetic agents is important for drug efficacy. Competition experiment between lidocaine-MTSBZ or lidocaine-benzocaine demonstrated that both MTSBZ and benzocaine were equally effective in competing with lidocaine for its binding site. Similar studies have demonstrated that lidocaine and benzocaine compete for the same receptor site on the channel (Hille. 1977: Schmidtmayer et al, 1980). Mutating a residue forming the putative local anesthetic receptor site (F1579A) resulted in a near complete

272

loss of MTSBZ effect on Na⁻ channel inactivation. This residue has been shown to reduce both tonic and phasic block by etidocaine and benzocaine on rat brain (Ragsdale et al., 1994) and skeletal muscle (Wang et al., 1998) Na⁻ channels leading to the suggestion that this residue forms an important part of the local anesthetic receptor. These data support the notion that MTSBZ interacts with local anesthetic binding site thereby leading to an alteration in channel inactivation as observed with benzocaine.

Collectively, MTSBZ irreversibly modifies both native and expressed cardiac Na⁻ channels but not skeletal muscle Na⁻ channels. The effects of anchored MTSBZ are largely indistinguishable from benzocaine alone suggesting that covalent tethering of benzocaine to methanethiosulfonate groups or to the channel protein allows interaction of the drug with the local anesthetic binding site. These effects of anchored MTSBZ, however, did not appear to involve nonspecific interactions of the drug with the channel. On this basis, we have created a local anesthetic agent which is heart-specific. Many treatments of ventricular tachycardia and fibrillation (Kuck et al., 1995) such as the use of class 1b antiarrhythmic agents (e.g. lidocaine, tocainide, mexilitine) are not warranted because of potential toxicity unrelated to the heart arising from the structural similarities between Na⁻ channels isoforms found in different tissues (Woosley et al., 1982). Specific targeting therapies are therefore highly desirable especially given local anesthetics inhibit Na⁻ channels in a variety of tissues leading to potentially serious side effects when used clinically.

The novel paradigm presented here can be extended to other agents or tissues to provide a novel therapeutic approach for drug delivery. One obvious limitation to our approach is the use of covalent disulfide anchors. Although the compounds investigated in this study were specific for the cardiac Na⁻ channel isoform, the methanethiosulfonate group may prove to be of limited usefulness as tissue-specific drugs due to reactions with other unidentified free sulfhydryl groups *in vivo*. The extracellular covalent modification of Na⁻ channels via the disulfide link may also produce long-lived complexes. However, it is important to point out that the anchor needs not be covalent. Our strategy simply

requires the anchor to specifically bind to a unique epitope on proteins which will promote selective binding. Therefore. this paradigm may prove to be of general utility in selectively targeting drugs to a single member of a homologous protein family. as shown in this study for MTS-based local anesthetics. Therefore. in principle tissue-specific drug delivery could be achieved provided a selected protein is uniquely expressed in a desired tissue.

7.6   *Acknowledgements*

CHAPTER 8

SUMMARY & FUTURE DIRECTIONS

8.1 *Summary*

8.1.1 *Molecular arrangements of P-loop residues*

P-loops form part of the Na^+ channel pore and are critical for ion permeation, but their precise molecular configuration is unknown. Current concepts of the Na^+ channel pore have assumed a static rigid structure, which allow certain properties to be explained using mathematical theories. Understanding the molecular basis of ion permeation and the structure of the Na^+ channel pore requires identification of amino acids that form the ion-selective pore. We employed single cysteine mutagenesis (i.e. Scanning Cysteine Accessibility Method) to probe for residues that line the extracellular phase of the Na^+ channel pore. The accessibility data (Chapter 3), as assessed by enhanced sensitivity to Cd^{2+} block and MTS modification of single cysteine mutant channels, illustrate that the side chains of as many as four consecutive P-loop residues in a row are facing the aqueous phase of the pore. Differences in affinity of Cd^{2+} binding for single cysteine mutants of sequence-aligned residues in the four different domains further suggest that the pore is asymmetrically arranged. This suggestion is consistent with single channel recordings which showed different electrical distances for Cd^{2+} binding for these putatively aligned residues (Chiamvimonvat et al., 1996). Overall, these single mutant data are in favor of random coil structure of the P-loops and are inconceivable of periodic structures such as α-helices and β-strands. However this conclusion is valid only when we assume 1) the pore is static in nature, 2) cysteine mutagenesis did not significantly alter channel structure, and that 3) application of such biophysical probes as Cd^{2+} and MTS agents did not result in trapping of a subset of channel states which may not be typical representatives of the real dominant states.

After identifying residues that putatively line the pore, we then probed the spatial

275

proximity of these residues by simultaneously substituting pairs of P-loop residues in distinct domains to cysteine. Our strategy allows identification of pairs of residues that are in close proximity to each other. We showed that there is extensive cross-talk between multiple P-loop residues especially within domain IV. One possible explanation for this phenomenon is that the Na⁺ channel pore is flexible on the time-scale of Cd^{2+} binding and sulfhydryl modification. Apparently, domain IV is the most flexible domain because of the exceptional ability of its residues to cross-talk with others. Interestingly, cross-linked double-mutant channels, whose pore motion was expected to be more restricted, became more selective for Na⁺ ion permeation following reduction of their disulfide bonds as indicated by rightward shifts of their reversal potentials in the presence of the reducing agent DTT. In addition, DTT application generally increased whole-cell peak currents of cross-linked double mutants by 2- to 10-fold indicating these channels are less capable of conducting current in the oxidized, cross-linked states versus the reduced state. These observations suggest a possible correlation between ion translocation and pore motion. Overall, our conclusion that the Na⁺ channel pore is flexible impacts on the traditional view of ion channel pores and provides easy explanations to many channel properties such as multi-ion behaviour that the current static model cannot accommodate.

8.1.2 *Na⁺ channel selectivity filter and its relations to pore flexibility*

To explore the role of pore-lining residues in Na⁺ channel ionic selectivity and to test if correlation exists between channel functions and pore motion, we examined for changes in the selectivity sequence of single cysteine mutant channels by measuring their ionic current ratios in the presence of different monovalents and divalents as the only extracellular cations. While mutating residues involved in the proposed putative selectivity filter (DEKA) showed little effects on ionic selectivity except the lysine residue in domain III, we identified three other residues (W1531, D1532, G1533), all in domain IV, which are critical determinants of ionic selectivity. Coincidentally, D-IV is the most flexible domain according to our double-cysteine mutant data. These selectivity data provide further supports to the notion that pore motion may correlate selectivity and

276

permeation. Using these results, we redefined the selectivity filter of Na⁻ channel.

8.1.3 *Identification of pore residues critical for μ-conotoxin (μ-CTX) binding*

Pharmacologically, we have identified pore residues which are critical for interacting with μ-CTX, a Na⁺ channel subtype-specific toxin, via electrostatic (E758, D1241) or hydrophobic (W402, W1239, W1531) interactions (Chapter 5). These results have not only allowed us to better understand the molecular mechanisms of μ-CTX binding to Na⁺ channels but have also permitted us to test several current models of the Na⁺ channel pore given the known structure of μ-CTX. In brief, our results that show neutralization of negative charges at aligned positions in the four internal repeats (i.e. E403, E758, D1241 and D1532) had differential effects on toxin binding further support the notion that the four domains contribute differently to channel properties. These results could reflect a non-symmetrical arrangement of the residues within the pore which is consistent with the data I presented in Chapter 3 and previous reports (Perez-Garcia et al., 1996; Chiamvimonvat et al., 1996).

8.1.4 *Identification of a pore residue critical for lidocaine binding to Na⁺ channel*

Local anesthetics (LA) such as lidocaine are commonly used to treat Na⁻ channel diseases such as cardiac arrhythmias and to achieve local anesthesia. The molecular constituents of the receptor for these agents are however not fully known. Based on previous single channel studies which show the electrical distances for Cd^{2+} and LA binding to the Na⁻ channel are 0.2 from the extracellular side and 0.7 from the cytoplasmic side respectively, we hypothesized that the P-loops and the LABS are adjacently close to each other. Indeed, we demonstrated that certain P-loop residues in the outer vestibule of the pore also regulate drug binding. In particular, the residue W1531 when mutated to cysteine completely abolish lidocaine block. Such effects were not results of change of drug access to the LABS. Mutations of the analogous residue (i.e. W1712) in the human heart Na⁺ channel produced similar effects on drug binding to the

skeletal channel. Our results demonstrate that this pore tryptophan plays a critical role in LA binding and is a common determinant in both skeletal muscle and cardiac Na⁻ channels. In order to accommodate both findings that W1531 lies on the extracellular side and that the LABS is located on the cytoplasmic face, we propose a translocation hypothesis. This hypothesis is also consistent with W1531's location in the most flexible domain (i.e. DIV) and our conclusion that the Na⁻ channel pore is flexible. Nonetheless, we cannot rule out the possibility that mutations of the residue W1531 has some long-range effects on the LABS thereby affecting LA block of the channel.

8.1.5 *Implications of Domain IV as the control centre of channel functions and properties: W1531 (DIV) is a critical residue*

It has been established that Domain IV of Na^+ channels controls many channel functional properties. For example, the inactivation gate located in the III-IV linker is situated at a position relative to D-IV which is homologous to the N-terminal ball in K^+ channels (Patton et al., 1992; West et al., 1992); DIVS4 plays a more significant role than the same segment in other domains in the voltage-dependent activation and inactivation of Na⁻ channel (Chen et al., 1996); certain residues in DIV are critical for channel activation and inactivation as well as the coupling between these two processess (Fan et al., 1996; Li et al., 1997c; see also Appendix); DIV contains regions responsible for β1 responsiveness (Makita et al., 1996b) and determinants for the differences in inactivation kinetics between skeletal and cardiac muscle sodium channels (Chahine et al., 1996; Makita et al., 1996b); pore residues in DIV determine ionic selectivity (Chapter 4); DIV is the most flexible domain (Chapter 3); mutations of residues lining DIVS6 disrupt inactivation and weaken local anesthetic binding (Ragsdale et al., 1994); and that a pore tryptophan (i.e. W1531) in DIV in rSkM1 and hH1 Na^+ channels is critical for lidocaine block (Chapter 6). Taken together, the non equivalence of contribution of domain IV in channel functions and properties compared with other domains could reflect an asymmetrical structural arrangements of these domains.

278

Remarkably, W1531 in domain IV in particular is responsible for governing several other major properties of the channel while analogous residues at equivalent locations in domains I, II and III are not as significant. In addition to its important role in local anesthetic binding as discussed in Chapter 6, W1531 also seems to be responsible for coupling inactivation to activation. Like D1413 located in DIVS3 (Appendix; Li et al., 1997c), which decouples inactivation from activation, the inactivation time constant (τ_h) of W1531C was apparently voltage independent (data not shown) while its mid-point of steady-state inactivation was negatively shifted and recovery from inactivation was slowed in comparison to WT channels. However, the role of W1531 in activation-inactivation still requires further studies. Furthermore, W1531 is also critical for one of the most fundamental properties of Na^+ channel - ionic selectivity (Chapter 4). When the aromatic residue is replaced with cysteine or alanine, the channel allows permeation of monovalent cations such as K^+, NH^{4+} and Cs^+. In additon to all these, W1531 is also a determinant of the wild-type sensitivity of Na^+ channel to μ-CTX block (Chapter 5). It should be noted that replacement of this tryptophan by tyrosine or phenylalanine (i.e. W1531Y and W1531F) often results in wildtype phenotypes (Chapter 4, 5, 6) implicating that the aromaticity at this location is critical for proper channel functioning. Since W1531 is located in the most flexible region of the channel (Chapter 3), the fact that it governs so many properties of the channel lends extra supports to the notion that channel flexibility is important for normal functions of Na^- channel.

8.1.6 *Mapping the spatial relationship between P-loop residues and the local anesthetic binding site (LABS)*

Knowing that certain P-loop residues also affect LA binding, we tried to probe the spatial relationship between these residues and the LABS using a novel paradigm where drugs are made up of three parts: an Anchor, a Linker and an active-Drug (i.e. ALD). Specifically, we synthesized the agent MTSBZ by tethering the LA benzocaine (the drug)

to the sulfhydryl reactive group methanethiosulfonate (the anchor) via a linker. MTSBZ targets specifically to a unique reactive cysteine residue present only in the pore of cardiac Na^+ channel but not other isoforms. Application of MTSBZ produced typical but irreversible local anesthetic effects in cardiac Na^+ channels. However, these effects were readily reversible in the muscle Na^+ channels upon drug washout indicating the specificity of these drugs to the cardiac subtype. On this basis, we have developed a cardioselective LA agent. This ALD paradigm is of general utility and could be applied to any protein or tissue. By varying the linker length, we were also able to map out the spatial relationship between the native pore cysteine (i.e. DI-C373) and the LABS in hH1 Na^+ channels. Based on these studies, the time-averaged optimal length between C373 and the LABS in hH1 channel is about 10Å.

8.1.7 Correlation between channel functions and pore flexibility

It is interesting to note that domain IV residues contribute uniquely to many of the channel properties. Coincidentally, DVI is the most flexible domain suggesting that correlations may exist between pore motions and ion channel properties. However, this hypothesis remains speculative as no definitive statement can be made regarding channel functions and pore flexibility since these experiments were performed independently. Some of the experimental designs to be described in the upcoming sections will specifically address this question and determine if there are direct correlations between channel functions and pore flexibility.

8.2 Future directions

8.2.1 Fluorescent labeling of pore residues to study pore flexibility

I have provided evidence that P-loops are remarkably flexible structures on the time-scale of Cd^{2+} binding and co-ordination using double cysteine mutagenesis (Chapter 3) and that Domain IV, as the most flexible region, is also critical for ionic selectivity

280

(Chapter 4). Since permeation occurs on a sub-microsecond time-scale while Cd^{2-} co-ordination occurs on a time-scale of milliseconds, the relationship between ion channel selectivity and P-loop flexibility is uncertain. In addition, our conclusion is probably an understatement of pore flexibility owing to the limitations of our technique. P-loop motions can be further investigated using fluorescence spectroscopy with substantial higher resolutions. Single cysteine pore mutants will be labeled with the fluorescent dye MTS-Rhod (a rhodamine linked to the highly reactive sulfhydryl specific reacting group MTS). Anisotropy and fluorescent intensity of the labeled channels will be measured under different experimental conditions.

Fluorescent anisotropy is commonly measured in protein chemistry and biophysics to measure molecular motion. Fluorescent molecules absorb light along a principal electronic dipolar axis upon excitation and emit fluorescent light along a separate axis after a characteristic time delay determined by the intrinsic spectroscopic properties of the fluorescent probe being used. If the probe rotates during the time gap between absorption and emission, there will be a loss of correlation between the polarization of the incident polarized light and the emitted light. Anisotropy A is therefore defined as:

$$A = (I_{pa} - I_{per}) / (I_{pa} + 2I_{per}) \qquad\qquad \text{Equation 9.1}$$

where I_{pa} and I_{per} are respectively the fluorescence intensities parallel and perpendicular to the plane of polarization of the incident light. If the fluorescent molecule does not rotate significantly prior to emission after absorption. A will be equal to 1 which means the polarization axes for absorption and emission are identical. A decl ves as the motion increases. Therefore, plot of A vs T(time) will allow identification of the number of spectral components present. It is not suprising to observe more than one component (i.e. $A(t) = \sum \alpha \exp(-t/\tau)$ where α is the relative amplitude of the corresponding time component τ) but in most cases only two can be resolved. If there is more than one correlation time constant (τ), I will: 1) try to identify what kind of motion is associated with each value of

τ. i.e. whether it represents internal (segmental. 10-100 ns) or entire protein motion (>100 ns) or intrinsic rotation of the probe (1-10 ns) itself. This can be done easily by first looking at the change of anisotropy of the probe itself and then comparing it to the experimental values of τ observed: 2) change experimental conditions (e.g. hyperpolarization vs depolarization. different concentrations of Na^+. presence and absence of drug. etc) such that the values of $τ_n$ (correlation time constant) and $α_n$ (contribution or relative amplitude) shifts. These shifts should be reversible upon restoration of conditions if reversible changes of conformational states of the channel are involved. This demonstration of reversibility between relative amplitudes of spectral components is crucial if we want to conclude that there are more than one conformation involved. These experiments also allow us to distinguish between an allosteric change and a shift of a pre-existing conformational equilibrium. Plot of the ratio of amplitudes of the spectral components in question may reflect the partitioning between the two states under different conditions. If the above changes are observed. I will then compare midpoints of changes of $τ_n$ and $α_n$ with other properties of the channel such as I-V. $V_{1/2}$ for steady-state activation and inactivation. etc to see if there is a correlation between these properties which may be responsible for the corresponding conformational change/shift.

If there are more than one rotational correlation time constant (τ). we may also look at the change of the prevailing τ under different experimental conditions (e.g. in the presence of different [Na^+]s. stepping to different voltages. etc) using steady state fluorescence. This series of experiments may allow determination of what kind of rotational motion is associated with a particular τ.

The length of anisotropy decay time may also reflect how flexible a particular residue is. Less flexible residues are expected to display longer decay times and vice versa. In cases where anisotropy (A) does not decay to zero. it implies that motion of the fluorophore is hindered (i.e. $A(t) = \sum α exp(-t/τ) + A(\infty)$). probably as a result of the presence of an energy barrier which prevents rotational diffusion from going beyond a

certain angle.

The degree of exposure of pore-lining residues (i.e. how much and how often a residue is buried within a certain timeframe assuming the pore is not rigid) can also be examined by performing viscosity-variation and quenching experiments. Solvent viscosity can be altered simply by adding glycerol/sucrose. A plot of $1/A$ vs. T/η where η represents solvent viscosity will be made for obtaining useful information from that kind of experiments. If a residue is more exposed, $1/A$ would correspondingly drop more rapidly even at very small values of T/η. In other words, it is more sensitive to change in viscosity. Similarly, specific quenchers can also be added to test the degree of which a residue is exposed to the outside. Residues of bigger exposure are expected to be more susceptible. Stern-Volmer Plot (i.e. Io/I - 1 vs. [quencher]) will be made to investigate these relationships. The fluorescence lifetime of an emitter decreases in the presence of quenchers according to the Stern-Volmer equation:

$$1/I = 1/I_o + k_q[Q] \hspace{4cm} \text{Equation 9.2}$$

where k_q may serve as a quantitative measure for the accessibility of the fluorophore: it approaches to zero at low accessibilities and approaches to the diffusion-control upper limit at high accessibilities. The average time in which a particular residue spends in the aqueous phase can therefore be reflected by this rate of quenching (k_q). These values of k_q will also allow us to construct a sequence in descending/ascending order of accessibilities which may complement with the order of polarity created by lifetime measurements and even the order of sensitivity to Cd^{2-} block of single cysteine mutants (Chapter 3). Moreover, the magnitudes of k_q may also reveal under what experimental conditions (depolarizing or hyperpolarizing, etc) are needed for a particular residue to be more accessible or more deeply buried. These experiments therefore allow differentiation between surface and buried residues since residues that are more exposed to the aqueous phase are expected to be more susceptible to viscosity and quenching. It will be necessary to consider internal shielding effect (if any) since a surface residue may appear to be less

susceptible if it is internally shielded by some other residues. Additionally, we need also to demonstrate that the quenching effects are not limited by the diffusion of the quencher to the residue.

In general, if correlation times detected by fluorescent probes located at different positions within the channel are dependent both upon the position of the probe (i.e. location of the residue attached with a probe) and experimental conditions, it is then possible to conclude that internal rotations might be present and are different for different portions of the channel under different conditions - i.e. channels are flexible. The only requirement for this anisotropy method to be applicable in our channels is that the delay time between absorption and emission (about 30-60 nsec) be on the same time scale as the molecular motions of the P-loops. Generally, it is necessary to use chemical models to extract meaningful information about fluorophore motion using anisotropic measurements. Fortunately, the results obtained from these experiments will be model independent since these experiments are designed to compare the anisotropy between different labeled single cysteine pore mutants. In other words, only the relative amount of motion between different pore residues is of interest.

Fluorescent intensity F can also be measured since F is strongly dependent on the local environment of the fluorophore. The quantum efficiency of fluorescent molecules is far higher in apolar compared to polar environments. Level of fluorescence will therefore reflect how deep a particular residue is buried within the protein over a certain time scale. In addition, fluorescence intensity, when normalized to the channel density, is predicted to vary between different single-cysteine mutants provided the polarity of the immediate local surroundings differs. The intensity of fluorescence is expected to change in a time- and voltage-dependent manner according to the conformational changes in channel structure as they go from one state to another following depolarization or hyperpolarization. P-loops are expected to involve in these conformational changes because they have been shown to affect ion selectivity, permeation (Tsushima et al., 1997a, b) and sometimes gating (Tomaselli et al., 1995; Balser et al., 1996; Li et al.,

284

1998). Provided these conformational changes are associated with alterations in the local polarity of the fluorescently labeled cysteine residues, the quantum efficiency will change as channels change their conformational state.

The first logical mutant to study is W1531C since this residue in located in the most flexible domain of the channel (Chapter 3) and possibly translocates during inactivation or drug binding (Chapter 7). Other residues such as A1529, G1530, D1532, G1533 and Y401 which I hypothesize are more mobile than other residues like E758 and W402, etc (Chapter 3) are the next candidates to examine. A pattern of flexibility that coincides with my previous observations of Cd^{2-} coordination and cross-linking in double cysteine pore mutants (Chapter 3) is expected. Fluorescence anisotropy will also be examined as a function of voltage and compared to gating properties such as channel activation and inactivation to see if there is any correlation between motion of the P-loops and these processes.

8.2.2 *Detailed spatial mapping of the P-loops with local anesthetic binding site*

The Na^+ channel pore and the local anesthetic binding site are distinct functional domains. I have already demonstrated that they are however structurally adjacent to each other. The molecular relationships of these domains can be further revealed by probing single cysteine pore mutants with ALD agents (Chapter 9). Initial success has been achieved by applying these ALD agents to Y401C rSkM1, hH1 and native rat cardiac Na^+ channels (Chapter 7). Making use of the single cysteine mutants available, ALD of various linker lengths will be anchored at selected positions in the P-loops via a disulfide bond as described in Chapter 7. The efficacy of channel modification by each ALD will be assessed by plotting the magnitude of selected efficacy parameters such as steady-state inactivation, rate of recovery from inactivation, tonic block, etc. against the linker length. For example, I will plot the time constant for the rate of recovery from inactivation or the degree of use-dependent block at steady-state as a function of linker length. The profile of efficacy with linker length of Toc- or Ben-ALDs for each of the different single-

285

cysteine mutant channels should depend on the distance between the P-loop residue (to which the Ben-ALD or Toc-ALD is anchored) and LABS. We anticipate that an "optimal length" linker will exist and this length reflects the distance between a particular P-loop residue and the LABS. The profile of the dependence of the selected parameter on linker length might also depend on the flexibility of the P-loop used to anchor the Toc-ALD and/or the flexibility of the LABS. In such case the "optimal length" more correctly represents a dynamically, time-averaged estimate of distance. Variable length Ben-ALDs (i.e. C2, C6, C10) and Toc-ALD (T2, T6, T10) have been synthesized and additional compounds will be created with 0-carbons (C/T0), 2-carbons (C/T2)... 14-carbons (C/T14) linker lengths (i.e. lengths of 0 Å, 3.1 Å.... 21.7 Å when fully extended). As a control, anchor with various linker lengths without the drug portion will also be synthesized and tested to ensure that the carbon-chain linker by itself does not exert any effects on channel gating.

Initially, the above experiments will be performed on Y401C (i.e. rSkM1) channels to determine the time-averaged distance between this pore cysteine residue and the LABS. My preliminary results have already shown that the optimal distance seems to be 2Å further supporting the two domains are extremely close to each other. It is interesting when MTSBZ was anchored at the native residue C373 in hH1, the optimal distance seems to be ~10 Å (Chapter 7) implying that structural/architectural differences between the two forms of channels, despite their extensive sequence homology, may exist in terms of the spatial relationships between their pores and the LABSs. This strategy may potentially provide an answer for why the affinity for LAs of cardiac channels is higher than that of the skeletal muscle channels.

As controls, the effects of pore mutations on local anesthetic binding will also be used as reference since some of these pore residues indeed affect drug binding (Chapter 7).

8.2.3 Identification of the location of the inactivation receptor in relation to the LABS and inactivation ball

Motivated by the observation that pore residues that are close enough to each other are capable of cross-linking with each other, we hypothesize further that detailed structural information of the interaction between the inactivation ball and its receptor can be obtained by simultaneously replacing two residues with cysteines: one substitution will be made in the putative ball region located on the III-IV linker (i.e. the IFM motif) while the other will be made in the suspected inactivation receptor region (i.e. S6 residues, W1531 and S4-S5 linker regions). It has been suggested that the LABS and the inactivation receptor are possibly overlapping domains (Hille, 1992). Since the inactivation particle and its receptor are postulated to come into close proximity and interact very strongly with each other in inactivated conformations (Hille, 1992), the inserted cysteines are expected to approach one another following channel depolarization. Depending on the distance, spontaneous cross-link may form between the two inserted cysteines or it can be promoted by applying various oxidizing agents or cross-linking reagents as probes to investigate the molecular distance as well as interactions between the substituted cysteines. Once cross-linked, the current should be eliminated because the channels are now locked into the inactivated conformation. If current inhibition is the result of cross-linking involving the formation of disulfide-bond, application of a reducing agent such as DTT should reverse the process.

8.2.4 Probing translocation of pore residues

We have hypothesized that the residue W1531 may translocate from the outside to the inside during either the inactivation process or following drug binding (Chapter 7). This possibility can be tested by modifying the substituted cysteine (i.e. W1531C) with the aqueous-specific sulfhydryl modifying agent MTSEA or MTSET under different experimental conditions. MTSEA is initially applied extracellularly to W1531C channels under control conditions while stimulated with a continuos train of depolarizations. The

287

degree and time course of current reduction is observed. Reduction of current by MTSEA is probably the result of modification of the permeation pathway (Tsushima et al., 1997a, b; Chiaminovat et al., 1997). The state-dependence of MTSEA modification will be investigated by applying MTSEA to the cysteine muatnt channels under different electrophysiological conditions such as a depolarizing potential favoring inactivation, a hyperpolarizing potential favoring the resting states, as well as in the absence and presence of drug for a certain period of time. The degree and time course of current reduction are then compared to that measured under control conditions over the same period of time. If translocation of the residue occurs during any of the above states, the degree and rate of current reduction occurred over the same time interval are expected to reduce when compared to the control. These experiments will reveal whether the residue C1531 is protected from MTSEA modification during a particular state of the channel. The degree of MTSEA modification can further be assessed by assaying Cd^{2+} sensitivity. Two populations of channels (Cd^{2+} insensitive modified channels and Cd^{2+} sensitive unmodified channels; c.f. Chapter 3) will be reflected as double-Cd^{2+} binding curves as a result of incomplete MTSEA modification. The relative amplitudes of the two populations can be used to assess the extent of MTSEA modification. Indeed, my preliminary data have indicated that the residue C1531 is protected from MTSEA modification in the presence of lidocaine during inactivation.

Translocation of W1531 is likely to involve nearby residues (such as G1530, D1532C, etc) as well. The same experiments can be repeated on other DIV pore mutants such as S1528C, A1529C, G1530C, D1532C, G1533C, etc. By examining the degree of MTSEA modification of these cysteine pore mutants, we can get an estimation of the degree of translocation or rearrangement of pore residues during inactivation or drug binding.

8.2.5 Single channel studies of W1531C to reveal the molecular mechanism of lidocaine binding

It is intriguing to find that though W1531C channels were less sensitive to use-dependent block by lidocaine, their sensitivity to tonic block was enhanced (Chapter 7). Single channel recordings reveal that the molecular mechanisms underlying such enhancement of tonic block is the result of enhanced open channel block of W1531C channels (see also Chapter 7). These single channel experiments will be repeated in the background of IFM/QQQ mutations (i.e. QQQ/W1531C: QQQ/W1531A, etc) to remove fast-inactivation. Recordings in the absence of fast-inactivation will avoid complications due to drug binding to the inactivated states and allow examination of the presence of discrete open channel block which is otherwise not observable in normal W1531C or W1531A channels due to their brief openings and rapid entry into the absorbing inactivated states.

8.2.6 Broader pharmacological study of W1531C channels

In Chapter 8, I have provided evidence that the mutation W1531C completely abolish lidocaine sensitivity suggesting W1531 may form part of the local anesthetic binding site. Other antiarrhythmic and related agents such as benzocaine. quinidine. flecainide. toccainide, mexilitene. procaine and etidocaine as well as anticonvulsants such as phenytoin and carbamazepine, etc also exert their clinical effects by preferentially inhibiting the Na^+ currents. They act by binding to the open and inactivated states of these channels during depolarized potentials. The sensitivity of W1531C (rSkM1) and W1712 (hH1) channels to these agents will be tested in comparison to the corresponding WT channels. Other pore mutants will also be tested if necessary. These experiments will reveal whether this pore tryptophan is a common determinant of binding of these drugs (i.e. whether these drugs block at identical, overlapping or separate receptor sites).

8.2.7   Binding of phenylalkylamines to L-type Ca^{2+} channels

Phenylalkylamines are a class of Ca^{2+} channel antagonist that are commonly used to treat electrical disturbances in diseases such as cardiac arrhythmias and angina pectoris in which L-type Ca^{2+} channels in the corresponding tissues play a significant role. Similar to the action of many tertiary local anesthetics such as lidocaine on Na^+ channels, tertiary phenylalkylamines also act on L-type Ca^{2+} channels in a voltage- and use-dependent manner (Lee and Tsien, 1983). Similarly, the permanently charged phenylalkylamine D890 blocks Ca^{2+} channel only when applied from the cytoplasmic side suggesting these drug molecules must bind to their receptor from the inside (Hescheler et al., 1982). This is analogous to QX-314 block observed in Na^+ channel (Strichartz, 1973; Hille, 1992). Furthermore, it has been demonstrated that binding of phenylalkylamines such as verapamil, desmethoxyverapamil ((-)-D888) and methoxyverapamil (D600), to Ca^{2+} channels are affected by mutations of residues in IVS6 of L-type Ca^{2+} channels (Hockerman et al., 1995; Doring et al., 1996; Johnson et al., 1996; Schuster et al., 1996). Interestingly, mutations of certain residues located in IVS6 of Na^+ channel also abolish binding of local anesthetics in a similar manner (Ragsdale et al., 1994). Given the similarity in action of phenylalkylamines and local anesthetics respectively on Ca^{2+} and Na^+ channels. These results suggest that the receptors for these agents of both types of channels may share some common molecular determinants. W1531 located in the pore of rSkM1 Na^+ channel is not only conserved among different Na^+ channel subtypes but is also found in Ca^{2+} channel. It is likely that the analogous residue of W1531 in Ca^{2+} channel also forms part of the receptor for phenylalkylamines. Further mutagenesis experiments will therefore provide a better molecular picture of the receptor for phenylalkylamines in the Ca^{2+} channels.

8.3   Conclusion

It should be aware that ionic channels are not the only proteins responsible for the control of membrane potential. It is becoming increasingly clear that these channels are

also under the control of other metabolic pathways and factors such as G proteins. Further insights into these areas will certainly allow developments of better antiarrhythmic agents. With advances in molecular techniques, the functionality of these ionic channels and the basis by which they are regulated will be revealed at the molecular level in details over the next decade. The importance of basic science therefore should not be understated. Knowledge gained from these researches should be applied and translated into better therapies for patients suffering from pathologies due to electrical disturbances. Once this step is achieved, one would see the true beauty of the marriage between basic science and clinical applications.

APPENDIX

THE ROLES OF CONSERVATIVE RESIDUES IN CHANNEL GATING: ACTIVATION & INACTIVATION

A. *Abstract*

Aspartates (i.e. D197, D640, D1094 and D1413) and phenylalanines (i.e. F198, F639, F1095 and F1412) found in the third transmembrane segment (S3) of all 4 domains of rat skeletal muscle Na^+ channel (rSkM1) are absolutely conserved residues among voltage-gated Na^+ and Ca^{2+} channel subtypes and highly conserved in K^+ channels. The S3 Asp residues may form salt bridges with the voltage sensor in S4 thereby influencing channel activation (Durell and Guy, 1996). Mutation F1412L causing the equine hyperkalemic periodic paralysis (HPP) in horse disrupts channel inactivation (Hanna et al., 1996). We therefore examined the roles of these residues in Na^+ channel activation and inactivation using single cysteine replacements and expression in *Xenopus* oocytes. All the D mutants studied but none of the F mutants displayed rightward shifts in steady-state activation curves by 5 to 15 mV. D-to-C mutants (except D1094C) also affected channel inactivation and the coupling between activation and inactivation (D197C and D1413C). Among 4 of the F residues studied, only F1412C displayed significant changes in inactivation including an increase in magnitude and reduced voltage-dependence of τ_h, faster recovery from inactivation and rightward shifts of the steady-state inactivation curve. Our results suggest that these highly conserved residues in S3 of all the four domains play a role in channel activation and inactivation.

B. *Introduction*

Voltage-gated Na^+ channels are reponsible for the initial rapid rising phase of action potentials in nerve, heart and skeletal muscle (Catterall, 1992, and Hille, 1992). At hyperpolarized membrane potentials, most Na^+ channels are in closed or resting states. Upon membrane depolarization, movements of charges contained in the voltage sensor lead

to channel opening or activation (Stuhmer et al., 1989; Sigworth, 1993; Yang et al., 1996). Open channels inactivate within a few milliseconds thereby restricting Na⁻ ion influx to brief periods following depolarization. Once the channels are inactivated, they require several milliseconds following membrane repolarization to recover from inactivation before they are ready to reopen upon subsequent depolarizations (Bezanilla and Stefani, 1994).

The fourth transmembrane spanning segment (S4) of each domain contains positively charged residues (either arginine or lysine) at every third or fourth position separated by hydrophobic residues (Noda et al., 1984). Mutations of these charged S4 basic residues often result in shifts in channel activation consistent with the putative role of these segments in voltage sensing for channel activation (Lopez et al., 1991; Papazian et al., 1991; Yang and Horn, 1995; Aggarwal and MacKinnon, 1996; Yang et al, 1996; Chen et al., 1996). However, studies in voltage-gated K⁺ channels have found that other transmembrane segments also influence voltage-dependent channel properties (Liman et al., 1991; Logothetis et al., 1992; Logothetis et al., 1993; Greenbalt et al., 1985; Sigworth, 1993; Seol et al., 1996). Within the S2 and S3 segments, there are many highly conserved negatively charged amino acid residues. Molecular models (Durell and Guy, 1996) and previous studies (Greenblat et al., 1985; Liman et al., 1991; Sigworth, 1993; Papazian et al., 1995; Planells-Cases et al., 1995; Seol et al., 1996) suggest that these negative residues may form salt bridges with the positive residues in the S4 segments thereby stabilizing S4 segments within the lipid bilayer and contributing to voltage-dependent properties. Mutations of these residues in S2 and S3 are therefore predicted to influence activation (Durell and Guy, 1996). Channel activation is a highly voltage-dependent process whereas channel inactivation is largely intrinsically voltage independent (Aldrich et al., 1983; O'Leary et al., 1995; Chen at al., 1996), deriving its voltage dependen..' from coupling to activation (Sigworth, 1993; Chahine et al., 1994). The molecular basis of this coupling is however poorly understood. Mutations of skeletal muscle sodium channels causing myotonias have been shown to affect this coupling mechanism (Chahine et al., 1994; Yang et al., 1994; Ji et al., 1996). A pair of tyrosine residues located on the III-IV linker when mutated to glutamines also disrupts this coupling (O'Leary et al., 1995).

We have previously shown that disruption of normal inactivation results from the mutation F1412L in rSkM1 sodium channels, which corresponds to the natural mutation associated with the disease equine hyperkalemic periodic paralysis (Hanna et al., 1996). This phenylalanine residue is absolutely conserved in all voltage-gated Na^- and Ca^{2-} channels as well as K^- channels. Furthermore, alignment of the S3 segments between the four internal repeat domains of Na^- and Ca^{2+} channels reveals absolute conservation of similar phenylalanine residues in domains I, II and III. Interestingly, these residues are situated either one residue upstream or downstream of the S3 aspartates.

In this study, we mutated aspartates (i.e. D197, D640, D1094 and D1413) and phenylalanines (i.e. F198C, F639C, F1095C, F1412C) located at the cytoplasmic end of S3 in all four domains (Figure AP.1) and examined their contribution to gating in rat skeletal muscle (rSkM1) Na^- channels. Our results indicate that S3 aspartates influence Na^- channel activation consistent with a role in voltage sensing. We also found that mutations of two S3 residues (i.e. D197C and D1413) alter the molecular coupling between activation and inactivation. In addition, our results indicate that none of these S3 phenylalanine mutations affect Na^- channel gating except F1412C which disrupts channel inactivation.

C.   Materials & Methods

C.1   Electrophysiology

Whole-cell current recordings were done at room temperature (20-22°C) using two-electrode voltage-clamp technique (2.3). The recording solution used , was ND96 (2.7). To ensure reasonable voltage control, only oocytes expressing peak currents less than 5 μA were used.

294

Figure AP.1

Putative transmembrane folding model of the Na⁺ channel α subunit showing internal repeat domains I-IV each with 6 transmembrane segments S1-6. Phenylalanine and aspartate found in the cytoplasmic end of the third transmembrane segment (S3) of each of the four domains (DI-IV) are highly conserved residues. They are absolutely conserved among voltage-gated Na⁺ and Ca²⁺ channels and are highly conserved in K⁺ channels. The S4 segments carries a ribbon of positively charged residues and are believed to be the voltage sensors. The S3 aspartates may act as countercharges and form electrostatic salt bridges with the S4 to stabilize the entire protein structure. A phenylalanine to leucine mutation in DIV (i.e. F1412L), which corresponds to the natural mutation found in the disease equine hyperkalemic periodic paralysis (HPP), is known to disrupt Na⁺ channel inactivation. Identical absolutely conserved residues (i.e. phenylalanine) are also found at equivalent locations in Domain I, II and III. Hydrophobic residues (IFM) in the III-IV linker region on the cytoplasmic side of the channel, which have been suggested to be the inactivation particle, are also indicated.
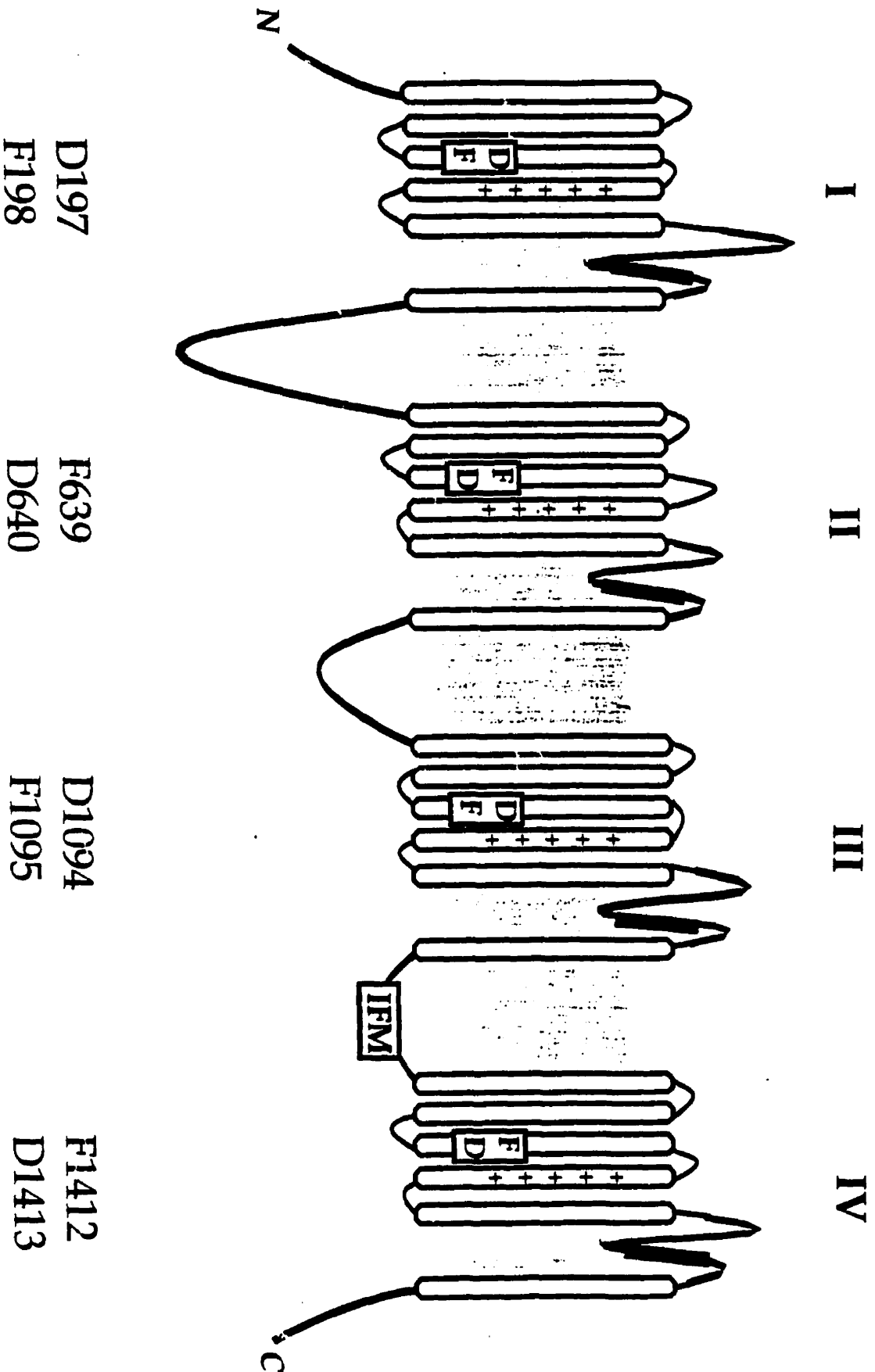
I   D197   F198

II   F639   D640

III D1094 F1095

IV   F1412 D1413

C.2   Experimental Protocols and Data Analysis

Current-voltage relationships were obtained by holding oocytes expressing the appropriate channels at -120 mV and stepping from -60 to +50 mV by increments of 10 mV. Steady-state activation curves of whole-cell currents were constructed from the current-voltage relationships of the corresponding channels using the transformation procedures described below. For steady-state inactivation, we recorded the current in response to a test depolarization to -20 mV ($I_{-20\,mV}$) which immediately followed a prepulse to a range of voltages. h_∞ was estimated as a function of the prepulse voltage by the ratio I_{-20} $_{mV}/ I_{-120\,mV}$ where $I_{-120\,mV}$ is the current measured in the absence of a prepulse.

Recovery from inactivation of rSkM1 and mutant channels were examined using a standard two-pulse protocol in which two identical depolarizing pulses (50 ms each) were separated by a recovery voltage (-80, -100 or -120 mV) applied for a variable period. The first conditioning pulse resulted in activation followed by inactivation of the channels. Recovery of channels from the inactivated state ensued during the time intervals between pulses. The peak current evoked by the second depolarizing pulse represents the fraction of channels which had recovered from inactivation during the interval at the recovery potential. Recovery from inactivation of each mutant was examined at holding potentials of -80, -100 and -120 mV.

C.3   Statistics and Curve fitting

Steady-state activation and inactivation curves were obtained by fitting data to the Boltzmann functions using the Marquardt-Levenberg algorithm in a non-linear-least-squares procedure:

$$m_\infty \text{ or } h_\infty = 1 / \{1 + \exp[(V_t - V_{1/2}) / k]\} \qquad \text{Equation 5.1}$$

297

where V_t is the test potential. $V_{1/2}$ is the half-point of the relationship and k (=RT/zF) is the slope factor. The holding potential in these experiments were -120 mV. For steady-state activation. m_∞ = g / g_{max} where the conductance g was obtained from the I-V relationship by scaling the peak current (I) by the net driving force using the equation g = I / (V_t -E_{rev}) where V_t is the test potential and V_{rev} is the reversal potential. Current-voltage data were fit to the equation I= m_∞ * g_{max} * (V-E_{rev}).

The time constant (τ_h) for decay of the whole-cell current was estimated by fitting the decaying phase of the whole-cell current beginning after the time of the peak current with a mono-exponential function:

$$I / Io = \exp(-t/\tau)$$ Equation 5.2

For fitting recovery from inactivation data, a bi-exponential function was used:

$$I / Io = 1 - [A1*\exp(-t/\tau_1) + (1-A1)*\exp(-t/\tau_2)]$$ Equation 5.3

Data presented are the means ± SEM. Statistical significance was determined using an unpaired Student's t-test with p<0.05 representing significance.

D.   *Result*

D.1   *Effects of cysteine mutations on macroscopic whole-cell current kinetics of rSkM1*

To examine the roles of S3 aspartates (i.e. D197. D640. D1094. D1413C) and phenylalanines (i.e. F198, F639, F1095 and F1412) in Na⁻ channel gating, we mutated these residues in rSkM1 channels individually to cysteine and co-expressed either WT or mutant channels with the rat brain β1 subunit in *Xenopus* oocytes. Figure AP.2A and 5.3A show the representative raw current traces recorded from aspartate-to-cysteine (D/C) and phenylalanine-to-cysteine (F/C) mutant channels in response to depolarizations from -120 mV to -10 mV using two-electrode voltage-clamp technique. The currents have been

normalized to make the peaks identical with the superimposed wild type rSkMl current (broken line). Upon depolarization. rSkMl channels elicited rapidly activating inward Na⁻ currents. peaked and then inactivated with a time constant (τ_h) of 0.97±0.08 ms (n=5) at this test potential. For most mutants. the estimated time constants for current decay. τ_h (see Materials and Methods) were identical (p>0.05) to WT (F198C: 1.10±0.07 ms. n=3: F639C: 1.04±0.07 ms. n=3; D640C: 1.07±0.03 ms. n=4; D1094C: 0.87±0.06 ms. n=3; F1095C:1.05±0.10 ms. n=3). However. the measured τ_h for D197C (2.54±0.18 ms; n=3). D1413C (4.11±0.60 ms; n=4) and F1412C (2.11±0.01 ms; n=4) channels. were significantly increased compared to WT channels (p<0.05). These effects can arise from defects in channel activation or inactivation or both. The mechanisms underlying these changes were further explored in the following sections.

D.2 *Aspartate-to-cysteine but not phenylalanine-to-cysteine mutants displayed shifts in steady-state activation*

Figures 5.2B and 5.3B show peak-current versus voltage relationships of WT rSkMl and selected cysteine mutant channels. Data points were fit to a modified Boltzmann relationship (see Materials and Methods). All D/C mutants (Figure AP.2B) displayed shifts of I-V curves in the depolarizing direction compared to WT while the F/C mutants (Figure AP.3B) were unchanged relative to WT channels. Effects on channel activation of these various mutants can be more readily seen by transforming the I-V relationships into steady-state activation curves (i.e. conductance-voltage or g-V curves) using the equation g = I / (V-E$_{rev}$) (Figure AP.2C and 5.3C). The parameters estimated from fitting the activation data to the Boltzmann equation are summarized in Table 5.1. D197C. D640C and D1413C (Figure AP.2C) displayed significant depolarizing (rightward) shi?: (p<0.05) in the midpoints of steady-state activation curves (D197C: -24.52 ± 0.96 mV, n=3; D640C: -8.59 ± 1.62 mV, n=8; D1413C: -21.76 ± 0.69 mV, n=7) compared to WT channels (WT: -26.70 ± 1.14 mV, n=3). Though not statistically significant, D1094C also displayed a slight rightward shift of steady-state activation ($V_{1/2}$ = -25.98 ± 1.20 mV, n=7). In contrast, none of the F/C mutants illustrated in Figure AP.3C showed measurable significant shifts

Figure AP.2

A) Representative traces of whole-cell currents recorded from rSkM1 (broken line) and aspartate-to-cysteine (D/C) mutant (solid line) channels expressed in *Xenopus* oocytes. The peak currents have been normalized such that the peaks at the baseline are equal. Peak currents for these sweeps are 4.2 μA for rSkM1. 1.1 μA for D197C, 4.4 μA for D640C, 4.1 μA for D1094C and 4.9 μA for D1413C.

B) The normalized peak Current-Voltage relationships of WT rSkM1 and D/C inactivation mutant channels. All D/C mutants displayed shifts of I-V curves in the depolarizing direction compared to WT suggesting there are shifts in stability toward the closed states of these channels.

C) Steady-state activation plots of rSkM1 and D/C mutant channels. Steady-state activation curves were derived from the I-V curves shown in Panel B using the equation $g=I/(V-E_{rev})$ and fit to the Boltzmann functions using the Marquardt-Levenberg algorithm in a non-linear least-squares procedure (see Materials and Methods). Steady-state activation curves of all D/C mutants examined were all shifted to the right. These observations are consistent with the suggestion that these aspartates form salt bridges with the positively charged residues in the S4 segments which are involved in the voltage sensing process.

A

D197C   D640C   D1094C   D1413C

WT

10 ms
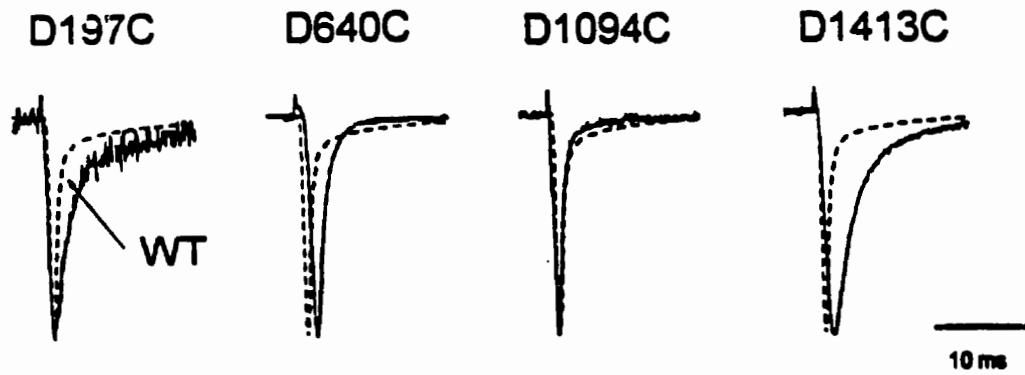
B
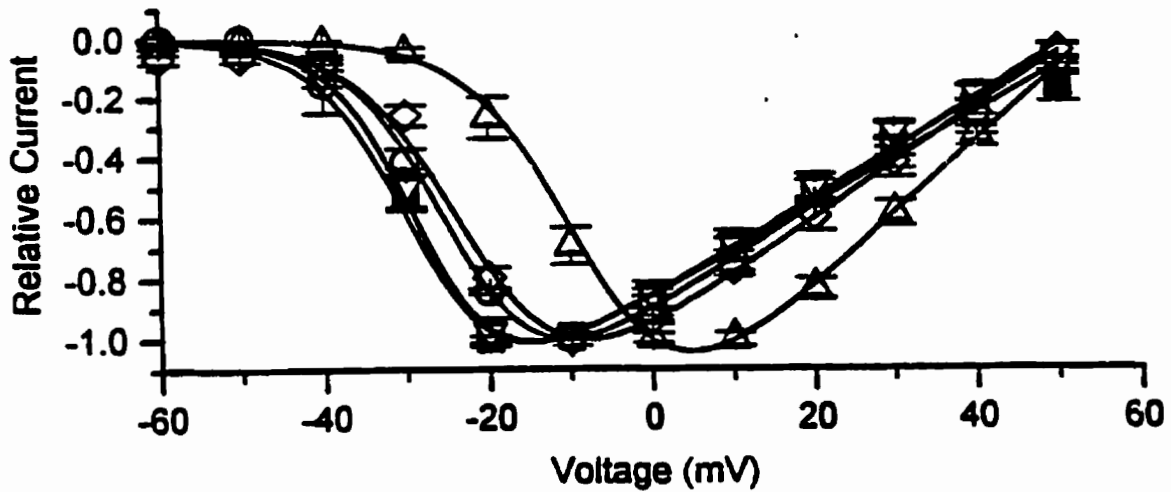
C
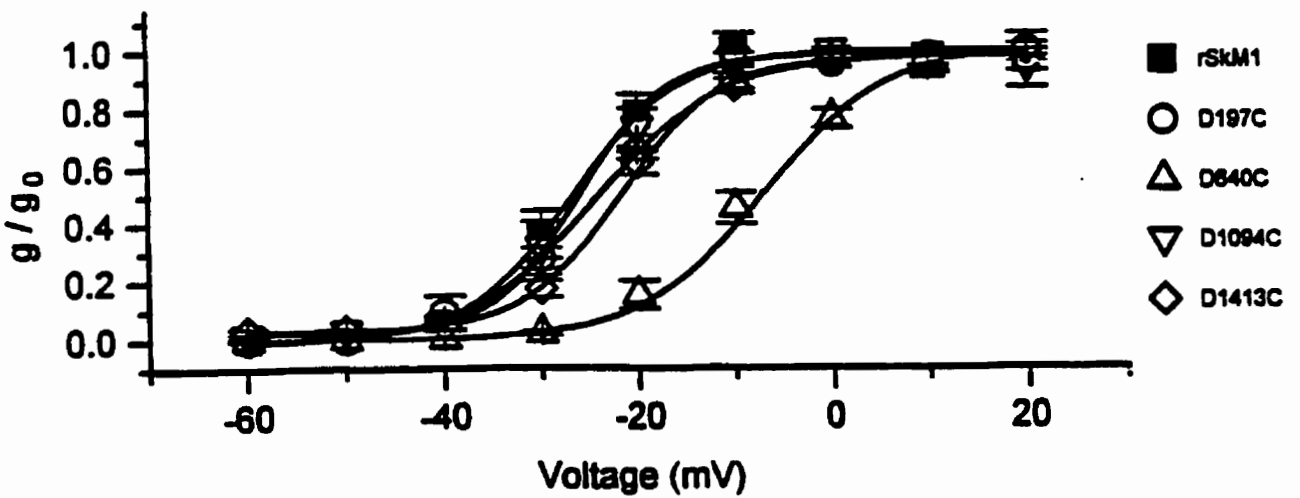
Figure AP.3

A) Representative traces of whole-cell currents recorded from rSkM1 (broken line) and phenylalanine-to-cysteine (F/C) inactivation mutant (solid line) channels expressed in *Xenopus* oocytes. The peak currents have been normalized to the peak and superimposed. Peak currents for these sweeps are 4.2 μA for rSkM1, 4.5 μA for F198C, 3.7 μA for F639C, 4.2 μA for F1095C and 4.7 μA for F1412C.

B) The normalized peak Current-Voltage relationships of rSkM1 and F/C mutant channels. Unlike the D/C mutants (Figure 2), the I-V relationships were identical for all the F/C mutant and WT channels indicating that activation was unaltered by these mutations.

C) Steady-state activation plots of rSkM1 and F/C mutant channels. Unlike D/C mutants, none of the F mutants displayed any shifts in steady-state activation suggesting these residues do not play a role in channel activation. Transformations of I-V relationships to steady-state activation curves were done as in Figure 2C.

A

F198C   F639C   F1095C   F1412C

10 ms

B

C
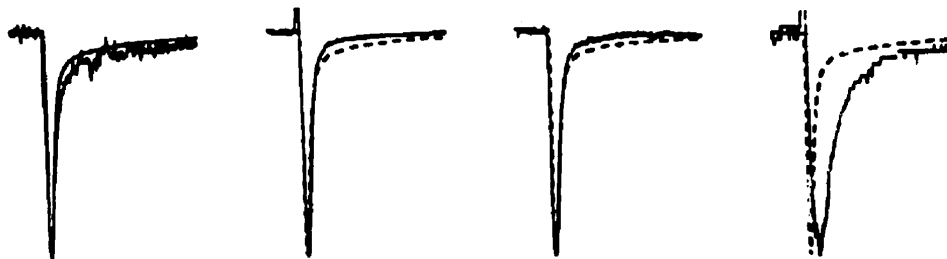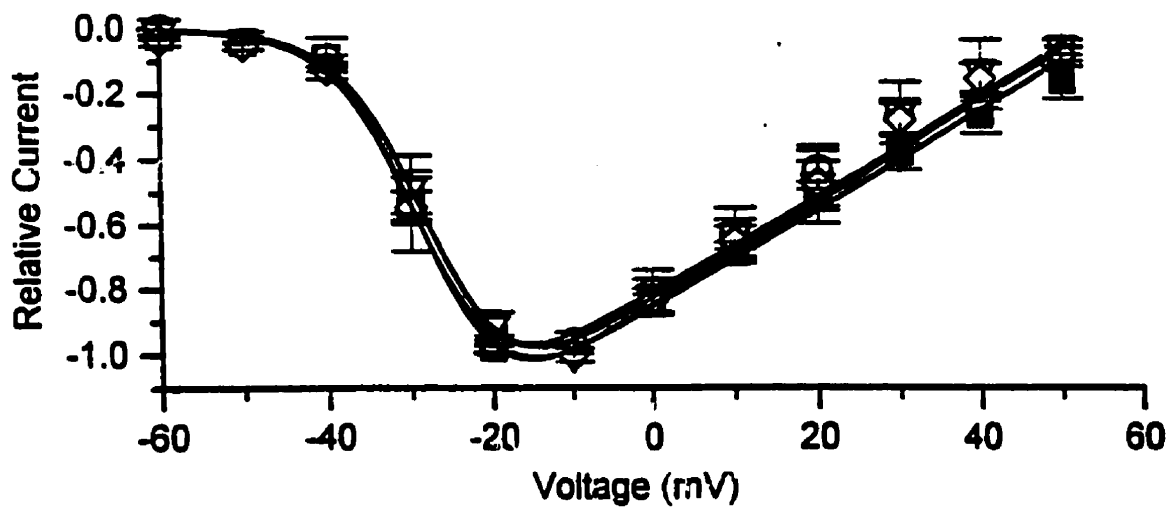
rSkM1
F198C
F639C
F1095C
F1412C
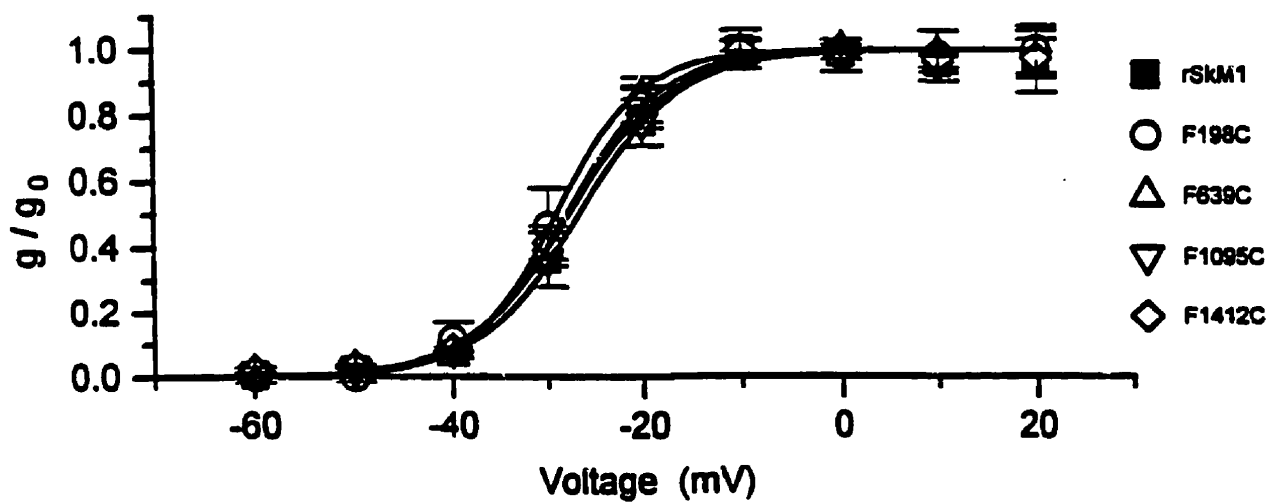
(p>0.05) in their steady-state activation curves (F198C: -27.73 ± 0.90 mV, n=5; F639C: -27.21 ± 2.37, n=3; F1095C: -26.69 ± 0.85 mV, n=4; F1412C: -27.87 ± 1.07 mV, n=4) when compared to WT. In addition to shifts in the midpoints observed in the D/C mutants, there were also changes in the slope factors (k) estimated from Boltzmann fits. Although limiting slope factors give a better measure of the "true" gating charge, these slope factors do provide some measure of the "apparent" gating charge (Almers, 1978). From the Boltzmann fits, the changes in voltage-dependence observed in D197C, D640C, D1094C and D1413C could be produced by "apparent" gating charge changes of +1.5, +1.0, -1.0 and +0.3 elementary charge (e_o) per channel, respectively. By contrast, the slope factors were not statistically different between the F/C mutants and WT channels (p>0.05). These data are consistent with the proposal that these S3 aspartate residues affect channel activation in Na⁻ channels possibly by forming salt bridges with the positively charged residues in S4. Our results also suggest that the phenylalanines located immediately adjacent to the aspartates, do not measurably affect Na⁻ channel activation.

D.3   Shifts of steady-state inactivation of D197C, D640C, F1412C and D1413C

To further explore the effects of these S3 mutations on channel gating, we next examined steady-state inactivation. Steady-state inactivation provides an energetic measure of the relative stability of the inactivated states compared to the closed states of the channel. Figure AP.4 shows the steady-state fast-inactivation curves of WT and cysteine mutants obtained by plotting the ratio between the peak current elicited in a test pulse to -20 mV recorded following 500 ms prepulses to various voltages and the peak current elicited following depolarization to -20 mV from a holding potential of -120 mV. A 500 ms prepulse was chosen to ensure equilibration between closed and fast-inactivated channels (Featherstone et al., 1996). Data points were fit with a Boltzmann equation and the estimated parameters are summarized in Table 1. Figure AP.4A shows that the midpoints for steady-state inactivation (i.e. $V_{1/2}$) of D197C (open circle, -56.77 ± 2.3 mV, n=3), D640C (open up triangle, -57.43 ± 0.50 mV, n=5) and D1413C (open diamond, -57.79 ± 1.52 mV, n=4) were significantly (p<0.05) shifted in the hyperpolarizing direction

Figure AP.4

Steady-state inactivation plots of rSkM1 and cysteine inactivation mutant channels (Panel A: D/C mutants; Panel B: F/C mutants). Steady-state fast-inactivation curves were derived by normalizing the current recorded in test pulses to -20 mV following 500 msec prepulses to various voltages to the maximum current recorded upon depolarization to -20 mV from a holding potential of -120 mV. Data were fit to the Boltzmann function using the Marquardt-Levenberg algorithm in a non-linear least-squares procedure (see Materials and Methods). Besides effects on steady-state activation, the D/C mutants D197C, D640C and D1413C also displayed effects on steady-state inactivation. Their mid-points for half-maximal inactivation (i.e. $V_{1/2}$) were shifted significantly in the rightward direction. Among the F/C mutants, only F1412C had an effect on inactivation and its steady-state inactivation curve was shifted 5 mV in the depolarizing direction suggesting a destabilization of its inactivated state.

A

Fraction of current vs. Prepulse Potential (mV)

- rSkM1
- D197C
- D640C
- D1094C
- D1413C

B

Fraction of current vs. Prepulse Potential (mV)

- rSkM1
- F198C
- F639C
- F1095C
- F1412C
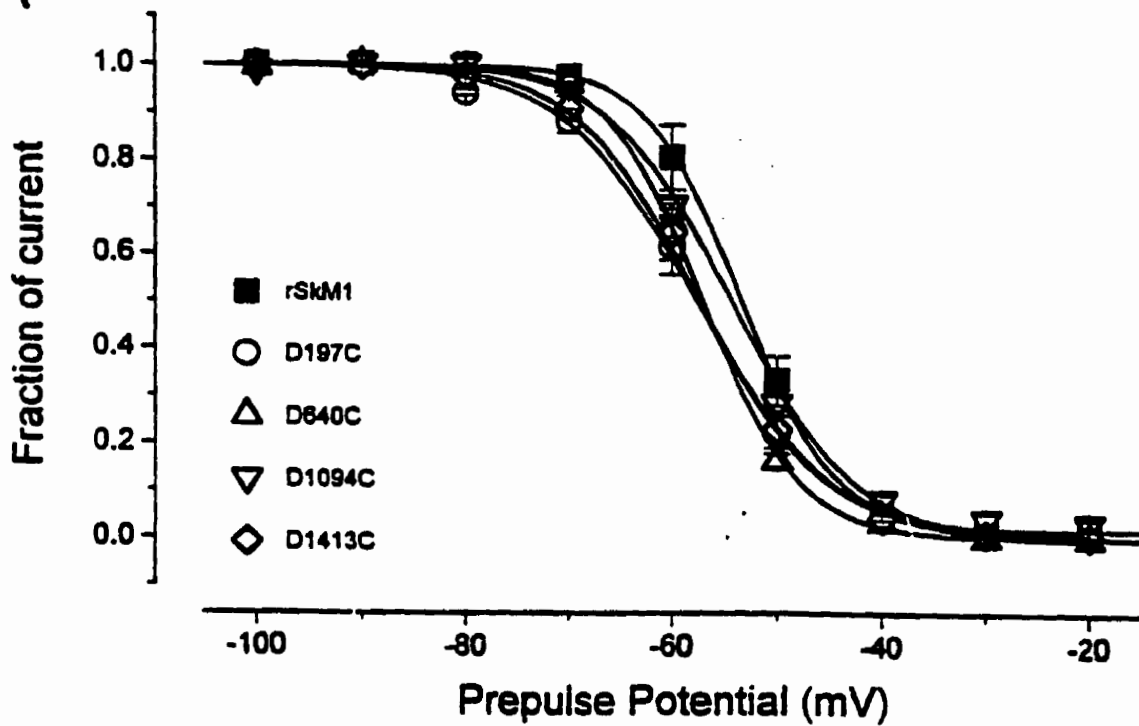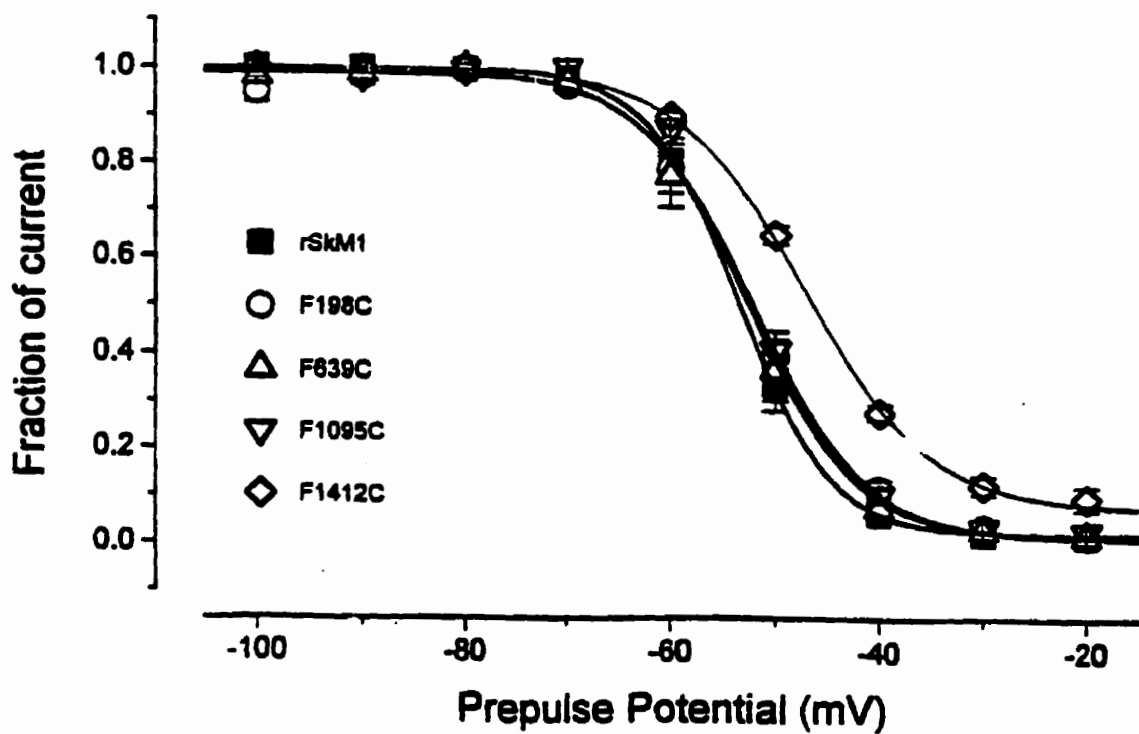
Table AP.1

Summary of $V_{1/2}$ and slope factor (k) for steady-state activation and inactivation of rSkM1 and cysteine mutant channels. Entries marked with asterisks are statistically different from WT (p<0.05).

Channels	Steady-state Activation		Steady-state Inactivation	
	$V_{1/2}$	Slope factor	$V_{1/2}$	Slope factor
rSkM1	-26.70 ± 1.14 (3)	5.37 ± 0.47 (3)	-53.41 ± 1.12 (8)	4.88 ± 0.22 (8)
D197C	-24.52 ± 0.96 (3)*	6.82 ± 0.73 (3)*	-56.77 ± 2.30 (3)*	6.62 ± 0.41 (3)*
F198C	-27.73 ± 0.90 (5)	4.72 ± 0.42 (5)	-52.40 ± 0.58 (7)	5.42 ± 0.16 (7)
F639C	-27.21 ± 2.37 (3)	5.49 ± 0.19 (3)	-53.97 ± 1.36 (4)	4.96 ± 0.12 (4)
D640C	-8.59 ± 1.62 (8)*	6.34 ± 0.21 (8)*	-57.43 ± 0.50 (5)*	4.23 ± 0.10 (6)*
D1094C	-25.98 ± 1.20 (7)	4.42 ± 0.58 (7)*	-55.08 ± 0.49 (7)	5.23 ± 0.04 (9)
F1095C	-26.69 ± 0.85 (4)	5.37 ± 0.47 (4)	-55.39 ± 0.81 (3)	4.43 ± 0.05 (3)
F1412C	-27.87 ± 1.07 (4)	5.12 ± 0.36 (4)	-48.51 ± 0.72 (8)*	5.68 ± 0.13 (13)*
D1413C	-21.70 ± 0.69 (7)*	5.03 ± 0.47 (7)	-57.79 ± 1.52 (4)*	5.29 ± 0.16 (4)

307

compared to WT channels (solid square, -53.41 ± 1.12 mV, n=8) while D1094C channels (open down triangle, $V_{1/2}$ = -55.08 ± 0.49 mV, n=7) were unaffected (p>0.05). Among the phenylalanine-to-cysteine mutants, only the F1412C mutation had an effect on inactivation with the midpoint (open diamond, $V_{1/2}$= -48.51 ± 0.72 mV, n=8) being shifted ≈5 mV in the depolarizing direction (Figure AP.4B). In addition to shifts in midpoints, some S3 mutations also affected the slope factors for D197C (6.62 ± 0.41, n=3), D640C (4.23 ± 0.12, n=6) and F1412C (5.68 ± 0.13, n=13) compared to WT (4.88 ± 0.22, n=8). These values correspond to a change in the effective gating charge by +1.7, -0.7 and +0.8 e_o respectively. The slope factors of other mutants were not statistically different from WT (p>0.05).

D.4 D197C, D640C and D1413C recover more slowly from inactivation whereas F1412C recovers faster

To further investigate the effects of these S3 mutations on channel inactivation, we also examined their rates of recovery from inactivation. The time constant of recovery from inactivation provides information on the rate of exit from inactivated states at a given holding potential. Figure AP.5 shows average recovery curves of each channel plotted as a function of the conditioning pulse for WT and cysteine mutant channels at -80 mV. A bi-exponential function was used to fit these recovery data. Using a 50 ms prepulse duration, recovery from inactivation of rSkM1 channels displayed only a single time constant (τ_1=6.6 ± 1.1 ms, A_1= 100%, n=4) suggesting slow inactivation was not induced under these experimental conditions. D197C, D640C and D1413C required considerably longer times for recovery (D197C: τ_1=3.5 ± 0.3 ms, A_1=67.5%, τ_2=50.8 ± 9.4, A_2=34.2%, n=3; D640C: τ_1=15.2 ± 1.7 ms, A_1=100%, n=5; D1413C: τ_1=3.3 ± 0.1 ms, A_1=58.7, τ_2=25.6 ± 1.6 ms, A_2=45.5%, n=4 where τ_1 and τ_2 represent the first and second time constants, A_1 and A_2 represent the relative amplitudes of the corresponding time constants). The presence of two components in D197C and D1413C may reflect entry into a slowly inactivated state of these channels similar to that observed in the fast-inactivation deficient F1304Q channels (Nuss et al., 1996). On the other hand, F1412C recovered 3-fold faster from inactivation (τ_1=2.1 ± 0.1 ms, A_1=96.8%, τ_2=153.8 ± 11.6 ms, A_2=5.0%, n=5) than WT at the same

308

Figure AP.5

Recovery from inactivation of rSkM1 and cysteine mutant channels. Holding potential was -80 mV. Two identical 50 ms depolarizations to -20 mV were given with various intervals of hyperpolarization to -80 mV in between to allow channels to recover from inactivation. Although not shown, data were collected to 50 ms. D197C, D640C and D1413C recovered more slowly than WT channels while F1412C displayed a 3-fold faster rate of recovery. Similar decelerated and accelerated rates of recovery from inactivation were also observed at holding potentials -100 and -120 mV. Time constants for recovery and their percent contributions are summarized in Table 2.

D197C
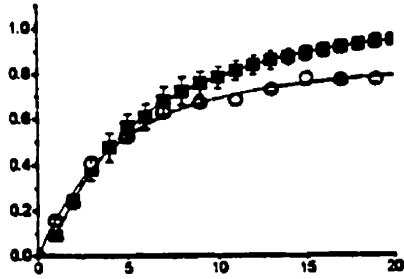
F198C
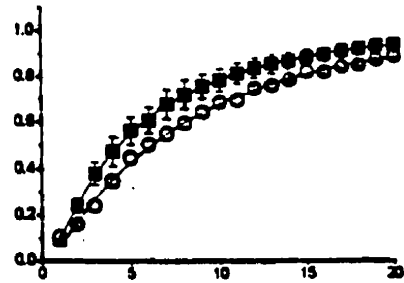
D640C
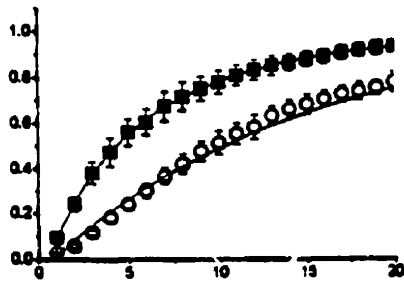
F639C
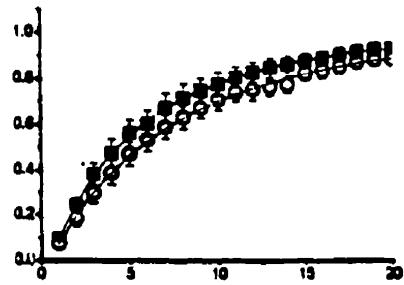
D1094C
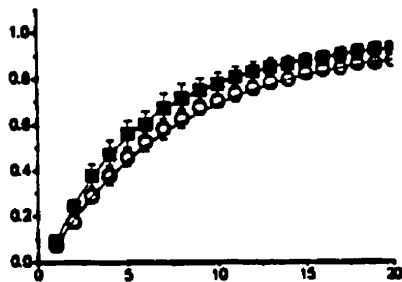
F1095C

D1413C

F1412C

Fraction recovered
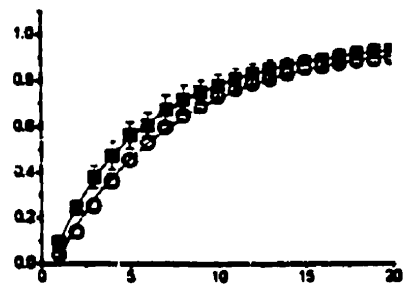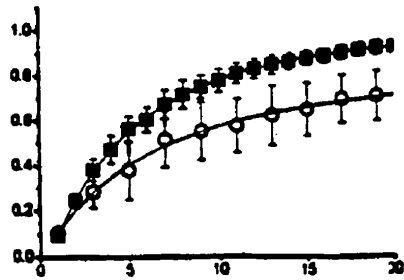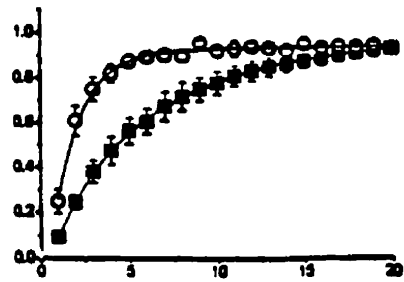
Inter-pulse interval (ms)

potential consistent with destabilization of the inactivated state (Hanna et al.. 1996). Though F1412C also displayed a second time component, the amplitude of this component was very small (A_2=5.0%). Similar differences in recovery curves compared to WT were also observed in D197C. D640C. F1412C and D1413C channels when measured at -120 and -100 mV. The time course of recovery for the other mutants were not different from WT (p>0.05). The time constants for recovery from inactivation of WT and all cysteine inactivation mutants at recovery potentials -120, -100 and -80 mV, including their percent contributions are summarized in Table 5.2.

D.5 *The rates of entry into the inactivated state of D197C, D1413C and F1412C are slower than WT*

Changes in activation are expected to result in changes in inactivation due to coupling between these two processes (Papazian et al.. 1991). The inactivation time constants (τ_h) have been shown to be influenced by both this coupling (Chahine et al.. 1994) and the rate of entry of open channels into the inactivated state (Hanna et al. 1996). As demonstrated in Figures 5.1A and 5.2A. several S3 mutants displayed changes in τ_h compared to WT channels. Since steady-state activation and inactivation curves were also affected in some of these mutants (Figures 5.1, 5.2 and 5.3), we investigated the relationship between steady-state gating properties and the voltage-dependent alterations in τ_h. Figure AP.6 summarizes the τ_h for the decay of macroscopic whole-cell currents of WT rSkM1 and cysteine mutants. Estimates of τ_h were obtained by fitting the decaying phase of the whole-cell current beyond the peak with a mono-exponential function. As shown in Figure AP.6, the values of τ_h for rSkM1 channels (solid squares) depended strongly on voltage between -40 mV and 0 mV, which coincides with the steep portion of the activation curve. This observation is consistent with the suggestion that inactivation, an intrinsically voltage independent process, derives its voltage dependence by being coupled to activation (Aldrich et al., 1983; Sigworth, 1993; Chahine et al., 1994). All S3 mutants except D197C, D640C. F1412C and D1413C displayed τ_h values which were unchanged compared to WT channels at all voltages examined (Figure AP.6A & B). These changes in τ_h might be

Table AP. 2.

Time constants for recovery from inactivation of of rSkM1 and cysteine mutant channels at different recovery potentials. Number in brackets indicated the percentage of contribution of each time constants to the total recovery at a particular recovery potential as indicated. Numbers in brackets may not sum up to unity because of rounding off. Mutants that are significantly different from rSkM1 are indicated by arterisks (p<0.05).

Channels	τ_1 @ -120 mV	τ_2 @ -120 mV	τ_1 @ -100 mV	τ_2 @ -100 mV	τ_1 @ -80 mV	τ_2 @ -80 mV
rSkM1	1.21 ± 0.07 (100%)	n.a.	2.11 ± 0.16 (100%)	n.a.	6.57 ± 1.09 (100 %)	n.a.
D197C *	1.25 ± 0.24 (79.2%)	8.16 ± 2.92 (22%)	1.45 ± 0.14 (83.6%)	16.42 ± 2.25 (26.9%)	3.49 ± 0.34 (67.5%)	50.79 ± 9.41 (34.2%)
F198C	1.46 ± 0.13 (96.0%)	9.07 ± 4.22 (5.5%)	2.62 ± 0.18 (95.1%)	4.54 ± 1.64 (5.3%)	6.99 ± 0.39 (86.6%)	21.62 ± 4.51 (15.3%)
F639C	0.98 ± 0.15 (100%)	n.a.	2.22 ± 0.32 (100%)	n.a.	5.91 ± 0.93 (100%)	n.a.
D640C *	2.00 ± 0.20 (100%)	n.a.	4.10 ± 0.42 (100%)	n.a.	15.22 ± 1.70 (100%)	n.a.
D1094C	1.08 ± 0.13 (97.5%)	11.41 ± 3.33 (6.0%)	2.33 ± 0.20 (97.6%)	18.51 ± 3.70 (7.6%)	5.76 ± 0.48 (89.2%)	23.29 ± 3.38 (13.2%)
F1095C	1.37 ± 0.08 (100%)	n.a.	1.87 ± 0.15 (100%)	n.a.	6.33 ± 0.55 (100%)	n.a.
F1412C *	0.69 ± 0.04 (95.2%)	16.68 ± 7.19 (5.7%)	1.21 ± 0.06 (97.2%)	58.68 ± 26.8 (3.7%)	2.13 ± 0.15 (96.8%)	153.8 ± 11.55 (5.0%)
D1413C *	1.62 ± 0.16 (95.3%)	3.23 ± 0.39 (4.6%)	2.07 ± 0.22 (88.0%)	10.52 ± 0.94 (22.2%)	3.30 ± 0.11 (58.7%)	25.61 ± 1.59 (45.5%)

resulted from changes in activation and inactivation or alteration in the coupling mechanism between these two gating processes. The voltage-dependence of τ_h of D197C channels (Figure AP.6A, open circle) were shifted to more depolarized potentials but with a far more shallow voltage-dependence. Interestingly, this flattening of the τ_h versus voltage relationship is mirrored by a marked reduction in the slopes of the steady-state activation and inactivation curves (Figure AP.2C and 5.4A). The voltage-dependence of τ_h for the D640C mutant channels (Figure AP.6A, open up trinagle) were also shifted to more depolarized potentials compared to WT channels in a manner similar to the corresponding shifts in the steady-state activation curves (Figure AP.2C). In contrast, D1413C channels (Figure AP.6A, open diamond) showed rates of current decay that were virtually voltage independent and these changes were not reflected in any of the changes in steady-state activation or inactivation (Figure AP.2C and 5.4A) suggesting a clear alteration in coupling between activation and inactivation. Of the F/C mutations, only F1412C channels (Figure AP.6B, open diamond) had notable changes in τ_h compared to WT channels. The rate of current inactivation showed a more shallow dependence on voltage when compared to WT. These changes in τ_h for F1412C channels were not reflected in changes in activation (Figure AP.3C) but rather were associated with a shift in steady-state inactivation curve to more depolarized potentials (Figure AP.4B).

E.   *Discussion*

In this report, we examined the effects of replacing highly conserved aspartate and phenylalanine residues located in S3 segments with cysteine on channel activation and inactivation in rat skeletal muscle Na^+ channel. Three of our S3 Asp-to-Cys mutants (i.e D197C, D640C and D1413C) displayed significant changes in channel behaviour compared to wild-type. For example, in D1413C channels the midpoint for steady-state inactivation was shifted in the hyperpolarizing direction while its steady-state activation curve was shifted in the opposite (depolarizing) direction. Associated with these steady-state changes, D1413C channels recovered more slowly from inactivation compared to WT channels while having slowed and largely voltage-independent rates of whole-cell current decay.

Figure AP.6

Inactivation time constants (τ_h) of whole-cell current decay of D/C mutants (Panel A) and F/C mutants (Panel B) plotted against test potentials. Inactivation time constants were estimated by fitting the decaying phase of whole-cell current beyond the peak to a mono-exponential function. The values of τ_h of rSkM1 (solid square) change steeply between -40 and 0 mV which is also the range within which activation is steeply dependent on voltage. This observation indicates that inactivation, an intrinsically voltage independent process, derives its voltage dependence by being coupled to activation. The voltage dependence of τ_h of D640C (Panel A, up triangle) was significantly shifted by 10 mV in the depolarizing direction. τ_h of D1094C (Panel A, down triangle) was also slightly shifted in the same direction. Though voltage-dependence was not completely lost, τ_h of D197C (Panel A, circle) was less dependent on voltage when compared to WT channels. Remarkably, τ_h of D1413C (Panel A, diamond) was virtually voltage independent. τ_h of F1412C (Panel B, diamond) was also less voltage dependent. However, such "apparent" decoupling was the result of its defects in channel inactivation. Other mutants displayed values of τ_h similar to those of the wild-type

.

A
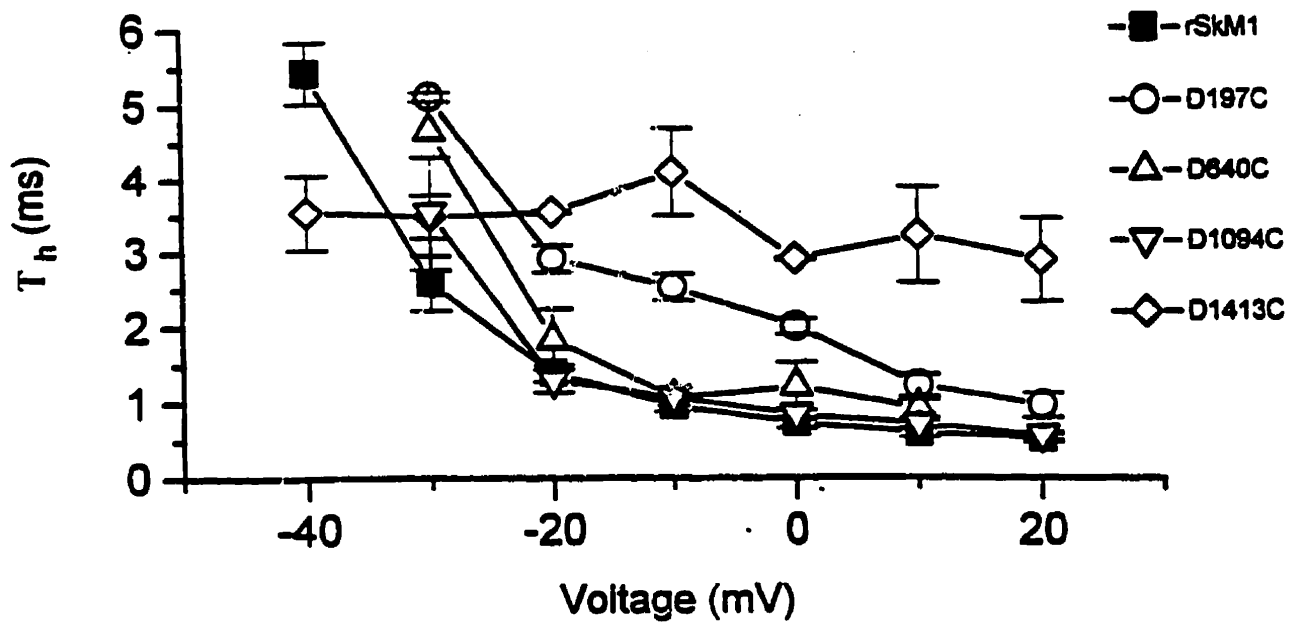
B
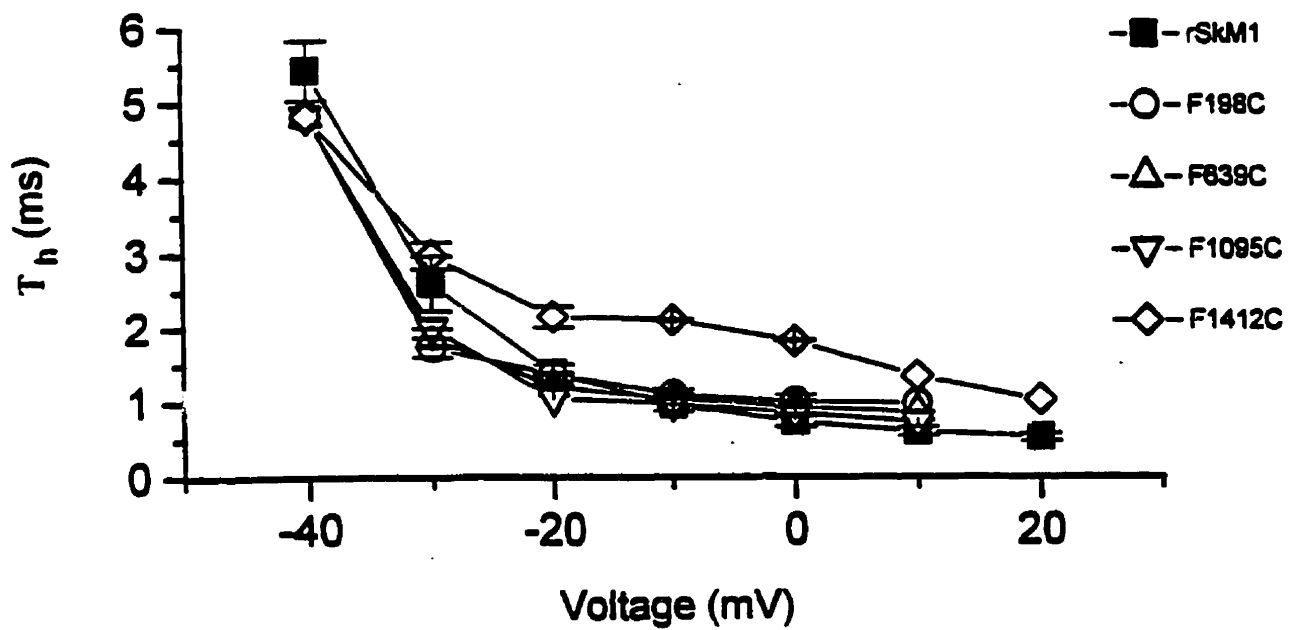
Interestingly. although there was a complete loss of voltage-dependence in τ_h. the voltage-dependences of steady-state properties. as reflected by the corresponding slope factors. were however not affected. Taken together. these results suggest that there was a clear decoupling of activation and inactivation for this mutant. Consistent with this notion. our single channel recordings showed an increased number of channel openings per sweep (WT: 1.12 ± 0.06. n=3; D1413C: 1.98 ± 0.08. n=2; HP=-120 mV, V_{test}=-20 mV). given that the channel opened at least once. We also observed a slight increase in the single channel mean first-latency time (WT: 0.93 ± 0.07 ms, n=4; D1413C: 1.19 ± 0.09 ms. n=2; HP=-120 mV, V_{test}=-20 mV) consistent with the small shift of steady-state activation observed at the whole-cell level. Since steady-state inactivation was leftward shifted and rates of recovery from inactivation were slowed. it seems probable that repeated late openings reflect a slowed entry into the inactivated state without evidence for destabilization of the inactivated conformation. This altered coupling between activation and inactivation caused by the mutation D1413C is similar to that observed in several natural mutations causing muscle myotonia (Chahine et al.. 1994; Yang et al.. 1994).

For D197C channels. the phenotypic changes observed were similar to D1413C channels except the voltage-dependence of τ_h was not completely lost. When the equivalent charge movement across the membrane field (δ) between -30 mV and 0 mV was quantified using the equation $\delta=(RT)/(\Delta V*F)*\ln[\tau_h(-30 \text{ mV})/\tau_h(0 \text{ mV})]$, the values of δ for WT and D197C were 1.5 e_o and 0.8 e_o respectively. This reduction of δ and flattening of the voltage-dependence of τ_h in D197C channels was accompanied by similar reductions in voltage-dependence of both steady-state activation and inactivation curves with reductions in effective gating charge by 1.5 and 1.7 e_o respectively when compared to WT channels. Taken together D197C also appears to be involved in coupling activation to inactivation. Furthermore, D197C channels consistently (after at least 10 rounds of injection) expressed current not more than 1 μA even after 5 days of incubation at room temperature. For this reason. we were unable to perform single-channel recordings on this mutant channel. This observation is however consistent with disruption of the structural integrity or maturation of the native channel protein in this mutant. Recently, similar

316

observations have been made in S3 in Shaker K⁻ channels at an analogous residue to D197 in Na⁻ channels (i.e. D316) which interacts with K374 in S4 within the same subunit (Tiwari-Woodruff et al., 1997). Given the analogy between K⁻ and Na⁻ channels, it seems possible that D197 may interact with a basic residue in DI/S4 (possibly K228 , the equivalence of the Shaker K374 in Domain I of rSkM1 Na⁻ channel). Further experiments examining channel protein maturation or introduction of a second rescue mutation to compensate for the structural disruptions created by mutating D197 may be useful to further study the potential roles of this residue.

Similar to D197C and D1413C, D640C channels also displayed significant changes in channel gating. However, unlike D197C and D1413C, the steepness of the voltage-dependence of τ_h for D640C channels was not noticeably affected but the entire relationship was shifted in a depolarized potential, by about 10 mV, when compared to WT channels. This shift of voltage-dependence of τ_h paralleled to the 18 mV depolarized shifts in steady-state activation curve. In addition, this mutation also caused a hyperpolarized shift in steady-state inactivation consistent with its slower rates of recovery from inactivation. At the single channel level, D640C channels showed a delay of mean first latency time (D640C: 1.52 ms, n=1; WT: 0.93 ● 0.07 ms, n=4; HP=-120 mV, V_{test}=-20 mV) without changes in the mean open time (D640C: 0.33 ms, n=1; WT: 0.31 ± 0.05 ms, n=3; HP=-120 mV, V_{test}=-20 mV) and the number of late openings (D640C: 1.07, n=1; WT: 1.12 ± 0.06, n=3, HP=-120 mV, V_{test}=-20 mV) when compared to WT channels. Given that wild-type channels normally open only once per depolarization, inactivate and do not reopen, and that activation rather than inactivation is rate-limiting (Aldrich et al., 1983), our observations suggest that this residue plays a critical role in channel activation and may affect coupling between activation and inactivation.

Overall, our D/C mutations D197C, D640C and D1413C demonstrate that these S3 aspartates play a unique role in modulating voltage-dependent channel activation as well as possibly coupling inactivation to activation. Indeed, not only were the mid-points for half-

maximal activation and inactivation shifted, but the slope factors (k) of many of these S3 mutant channels were also changed. These changes in steady-state voltage-dependence suggest that these residues may contribute to the gating charge. However, since these slope factors merely provide an indication of "apparent" gating charge, the potential roles of these residues in gating charge movement will require further studies by examining the change of gating current or the slope of the activation curve at very negative potentials (Seol et al., 1996).

Furthermore, our results indicate that these residues are not functionally equivalent and contribute differently to channel gating. In other words, individual residues at equivalent positions in all four domains contribute differently to the voltage-sensing process. In general, our data are also consistent with previous studies. It has been proposed that the S3 aspartates may form electrostatic salt bridges with the positively charged residues in S4 (Papazian et al., 1995; Durell and Guy, 1996; Ti·vari-Woodruff et al., 1997). Therefore, mutations of these residues might influence gating. Our results show that only the aspartate-to-cysteine but not the phenylalanine-to-cysteine mutants displayed significant shifts in steady-state activation despite their proximity. Neutralization of positively charged residues in S4 generally alter the voltage dependent activation and may decouple inactivation from activation (Stumer et al., 1989; Papazian et al., 1991; Logothetis et al., 1993; Chahine et al. 1994; Perozo et al., 1994; Yang and Horn; 1995; Aggarwal and MacKinnon; 1996).

In addition to shifts in channel activation, we also observed that D197C and D1413C altered coupling between activation and inactivation. These changes are similar to those observed with replacement of positive S4 charges in Na^- chann. '- and negative S2 and S3 charges in Shaker K^- channels (Papazian et al., 1995; Planells-Cases et al., 1995). Presumably, these S3 residues move during gating in a direction opposite to the movement of basic S4 residues or alternatively they may be anchored within the channel and serve to govern the cooperativity between different voltage-sensing domains during activation (Planells-Cases et al., 1995).

318

Among the S3 F/C mutants. only F1412C in domain IV displayed significant changes in channel gating. While mutations at equivalent positions in domains I. II and III (i.e. F198C. F639C and F1095C respectively) had no effects establishing that these highly conserved residues also do not contribute equally to channel gating. For F1412C channels. the magnitude of τ_h and voltage-dependence were modified compared to WT channels. Unlike the D/C mutants. these changes in τ_h were associated with rightward shifts of steady-state inactivation curve and accelerated rates of recovery from inactivation. At the single channel level. these channels had prolonged mean open times (F1412C: 0.54 ± 0.08 ms. n=3; WT: 0.31 ± 0.05 ms. n=3) and increased number of openings per sweep (F1412C: 1.79 ± 0.18 ms. n=3; WT: 1.12 ± 0.06 ms. n=3). These observations are consistent with the natural mutation (i.e. F1412L in rSkM1) associated with the horse disease hyperkalemic periodic paralysis which showed evidence for destabilization of the inactivated state (Hanna et al.. 1996). Since channel activation was not affected by this mutation. alterations of inactivation cannot be ascribed to changes in activation.

Overall. our observations are consistent with previous studies suggesting that DIV plays a unique role in sodium channel inactivation (Chahine et al., 1994; Chen et al.. 1996; Yang et al.. 1996). Previous studies have established that S4/DIV contributes to channel gating as well as the coupling between activation and inactivation. Our observations showing that D1413C decouples activation from inactivation while F1412C displayed defects in inactivation are consistent with these suggestions.

In summary, our results establish that the conservative S3 aspartate residues in rat skeletal muscle Na channel play a significant role in channel activation. These observations support the notion that the S4 segments are not solely responsible for sensing changes in transmembrane potential. In addition, the mutations of D197 and D1413 to cysteine altered coupling between activation and inactivation. Mutations of phenylalanines that are located either one residue downstream or upstream of these aspartates within the S3 segments however did not display any noticeable effects on channel activation. Nonetheless. the

mutation F1412C disrupted inactivation suggesting that this residue might be important for interactions between the inactivation gate and its receptor. Though these aspartates and phenylalanines are both highly conserved and are in such close proximity to each other, they play different roles in modulating channel activation and inactivation.

F.   *Acknowledgment*

REFERENCE

Adelman, W.J. and Y. Palti. 1969. The effects of external potassium and long duration voltage conditioning on the amplitude of sodium currents in the giant axon of the squid. *J. Gen. Physiol.* 54: 589-606.

Aggarwal, S.K., R. MacKinnon 1996. Contribution of the S4 segment to gating charge in the Shaker K^+ channel. *Neuron* 16, 1169-1177.

Akabas, M.H., D.A. Stauffer, M. Xu, and A. Karlin. 1992. Acetylcholine receptor channel structure probed in cysteine-substitution mutants. *Science* 258:307-310.

Akabas, M.H., C. Kauffmann, P. Archdeacon and A. Karlin. 1994a. Identification of acetylcholine receptor channel-lining residues in the entire M2 segment of the alpha-subunit. *Neuron* 13:919-927.

Akabas, M.H., C. Kauffmann, T.A. Cook and P. Archdecon. 1994b. Amino acid residues lining the chloride channel of the cystic fibrosis transmembrane regulator. *J. Biol. Chem.* 269:14865-14868.

Akopian, A.N., Sivilotti, L. & Wood, J.N. A tetrodotoxin-resistant voltage-gated sodium channel expressed by sensory neurons. *Nature* 379, 257-262 (1996).

Aldrich, R.W., D.P. Corey, C.F. Stevens. 1983. A reinterpretation of mammalian sodium channel gating based on single channel recording. *Nature* 306(5942):436-441.

Almers, W. (1978). Gating currents and charge movements in excitable membranes. *Rev. Physiol. Biochem. Pharmacol.* 82, 96-190.

Almers, W. and E.W. McCleskey. 1984. Non selective conductance in calcium channels of frog muscle: calcium selectivity in a single file pore. *J. Physiol.* 353: 585-608.

Almers. W.. E.W. McClesky and P.T. Palade. 1984. A non-selective cation conductance in frog muscle membrane blocked by micro-molar external calcium ions. *J. Physiol. (Camb.).* 353:565-583.

Albuquerque EX, Daly JW, Witkop B. 1971. Batrachotoxin: chemistry and pharmacology. *Science* 172(987):995-1002

Albuquerque EX, Warnick JE, Sansone FM. Daly J. 1973. The pharmacology of *batrachotoxin. V.* A comparative study of membrane properties and the effect of batrachotoxin on sartorius muscles of the frogs *Phyllobates aurotaenia* and *Rana pipiens. J Pharmacol Exp Ther* 184(2):315-329

Alpert L.A.. H.A. Fozzard. D.A. Hanck. J.C. Makielski. 1989. Is there a second external lidocaine binding site on mammalian cardiac cells? Am J Physiol 257: H79-H84.

Anderson PA. Holman MA. Greenberg RM. Deduced amino acid sequence of a putative sodium channel from scyphozoan jellyfish *Cyanea capillata. Proc Nat Aca-d Sci 1993;* 90:7419-7423.

Armstrong, C.M. 1971. Interaction of tetraethylammomium ion derivatives with the potassium channels of giant squid axons. *J. Gen. Physiol.* 58:413-437

Armstrong, C.M. 1975. Ionic pores, gates, and gating currents. *Q. Rev. Biophys.* 7:179-210

Armstrong, C.M. 1981. Sodium channels and gating currents. *Physiol. Rev.* 61:644-683.

Armstrong, C.M. 1998. The vision of the pore. *Science (Wash. D.C.)* 280:56-57.

Armstrong, C. M. and F.. Bezanilla. 1973. Currents related to movement of the gating

particles of the sodium channels. *Nature (London)* 242, 459-461.

Armstrong, C. M., F., Bezanilla, E. Rojas. 1973. Destruction of sodium conductance inactivation in squid axons perfused with pronase. *J. Gen. Physiol.* 62, 375-391

Armstrong, C. M. and F., Bezanilla. 1974. Charge movement associated with the opening and closing of the activation gates of the Na+ channels. *J. Gen. Physiol.* 63, 533-552.

Armstrong CM, Bezanilla F. 1977. Inactivation of the sodium channel. II. Gating current experiments. *J Gen Physiol* 70(5):567-590

Armstrong, C.M. and J. Neyton. 1992. Ion permeation through calcium channels: a one-site model. *Ann. NY Acad. Sci.* 635: 18-25

Arnold, G.E., Manchester J.i., Townsend B.D. and Ornstein R.L. 1994. Investigation of domain motions in bacteriophage T4 lysozyme. *J. Biomol. Struct. Dyn.* 12:457-474

Auld V.J., A.L. Goldin, D.S. Krafte, J. Marshall, J.M. Dunn, W.A. Catterall, H.A. Lester, N. Davidson, R.J. Dunn. 1988. A rat brain Na$^+$ channel a subunit with novel gating properties. *Neuron* 1:449-461.

Auld VJ, Goldin AL, Krafte DS, Catterall WA, Lester HA, Davidson N, Dunn RJ. 1990. A neutral amino acid change in segment IIS4 dramatically alters the gating properties of the voltage-dependent sodium channel. *Proc Natl Acad Sci U S A* 87(1):323-327

Backx, P., D. Yue, J. Lawrence, E. Marban, and G. Tomaselli. 1992. Molecular localization of an ion-binding site within the pore of mammalian sodium channels. *Science.* 257:248-251.

Balaji, V.N., Mobasser A. and Rai S.N. 1989. Modification of protein stability by introduction of disulfide bridges and prolines: geometric criteria for mutation sites.

Biochem. Biophys. Res. Commun. 160:109-114

Balser, J.R., H.B. Nuss, N. Chiamvirnonvat, M.T. Perez-Garcia, E. Marban, and G.F. Tomaselli. 1996. External pore residues mediates slow inactivation in μ1 rat skeletal muscle sodium channels. *J. Physiol. (London)* 494.2:431-442.

Barchi RL. 1988. Probing the molecular structure of the voltage-dependent sodium channel. *Annu Rev Neurosci* 11: 455-495.

Barnard, E.A., Mileai, F., Sumikawa, K. 1982. Translation of exogenous messenger RNA coding for nicotinic acetylcholine receptors induces functional receptor in Xenopus oocytes. *Proc. R. Soc. Lond.* B215:241-246.

Baumann A, Grupe A, Ackermann A, Pongs O. 1988. Structure of the voltage-dependent potassium channel is highly conserved from Drosophiia to vertebrate central nervous systems. *EMBO J* (8):2457-2463

Becker, S., E. Prusak-Sochazewski, G.Zamponi, A.G. Beck-Sickinger, R.D. Gordon, and R.J. French. 1992. Action of derivatives of μ-conotoxin GIIIA on sodium channels. Single amino acid substitutions in the toxin separately affect association and dissociation rates. *Biochemistry.* 31:8229-8238.

Begenisich, T. 1987. Molecular properties of ion permeation through sodium channels. *Ann. Rev. Biophys. Chem.* 16: 247-263.

Bendahhou, S., Cummins, T., Potts, J., Tong, J. & Agnew, W. (1995). Serine-1321-independent regulation of the μ1 adult skeletal muscle Na+ channel by protein kinase C. *Proceedings of the National Academy of Sciences of the USA* 92, 12003-12007.

Benitah, J.P., G.F. Tomaselli, and E. Marban. 1996. Adjacent porelining residues within sodium channels identified by paired cvsteine replacements. *Proc. Natl Acad. Sci.*

USA. 93:7392-7396.

Benitah, J.P., R. Ranjan, T. Yamagishi, M. Janecki, G.F. Tomaselli, and E. Marban. 1997. Molecular motions within the pore of voltage-dependent sodium channels. *Biophys. J.* 73: 603-613.

Bennett PB Jr, Makita N, George AL Jr. 1993. A molecular basis for gating mode transitions in human skeletal muscle Na$^+$ channels. *FEBS Lett* 326(1-3):21-24

Bennett, P.B., C. Valenzuela, L.Q. Chen and R.G. Kallen. 1995. On the molecular nature of the lidocaine receptor of cardiac Na$^+$ channels. Modification of block by alterations in the α-subunit III-IV interdomain. *Cir. Res.* 77: 584-592.

Bennett, E., Urcan, M., Tinkle, S., Koszowski, A. & Levinson, S. (1997). Contribution of sialic acid to the voltage dependence of sodium channel gating. A possible electrostatic mechanism. Journal of General Physiology 109, 327-343.

Berger HA, Travis SM, Welsh MJ. 1993. Regulation of the cystic fibrosis transmembrane conductance regulator Cl- channel by specific protein kinases and protein phosphatases. *J Biol Chem* 268(3):2037-2047

Bezanilla, F. and C. Armstrong. 1972. Negative conductance caused by entry of sodium and cesium ions into the potassium channel in squid axons. *J. Gen. Physiol.* 60. 588, 50: 533-575.

Bezanilla F, Armstrong CM. 1974. Gating currents of the sodium channels: three ways to block them. *Science* 183(126):753-754

Bezanilla F, Armstrong CM. 1975. Kinetic properties and inactivation of the gating currents of sodium channels in squid axon. *Philos Trans R Soc Lond B Biol Sci* 270(908):449-458

Bezanilla F. Armstrong CM. 1977. Inactivation of the sodium channel. I. Sodium current experiments. *J Gen Physiol* 70(5):549-566

Bezanilla, F. and E. Stefani. 1994. Voltage-dependent gating of ionic channels. *Annual Review of Biophysics and Biomolecular Structure* 23, 819-846.

Bogartz, R.S. 1994. An Introduction to the Analvsis of Variance. Praeger Publishers Inc.. Westport, CT. 233-348.

Branden, C. and Tooze. J. (1991). Introduction to protein structure. Garland Publishing Inc, New York. pp 11-77.

Brown GB. 1988. Batrachotoxin: a window on the allosteric nature of the voltage-sensitive sodium channel. *Int Rev Neurobiol* 29:77-116

Butterworth, J. F. IV, and G. R. Strichartz. Molecular mechanisms of local anaesthesia: A Review. *Anesthesiology* 72: 711-734, 1990.

Camm AJ, Redwood SR.. Peri-infarction arrhythmias. 1995. Chapter 60 in Cardiac Arrhythmia: mechanisms, diagnosis and management. Editors: Podrid and Kowey. Williams and Wilkins. Baltimore. pp 1239-1252.

Cannon, S.C., A. I. McClatchey, and J.F. Gusella. 1993. Modification of the Na$^+$ current conducted by the rat skeletal muscle α subunit by coexpression with a human brain β subunit. *Pflugers Archiv.* 423:155-157.

Cannon, S.C. and S.M. Strittmatter. 1993. Functional expression of sodium channel mutations identified in families with periodic paralysis. *Neuron* 10, 317-326.

Cannon, S.C. 1996. Slow inactivation of sodium channels: more than just a laboratory curious. *Biophys. J.* 71: 5-7.

Cantrell. A.. Smith. R.. Goldin. A.. Scheuer. T. & Catterall. W. (1997). Dopaminergic modulation of sodium current in hippocampal neurons via cAMP-dependent phosphorylation of specific sites in the sodium channel subunit. Journal of Neuroscience 17, 7330-7338.

Careaga. C.L.. and J.J. Falke. 1992. Structure and dynamics of Escherichia coli chemosensory receptors. Engineered sulfhydryl studies. *Biophys.J.* 62:209-216.

Catterall WA. 1981. Localization of sodium channels in cultured neural cells. *J Neurosci* 1(7):777-783

Catterall. W.A. 1988. Structure and function of voltage-sensitive ion channels. *Science* 242. . 50-61

Catterall. W. A. 1992. *Physiol. Rev.* 72 (Suppl.). S15-S48.

Catterall, W.A. 1995. Structure and function of voltage-gated ion channels. *Annu. Rev. Biochem.* 64:493-531.

Catterall WA. Beneski DA. 1980. Interaction of polypeptide neurotoxins with a receptor site
associated with voltage-sensitive sodium channels. *J Supramol Struct* 14(3):295-303

Catterall WA, Gainer M. 1985. Interaction of brevetoxin A with a new receptor site on the sodium channel. *Toxicon* 23(3):497-504

Catterall, W.A. and J. Striessnig. 1992. *Trends Pharmacol. Sci. 13*, 256-262.

Cha. A.. F. Bezanilla. 1997. Characterizing voltage-dependent conformational changes in the Shaker K$^-$ channel with fluorescence. *Neuron* 19: 1127-1140.

Chahine. M.. A.L. George. Jr.. M. Zhou. S. Ji. W. Sun, R.L. Barchi, R. Hom. 1994. Sodium channel mutations in paramyotonia congenita uncouple inactivation from activation. *Neuron* 12. 281-294.

Chahine. M.. L.-Q. Chen, N. Fotouhi, R. Walsky, D. Fry, R. Horn, and R.G. Kallen. 1995. Characterizing the μ-Conotoxin binding site on Na channel with toxin analogues and channel mutations. *Receptors and Channels*. 3(3):164-74.

Chahine M.. L. Deschene, L.Q. Chen, R.G. Kallen. 1996. Electrophysiological characteristics of cloned skeletal and cardiac mucle sodium channels. *Am. J. Physiol.* 271:H498-H506

Chahine. M.. J. Sirois. P. Marcotte. L.-Q. Chen and R.G. Kallen. 1998. Extrapore residues of the S5-S6 loop of domain 2 of the voltage-gated skeletal muscle sodium channel (rSkM1) contribute to the μ-Conotoxin GIIIA binding site. *Biophys. J.* 75: 236-246.

Chandler WK, Meves H. 1970. Slow changes in membrane permeability and long-lasting action potentials in axons perfused with fluoride solutions. *Physiol (Lond)* 211(3):707-728

Chang SY. Satin J. Fozzard HA. 1996. Modal behavior of the μ1 Na$^+$ channel and effects of coexpression of the beta I-subunit. *Biophys J* 70(6):2581-2592

Chang, N.S.. R.J. French. G.M. Lipkind, H.A. Fozzard and S. Dudley Jr. 1998. Predominant interactions between μ-conotoxin Arg-13 and the skeletal muscle Na$^+$ channel localized by mutant cycle analysis. *Biochemistry* 37: 4407-4419.

Chen, C.F. and S.C. Cannon. 1995. Modulation of Na$^+$ channel inactivation by the beta 1 subunit: a deletion analysis. *Pfluegers Arch.* 431: 186-195

Chen, L.-Q., M. Chahine, R.G. Kallen, R.L. Barchi, and R. Horn. 1992. Chimeric study of sodium channels from rat skeletal and cardiac muscle. *FEBS Lett.* 309:253-257

Chen, L.Q., V. Santarelli, R. Horn, R.G. Kallen. 1996. A unique role for the S4 segment of domain 4 in the inactivation of sodium channels. *J.Gen. Physiol.* 108. 549-556.

Chiamvimonvat, N., M. Perez-Garcia, R. Ranjan, E. Marban, and G.F. Tomaselli. 1996. Depth assymetries of the pore-lining segments of the sodium channel revealed by cysteine mutagenesis. *Neuron.* 16:1037-1047.

Chiamvimonvat, N., M.T. Pérez-García, G.F. Tomaselli, and E. Marban. 1996b. Control of ion flux and selectivity by negatively charged residues in the outer mouth of rat sodium channels. *J. Physiol. (Lond.)* 491:51-59.

Choi, K.L., R.W. Aldrich and G. Yellen. 1991. Tetraethylammonium blockade distinguishes two inactivation mechanisms in voltage-activated K^+ channels. *Proc. Natl. Acad. Sci. U.S.A.* 88: 5092-5095.

Choi, K.L., C. mossman, J. Aube and G. Yellen. 1993.. *Neuron.* 10: 533-541.

Ciani S. 1984. Coupling between fluxes in one-particle pores with fluctuating energy profiles. A theoretical study. *Biophys J.* 46(2): 249-252.

Cohen SA, Levitt LK. 1993. Partial characterization of the rH1 sodium channel protein from rat heart using subtype-specific antibodies. *Circ Res* 73(4):735-742

Cohn JN. Drug treatment of heart failure. Advances in Therapeutic Conununications International, Secaucus, New Jersey, USA. 1988.

Cole, K.S., 1968. *Membranes, Ions and Impulses: A Chapter of Classical Biophysics.* University of California Press, Berkeley, pp.569

Colquhoun, D. and F.J. Sigworth. 1983. Fitting and statistical analysis of single-channel records. In Single-Channel Recording, ed. Sakmann, B. and Neher E., pp 191-263

Plenum Press. New York.

Colquhoun LM. Patrick JW. 1997. Pharmacology of neuronal nicotinic acetylcholine receptor subtypes. *Adv Pharmacol* 39:191-220

Cotton. F.A., and G. Wilkinson. 1992. Advanced Inorganic Chemistry. A Comprehensive Text 3rd ed. Interscience Publishers, New York.503-527.

Cottrell. T.J., Harris, L.J., Tanaka. T. and Yada, R.Y. (1995). The sole lysine residue in porcine pepsin works as a key residue for catalysis and conformational flexibility. *J. Biol. Chem.* 34, 19974-19978.

Courtney, K.R. 1975. Mechanisms of frequency-dependent inhibition of sodium currents in frog myelinated berve by the lidocaine derivative GEA 968. *J. Pharmacol. Exp. Ther.* 195:225-236

Creighton, T.E. 1993. Proteins. Structures and Molecular Properties. W. H. Freeman and Company, New York.

Cruz. L. J., W.R. Gray, B.M. Olivera. R.D. Zeikus, L. Kerr. D. Yoshikami, and E. Moczydlowski. 1985. Conus geographus toxins that discriminate between neuronal and skeletal muscle sodium channels. *J. Biol. Chem.* 260:9280-9288.

Cummins, T.R., and F.J. Sigworth. 1996. Comparison of slow inactivation in HYPP-T698M and F1304Q mutant rat skeletal muscle Na$^+$ channels. *Biophys. J.* 70: A132.

Cummins, T.R., and F.J. Sigworth, 1996. Impaired slow inactivation in mutant skeletal muscle Na$^+$ channels. *Biophys. J.* 71: 227-236.

Dang T.X. and E.W. McCleskey. 1998. Ion channel selectivity through stepwise changes in binding affinity. *J. Gen. Physiol.* 111: 185-193.

330

DeLuca. A., T. Probstle. H. Braeier. and R. Riidel. The different use dependences of tocainide and benzocaine are correlated with different effects on sodium channel inactivation. *Naunyn-Schmiedeberg's Arch. Pharmacol.* 344: 596-601, 1991.

Diebler. H.. M. Eigen. G. Iigenfritz. G. Maas and R. Winkler. 1969. Kinetics and mechanism of reactions of main group metal ions with biological carriers. *Pure Appl. Chem.* 20:93-115.

Doring, F.. V.E. Degtiar. M. Grabner. J. Stressnig. S. Hering and H. Glossman. 1996. Transfer of L-type Ca^{2+} channel IVS6 segment increases phenylalkylamine sensitivity of α_{1A}. *J. Biol. Chem.* 271: 11745-11749.

Dougherty. D.A. 1996. Cation-π interactions in chemistry and biology: A new view of benzene. Phe. Tyr. and Trp. *Science (Wash. DC)* 271:163-168.

Doyle DD. Guo Y. Lustig SL. Satin J, Rogart RB. Fozzard HA. 1993. Divalent cation competition with [3H]saxitoxin binding to tetrodotoxin-resistant and -sensitive sodium channels. A two-site structural model of ion/toxin interaction. *J Gen Physiol* 101(2):153-82

Doyle. D.A.. J.M. Cabral. R.A. Pfuetzner. A. Kuo. J.M. Gulbis. S.L. Cohen. B.T. Chait and R. MacKinnon. 1998. The structure of the potassium channel: Molecular Basis of K^+ conduction and selectivity. *Science (Wash. D.C.)* 280:69-77.

Dudley S.C. Jr., T. Hannes, Lipkind G., Fozzard H.A. 1995. A μ-Conotoxin-Insensitive Na^+ Channel Mutant: Possible localization of a binding site at the outer vestibule. *Biophys. J.* 69(5):1657-65.

Duff, H.. Offord. J.. West. J. & Catterall. W. (1992). Class I and IV antiarrhythmic drugs and cytosolic calcium regulate mRNA encoding the sodium channel subunit in rat cardiac muscle. *Molecular Pharmacology* 42, 570-574.

Durell S.R. and R.H. Guy. 1996. Structural model of the outer vestibule and selectivity filter of the Shaker voltage-gated K⁺ channel. *Neuropharmacology* 35(7): 761-773

Durell. S.R. and H.R. Guy. 1992. Atomic scale structure and functional models of voltage-gated potassium channels. *Biophys. J.* 62:238-250.

Eaholtz G, Scheuer T, Catterall WA. 1994. Restoration of inactivation and block of open sodium channels by an inactivation gate peptide. *Neuron* 12(5):1041-1048

Eaton DC, Brodwick MS, Oxford GS, Rudy B. 1978. Arginine-specific reagents remove sodium channel inactivation. *Nature* 271(5644):473-476

Ehring, G.R.. Moyer, J.W. & Hondeghem. L.M. Quantiative structure activity studies of antiarrhythmic properties in a series of lidocaine and procainamide derivatives. *J Pharmacol Expt Ther* **244**. 479-492 (1988)

Eigen M, Winkler R. 1971. Carriers and specificity in membranes. II. Characteristics of carriers. Alkali ion carriers: specificity, architecture. and mechanisms: an essay. *Neurosci Res Program Bull* 9(3):330-338

Eisenberg, R. 1990. Channels as enzymes. *J. Membr. Biol.* 115:1-12.

Eisenman, G. 1984. Ion Transport Through Membranes. B. Pullman and K. Yagi, editors. Academic Press, NewYork. 101-129.

Eisenman, G. and R. Horn. 1983. Ionic selectivity revisited: The role of kinetic and equilibrium processes in ion permeation through channels. *J. Membr. Biol.* 76:197-225.

Elliott, J.R., Haydon. D.A. & Hendry, B.M. Local anaesthetic effects of benzene and structurally related molecules, including benzocaine, on the squid giant axon. *Pflügers Arch.* **409**, 589-595 (1987).

Ellinor. P.T.. J. Yang. W.A. Sather. J.-F. Zhang. and R.W. Tsien. 1995. Ca^{2-} channel selectivity at a single locus for high-affinity Ca^{2+} interactions. *Neuron* 15:1121-1132.

Elliott JR, Haydon DA. Hendry BM. Local anaesthetic effects of benzene and structurally related molecules, including benzocaine, on the squid giant axon. *Pflügers Arch.* 1987;409:589-595.

Ellis SB. Williams ME. Ways NR. Brenner R. Sharp AH. Leung AT. Campbell KP, McKenna
E. Koch WJ. Hui A. et al. 1988. Sequence and expression of mRNAs encoding the alpha 1 and alpha 2 subunits of a DHP-sensitive calcium channel. *Science* 241(4873):1661-1664

Eyring. H.. R. Lumry and J.W. Woodbury. 1949. Some applications of modem rate theory to physiological systems. *Rec. chem. Prog.* 100:100.

Falke, J.J. A.F. Dernburg, D.A. Sternberg, N. Zalkin. D.L. Milligan and D.E. Koshland. 1988. Structure of a bacterial sensory receptor. A site-directed sulfhydryl study. J. Biol. Chem. 263:14850-14858.

Favre. I.. E. Moczydlowski. and L. Schild. 1996. On the structural basis for ionic selectivity among Na^+. K^+, and Ca^{2+} in the voltage-gated sodium channel. *Biophys. J.* 71:3110-3125.

Featherstone D.E.. J.E. Richmond. P.C. Ruben (1996). Interaction between fast and slow inactivation in rSkM1 sodium channels. *Biophys J* 71(6):3098-3109.

Fersht, A. (1985). *Enzyme structure and mechanism.* W. H. Freeman and Company. New York. NY. 2nd Edition. pp 311-344.

Filatov, G.N., S.D. Kraner and R.L. Barchi. 1997. *Biophys. J.* 72: A260.

Fleig A. Fitch JM, Goldin AL. Rayner MD. Starkus JG. Ruben PC. 1994. Point mutations in

IIS4 alter activation and inactivation of rat brain IIA Na channels in *Xenopus* oocyte macropatches. *Pflugers Arch* 427(5-6):406-413

Fox, J.M. 1976. Ultra-slow inactivation of the ionic currents through the membrane of myelinated nerve. *Biochim. Biophys. Acta.* 426: 232-244.

Fozzard H.A., D.A. Hanck. 1996. Structure and function of voltage-dependent sodium channels: comparison of brain Ii and cardiac isoforms. *Physiol Rev* 76: 887-926

Frazier, .T., T. Narahashi and M Yamada. 1970. The site of action and active form of local anesthetics. II. Experiments with quaternary compunds. *J. Pharmacol. Exp. Ther.* 171: 45-51.

French RJ. Shoukimas JJ. 1985. An ion's view of the potassium channel. The structure of the permeation pathway as sensed by a variety of blocking ions. *J Gen Physiol.* 85(5):669-698

French, R.J., Prusak-Sochaczewski. E., Zamponi. G.W., Becker. S., Kularanta. A.S., Horn, R. 1996. Interactions between a pore-blocking peptide and the voltage-sensor of the sodium channel: An electrostatic approach to channel geometry. *Neuron. 16, 407-413.*

Frelin C, Cognard P, Vigne P, Lazdunski M: Tetrodotoxin-sensitive and tetrodotoxin-resistant Na⁻ channels differ in their sensitivity to Cd^{2+} and Zn^{2+}. *Eur J Pharmacol* 1986: 122:245-250.

Friel, D.D. and R.W. Tsien. 1989. Voltage-gated calcium channels: direct observation of the anomalous mole fraction effect at the single channel level. *Proc. Natl. Acad. Sci. USA* 86: 5207-5211.

Frohnwieser, B., Chen, L., Schreibmayer, W. & Kallen, R. (1997). Modulation of the human cardiac sodium channel -subunit by cAMP-dependent protein kinase and the

responsible sequence domain. Journal of Physiology 498. 30ᵒ-318.

Frohnwieser, B., Weigl, L. & Schreibmayer, W. (1995). Modulation of cardiac sodium channel isoform by cyclic AMP dependent protein kinase does not depend on phosphorylation of serine 1504 in the cytosolic loop interconnecting transmembrane domains III and IV. Pflügers Archiv 430, 751-753.

Garcia J, Nakai J, Imoto K, Beam KG. 1997. Role of S4 segments and the leucine heptad motif in the activation of an L-type calcium channel. *Biophys J* 72(6):2515-2523

Gellens, M.E., George, A.L., Chen, L., Chahine, M., Horn, R., Barchi, R.L & Kallen, R.G. Primary structure and functional expression of the human cardiac tetrodotoxin-insensitive voltage-dependent sodium channel *Proc. Natl. Acad. Sci. U.S.A.* **89**, 554-558 (1992).

Gershon, E., Weigl, L., Lotan, I., Schreibmayer, W. & Dascal, N. (1992). Protein kinase A reduces voltage-dependent Na+ current in Xenopus oocytes. Journal of Neuroscience 12, 3743-3752.

Gianelly, R., J. O. van der Groeben, A. P. Spivack and D.C. Harrison. 1967. Effects of lidocaine on ventricular arrhythmias in patients with coronary heart diseases. *N. Eng. J. Med.* 277: 1215-1219.

Gingrich K.J., D. Beardsley D., D.T. Yue. 1993. Ultra-deep blockade of Na^+ channels by a quaternary ammonium ion: catalysis by a transition-intermediate state? *J. Physiol. (London)* 471:319-341.

Goldin, A. L. 1994. Voltage-gated sodium channels. Handbook of receptors and channels. Ligand and voltage-gated ion channels, edited by R.A. North. *Boca Raton, FL:* CRC. 1994. vol II, p73-112.

Goldman. L. and C.L. Schauf. 1972. Inactivation of the sodium current in Myxiola giant axons. Evidence of coupling to the actiavtion process. *J. Gen. Physiol.* 59: 659-675.

Goldstein. S.A.N.. D.J. Pheasant. C. Miller. 1994. The charybdotoxin receptor of a Shaker K⁺ channel: peptide and channel residues mediating molecular recognition. *Neuron. 12. 1377-1388.*

Gray, W.R., B.M. Olivera. L.J. Cruz. 1988. Peptide toxins from venomous Conus snails. *Annu. Rev. Biochem.* 57, 665-700.

Grant A.O.. M.A. Dietz. F.R. Gilliam 3rd. C.F. Starmer. 1989. Blockade of cardiac sodium channels by lidocaine. Single-channel analysis. *Circ Res* 65: 1247-1262

Grant. A.O. 1991. Models of drug interaction with the sodium channel. *Clin. Invest. Med.* 14: 447-457

Greenblat. R.E.. Y. Blatt and M. Montal (1985). The structure of the voltage-gated sensitive Na⁺ channel. Inferences derived from computer aided analysis of the Electrophorous eletricus channel primary structure. *FEBS Lett.* 193, 125-134.

Grenningloh G. Gundelfinger E. Schmitt B. Betz H. Darlison MG. Barnard EA. Schofield PR, Seeburg PH. 1987a. Glycine vs GABA receptors. *Nature* 330(6143):25-26

Grenningloh G, Rienitz A, Schmitt B, Methfessel C. Zensen M, Beyreuther K. Gundelfinger ED. Betz H. 1987b. The strychnine-binding subunit of the glycine receptor shows homology with nicotinic acetylcholine receptors. *Nature* 328(6127):215-220

Gross. A and R. MacKinnon. 1996. Agitoxin footprinting the Shaker potassium channel pore. *Neuron. 16, 399-406.*

Gurdon, J.B. Lane. C. D.. Woodliand, H.R.. Marbaix, G. 1971. Use of frog eggs and oocytes

for the study of messenger RNA and its translation in living cells. *Nature.* 233:177-178.

Guy, H. R. and F. Conti. 1990 *Trends Neurosci.* 201-206

Guy, H.R.. and S.R. Durell. 1995. Structural models of Na', Ca2' and K' channels. In Ion Channels and Genetic Diseases. D.C. Dawson and R.A. Frizzell, edito rs. Rockefeller University Press, New York. 1-16.

Hamill, O.P., Marty, A.. Neher, E.. Sakmann, B. and Sigworth. F.J. 1981. Improved patch-clamp techniques for high-resolution current recording from cells nad cell-free membrane patches. *Pflugers Archiv* 391. 85-100.

Hanna W.J.B.. R.G. Tsushima. R. Sah. L.J. McCutcheon. E. Marban. P.H. Backx. 1996. The equine periodic paralysis Na$^+$ channel mutation alters molecular transitions between the open and inactivated states. *J. Physiol. (London)* 1996: 497-364.

Harrison D.A.. Winkle R.A.. Sami M., Mason J. (1981) in Cardiac arrhythmias: A decade of progress. Boston. Mass. GK Hall.

Hartmann, H.A.. G.E. , J.A. Drewe. M. Taglialatela, R.H. Joho. and A.M. Brown. 1991. Exchange of conduction pathways between two related K$^+$ channels. *Science (Wash. DC)* 251:942-944.

Hayward, L.J.. R.H. Brown Jr. and S.C. Cannon. 1997. Slow inactivation differs among mutant Na channels associated with myotonia and periodic paralysis. *Biophys. J.* 72: 1204-1219.

Heginbotham, L.. T. Abramson. and R. MacKinnon. 1992. A functional connection between the pores of distinctly related ion channels as revealed by mutant K$^+$ channels. *Science (Wash. DC).* 258:1152-1155.

Heginbotham, L and R. MacKinnon. 1992. The aromatic binding site for tetraethylammonium ion on potassium channels. *Neuron* 8:483-491.

Heginbotham, L., Z. Lu, T. Abramson, and R. MacKinnon. 1994. Mutations in the K⁻ channel signature sequence. *Biophys. J.* 66:1061-1067.

Heinemann, S.H., H. Terlau, W. Stühmer, K. Imoto, and S. Numa. 1992a. Calcium channel characteristics conferred on the sodium channel by single mutations. *Nature (Lond.)* 356:441-443.

Heinemann SH, Terlau H, Stuhmer W, Imoto K, Numa S. 1992b. Calcium channel characteristics conferred on the sodium channel by single mutations. *Nature* 356(6368):441-3

Hescheler, J., G. Pelzer, G. Trube abd W. Trautwein. 1982. Does the organic Ca^{2+} channel blocker D600 act from the outside or inside of the cell membrane? *Pflueg. Arch. Eur. J. Physiol.* 393: 287-291.

Hess, P., J.B. Lansman, and R.W. Tsien. 1986. Calcium channel selectivity for divalent and monovalent cations. Voltage and concentration dependence of single channel currnet in ventricular heart cells. *J. Gen. Physiol.* 88:293-319.

Hess, P. and R.W. Tsien. 1984. Mechanism of ion permeation through calcium channels. *Nature.* 309:453-456.

Heinemann, S.H., H. Terlau, and K. Imoto. 1992. Molecular basis f·r pharmacological differences between brain and cardiac sodium channels. *Pflügers Arch* 422:90-92.

Heinemann, S.H., H. Terlau, W. Stuhmer, K. Imoto, S. Numa. 1992. Calcium channel characteristics conferred on the sodium channel by single mutations. *Nature* 356, 441-444.

Hess P. Tsien RW. 1984. Mechanism of ion permeation through calcium channels. *Nature* 309(5967):453-456

Hidalgo, P., and R. Mackinnon. 1995. Revealing the architecture of a K+ channel pore through mutant cycles with a peptide inhibitor. *Science (Wash. DC)*. 268:307-3 1 0.

Hill J.M., P.F. Alewood, D.J. Craik. 1996. Three-dimensional solution structure of μ-conotoxin GIIIB, a specific blocker of skeletal muscle sodium channels. *Biochemistry*. 35(27):8824-35.

Hille, B. 1971. The permeability of the sodium channel to organic cations in myelinated nerve. *J Gen Physiol*; 58:599-619.

Hille, B. 1972. The permeability of the sodium channel to metal cations in myelinated nerve. *J. Gen. Physiol.* 59:637-658.

Hille, B. 1973. Potassium channels in myelinated nerve. Selective permeability to small cations *J. Gen. Physiol.* 61, 669-686.

Hille, B. 1975. Ionic selectivity, saturation and block in sodium channels. A four-barrier model. *J. Gen. Physiol.* 66: 535-560.

Hille, B. 1977. Local anesthetics: hydrophilic and hydrophobic pathways for the drugreceptor reaction. *J. Gen. Physiol.* 69:479-515.

Hille, B. 1978. Local anesthetic action on inactivation of the Na$^+$ channel in nerve and skeletal muscle. Biophysical Aspects of Cardiac Muscle. M. Morad, editor. *Academic Press Inc.. New York*. 55-74.

Hille, B. 1992. *Ionic Channels of Excitable Membranes* , Second Edition. Sinauer Associates Inc.. Sunderland, Massachussetts.

Hille. B. and W. Schwartz. 1978. Potassium channels as multi-ion single-file pores. *J. Gen. Physiol.* 72:409-442.

Hockerman. G.H., B.D. Johnson. T. Scheuer and W.A. Catterall. 1995. Molecular determinants of high-affinity phenyalkylamine block of L-type calcium channel. *J. Biol. Chem.* 270: 22119-22122.

Hodgkin, A.L. and P. Horowicz. 1960. Potassium contracture in single muscle fibres. *J. Physiol. (London)* 153: 386-403.

Holmgren. M., M.E. Jurman and G. Yellen. 1996. *J. Gen. Physiol.* 108: 195-206.

Hondeghem. L.M. and B.G. Katzung. 1977. Time- and voltage-dependent interactions of anti-arrhythmic drugs with cardiac sodium channels. *Biochim. Biol)hys. Acta* 472:373-398

Horn R. Patlak J. Stevens CF. 1981. Sodium channels need not open before they inactivate. *Nature* 291(5814):426-427

Hoshi. T., W.N. Zagotta and R.W. Aldrich. 1990. Biophysical and molecular mechanisms of Shaker potassium channel inactivation. *Science (Wash. DC).* 250: 533-538.

Hoyt. R.C. 1965. The squid giant axon: mathematical models. *Biophys. J.* 3: 399-431.

Hudson A.J., G. C. Ebers and D. E. Bulman. 1995. Review: The skeletal muscle sodium and chloride channel diseases. *Brain* 118:547-563.

Isacoff EF, Jan LY. 1991. Putative receptor for the cytoplasmic inactivation gate in Shaker K *channels. Nature (Lond)* 353:86-90.

Isom. L.L.. K.S. DeJongh. D.E. Patton. B.F.X. Reber. J. Offord. H. Carbonneau. K. Walsh. A.L. Goldin. and W.A. Catterall. 1992. Primary structure and functional expression of the ß₁-subunit of the rat brain sodium channel. *Science* 256:839-842.

Isom. L.. Ragsdale. D.. De Jongh. K.. Westenbroek. R., Reber. B.. Scheuer. T. & Catterall, W. (1995). Structure and function of the 2 subunit of brain sodium channels. a transmembrane glycoprotein with a CAM motif. Cell 83. 433-442.

James. W. & Agnew. W. (1989). Alpha-(2-8)-polysialic acid immunoreactivity in voltage-sensitive sodium channel of eel electric organ. Proceedings of the Royal Society B 237. 233-245.

Jan. L.Y. and Y.N. Jan. 1989. Voltage-sensitive ion channel. *Cell.* 56: 13-25.

Jewitt. D. E., Y. Kishon and M. Thomas. 1968. Lidocaine in the management of arrhythmias after acute myocardial infarction. *Lancet.* 1:266-270.

Ji.. S.. A.L. George. Jr.. R. Horn. R.L. Barchi. 1996. Paramyotonia congenita mutations reveal different roles for segments S3 and S4 of domain D4 in hSkM1 sodium channel gating. *J. Gen. Physiol.* 107. 183-194.

Johnson. B.D.. G.H. Hockerman. T. Scheuer. W.A. Catterall. 1996. Distinct effects of mutations in transmembrane segment IVS6 on block of L-type calcium channels by structurally similar phenylalkylamines. *Mol. Pharm.* 50: 1388-1400.

Kao, C.Y. 1986. Structure-activity relations of tetrodotoxin. saxitoxin and analogues. *Ann. N. Y. Acad. Sci. U.S.A.* 479:52-67.

Kallen RG. Sheng ZH, Yang J, Chen LQ, Rogart RB, Barchi RL. 1990. Primary structure and expression of a sodium channel characteristic of denervated and immature rat skeletal muscle. *Neuron* 4(2):233-242

Kayano T, Noda M, Flockerzi V, Takahashi H, Numa S. 1988. Primary structure of rat brain sodium channel III deduced from the cDNA sequence. *FEBS Lett* 228(1):187-194

Keating M.T., M.C. Sanguinetti. Pathophysiology of ion channel mutations. 1996. *Curr Opin Genet Dev* 6: 326-333

Kellenberger, S., T. Scheuer and W.A. Catterall. 1996. Movement of the Na$^+$ channel Inactivation gate during inactivation. *J. Biol. Chem.* 271: 30971-30979.

Keynes RD, Rojas E. 1973. Characteristics of the sodium gating current in the squid giant axon. *J Physiol (Lond)* 233(1):28P-30P

Kim, M S., T. Morii, L.X. Sun, K. Imoto, and Y. Mori. 1993. Structural determinants of ion selectivity in brain calcium channel. *FEBS Lett.* 318-145-148.

Kimura I. 1998. Calcium-dependent desensitizing function of the postsynaptic neuronal-type nicotinic acetylcholine receptors at the neuromuscular junction. *Pharmacol Ther* 77(3):183-202

Kirsh, G.E., C.C. Shieh, J.A. Drewe, D.F. Vener and A.M. Brown. 1993. Segmental exchanges define 4-aminopyridine binding and the inner mouth of K$^+$ pores. *Neuron.* 11: 503-512.

Kirsch, G.E., M. Alam, and H.A. Hartmann. 1994. Differential effects of sulfhydryl reagents on saxitoxin and tetrodotoxin block of voltage-dependent Na channels. *Biophys. J.* 67:2305-2315.

Kiss, L., D. Immke, J. LoTurco and S.J. Korn. 1998. The interaction of Na$^+$ and K$^+$ in voltage-gated potassium channels. Evidence for cation binding sites of different affinity. *J. Gen. Physiol.* 111: 195-206

Kontis. K.J. and A.L. Goldin. 1993. Site-directed mutagenesis of the putative pore region of the rat IIA sodium channel. *Mol. Pharmacol.* 43:635-644.

Kontis K.J. and Goldin A.L. 1997a. Sodium channel activation gating is altered by subsitution of voltage sensor positive charges in all four domains. *J. Gen. Physiol.* 110: 391-401.

Kontis K.J. and Goldin A.L. 1997b. Sodium channel inactivation is altered by subsitution of voltage sensor positive charges. *J. Gen. Physiol.* 110: 403-413.

Krafte. D.S.. T.P. Snutch. J.P. Leonard. N. Davidson. and H.A. Lester. 1988. Evidence for the involvement of more than one mRNA species in controlling the inactivation process of rat and rabbit brain Na channels expressed in *Xenopus* oocytes. *Neuroscience.* 8:2859-2868.

Kreusch A., P.J. Pfaffinger. C.F. Stevens. S. Choe. 1998. Crystal structure of the tetramerization domain of the Shaker potassium channel. *Nature* 392:945-948

Krovetz. H.S.. H.M.A. Vandongen. and A.Mj. Vandongen. 1997. Atomic distance estimates from disulfides and high affinity inetal-binding sites in a KI channel pore. *Biophys. J.* 72:117-126.

Kuck KH, Siebels J. Schneider MA. 1995. Therapeutic consequences of newer studies addressing the problem of myocardial ischemia and ventricular arrhythmias. *Herz* 20: 213-218.

Kumpf, R.A. and D.A. Dougherty. 1993. A mechanism for ion selectivity in potassium channels: computational studies of cation-p interactions. *Science (Wash. DC)* 261:1708-1710.

343

Kunkel. T.A. 1985. Rapid and efficient site-specific mutagenesis without phenotypic selection. *Proc. Natl. Acad. Sci. U.S.A.* 82:488-492.

Kuo C.C. and P. Hess. 1993a. Ion permeation through the L-type Ca^{2+} channel in rat PC12 cells: two sets of binding sites in the pore. *J. Physiol.* 466, 629-655.

Kuo C.C. and P. Hess. 1993b. Characterization of the high-affinity Ca^{2+} binding sites in the L-type Ca^{2+} channel in rat PC12 cells. *J. Physiol.* 466, 657-682.

Kuo CC, Bean BP. 1994. Na^+ channels must deactivate to recover from inactivation. *Neuron* (4):819-829

Kürz, L.L., R.D. Zühlke. H.-J. Zhang. and R.H. Joho. 1995. Side-chain accessibilities in the pore of a K^+ channel probed by sulfhydryl-specific reagents after cysteine-scanning mutagenesis. *Biophys. J.* 68:900-905.

Lan, Y., Lu, T., Lovett. P.S. and Creighton. D.J. (1995). Evidence for a (triosephosphate-like) "catalytic loop" near the active site of glyoxalase 1. *J. Biol. Chem.* 270, 12957-12960.

Lancelin. J.M., D. Knoda. S. Tate. Y. Yanagawa. T. Abe. M. Satake. F. Inagaki. 1991. Tertiary structure of conotoxin GIIIA in aqueous solution. *Biochemistry.* 30(28):6908-16.

Larson, E.M., Larimer, F.W. and Hartman. F.C. (1995). Mechanistic insights provided by deletion of a flexible loop at the active site of ribulose-1,5-biphosphate carboxylase/oxygenase. *Biochemistry* 34, 4531-4537.

Larsson HP, Baker OS, Dhillon DS. Isacoff EY. 1996. Transmembrane movement of the shaker K^+ channel S4. *Neuron* 16(2):387-397

Lauger, P. 1973. Ion transport through pores: A rate theory analysis. *Biochim. Biophys.*

Acta. 311: 423-441.

Lauger, P. 1987. Dynamics of ion transport svstems in membranes. *Physiol. Rev.* 67:1296-1331.

Lawrence J.H., D.T. Yue, W.C. Rose, E. Marban. 1991. Sodium channel inactivation from resting states in guinea-pig ventricular myocytes. *J Physiol (Lond)* 443:629-650

Lee, K.S. and R.W. Tsien. 1983. Mechanism of calcium channel blockade by verapamil, D600, diltiazem and nitrendipine in single dialyzed heart cells. *Nature (Lond.).* 302: 790-794.

Li, M., West, J., Numann, R., Murphy, B., Scheuer, T. & Catterall, W. (1993). Convergent regulation of sodium channels by protein kinase C and cAMP-dependent protein kinase. *Science* 261, 1439-1442.

Li R., R. Tsushima, P.H. Backx. 1996. Determination of Na+ channel pore structure using single- and multiple-cysteine substitutions. *Biophys. J.* 70:A24.

Li R.A., R.G. Tsushima, P.H. Backx. 1997a. Critical pore residues for μ-conotoxin binding to rat skeletal muscle Na^+ channel. *Biophys. J.* 73:1874-1884

Li R.A., R.G. Tsushima, P.H. Backx. 1998. Highly conserved residues in the S3 segments of rat skeletal muscle Na^+ channel play a role in channel activation and inactivation. *Biophys. J.* (submitted)

Li R.A., R.G. Tsushima, P.H. Backx. 1998. pore residue in mammalian Na^+ channel is critical for lidocaine binding. *J. Gen. Physiol.* (submitted)

Li R.A., R.G. Tsushima, P.H. Backx. 1998. Local anesthetics targeting to cardiac Na^+ channels. *Cir. Res.* (submitted)

Liman, E.R., P. Hess. F. Weaver and G. Koren (1991). Voltage-sensing residues in the S4 region of a mammalian K$^+$ channel. *Nature* 353, 752-756.

Lipkind, G M., and H.A. Fozzard. 1994. A structural model of the tetrodotoxin and saxitoxin binding site of the NaI channel. *Biophys. J* 66:1-13.

Liu Y., M.E. Jurman. G. Yellen. 1996. Dynamic rearrangement of the outer mouth of a K$^+$ channel during gating. *Neuron* 16 (4):859-867

Logothetis. D.E.. S. Movahedi. C. Salter. K. Linpaintner and B. Nadal-Ginard (1992). Incremental reductions of positive charge within the S4 region of a voltage-gated K+ channel result in corresponding decreases in gating charge. *Neuron* 8: 531-540.

Logothetis. D.E.. B. F. Kammen. K. Lindpaintner, D. Bisbas. B. Nadal-Ginard (1993). Gating charge differences between two voltage-gated K+ channels are due to the specific charge content of their respective S4 regions. *Neuron* 10: 1121-1129

Lopez, G.A. Y. N. Jan, and L.Y. Jan. 1991. Hydrophobic substitution mutations in the S4 sequence alter voltage-dependent gating in Shaker K$^+$ channels. *Neuron* 7(2):327-336

Lopez, G.A. Y. N. Jan, and L.Y. Jan. 1994. Evidence that the S6 segment of the voltage-gated K+ channel comprises part of the pore. *Science (Wash. DC).* 367:179-182.

Lü, Q. and C. Miller. 1995. Silver as a probe of pore-forming residues in a potassium channel. *Science (Wash. DC)* 268:304-307.

MacKinnon. R. 1991. New insights into the structure and function of potassium channels. Curr. Opin. Neurobiol. 1, 14-19

MacKinnon R. 1995. Pore loops: an emerging theme in ion channel structure. *Neuron* 14(5): 889-892.

MacKinnon, R., and C. Miller. 1989. Mutant potassium channels with altered binding of charybdotoxin, a pore-blocking peptide inhibitor. *Science (Wash. DC)*. 245:1382-1385.

Makielski JC, Limberis JT, Chang SY, Fan Z, Kyle JW. 1996. Coexpression of beta 1 with cardiac sodium channel alpha subunits in oocytes decreases lidocaine block. *Mol Pharmacol* 49(1):30-39

Makita N., P.B. Bennette, A. George Jr. 1996a. Multiple domains contribute to the distinct inactivation properties if human heart and skeletal muscle Na^+ channels. *Cir. Res.* 78(2):244-252

Makita N, P.B. Bennette, A. George Jr. 1996b. Molecular determinants of $\beta1$ subunit-induced gating modulation in voltage-dependent Na^+ channels. *J. Neurosci.* 16(22):7117-7127

Mannuzzu LM, Moronne MM, Isacoff EY. 1996. Direct physical measure of conformational rearrangement underlying potassium channel gating. *Science* 271(5246):213-216

McCormack, K., M.A. Tanouye, L.E. Iverson, J.W. Lin, M. Ramaswami. T. McCormack, J.T. Campanelli, M.K. Matthews and B. Ruby. 1991. A role for hydrophobic residue in the voltage dependent gating of Shaker K^+ channels. *P.N.A.S.* 88: 2931-2935.

McCormack, K., L. Lin and F.J. Sigworth. 1993. Subsitution of a hydrophobic residue alters the conformational stability of Shaker K^+ channels during gating and assembly. *Biophys. J.* 65: 1740-1748.

McCormick, K.A., L.L. Isom, D. Ragsdale, D. Smith, T. Scheuer and W.A. Catterall. 1998. Molecular determinants of Na^+ channel function in the extracellular domain of the b1 subunit. *J. Biol. Chem.* 273: 3954-3962.

McPhee, J.C., D.S. Ragsdale, T. Scheuer and W.A. Catterall. 1994. A mutation in segment IVS6 disrupts fast inactivation of sodium channels. *Proc. Natl. Acad. Sci. U.S.A.* 91: 12346-12350.

McPhee, J.C., D.S. Ragsdale, T. Scheuer and W.A. Catterall. 1995. A critical role for transmembrane segment IVS6 of the sodium channel α subunit in fast-inactivation. *J. Biol. Chem.* 270: 12025-12034.

McPhee, J.C., D.S. Ragsdale, T. Scheuer and W.A. Catterall. 1998. A critical role for the S4-S5 intracellular loop in Domain IV of the sodium channel α subunit in fast-inactivation. *J. Biol. Chem.* 273: 1121-1129.

Mikala, G., A. Bahinski, A. Yatani, S. Tang, and A. Schwartz. 1993. Differential contribution by conserved glutamate residues to an ion-selectivity site in the L-type Ca^{2+} channel pore. *FEBS Lett.* 335:265-269.

Miller C. 1991. 1990: Annus mirabilis of potassium channels. *Science* 252:1092-1096.

Miller, C. 1992. Ion channel structure and function. *Science* 258:240-241.

Miller C. 1996. A chloride channel model? *Science* 274(5288): 738

Mitrovic, N., H. Lerche and F. Lehmann-Horn. 1996. Role in fast inactivation of conserved amino acids in the IV/S4-S5 loop of the human muscle Na^+ channel. *Neurosci. Lett.* 214:9

Moczydlowski, E., B.M. Olivera, W.R. Gray, and G.R. Strichartz. 1986. Discrimination of

muscle and neuronal Na-channel subtypes by binding competition between [^{3}H] saxitoxin and μ-Conotoxins. *Proc. Natl. Acad. Sci. USA.* 83:5321-5325

Murphy, B., Rogers, J., Perdichizzi, A., Colvin, A. & Catterall, W. (1996). cAMP-dependent phosphorylation of two sites in the subunit of the cardiac sodium channel. *J. Biol. Chem.* 271, 28837-28843.

Murphy, B., Rossie, S., De Jongh, K. & Catterall, W. (1993). Identification of the sites of selective phosphorylation and dephosphorylation of the rat brain Na+ channel subunit by cAMP-dependent protein kinase and phosphoprotein phosphatases. *J. Biol. Chem.* 268. 27355-27365.

Murray, K., Hu, N., Daw, J., Shin, H., Watson, M., Mashburn, A. & George, A. Jr (1997). Functional effects of protein kinase C activation on the human cardiac Na+ channel. Circulation Research 80, 370-376.

Myerberg RJ, Castellanos A. Cardiac arrest and sudden cardiac death. In Braunwald E ed. *Heart Disease: A Textbook of Cardiovascular Medicine.* vol. 1 Toronto. Canada: WB Saunders Co; 1997:742-779.

Nakamura, H., J. Kobayashi, Y. Ohizumi, Y. Hirata. 1983. Isolation and amino acid compositions of geographutoxin I and II from the marine snail *Conus geographus Linne. Experientia (Basel).* 39, 590-591.

Narahashi T. 1986. Toxins that modulate the sodium channel gating mechanism. *Ann N Y Acad Sci* 479:133-151

Naranjo, D., and C. Miller. 1996. A strong interacting pair of residues on the contact surface of charydotoxin and *Shaker* K$^+$ channels. *Neuron.* 16:123-130.

Neyton, J. and C. Miller. 1988. Discrete Ba^{2+} block as a probe of ion occupancy and pore

structure in the high conductance Ca^{2+}-activated K^+ channel. *J. Gen. Physiol.* 92:569-586.

Nicholson, L.K-, T. Yamazaki, D.A. Torchia, S. Grzesiek, A. Bax, S.J. Stahl, J.D. Kaufman, P.T. Wingfield, P.Y.S. Lam, P.K. jadhav, et al. 1995. Flexibility and function in HIV-I protease. *Nature Structural Biology.* 2:274-280.

Noda M, Shimizu S, Tanabe T, Takai T, Kayano T, Ikeda T, Takahashi H, Nakayama H, Kanaoka Y, Minamino N, Kangawa K, Matsuo H, Raftery MA, Hirose T, Inayama S, Hayashida H, Miyata T, Numa S. 1984. Primary structure of *Electrophorus electricus* sodium channel deduced from CDNA sequence. *Nature* 312:121-127.

Noda M, Ikeda T, Kayano T, Suzuki H, Takeshima H, Kurasaki M, Takahashi H, Numa S. Existence of distinct sodium channel messenger RNAs in rat brain. *Nature.* 1986:320:188-192.

Noda M, Ikeda T, Suzuki H, Takeshima H, Takahashi H, Kuno M, Numa S. 1986. Expression of functional sodium channels from cDNA. *Nature* 322:826-828.

Noda, M., H. Suzuki, S Numa, W. Stuhmer. 1989. A single point mutation confers tetrodotoxin and saxitoxin insensitivity on the sodium channel-II. *FEBS Lett.* 259, 213

Nonner W, Spalding BC, Hille B. 1980. Low intracellular pH and chemical agents slow inactivation gating in sodium channels of muscle. *Nature* 284(5754):360-363

Numa, S. 1989 A molecular view of neurotransmitter receptors and ionic channels. *Harvey Lect.* 83, 121-165

Numann, R., Catterall, W. & Scheuer, T. (1991). Functional modulation of brain sodium channels by protein kinase C phosphorylation. *Science* 254, 115-118.

Numann R, Hauschka SD, Catterall WA, Scheuer T. 1994. Modulation of skeletal muscle

sodium channels in a satellite cell line by protein kinase C. *J Neurosci* 14(7):4226-4236

Nuss, H.B., N. Chiamvimonvat, M.T. Perez-Garcia, G.F. Tomaselli, E. Marban. 1995. Functional association of the ß1 subunit with human cardiac (hH1) and rat skeletal muscle (μ1) sodium channel α subunits expressed in *Xenopus* oocytes. *J. Gen. Physiol.* 106, 1171-1191.

Nuss HB, Tomaselli GF, Marbán E. Cardiac sodium channels (hH1) are intrinsically more sensitive to block by lidocaine than are skeletal muscle (μ1) channels. *J Gen Physiol.* 1995;106:1193-1209.

O'Leary, M.E., L.Q. Chen, R.G. Kallen, R. Horn. 1995. A molecular link between activation and inactivation of sodium channels. *J. Gen. Physiol.* 106, 641-658.

Olivera, B.M., J. Rivier, C. Clark, C.A. Ramilo, G.P. Corpuz, F.C. Abogadie, E.E. Mena, S.R. Woodward, D.R. Hilliyard, L.J. Cruz. 1990. Diversity of Conus neuropeptides. *Science* 249, 257-263.

Oxford GS, Wu CH, Narahashi T. 1978. Removal of sodium channel inactivation in squid giant axons by n-bromoacetamide. *J Gen Physiol* 71(3):227-247

Papazian DM, Schwarz TL, Tempel BL, Jan YN, Jan LY. 1987. Cloning of genomic and complementary DNA from *Shaker*, aputative potassium channel gene from *Drosophila*. *Science* 237(4816):749-753

Papazian, D.M., L.C. Timple, Y.N. Jan and L.Y. Jan. 1991. Alterations of Shaker potassium channel by mutations in the S4 sequence. *Nature* 349, 305-310.

Papazian, D.M., X.M. Shao, S.A. Seol, A.F. Mock, Y. Huang, D.H. Wainstock. 1995. Electrostatic interactions of S4 voltage sensor in Shaker K+ channel. *Neuron* 14, 1293-1301.

351

Park. C.S. and C. Miller. 1992. Mapping function to structure in a channel-blocking peptide: electrostatic mutants of charybdotoxin. *Biochemistry* 31, 7749-7755.

Pascual, J.M., C.-C. Shieh, G.E. Kirsch, and A.M. Brown. 1995. K^+ pore structure revealed by reporter cysteines at inner and outer surfaces. *Neuron* 14:1055-1063.

Patlak J. 1991. Molecular kinetics of voltage-dependent Na^+ channels. *Physiol Rev* 71(4):1047-1080

Patton, D.E., W.W. James, W.A. Catterall and A.L. Goldin. 1993. A peptide segment critical for sodium channel inactivation functions as an inactivation gate in a potassium channel. *Neuron.* 11: 947-974.

Perez-Garcia. M.T., N. Chiamvimonvat, E. Marban, and G.F. Tomaselli. 1996. Structure of the sodium channel pore revealed by serial cysteine mutagenesis. *Proc. Natl. Acad. Sci. USA.* 93:300-304.

Perozo, E., L. Santacruz-Toloza, E. Stefani, F. Benzailla, D.M. Papazian. 1994. S4 mutations alter gating currents of Shaker K channels. *Biophys. J.* 66, 345-354.

Planell-Cases, R., A.V. Ferrer-Montiel, C.D. Patten, M. Montal. 1995. Mutation of conserved negatively charged residues in the S2 and S3 transmembrane segments of a mammalian K^+ channel selectively modulates channel gating. *PNAS.* 92, 9422-9426.

Pompliano, D. L., Peyman, A. and Knowles, J. R. (1990). Stabilization of a reaction intermediate as a catalytic device: definition of the functional role of the flexible loop in triosephosphate isomerase. *Biochemistry* 29, 3186-3194.

Qu Y, J. Rogers, T. Tanada, T. Scheuer, W.A. Catterall. 1995. Molecular determininat of drug access to the receptor site for antiarrhythmic drugs in the cardiac Na^+ channel. *Proc.*

Natl. Acad. Sci. USA. 92:11839-11843

Ragsdale. D.S.. J.C. McPhee. T. Scheuer. W.A. Catterall. 1994. Molecular determinants of state-dependent block of Na⁺ channels by local anesthetics. *Science* 265:1724-1728.

Ragsdale. D.S.. J.C. McPhee. T. Scheuer. W.A. Caterall. 1996. Common molecular determinants of local anesthetic. antiarrhythmic and anticonvulsant block of voltage-gated Na⁺ channels. *Proc. Natl. Acad. Sci. USA.* 93:9270-9275.

Ranganathan. R.. J.H. Lewis. and R. MacKinnon. 1996. Spatial localization of the K⁺ channel selectivity filter by mutant cyclebased structure analysis. *Neuron.* 16:131-139.

Rogart RB. Cribbs LL. Muglia LK. Kephart DD. Kaiser MW. Molecular cloning of a putative tetrodotoxin-resistant rat heart Na⁺ channel isoform. *Proc Natl Acad Sci USA.* 1989;86:8170-8174.

Rojas E. Armstrong C. 1971. Sodium conductance activation without inactivation in pronase-perfused axons. *Nat New Biol* 229(6):177-178

Rojas. C.V.. J.Z. Wang, L.S. Schwartz. E.P. Hoffman. B.R. Powell and R.B. Brown Jr. 1991. Nature (Lond.). 354: 387-389.

Role LW. Berg DK 1996. Nicotinic receptors in the development and modulation of CNS synapses. *Neuron* 16(6):1077-1085

Rosenberg, R.L. and X. H. Chen. 1991. Characterization and localization of two ion binding sites within the pore of cardiac L-type calcium channels. *J. Gen. Physiol.* 97: 1207-1225.

Ruben, P.C., J.G. Starkus and M.D. Rayner. 1992. Steady-state availability of sodium channels. Interactions between activation and slow inactivation. *Biophys. J.* 61: 941-955.

Rudy B. 1978. Slow inactivation of the sodium conductance in squid giant axons. Pronase resistance. *Physiol (Lond)* 283:1-21

Ruff. R.L.. L. Simoncini and W. Stumer. 1987. Comparison between slow sodium channel inactivation in rat slow- and fast-twitch muscle. *J. Physiol.* 383: 339-348.

Ruff. R.L.. L. Simoncini and W. Stumer. 1988. Slow sodium channel inactivation in mammalian muscle: a possible role in regulating excitability. *Muscle Nerve.* 11: 502-510.

Sah R:L.. R.G. Tsushima. P.H. Backx. 1998. Effects of local anesthetics on Na+ channels containing the equine hyperkalemic periodic paralysis mutation. *Am. J. Physiol.* 275: C389-C400.

Salkoff L. Butler A. Wei A. Scavarda N. Giffen K. Ifune C. Goodman R. Mandel G: Genomic organization and deduced amino acid sequence of a putative sodium channel gene in *Drosophila. Science* 1987; 237:744-749.

Salkoff L. Baker K. Butler A. Covarrubias M. Pak MD. Wei A. 1992. An essential 'set' of K+ channels conserved in flies. mice and humans. Trends Neurosci 15(5):161-166

Sanchez-Chapula. J.. Tsuda. Y. & Josephson. 1.R. 1983. Voltage- and use-dependent effects of lidocaine on sodium current in rat single ventricular cells. *Circ. Res.* **52**:557-565

Sanger. F.. S. Nicklen. A.R. Coulson. 1977. DNA sequencing with chain-terminating inhibitors. *Proc. Natl. Acad. Sci. U.S.A.* 74:5463-5467.

Satin, J.. J.W. Kyle. M. Chen. P. Bell. L.L. Cribbs. H.A. Fozzard, R.B. Rogart 1992. A mutant of TTX-resistant cardiac sodium channels with TTX-sensitive properties. *Science. 256:1202-1205.*

Sato. K. Y. Ishida.. K. Wakamatsu.. R. Kato. H. Honda. Y. Ohizumi. H. Nakamura. M. Ohya. J.M. Lancelin. D. Kohda. and F. Inagaki. 1991. Active site of μ-Conotoxin GIIIA. a peptide blocker of muscle sodium channels. *J. Biol. Chem.* 266:16989-16991.

Seol. S.A.. D. Sigg. D.M. Papazian. F. Bezanilla. 1996. Voltage-sensing residues in the S2 and S4 segments of the Shaker K⁺ channel. *Neuron* 16. 1159-1167.

Schild. L.. E. Moczydlowski. 1991. Competitive binding interaction between Zn^{2+} and saxitoxin in cardiac Na⁺ channels. *Biophys. J.* 59: 523-537.

Schmaker. M.F. and R. MacKinnon. 1990. A simple model for multi-ion permeation. Single-vacancy conduction in a simple pore model. *Biophys. J.* 58:975-984.

Schmidt. J.. S. Rossie & W. Catterall. 1985. P.N.A.S. 82: 4847

Schmidt. J. & Catterall. W. (1987). Cell. 46: 437

Schmidt. J. & Catterall. W. (1987). Palmitylation. sulfation. and glycosylation of the subunit of the sodium channel. Role of post-translational modifications in channel assembly. Journal of Biological Chemistry 262. 13713-13723.

Schmidtmayer. J. & Ulbricht. W. Interaction of lidocaine and benzocaine in blocking sodium channels *Pflügers Arch.* 387. 47-54 (1980).

Schofield PR, Darlison MG, Fujita N. Burt DR, Stephenson FA. Rodriguez H. Rhee LM. Ramachandran J. Reale V. Glencorse TA 1987. Sequence and functional expression of the GABA A receptor shows a ligand-gated receptor super-family. *Nature* 328(6127):221-227

Schoppa NE. McCormack K. Tanouye MA. Sigworth FJ. 1992. The size of gating charge in wild-type and mutant *Shaker* potassium channels. *Science* 255(5052):1712-1715

Schreibmayer, W., Frohnwieser, B., Dascal, N., Platzer, D., Spreitzer, B., Zechner, R., Kallen, R. & Lester, H. (1994). -Adrenergic modulation of currents produced by rat cardiac Na+ channels expressed in Xenopus laevis oocytes. Receptors and Channels 2. 339-350.

Schuster, A., L. Lacinova, N. Klugbauer, H. Ito, L. Birnbauer and F. Hoffman. 1996. The IVS6 segment of the L-type calcium channel is critical for the action of dihydropyridines and phenylalkylamines. EMBO J. 15: 2365-2370.

Seoh SA, Sigg D, Papazian DM, Bezanilla F. 1996. Voltage-sensing residues in the S2 and S4 segments of the Shaker K⁺ channel. Neuron 16(6):1159-1167

Shaw, C.F., III, M.J. Stillman, and K.T. Suzuki. 1992. Metallothioneins: Synthesis, Structure and Properties of Metallothioneins. Phytochelations and Metal-Thiolate Complexes. VCH Publishers Inc., New York. 1-1 3.

Sheldon R.S., R.J. Hill, M. Taouis, L.M. Wilson.1991. Aminoalkyl structural requirements for interaction of lidocaine with the class I antiarrhythmic drug receptor on rat cardiac myocytes. Mol Pharmacol 39: 609-614 .

Sigg, D., and F. Bezanilla. 1997. Total charge movement per channel. The realtion between gating charge displacement and the voltage sensitivity of activation. J Gen. Physiol. 109: 27-39.

Sigworth, F. J. 1993. Voltage gating of ion channels. Q. Rev. Biophysicis 27:1-40.

Simoncini, L. and W. Stumer. 1987. Slow sodium channel inactivation in rat fast-twitch muscle. J. Physiol. (Lond.). 383-339-348

Smith, M.R. and A.L. Goldin. 1997. Interaction between the sodium channel inactivation linker and Domain III S4-S5. Biophys. J. 73: 1885-1895.

Smith. R. & Goldin. A. (1992). Protein kinase A phosphorylation enhances sodium channel currents in Xenopus oocytes. American Journal of Physiology 263. C660-666.

Smith. R. & Goldin. A. (1995). Phosphorylation of brain sodium channels in the I-II linker modulates channel function in *Xenopus* oocytes. Journal of Neuroscience 16. 1965-1974.

Smith. R. & Goldin. A. (1997). Phosphorylation at a single site in the rat brain sodium channel is necessary and sufficient for current reduction by protein kinase A. Journal of Neuroscience 17. 6086-6093.

Soman. K.V.. J.A. McCammon. and A.M. Brown. 1995. Secondary structure prediction of the H5 pore of potassium channels. *Protein Eng.* 8:397-40 1.

Stampe, P.. L. Kolmakova-Partensky. C. Miller. 1994. Intimations of K^+ channel structure from a complete functional map of the molecular surface of charybdotoxin. *Biochemistry* 33, 443-450.

Starmer. C.F.. A.O. Grant. H.C. Strauss. 1984. Mechanisms of use-dependent block of sodium channels in excitable membranes by local anesthetics. *Biophys. J.* 46: 15-27.

Starmer. C.F.. A.O. Grant. 1985. Phasic ion channel blockade: A kinetic model and parameter estimation procedure. *Mol. Pharmacol* 28: 348-356.

Starmer, C.F., K.R. Courtney. 1986. Modelling ion channel blockade at guarded binding sites: Application to tertiary drugs. *Am J. Physiol.* 251: H848-H856.

Starmer C.F., J.Z. Yeh, J. Tanguy. 1989. A quantitative description of QX222 blockade of sodium channels in squid axons. *Biophys J* 49:913-920.

Steinmeyer K. Klocke R. Ortland C. Gronemeier M. Jockusch H. Grunder S. Jentsch TJ. 1991. Inactivation of muscle chloride channel by transposon insertion in myotonic mice. *Nature* 354:304-308

Stephan M.M., J.F. Potts, W.S. Agnew. 1994. The μ1 skeletal muscle sodium channel: mutation E403Q eliminated sensitivity to tetrodotoxin but not to μ-conotoxin GIIIA and GIIIB. *Journal of Membrane Biology.* 137(1):1-8.

Stevens, CF: Making a microscopic hole in one. *Nature* 1991;349:657.

Stone. Mj., NVJ. Fairbrother, A.G. Palmer III, J. Reizer, M.H. Saier, Jr., and P.E. Wright. 1992. Backbone dynamics of the *Bacillus substilis* glucose permease IIA domain determined from 15N NMR relaxation measurements. *Biochemistiy.* 31:4394-4406.

Strichartz G.R. 1973. The inhibition of sodium currents in myelinated nerve by quaternary derivatives of lidocaine. *J. Gen. Physiol.* 62:37-57.

Striessnig, J., H. Glossman and W.A. Catterall. 1990. *Proc. Natl. Acad. Sci. U.S.A.* 88: 9203-9207.

Stühmer, W., F. Conti, H. Suzuki, X. Wang, M. Noda, N. Yahagi, H. Kubo, and S. Numa. 1989. Structural parts involved in activation and inactivation of the sodium channel. *Nature (Lond.)* 339:597-603.

Sun, Z.-P., M.H..kkabas, E.H. Goulding, A. Karlin, and S.A. Siegelbaum. 1996. Exposure of residues in the cyclic nucleotide-gated channel pore: P-region structure and function. *Neuron.* 16:141149.

Sun, Y.M., I. Favre, L. Schild, and E. Moczydlowski. 1997. On the structural basis for selective permeation of organic cations through voltage-gated sodium channel. Effect of alanine mutations at the DEKA locus on selectivity, Inhibition by Ca2+ and H+ and

molecular seiving. *J. Gen. Physiol.* 110: 693-715.

Sunami A. Dudley Jr SC. Fozzard HA. 1997. Sodium channel selectivity filter regulates antiarrhythmic drug binding. *Proc Natl Acad Sci USA*. 94:14126-14131.

Taglialatela. M., J.A. Drewe, G.E. Kirsch, M. De Biasi, H.A. Hartmann, A.M. Brown. 1993. Regulation of K^+/Rb^+ selectivity and internal TEA blockade by mutations at a single site in K^+ pores. *Pflügers Arch* 423:104-112.

Tanabe T, Takeshima H. Mikami A. Flockerzi V, Takahashi H. Kangawa K. Kojima M. Matsuo H, Hirose T, Numa S. 1987. Primary structure of the receptor for calcium channel blockers from skeletal muscle. *Nature* 328(6128):313-318

Tanaka, T., Yamaguchi, H., Kato, H., Nishioka, T., Katsube, Y. and Oda, J. (1993). Flexibility impaired by mutations revealed the multifunctional roles of the loop in glutathione synthetase. *Biochemistry* **32**, 12398-12404.

Tang, L., R.G. Kallen and R. Horn. 1996. Role of an S4-S5 linker in sodium channel inactivation probed by mutagenesis and a peptide blocker. *J. Gen. Physiol.* 108: 89-104.

Tempel BL. Papazian DM. Schwarz TL, Jan YN, Jan LY. 1987. Sequence of a probable potassium channel component encoded at Shaker locus of Drosophila. *Science* 237(4816):770-775

Terlau, H., S.H. Heinemann, W. Stühmer, M. Pusch, F. Conti, K. Imoto, and S. Numa. 1991. Mapping the site of block by tetrodotoxin and saxitoxin of sodium channel II. *FEBS Lett.* 293:93-96.

Todt, H., S. Dudley and H. Fozzard. 1997. ultra-slow inactivation in the skeletal muscle sodium channnle is influenced by pore residues. *Biophys. J.* 72: A261.

Tomaselli. G.F.. H.B. Nuss.J.R. Balser. M.T. Perez-Garcia. K. Kluge. D.W. Orias. P.H. Backx. and E. Marban. 1995. A mutation in the pore of the sodium channel alters gating. *Biophys. J.* 68:18141827.

Torchinsky, Y.M. 1981. Sulfur in Proteins. Pergamon Press, Oxford. pp1-98.

Townend, C. and R. Horn. 1997. Effect of alkali metal cations on slow inactivation of cardiac Na$^+$ channels. *J. Gen. Physiol.* 110: 23-33.

Trimmer. J.S.. Cooperman. S.S.. Tomiko, S.A.. Zhou, J., Crean. S.M.. Boyle, M.B.. Kallen. R.G.. Sheng, Z.. Barchi. R.L.. Sigworth, F.J., Goodman. R.H.. Agnew, W.S. and Mandel. G. 1989. Primary structure and functional expression of a mammalian skeletal muscle sodium channel. *Neuron* 3, 33-49.

Trimmer, J.S., S.S. Cooperman, S.A. Tomiko, J. Zhou, S.M. Crean, M.B. Boyle. R.G. Kallen, Z. Sheng, R.L. Barchi. F.J. Sigworth, R.H. Goodman, W.S. Agnew. and G. Mandel. 1989. Primary structure and functional expression of a mammalian skeletal muscle sodium channel. *Neuron. 3:33-49.*

Tsien. R.W.. P. Hess, E.W. McCleskey and R.L. Rosenberg 1987. Calcium channels: Mechanism of selectivity, permeation. and block. *Ann Rev Biophys Biophys Chem* 16:265-290.

Tsushima, R.G.. R.A. Li. P.H. Backx. 1997. Altered ionic selectivity of Na$^+$ channel revealed by cysteine mutagenesis within the pore. *J. Gen. Physiol.* 109:463-475

Tsushima, R.G., R.A. Li. P.H. Backx. 1997. P-loop flexibility in Na+ channel pores revealed by single- and double-cysteine replacements. *J. Gen. Physiol.* 110:59-72

Tiwari-Woodruff, S.K., C.T. Schulteis , A.F. Mock. D.M. Papazian. 1997. Electrostatic interactions between transmembrane segments mediate folding of Shaker K$^+$ channel

subunits. *Biophys. J.* 72: 1489-1500.

Trimmer, J.S., S.S. Cooperman, S.A. Tomiko, J. Zhou, S.M. Crean, M.B. Boyle, R.G. Kallen, Z. Sheng, R.L. Barchi, F.J. Sigworth, R.H. Goodman, W.S. Agnew, G. Mandel (1989). Primary structure and functional expression of a mammalian skeletal muscle sodium channel. *Neuron* 3, 33-49.

Tytgat J, Nakazawa K, Gross A. Hess P. 1993. Pursuing the voltage sensor of a voltage-gated mammalian potassium channel. *J Biol Chem* 268(32):23777-23779

Vallee. B.L., and K.H. Faichuk. 1993. The biochemical basis of zinc physiology. *Physiol. Rev.* 73:79-1 IS.

Vassilev PM, Scheuer T, Catterall WA. 1988. Identification of an intracellular peptide segment involved in sodium channel inactivation. *Science* 241(4873):1658-1661

Vassilev P, Scheuer T, Catterall WA. 1989. Inhibition of inactivation of single sodium channels by a site-directed antibody. *Proc Natl Acad Sci U S A* 86(20):8147-8151

Vaughan Williams E.M. 1980. Classification of anti-arrhythmic drugs. In Sandoe E. Flensted-Jensen E. Olesen K (eds): Cardiac arrhythmias. Sweden, Astra. Sodertalje. 449-472.

Vedantham, V. and S.C. Cannon. 1998. Slow inactivation does not affect movement of the fast inactivation gate in voltage-gated Na^+ channels. *J. Gen. Physiol.* 111: 83-93.

Wade. R.C., M.E. Davis, B.A. Lutv, J.D. Madura, and J.A. McCammon. 1993. Gating of the active site of triose phosphate isomerase: Brownian dynamics simulations of flexible peptide loops in the enzyme. *Biophys. J.* 64:9-15.

Wakamatsu, K., D. Kohda, H. Hatanaka, J.M. Lancelin, Y. Ishida, M. Oya, H. Nakamura, F.

Inagaki, K. Sato. 1992. Structure-activity relationships of μ-conotoxin GIIIA: structure determination of active and inactive sodium channel blocker peptide by NMR and simulated annealing calculations. *Biochemistry*. 31(50):12577-84.

Wang D.W., N. Li, A.L. George Jr., P.B. Bennett. 1996. Distinct local anesthetic affinities in Na$^+$ channel subtypes. *Biophys. J.* 70:1700-1708.

Wang, G.K., Quan, C. & Wang, S.-Y. A common local anesthetic receptor for benzocaine and etidocaine in voltage-gated μ1 Na$^+$ channels. *Pflügers Arch.* 435. 293-302 (1998).

Welch, G.R, B. Somogvi. and S. Damjanovich. 1982. The role of protein fluctuations in enzyme action: a review. *Prog. Biophys. Mol. Biol.* 39:109-146.

West, J., Numann, R., Murphy, B., Scheuer, T. & Catterall, W. (1991). A phosphorylation site in the Na$^+$ channel required for modulation by protein kinase C. *Science* 254, 866-868.

West, J.W., D.E. Patton, T. Scheuer, Y. Wang, A.L. Goldin, and W.A. Catterall. 1992. A cluster of hydrophobic amino acid residues required for fast Na$^+$-channel inactivation. *Proc. Natl. Acad. Sci. U.S.A.* 89:10910-10914.

Wickenden, A.D., Kaprieleian, R., Parker, T.G., Jones, O.T. & Backx, P.H. Effects of development and thyroid hormone on K$^+$ currents and K$^+$ channel gene expression in rat ventricle. *J Physiol* 504. 271-286 (1997).

Wollner, D.A., D.J. Messner and W.A. Catterall. 1987. J. Biol. Chem. 262: 14709

Woodhull, A.M. 1973. Ionic blockade of sodium channels in nerve. *J. Gen. Physiol.* 61:687-708.

Woosley. R.L.. Roden. D.M.. Duff. H.J. & Oates. J.A. Selection of an antiarrhythmic drug for a sudden-death-prevention trial. *Am Heart J* **103**. 737-745 (1982).

Wright SN. Wang S-Y. Kallen RG. Wang GK. Differences in steady-state inactivation between Na channel isoforms affect local anesthetic binding affinity. *Biophys J.* 1997;73:779-788.

Yang, J.. Sladky, J., Kallen. R. & Barchi. R. (1991). TTX-sensitive and TTX-insensitive sodium channel mRNA transcripts are independently regulated in adult skeletal muscle after denervation. *Neuron* 7, 421-427.

Yang. J.S.. Bennett. P.B.. Makita. N.. George. A.L. & Barchi, R.L. Expression of the sodium channel β_1 subunit in rat skeletal muscle is selectively associated with the tetrodotoxin-sensitive a subunit isoform. *Neuron* **11**, 915-922 (1993).

Yang, J.. P.T. Ellinor. W.A. Sather. J-F. Zhang, and R.W. Tsien. 1993. Molecular determinants of Ca^{2+} selectivity and ion permeation in L-type Ca^{2+} channels. *Nature (Lond.)* 366:158-161.

Yang. N . S. Ji, M. Zhou. L.J. Ptacek. R.L. Barchi, R. Horn and A.L. George Jr. 1994. Sodium channel mutations in paramyotonia congenita exhibit similar biophysical phenotypes in vitro. *Proc. Natl. Acad. Sci. U.S.A.* 91: 12785-12789.

Yang N. Horn R. 1995. Evidence for voltage-dependent S4 movement in sodium channels. *Neuron* 15(1):213-218

Yang, N., A.L. George, Jr., R. Horn. 1996. Molecular Basis of charge movement in voltage-gated sodium channels. *Neuron* 16, 113-122.

Yang, N., A.L. George. Jr.. R. Horn (1997). Probing the outer vestibule of a sodium channel voltage sensor. *Biophys J* 73(5):2260-2268.

Yatani, A., A. Bahinski, G. Mikala, S. Yamamoto and A. Schwartz. 1994. Single amino acid substitutions within the ion permeation pathway alter single-channel conductance of the human L-type cardiac Ca^{2+} channel. *Circ. Res.* 75: 315-323.

Yeh, J. Z. and J. Tanguy. 1985. Na channel activation gate modulates slow recovery from use-dependent block by local anesthetics in squid giant axons. *Biophys. J.* 47, 685.

Yellen G. 1984. Ionic permeation and blockade in Ca^{2+}-activated K^+ channels of bovine chromaffin cells. *J Gen Physiol.* 84(2): 157-186.

Yellen, G., M.E. Jurman, T. Abramson, and R. MacKinnon. 1991. Mutations affecting internal TEA blockade identify the probable pore-forming region. *Science (Wash. DC)* 251:939-942.

Yellen G, Sodickson D, Chen TY, Jurman ME. 1994. An engineered cysteine in the external mouth of a K^+ channel allows inactivation to be modulated by metal binding. *Biophysical J.* 66:1068-1075.

Yool, A.J., and T.L. Schwartz. 1991. Alteration of ionic selectivity of a K^+ channel by mutation of the H5 region. *Nature (Lond.)* 349:700-704.

Yue, D. and E. Marban. 1990. Permeation in the dihydropyridine-sensitive calcium channel: multiple occupancy but no anomalous mole-fraction effect between Ba^{2+} and Ca^{2+}. *J. Gen. Physiol.* 95: 911-939.

Zagotta WN, Hoshi T, Aldrich RW. 1990. Restoration of inactivation in mutants of *Shaker* potassium channels by a peptide derived from *ShB*. *Science.* 250:568-571.

Zagotta WN, Hoshi T, Dittman J, Aldrich RW. 1994a. *Shaker* potassium channel gating. II: Transitions in the activation pathway. *J Gen Physiol* 103(2):279-319

Zagotta WN, Hoshi T, Aldrich RW. 1994b. *Shaker* potassium channel gating. III: Evaluation of kinetic models for activation. *J Gen Physiol* 103(2):321-362

Zamponi GW, French RJ. Dissecting lidocaine action: diethylamide and phenol mimic separate modes of lidocaine block of sodium channels from heart and skeletal muscle *Biophys J.* 1993;65:2335-2347.

Zamponi GW, French RJ. Amine blockers of the cytoplasmic mouth of sodium channels: a small structural change can abolish voltage dependence. *Biophys J.* 1994;67:1015-1027.

Zar, J.H. *Biostatisical Analysis* Prentice Hall, Upper Saddle River, NJ (1996)

Zhou, J., J.F. Potts, J.S. Trimmer, W.S. Agnew, F.J. Sigworth. 1991. Multiple gating modes and the effect of modulating factors on the μ1 sodium channel. *Neuron.* 7:775-785.

Zipes DP. Management of carrdiac arrhythmias: pharmacological, electrical, and surgical techniques. In Braunwald E ed. *Heart Disease: A Textbook of Cardiovascular Medicine.* vol. 1 Toronto, Canada: WB Saunders Co; 1997:593-639.